

On Stability of Sustainable Power Systems

Network Fault Response of Transmission Systems
with Very High Penetration of Distributed Generation

Jens C. Boemer

Cover design: Becky L. Crook

On Stability of Sustainable Power Systems

Network Fault Response of Transmission Systems with Very High Penetration of Distributed Generation

Proefschrift

ter verkrijging van de graad van doctor
aan de Technische Universiteit Delft,
op gezag van de Rector Magnificus prof.ir. K.C.A.M. Luyben,
voorzitter van het College voor Promoties,
in het openbaar te verdedigen op donderdag 16 juni 2016 om 10.00 uur

door

Jens Christian BOEMER

Diplom-Ingenieur Elektrotechnik,
geboren te Dortmund, Duitsland.

This dissertation has been approved by:
promotor: Prof.ir. M.A.M.M. van der Meijden
copromotor: Dr. M. Gibescu

Composition of the doctoral committee:

Rector Magnificus	chairman
Prof.ir. M.A.M.M. van der Meijden	Delft University of Technology
Dr. M. Gibescu	Eindhoven University of Technology

Independent members:

Prof.dr. P. Palensky	Delft University of Technology
Prof.dr. J. Milanovic	The University of Manchester
Prof.dr.-ing. R. Witzmann	Technische Universität München
Prof.dr. F.M. Brazier	Delft University of Technology

Other members:

Dr. B. Rawn	Brunel University London
-------------	--------------------------

The research described in this thesis was partly supported by the Forum network technology / network operation in the VDE (FNN).

Cover design by Becky L. Crook

Published and distributed by: Jens Christian BOEMER

E-mail: mail@jens-boemer.de

WWW: <http://www.jens-boemer.de>

ISBN 978-94-6186-646-2

Keywords: power system stability, distributed generation, dynamic equivalents, grid codes.

Copyright © 2016 by Jens Christian BOEMER

All rights reserved. No part of the material protected by this copyright notice may be reproduced or utilized in any form or by any means, electronic or mechanical, including photocopying, recording or by any information storage and retrieval system, without written permission of the author.

An electronic version of this dissertation is available at <http://repository.tudelft.nl/>.

Printed by CPI-Koninklijke Wöhrmann – Zutphen in The Netherlands

Summary

Electrical power systems are being transformed: renewable power generating facilities, excluding large hydro power plants, accounted for 48 % of new generation capacity added worldwide in 2014. The drivers for this change are: policies to reduce emissions of greenhouse gases, efforts to decrease the dependency on fuel imports and to maintain the security of supply in the long-term, and the liberalisation of the electricity sector as well as a public movement towards a ‘democratisation’ of power generation.

As a consequence, power systems are nowadays undergoing an unprecedented *structural* and *technological* transformation. The increase of distributed generation (DG), primarily wind power park modules (WPPMs) and photovoltaic power park modules (PVPPMs), is already changing the way power systems are structured and operated. Power systems are being transformed from vertically-designed systems with unidirectional power flows to horizontally-designed systems with bidirectional power flows. Distribution systems are turning from ‘passive’ into ‘active’ distribution systems (ADSs). Conventional (thermal) power plants with synchronous generators are being replaced by power park modules that are connected to the network non-synchronously and/or via power electronic converters. This structural and technological transformation influences the power system’s network fault response and stability properties.

This thesis investigates the network fault response of integrated transmission and distribution systems with very high penetration of distributed renewable and conventional generation. Network fault response is the dynamic response of the whole or of parts of the power system during and shortly following sudden faults in the network. The response is calculated in terms of changes in system variables over a time frame of interest, such as bus voltage magnitudes and angles, generator rotor angles, and fundamental system frequency. In summary, the impacts of DG on transient stability, large disturbance voltage stability, and frequency stability are analysed in this thesis. The analysis focuses on symmetrical, three-phase transmission network faults. Other classes of power system stability problems and unbalanced faults are not within the scope of this thesis.

Requirements for the response of all generation types and in particular distributed generation to network faults are defined in grid connection requirements (GCRs), which are a set of legally binding technical rules to ensure system security. The massive insertion of DG into distribution systems (DSs) leads to new challenges like the regular occurrence of reverse power flow (RPF) situations from the distribution to transmission level, the potential increase of the inductive reactive power demand when DG control their terminal voltage, and local stability problems with the connection of DG to ‘weaker’ points of common coupling (PCC). Furthermore, with distributed generation being located very close to the loads,

DG is more likely to be exposed to fault-induced delayed voltage recovery (FIDVR) events than transmission and sub-transmission connected generating facilities. This leads to the identification of the following *shortcomings in the state of the art*:

- Current modelling approaches to study the impact of DG on transient stability, large disturbance voltage stability, and frequency stability fall short with very high penetration of DG with regard to the accuracy in the periphery region ('annulus') of a voltage funnel.
- Hence, grid connection requirements currently in force have undergone insufficient technical impact assessment for systems with reverse power flow situations and 'weak' points of common coupling (PCCs).
- Furthermore, the actual implementation of these grid connection requirements by distribution system operators (DSOs) for DG connected at medium voltage level can have undesired consequences for system stability under certain conditions.
- After all, state of the art requirements regarding network fault response of DG have so far been implemented insufficiently at low voltage (LV) levels.

The *overall objective* of this thesis, therefore, is to critically review current and proposed grid connection requirements with regard to the network fault response of transmission systems with very high penetration of distributed generation and to propose changes to the specifications where needed. This is achieved through the following *scientific contributions*:

- Analysis of the stability of evolving sustainable power systems in a system-wide, accurate and computational-efficient way that considers dynamic interactions between the transmission and distribution system levels.

This thesis proposes a comprehensive methodology of aggregation of DGs and their dynamic equivalencing for stability studies. The dynamic response of DG models is very sensitive to the retained terminal voltage during a network fault. The spatial voltage profile (voltage funnel) in the fault period has a periphery region (annulus) in which the retained voltage is very close to the undervoltage protection threshold of DG. The accurate modelling of the voltage contour that delineates all system nodes where the retained voltage is smaller than the DG's undervoltage protection threshold will have a significant impact on the bifurcation point of the system-wide stability response: the aggregate MW-value of DG units that trip will be quite sensitive to the modelling assumptions, network representation, and network fault response of individual DG units.

The thesis derives dynamic equivalent models of ADSs that are highly accurate in the voltage funnel's annulus. The equivalent models also consider the 'legacy' performance through the composition of DG classes in terms of their technology and grid code performance. The derived equivalent ADSs models have been validated against detailed models and show a high accuracy.

- Improved understanding of the effects of very high penetration of DG, including renewable energy sources for electricity (RES-E), on power system stability.

This thesis demonstrates that current undervoltage protection schemes for small-scale and medium-scale DG connected in LV distribution networks may become a risk for power system stability. It further demonstrates that a low voltage ride-through (LVRT) operation of distribution connected DG with blocking of the inverter current (also known as 'momentary cessation', 'zero-power' mode, or 'limited dynamic voltage support') for terminal voltages immediately below the continuous operating region can compound fault-induced delayed voltage recovery and negatively impact power system stability.

- Identification of minimum requirements for LV connected DG and improvement of existing grid connection requirements for MV connected DG to maintain power system stability.

This thesis proposes new requirements for the network fault response of LV connected, inverter-based DG, analyses the opportunities and challenges of a full dynamic voltage support by additional reactive current injection (aRCI) from distribution connected DG, and studies LVRT requirements for LV connected, low-inertia, synchronous generator-based DG. A new fault control mode is proposed that shows robust performance under a large number of system conditions and control parameter variations. Finally, the opportunities and challenges are studied of using both additional reactive/active current injection to achieve a dynamic voltage support optimised for the network impedance angle.

The most important *conclusions* from this research are:

- When aggregating ADSs for stability studies of sustainable power systems, radial parts of distribution systems can be aggregated, but individual voltage levels should be explicitly modeled with their respective transformer impedance, as well as an equivalent impedance to represent the feeders. DG prevalent at each voltage level should be clustered into equivalent models of the same technology type and network fault response performance. On-load tap-changers of transformers and the quasi-stationary voltage control of DGs should be explicitly modelled, so as to correctly initialise the dynamic simulation.
- It has been shown that, with DG being located very close to the loads, the network fault response of DG is even more influenced by the load characteristics than this is the case for transmission connected generation. Fault-induced delayed voltage recovery caused by induction motors (e.g., air conditioning systems) can prolong LVRT operation in blocking mode. This could trigger a large frequency deviation in the post-fault period, thereby increasing the risk of load-shedding and frequency instability.
- Significant active power from LV connected DG can be lost following a transmission system fault. It is recommended that, in the short term, LV connected photovoltaic power park modules ride through voltage dips caused by transmission system faults in blocking mode ('limited dynamic voltage support'). In the

long term, the aRCI mode is recommended ('full dynamic voltage support'). As long as penetration levels for synchronous generation-based DG are low, a LVRT requirement for shallow voltage dips is deemed sufficient.

- The opportunities and challenges of a short-circuit current injection from DG are complex. In the fault period, full dynamic voltage support can increase the voltage at distribution level in the annulus of a voltage funnel and thereby move the voltage contour that delineates all system nodes where the retained voltage is smaller than the DG's undervoltage protection threshold. This reduces the aggregate MW-value of DG units that trip. In the post-fault period, it can prevent a prolonged LVRT operation of DG units at all locations in the system where FIDVR occurs in active distribution systems with large amounts of induction motors (e.g., air conditioning systems). However, injection of a short-circuit current may require a complete revision of the distribution system protection scheme and anti-islanding techniques.
- To better manage the risk associated with implicit assumptions in grid connection requirements, such as modest penetration levels for certain DG technologies and a dominance of PV systems in inverter-based DG, a performance-based approach to network fault response requirements of DG could be considered to replace the technology-based approach of current GCRs.

From a practical viewpoint, the contributions and conclusions of this thesis can inform distribution system operators and national grid code committees as they define justified and effective grid connection requirements. The recommendations on modelling of DG in bulk power system stability studies can contribute to ongoing activities related to power system dynamic performance in IEEE and CIGRÉ.

Samenvatting

Elektriciteitsvoorzieningssystemen ondergaan een transformatie: productiefaciliteiten voor hernieuwbare energie, exclusief grote waterkrachtinstallaties, waren in 2014 goed voor 48% van de nieuw toegevoegde opwekkingscapaciteit voor elektrische energie. De aanjagers van deze verandering zijn het beleid dat is gericht op het verminderen van broeikasgassen, de inspanningen om de afhankelijkheid van geïmporteerde brandstof te verminderen en het veilig stellen van de levering voor de langere termijn. Daarnaast spelen de liberalisering van de elektriciteitssector en de publieke opinie richting een 'democratisering' van elektrische energieopwekking een rol.

Als gevolg hiervan ondergaan de elektriciteitssystemen van vandaag een ongekende *structurele* en *technologische* transformatie. De toename van gedistribueerde opwekking (DG, *distributed generation*), in het bijzonder windparken (WPPM, *wind power park modules*) en zonneparken (PVPPM, *photovoltaic power park modules*), verandert nu al de manier waarop elektriciteitssystemen worden gestructureerd en worden bedreven. Elektriciteitssystemen gaan van verticaal ontworpen systemen waarin energie in één richting stroomt naar horizontaal ontworpen systemen waarin energie in twee richtingen stroomt. Distributiesystemen veranderen van 'passieve' naar 'actieve' distributiesystemen (ADS, *active distribution system*). Conventionele (thermische) energiecentrales met synchrone generatoren worden hierbij vervangen door opwekeenheden die asynchroon of via elektronische omvormers verbonden zijn met het netwerk. Deze structurele en technologische transformatie heeft invloed op de kortsluitreactie en de stabiliteit van het elektriciteitsnetwerk.

Dit proefschrift onderzoekt de kortsluitreactie van het netwerk van de geïntegreerde transmissie- en distributiesystemen met een zeer hoge penetratie van gedistribueerde hernieuwbare en conventionele opwekkers. De kortsluitreactie is de dynamische reactie van het volledige of gedeeltelijke elektriciteitssysteem, gedurende en kort na plotselinge fouten in het netwerk. De reactie wordt berekend aan de hand van veranderingen in systeemvariabelen gedurende een bepaalde periode, zoals de toename en de hoeken van knooppuntspanningen, de lasthoeken van generatoren en de systeemfrequentie. Samenvattend: in dit proefschrift worden de invloed van gedistribueerde opwekking op kortstondige stabiliteit, de spanningsstabiliteit bij langdurige storingen en de frequentiestabiliteit geanalyseerd. De analyse richt zich op symmetrische driefasenfouten in het transmissienetwerk. Andere soorten stabiliteitsproblemen en asymmetrische fouten vallen niet binnen het kader van dit proefschrift.

Vereisten voor de reactie van alle soorten opwekkers en in het bijzonder van gedistribueerde opwekkers op netwerkfouten worden beschreven in netcodes (GCR, *grid connection requirements*). Dit betreft een reeks wettelijk bindende technische regels die systeemvei-

ligheid moeten garanderen. De grootschalige toepassing van gedistribueerde opwekking in distributiesystemen (DS) leidt tot nieuwe uitdagingen, waaronder het regelmatig vóórkomen van omgekeerde vermogensstromen (RPF, *reverse power flow*) van distributie- naar transmissieniveau, de mogelijke toename van de inductieve, resp. reactieve elektriciteitsvraag indien gedistribueerde opwekkers lokaal de klemspanning beïnvloeden en de lokale stabiliteitsproblemen bij de verbinding van gedistribueerde opwekkers aan 'zwakke' netaankoppelingen (PCC, *points of common coupling*). Gezien het feit dat gedistribueerde opwekkers zich doorgaans dichtbij het elektriciteitsverbruik (de belasting) bevinden, is in vergelijking met (sub-)transmissiesystemen de kans groter dat gedistribueerde opwekkers worden blootgesteld aan situaties waarbij door fouten geïnduceerd vertraagd spanningsherstel (FIDVR, *fault-induced delayed voltage recovery*) optreedt. Het voorgaande leidt tot de identificatie van de volgende *tekortkomingen in de huidige stand van zaken*:

- Huidige modelleringsbenaderingen om de invloed te bestuderen van gedistribueerde opwekking op kortstondige stabiliteit, spanningsstabiliteit bij zware verstoringen en tekortkoming van frequentiestabiliteit met een zeer hoge penetratie gedistribueerde opwekkers schieten bij een zeer hoge penetratie gedistribueerde opwekkers te kort met betrekking tot de nauwkeurigheid van de spanningstrechter in de perifere regio ('annulus').
- Dientengevolge heeft de huidige regelgeving voor netwerkaansluitingen onvoldoende technische impactbeoordeling ondergaan voor systemen met situaties met omgekeerde energiestroom en 'zwakke' netaankoppelpunten.
- Ook kan de daadwerkelijke implementatie van deze netcodes door distributiesysteembeheerders (DSO, *distribution system operator*) voor gedistribueerde opwekkers verbonden op het middenspanningsniveau (MV) onder bepaalde omstandigheden ongewenste gevolgen hebben voor de systeemstabiliteit.
- Uiteindelijk zijn de laatste vereisten met betrekking tot de kortstsluitreactie van gedistribueerde opwekkers tot op heden onvoldoende op het laagspanningsniveau (LV) geïmplementeerd.

Het *overkoepelende doel* van dit proefschrift is daarom het kritisch evalueren van de huidige en de nieuw voorgestelde netcodes met betrekking tot de kortstsluitreactie van transmissiesystemen met een zeer hoge penetratie van gedistribueerde opwekkers en het, waar nodig, voorstellen van aanpassingen in de specificaties. Dit doel wordt bereikt door middel van de volgende *wetenschappelijke bijdragen*:

- Analyse van de stabiliteit van in ontwikkeling zijnde duurzame elektriciteitssystemen op een systeem brede, nauwkeurige en numeriek efficiënte manier, die bovendien rekening houdt met dynamische interacties tussen de transmissie- en distributiesystemen.

Dit proefschrift introduceert een uitgebreid raamwerk van methodes voor stabiliteitsonderzoeken aan de hand van aggregatie van gedistribueerde opwekkers en hun dynamische equivalenten. De dynamische respons van modellen voor gedistribueerde opwekkers is zeer gevoelig voor de restspanning tijdens een netwerkfout. Het ruimtelijke spanningsprofiel (spanningstrechter) heeft tijdens de

foutperiode een perifere regio (annulus) waarin restspanning dicht bij de onderspanningsdrempel van de beveiliging van gedistribueerde opwekkers ligt. Het nauwkeurig modelleren van de spanningsomtrek die alle systeemknooppunten bevat waar de restspanning lager is dan de aanspreekwaarde van de onderspanningsbeveiliging van de gedistribueerde opwekking heeft een belangrijke invloed op het zadel-knoop bifurcatiepunt van de systeem brede stabiliteitsreactie: het geaggregeerde afgeschakelde MW vermogen van de gedistribueerde opwekkers zal zeer gevoelig zijn voor de modelleeraannames, netwerkrepresentatie en de kortsluitreactie van individuele gedistribueerde opwekeenheden.

Het proefschrift leidt dynamisch equivalente modellen af van actieve distributiesystemen die vooral zeer nauwkeurig zijn in de annulus van de spanningstrechter. Deze equivalente modellen houden ook rekening met de prestatie van de bestaande systemen door middel van de samenstelling van gedistribueerde opwekkingsklassen voor hun technologieën en het voldoen aan de netcode. De afgeleide equivalenten van actieve distributiesystemen zijn gevalideerd aan de hand van gedetailleerde modellen en laten derhalve een zeer hoge nauwkeurigheid zien.

- Verbeterd begrip van de effecten van een zeer hoge penetratie van gedistribueerde opwekkers op de stabiliteit van elektriciteitssystemen. Dit is inclusief hernieuwbare energiebronnen voor elektriciteit (RES-E, *renewable energy sources for electricity*).

Dit proefschrift laat zien dat de huidige onderspanningsbeveiligingsfilosofieën voor kleine en middelgrote verbindingen van gedistribueerde opwekking in laagspannings-distributienetwerken een risico kunnen vormen voor de stabiliteit van het elektriciteitsvoorzieningssysteem. Het laat ook zien dat het tijdens kortsluitingen (LVRT, *low voltage ride-through*) behouden van de netverbinding van gedistribueerde opwekkers met geblokkeerde inverterstroom (ook wel bekend als '*momentary cessation*', '*zero-power*' mode of 'beperkte dynamische spanningsondersteuning') voor de klemspanningen direct onder het continue werkingsgebied (in de LVRT curve) het fout-geïnduceerd vertraagd stroomherstel kan verergeren en daardoor een negatieve invloed kan hebben op de stabiliteit van het elektriciteitssysteem.

- Identificatie van de minimale vereisten voor gedistribueerde opwekkers op laagspanning en verbetering van bestaande netwerkverbindingsvereisten voor gedistribueerde opwekking op middenspanning om de stabiliteit van het elektriciteitssysteem te behouden.

Dit proefschrift stelt nieuwe vereisten voor de netwerkfoutreactie van met omvormers op laagspanning aangesloten gedistribueerde opwekkers voor, analyseert de kansen en uitdagingen van een volledig dynamische spanningsondersteuning door aanvullende reactieve stroominjectie (aRCI, *additional reactive current injection*) vanaf de DG en onderzoekt de LVRT-vereisten voor gedistribueerde opwekking op laagspanningsniveau via synchrone generator met kleine massastraagheid. Er wordt een nieuwe foutcontrolemodus voorgesteld die robuuste prestaties laat zien in veel verschillende systeemomstandigheden en vari-

aties in regelparameters. Tot slot worden kansen en uitdagingen bestudeerd van het gebruik van zowel aanvullende reactieve/actieve stroominjectie om te zorgen voor een dynamische spanningsondersteuning die geoptimaliseerd is voor de lokale netwerkimpedantiehoek.

De belangrijkste *conclusies* van dit onderzoek zijn:

- Als actieve distributiesystemen geaggregeerd worden ten behoeve van stabiliteitsonderzoeken inzake duurzame elektriciteitssystemen, kunnen radiale delen van distributiesystemen geaggregeerd worden. Individuele spanningsniveaus dienen echter nadrukkelijk gemodelleerd te worden met hun respectievelijke transformatorimpedantie en een equivalente impedantie om de aanvoerverbindingen weer te geven. Op ieder spanningsniveau dienen de aanwezige gedistribueerde opwekkers geclusterd te worden in equivalente modellen van hetzelfde type technologie. Daarnaast behoort de (quasi-stationaire) spanningsregeling van gedistribueerde opwekking expliciet gemodelleerd te worden, zodanig dat de dynamische simulatie op de juiste wijze gestart kan worden.
- Het is aangetoond dat als de gedistribueerde opwekking erg dicht bij de belasting staat, de netwerkfoutreactie van gedistribueerde opwekking nog meer beïnvloed wordt door de kenmerken van de belasting dan het geval is bij opwekking verbonden op transmissieniveau. Fout-geïnduceerd vertraagd spanningsherstel, veroorzaakt door inductiemotoren (b.v. aircosystemen), kunnen de LVRT-werking in blokkeermodus verlengen. Dit kan een grote frequentieafwijking initiëren in de periode die volgt na de kortsluiting. Dit kan vervolgens weer leiden tot een risico op belastingafschakelen en frequentie-instabiliteit.
- Een significante hoeveelheid actief vermogen van gedistribueerde opwekking op laagspanning kan verloren raken na een fout in het transmissiesysteem. Aanbevolen wordt om op de korte termijn de zonneparken op laagspanningsniveau door de spanningsdips, die veroorzaakt worden door fouten in transmissiesystemen, in blokkeermodus ('beperkte dynamische spanningsondersteuning') heen te loodsen. Op de lange termijn wordt de aRCI-modus geadviseerd ('volledige dynamische spanningsondersteuning'). Zolang de penetratieniveaus van gedistribueerde opwekkers op basis van synchrone opwekking laag zijn, is een LVRT-eis voor kleine spanningsdips voldoende.
- De kansen en uitdagingen van een kortsluitstroominjectie door gedistribueerde opwekkers zijn complex. Gedurende de fout kan een volledig dynamische spanningsondersteuning de spanning op distributieniveau in de annulus van een spanningstrechter verhogen. Hierdoor verplaatst de spanningsomtrek die alle systeemknooppunten markeert waarvan de restspanning lager is dan de drempel voor onderspanningsbeveiliging van de gedistribueerde opwekkingseenheden. Dit vermindert de geaggregeerde MW-waarde van gedistribueerde opwekkingseenheden die afgeschakeld wordt. In de periode na de fout kan het een verlengde LVRT-operatie voorkomen van de gedistribueerde opwekkingseenheden op alle locaties in het systeem waar FIDVR voorkomt in actieve distributiesystemen met grote aantallen inductiemotoren (b.v. aircosystemen). Kortsluitstroominjectie

kan echter een complete herziening van het distributiebeveiligingssysteem en anti-eiland beveiligingstechnieken met zich meebrengen.

- Om de risico's die verbonden zijn aan de impliciete aannames in de netcodes beter te kunnen beheren, zoals bijvoorbeeld risico's verbonden aan bescheiden penetratieniveaus voor bepaalde technologieën van gedistribueerde opwekking en een dominantie van PV-systemen in invertergebaseerde gedistribueerde opwekking, kan een op prestaties gebaseerde benadering van netwerkfoutreactie-eisen van gedistribueerde opwekking overwogen worden ter vervanging van de op technologie gebaseerde benadering van de huidige netcodes.

Vanuit praktisch opzicht kunnen de bijdragen en conclusies van dit proefschrift distributiesysteembeheerders en nationale netcodecommissies informeren met betrekking tot het bepalen van gerechtvaardigde en effectieve eisen voor nieuwe netaansluitingen. De aanbevelingen inzake het modelleren van gedistribueerde opwekking in grootschalige stabiliteitsonderzoeken kunnen bijdragen aan lopende activiteiten in IEEE en CIGRÉ verband aangaande de dynamische prestaties van het elektriciteitsvoorzieningssysteem.

Nomenclature

Abbreviations

aRACI	additional reactive/active current injection
aRCI	additional reactive current injection
ac	alternating current
ANN	artificial neural network
ADS	active distribution system
AS	ancillary service
AVR	automatic voltage regulator
BM	blocking mode
CAG	conventional asynchronous generator
CCT	critical clearance time
CE	Continental Europe
CENELEC	European Committee for Electrotechnical Standardization
CHP	combined heat and power
CM	control mode
dAPR	delayed active power recovery
dc	direct current
DER	distributed energy resource
DFAG	doubly fed asynchronous generator
DG	distributed generation
DGF	DIgSILENT PowerFactory© v15.1

DRS	dynamic reactive support
DS	distribution system
DSO	distribution system operator
eHV	extra-high voltage
emt	electro-magnetic transient value
ENTSO-E	European Network of Transmission System Operators for Electricity
NC RfG	Network Code for Requirements for Grid Connection Applicable to all Generators
FC	full converter interface unit
FIDVR	fault-induced delayed voltage recovery
FNN	Forum network technology / network operation in the VDE
FRT	fault ride-through
GC	grid code
GCR	grid connection requirement
HV	high voltage
HVRT	high voltage ride-through
IEEE	Institute of Electrical and Electronics Engineers
KCL	Kirchhoff current law
KVL	Kirchhoff voltage law
LV	low voltage
LVRT	low voltage ride-through
MPPT	maximum power point tracking
MV	medium voltage
NE	New England
OLTC	on load tap changer
OS	operational scenario
PCC	point of common coupling
PEC	power electronic converter
PGM	power generating module

sPGM	synchronous power generating module
PLL	phase locked loop
PSS	power system stabiliser
PPM	power park module
PM	prime mover
PV	photovoltaic
PVPPM	photovoltaic power park module
RES-E	renewable energy sources for electricity generation
rms	root mean square
ROCOF	rate of change of frequency
RPF	reverse power flow
SCR	short-circuit ratio
SG	synchronous generator
ST	sub-transmission
TS	transmission system
TSO	transmission system operator
VRRAG	variable rotor resistance asynchronous generators
VSC	voltage source converter
WECC	Western Electricity Coordinating Council
WPPM	wind power park module
WTG	wind turbine generator

Notation

Typeface	Examples	Explanation
<i>italic</i>	y, Y, I_d or i, j	scalar physical quantities or numerical variables
<u>underscored</u>	$\underline{y}, \underline{Y}, \underline{S}, I_{DG}$	phasors and complex quantities, complex conjugated quantities denoted as $\underline{y}^*, \underline{Y}^*$
<i>italic, lower case</i>	$y, f, v(t)$	normalised quantities in per unit values; time dependent instantaneous variables, denoted as $y(t)$
UPPER CASE	Y, \underline{Y}, F	absolute quantities in physical units
boldface lower case	y	vectors
boldface UPPER CASE	Y	matrices
<i>italic</i>	$f(x), G(s)$	functions in general
roman	sin, cos, tan	explicitly defined functions
roman	kV, A, Hz	unit symbols
roman	$\frac{df}{dt}$ and $\frac{\partial p}{\partial x}$	ordinary derivatives and partial derivatives
roman	1, Flt, π	descriptive terms incl. subscripts and superscripts, mathematical constants that never change

General Definitions

Symbol	Notation	Definition
\underline{z}, r, x	<i>lower case</i>	complex impedance, scalar resistance and reactance in per unit values on a machine base value
$\underline{V}, \underline{I}, \underline{Z}, R, X$	UPPER CASE	complex rms voltage and current, scalar impedance, resistance and reactance
$\langle x \rangle$	<i>angle brackets</i>	mean value over a sample of values
\bar{x}	<i>bar accent</i>	average value over time period T
$[x]$	<i>half brackets</i>	ceiling function (round up towards next integer)
$\max_y(x)$		maximum function with lower limit of y
$\min^y(x)$		minimum function with upper limit of y

General Symbols

P	active power in [W]
Q	reactive power in [VAr]
S	apparent power in [VA]
t	time in [p.u.]
t'	time in [s]
H	inertia time constant in [p.u.]
J	inertia constant in [kg · m ²]
Δ	difference between two values in [p.u.]
F	instantaneous frequency in [Hz]
ω	angular frequency in [p.u.]
Ω	angular frequency in [rad/s]
v	instantaneous voltage in [p.u.]
V	voltage phasor magnitude in [V]
i	instantaneous current in [p.u.]
I	current phasor magnitude in [A]
ϕ	voltage or current phasor angle in [rad] or [deg]
r	resistance in [p.u.]
x	reactance in [p.u.]
z	impedance in [p.u.]
δ	rotor angle in [rad] or damping coefficient in [p.u.]
τ	mechanical or electromagnetic torque in [p.u.]
T	time constant in [s]
k	controller gain in [p.u.]
φ	phase angle in [rad]
ψ	network impedance angle in [rad] or [deg]
\underline{x}'	complex transient reactance in [p.u.]

\underline{x}''	complex subtransient reactance in [p.u.]
\underline{s}	complex power in [p.u.]

Subscripts

0	initial value or pre-fault value
b	base quantity for per unit values
n	nominal quantity
r	rated quantity
s	synchronous quantity
i	instantaneous or actual quantity
i	internal quantity of generator
σ	leakage quantity
e	electromagnetic (torque)
m	mechanic (torque) or magnetising (reactance)
a,b,c	phase quantities
1,2,0	symmetrical components
d,q	components in rotating reference frame
α, β	components in stationary reference frame
G	network quantity
ST	sub-transmission network quantity
DS	distribution network quantity
f	frequency related quantity
meas	measured quantity
sum, Σ	sum
ref	reference value
DB	deadband

max	maximum value
min	minimum value
fund	fundamental frequency component
prio	component with assigned priority
p	peak value
stat	stationary component
P	active component
Q	reactive component
Ld	quantity of load
Ld,dyn	dynamic part of load
Ld,stat	static part of load
Ln	quantity of line
DG	quantity of distributed generation
SG	quantity of synchronous generation
Tr	quantity of transformer
k, Flt	quantity of fault or short-circuit
WP	quantity of wind power park module

Superscripts

\angle	arbitrary coordinate system
$\angle 0$	stationary reference frame
$\angle v_G$	reference frame aligned to network voltage
*	conjugated complex quantity
\diamond	non-limited quantity

Specific Symbols Used

Power quantities

\underline{S}	apparent power phasor	[VA]
S	apparent power phasor magnitude	[VA]
P	active power magnitude	[W]
Q	reactive power magnitude	[VAr]
P_{WPPM}	active power magnitude at WPPM terminal (PCC)	[W]
Q_{WPPM}	reactive power magnitude at WPPM terminal (PCC)	[VAr]
\underline{S}_{DG}	apparent power phasor at DG terminal (PCC)	[VA]
S_{DG}	apparent power magnitude at DG terminal (PCC)	[VA]
P_{DG}	active power magnitude at DG terminal (PCC)	[W]
Q_{DG}	reactive power magnitude at DG terminal (PCC)	[VAr]
S_{Ld}	apparent power magnitude at load terminal	[VA]
P_{Ld}	active power magnitude at load terminal	[W]
Q_{Ld}	reactive power magnitude at load terminal	[VAr]
S_{Tr}	apparent power magnitude of transformer	[VA]
P_{Tr}	active power magnitude of transformer	[W]
\underline{S}_k''	short-circuit power	[VA]
S_k''	short-circuit power magnitude	[VA]

Voltage quantities

\underline{V}	voltage phasor	[V]
V	voltage phasor magnitude	[V]
\underline{V}_0	initial voltage phasor	[V]
V_0	initial voltage phasor magnitude	[V]
\bar{V}_0	voltage phasor magnitude average	[V]
ΔV	voltage deviation from pre-fault value	[V]

V_{DB}	voltage deadband for fast voltage control	[p.u.]
ΔV_{Flt}	voltage support phasor during fault	[p.u.]
ΔV_{Flt}	voltage support phasor magnitude during fault	[p.u.]
$\Delta V_{Flt,max}$	maximum voltage support during fault	[p.u.]
\underline{V}_G	voltage phasor of grid Thevenin equivalent	[V]
V_G	voltage phasor magnitude of grid Thevenin equivalent	[V]
\underline{V}_{TS}	transmission system voltage phasor = Voltage phasor including retained voltage during fault	[V]
V_{TS}	transmission system voltage phasor magnitude = Voltage phasor magnitude including retained voltage during fault	[V]
\underline{V}_{ST}	sub-transmission system voltage phasor = Voltage phasor including retained voltage during fault	[V]
V_{ST}	sub-transmission system voltage phasor magnitude = Voltage phasor magnitude including retained voltage during fault	[V]
\underline{V}_{DS}	distribution system voltage phasor = Voltage phasor at PCC	[V]
V_{DS}	distribution system voltage phasor magnitude = Voltage phasor magnitude at PCC	[V]
\underline{V}_{WTG}	voltage phasor at WTG terminals	[V]
V_{WTG}	voltage phasor magnitude at WTG terminals	[V]
\underline{V}_{DG}	voltage phasor at DG terminal (PCC)	[V]
V_{DG}	voltage phasor magnitude at DG terminal (PCC)	[V]
\underline{V}_{Flt}	voltage phasor at DG terminal (PCC) during fault	[V]
V_{Flt}	voltage phasor magnitude at DG terminal (PCC) during fault	[V]
V_b	d-axis current control DC base voltage	[kV]

Current quantities

\underline{I}	current phasor	[A]
I	current phasor magnitude	[A]
\underline{I}_G	current phasor of grid Thevenin equivalent	[A]
I_G	current phasor magnitude of grid Thevenin equivalent	[A]
\underline{I}_{TS}	transmission current voltage phasor = current phasor including retained voltage during fault	[A]
I_{TS}	transmission system current phasor magnitude = Current phasor magnitude including retained voltage during fault	[A]
\underline{I}_{DS}	distribution system current phasor = Current phasor at PCC	[A]
I_{DS}	distribution system current phasor magnitude = Current phasor magnitude at PCC	[A]
\underline{I}_{WP}	current phasor at WPPM point of common coupling	[A]
I_{WP}	current phasor magnitude at WPPM point of common coupling	[A]
\underline{I}_{WTG}	current phasor at WTG terminals	[A]
I_{WTG}	current phasor magnitude at WTG terminals	[A]
\underline{I}_{Flt}	current phasor at DG terminal (PCC) during fault	[A]
I_{Flt}	current phasor magnitude at DG terminal (PCC) during fault	[A]
$I_{Tr,r}$	transformer rated current magnitude	[A]
\underline{I}_d	direct-axis current phasor magnitude	[A]
\underline{I}_q	quadrature-axis current phasor magnitude	[A]
\bar{I}_0	total current phasor magnitude pre-fault average	[A]
$\bar{I}_{d,0}$	direct-axis current phasor magnitude pre-fault average	[A]
$\bar{I}_{q,0}$	quadrature-axis current phasor magnitude pre-fault average	[A]
$I_{d,Flt}$	direct-axis current phasor magnitude during fault mode	[A]
$I_{q,Flt}$	quadrature-axis current phasor magnitude during fault mode	[A]
ΔI	additional current injection during fault mode	[A]

I_{DG}	current phasor at DG terminal (PCC)	[A]
\underline{I}_{DG}	current phasor magnitude at DG terminal (PCC)	[A]
I_{base}	base current to which all PI controller parameters are tuned	[A]

Angle quantities

φ	current phase angle	[deg]
ϕ	voltage angle with reference to reference generator	[deg]
ϕ_0	initial voltage angle with reference to reference generator	[deg]
ϕ_G	voltage angle of grid Thevenin equivalent	[deg]
ϕ_{TS}	transmission system voltage angle	[deg]
ϕ_{ST}	sub-transmission system voltage angle	[deg]
ϕ_{DS}	distribution system voltage angle = voltage phase angle at PCC	[deg]
ϕ_{WTG}	voltage angle at WTG terminals	[deg]
ϕ_{WP}	voltage angle at PCC of WPPM with reference to the reference generator	[deg]
δ_i	internal rotor angle of SG with reference to the reference generator	[deg]
δ_{CC}	critical clearing angle of SG in transient stability studies	[deg]
ψ_G	network impedance angle, $\psi_G = \arctan(X/R)$	[deg]
$\Delta\phi_{max}$	maximum voltage angle deviation	[deg]
ψ_{aRACI}	angle for aRACI	[deg]
ϕ_G	angle aligned to voltage at DG terminals	[deg]
$\Delta\delta_m$	mechanical rotor angle	[deg]
$\Delta\delta_e$	electrical rotor angle	[deg]

Frequency quantities

f	system frequency	[p.u.]
ω	angular frequency	[p.u.]

ω_n	nominal angular frequency	[p.u.]
ΔF_{\max}	maximum system frequency deviation	[Hz]
$\Delta \delta_{t,\max}$	maximum rotor angle deviation	[deg]

Impedance quantities

\underline{Z}	complex impedance	$[\Omega]$
Z	impedance magnitude	$[\Omega]$
R	complex impedance, real part (resistance)	$[\Omega]$
X	complex impedance, imaginary part (inductance)	$[\Omega]$
\underline{Z}_G	network or grid impedance	$[\Omega]$
\underline{Z}_{DS}	distribution system equivalent impedance	$[\Omega]$
\underline{Z}_{ST}	sub-transmission system equivalent impedance	$[\Omega]$
\underline{Z}_{TS}	transmission system equivalent impedance	$[\Omega]$
\underline{Z}_{WPPM}	impedance of WPPM connection line	$[\Omega]$
\underline{Z}_{DG}	impedance of DG connection line	$[\Omega]$
\underline{Z}_{Flt}	impedance of network fault	$[\Omega]$
Z_{Flt}	impedance magnitude of network fault	$[\Omega]$
\underline{Z}_{PCC}	equivalent shunt impedance at PCC	$[\Omega]$
x_m	magnetising reactance at P_{base}	[p.u.]
X	coupling reactance	[%]
r_2	negative sequence resistance	[p.u.]
x_2	negative sequence reactance	[p.u.]
X_d	direct axis synchronous reactance	[p.u.]
X'_d	direct axis transient reactance	[p.u.]
X''_d	direct axis subtransient reactance	[p.u.]
X_q	quadrature axis synchronous reactance	[p.u.]
X''_q	quadrature axis subtransient reactance	[p.u.]
r_S	stator resistance	[p.u.]
x_S	stator reactance	[p.u.]

x_m	magnetising reactance	[p.u.]
r_R	rotor resistance	[p.u.]
x_R	rotor reactance	[p.u.]

Controller gain quantities

k_p	active power control gain	[p.u.]
k_q	reactive power control gain	[p.u.]
$FRT_{CI,k}$	short-circuit current gain	[p.u.]
k_{RCI}	reactive current gain (positive sequence)	[p.u.]
k_{RACI}	reactive/active current gain (positive sequence)	[p.u.]
G	gain of lead lag block in DC voltage PI control	[-]
K	1 st order filter gain for aACI only	[p.u.]
K_1	1 st order filter gain for aRCI only	[p.u.]
K_a	controller gain	[p.u.]
K_{ac}	ac voltage controller gain	[-]
K_{aRCI}	gain for aRCI	[p.u.]
K_c	rectifier regulation constant	[p.u.]
K_d	exciter armature reaction factor	[p.u.]
K_{dc}	dc voltage controller gain	[-]
K_e	exciter constant	[p.u.]
K_f	stabilisation path gain	[p.u.]
$K_{i,d}$	gain for aACI	[p.u.]
$K_{q,ac}$	reactive power controller gain	[-]
$K_{\Delta V}$	reactive support gain	[-]

Time quantities and controller time constants

t'	time, absolute value	[s]
t	time, normalised value	[p.u.]
T_{aP}	acceleration time constant on active power base	[s]

T_{aS}	acceleration time constant on apparent power base	[s]
H_P	inertia time constant on active power base	[s]
H_S	inertia time constant on apparent power base	[s]
T_p	active power control time constant	[s]
T_q	reactive power control time constant	[s]
$T_{FRT_i_d_v}$	voltage dependent active current reduction control time constant	[s]
T_{FRT_detect}	time to detect a fault: voltage support delay	[s]
$T_{FRT_CI_CONT}$	voltage support continuation period after fault for $i_{FRT_CI_CONT} = 1$	[s]
T_{back_delay}	voltage support continuation period after fault	[s]
T_{FIDVR}	time constant for FIDVR	[s]
T_q	reactive power control time constant	[s]
T_{q_RCI}	reactive current control rise time	[s]
T	1 st order filter time constant for aACI only	[s]
T_1	1 st order filter time constant for aRCI only	[s]
T_a	controller time constant	[s]
T_{ac}	ac voltage controller time constant	[s]
T_b	filter time delay	[s]
T_c	filter derivative time constant	[s]
T'_d	direct axis transient time constant	[s]
T''_d	direct axis subtransient time constant	[s]
T_{dc}	dc voltage controller time constant	[s]
T_{drop}	only in nLVRT mode: resynchronisation time constant	[s]
T_e	exciter time constant	[s]
T_f	stabilization path delay time	[s]
T_{f_ac}	ac voltage filter time constant	[s]
$T_{q_f_ac1}$	(directly controlled) q-axis current filter time constant	[s]
T_{f_dc}	dc voltage filter time constant	[s]

T_{I_d}	dc voltage controller time lead constant	[s]
T_{I_g}	dc voltage controller time lag constant	[s]
T_p	active power control time constant	[s]
T_q	reactive power control time constant	[s]
T_q''	quadrature axis subtransient time constant	[s]
T_{q_ac}	reactive power controller time constant	[s]
$T_{q_f_ac}$	reactive power filter time constant	[s]
T_r	measurement delay	[s]
T_{relay}	delay time for relay disconnection for nLVRT	[s]
T_{sr}	delay time for returning to normal operating mode after fault	[s]
T_{u_delay}	voltage support delay	[s]

Error values

F_1	validation error for average value in (quasi-) stationary period	[-]
F_2	validation error for average value in transient period	[-]
F_3	validation maximum instantaneous error for positive or negative sequence values in a (quasi-) stationary period	[-]
F_G	overall validation error	[-]
$F_{P,period}$	Weighted validation error in case period contains multiple sub-periods	[-]

Controller flags

$i_{FRT_CL_DB}$	0 = TC curve; 1 = SDL curve	[0/1]
i_{EEG}	aRCI mode	[-]
$i_{FRT_CL_MOD}$	current injection during fault: 0 = total (TC mode); 1 = additional to pre-fault value (SDL mode)	[0/1]

$i_{\text{FRT_CL_PRIO}}$	current priority given to 0 = id; 1 = iq (TC & SDL mode); other = equal (RACI mode)	[0/1/2]
$i_{\text{FRT_CL_PRIO_MOD}}$	Current priority mode: 1 = arithmetic (abs); 2 = geometric (sqrt); other = set other value to zero	[0/1/2]
$i_{\text{FRT_CL_STAB}}$	stability improvement during fault by voltage dependent id reduction: 0 = no; 1 = yes	[0/1]
$i_{\text{FRT_CL_ANG}}$	current angle (a)RACI, best set equal to $\varphi = \angle(\underline{Z}_G)$	[deg]
$i_{\text{FRT_CL_CONT}}$	current injection continuation after fault for $T_{\text{FRT_CL_CONT}}$ seconds: 0 = no; 1 = yes	[0/1]
$i_{\text{FRT_CL_dAPR}}$	delayed active power recovery after fault for $FRT_{\text{dAPR_ramp}}$: 0 = no; 1 = yes	[0/1]
$i_{\text{FRT_Mode}}$	PV fault control mode	[-]
$i_{\text{Q_Mode}}$	Reactive current mode	[-]

Controller limit quantities

E_1	saturation factor 1	[p.u.]
E_2	saturation factor 3	[p.u.]
S_{e_1}	saturation factor 2	[p.u.]
S_{e_2}	saturation factor 4	[p.u.]
$\Delta V_{\text{FRT_DB_FAULT}}$	voltage deadband for fault detection (hysteresis low)	[p.u.]
$\Delta V_{\text{FRT_DB_CLEAR}}$	voltage deadband for fault clearance (hysteresis high)	[p.u.]
$P_{\text{FRT_dAPR_ramp}}$	active power ramp after fault is cleared	[%/s]
$I_{\text{max}}, I_{\text{min}}$	combined current limits during fast voltage control	[p.u.]
$i_{\text{d_max}}$	I_{d} current limit during fast voltage control	[p.u.]
$i_{\text{q_max}}$	I_{q} current limit during fast voltage control	[p.u.]
u_{max}	maximum allowed internal voltage	[p.u.]
$V_{\text{r_max}}$	controller maximum output	[p.u.]
$V_{\text{r_min}}$	controller minimum output	[p.u.]
$i_{\text{PV_max}}$	PVPPM maximum current output	[-]

i_{PV,q_max}	PVPPM maximum current output	[-]
F_{max}	Scaling factor for current limitation during fault control mode	[-]

Load model parameters

a_P	coefficient a_P for voltage dependence of P	[-]
a_Q	coefficient a_Q for voltage dependence of Q	[-]
e_{aP}	exponent e_{aP} for voltage dependence of P	[-]
e_{aQ}	exponent e_{aQ} for voltage dependence of Q	[-]

Mechanical quantities

n_s	synchronous speed	[r/min]
n_R	rotor speed	[r/min]
s	slip speed of the rotor on synchronous speed n_s base	[p.u.]
τ_m	mechanical torque	[p.u.]
τ_e	electromagnetic torque	[p.u.]
$\tau_{m,s=0}$	torque at synchronous speed	[p.u.]
$\tau_{m,s=1}$	torque at standstill	[p.u.]
$\tau_{m,min}$	minimum torque	[p.u.]
$s\tau_{m,min}$	slip at minimum torque	[p.u.]
$\tau_{m,1}$	torque of 1 st polynomial torque function	[p.u.]
$\tau_{m,2}$	torque of 2 nd polynomial torque function	[p.u.]
$e_{\tau_{m,1}}$	exponent of 1 st polynomial torque function	[-]
$e_{\tau_{m,2}}$	exponent of 2 nd polynomial torque function	[-]

Other quantities

ρ_{DGr}	rated DG penetration	[%]
ρ_{DGi}	actual DG penetration	[%]
SCR_{PCC}	short-circuit ratio at PCC	[-]

γ_{Ld}	ratio between minimum and maximum load	[-]
$\eta_{Tr/Ld}$	transformer overrating factor for load supply	[-]
$\cos(\varphi)_{Ld}$	power factor of load	[-]
$\cos(\varphi)_{DG,r}$	rated power factor of any DG	[-]
$\langle \cos(\varphi)_{DS} \rangle$	mean power factor of any system level	[-]
$\xi_{DG,i}$	split of any rated DG power installed at different voltage levels i , i.e. $\sum_i \xi_{DG,i} = 1$	[-]

Contents

Summary	v
Samenvatting	ix
Nomenclature	xv
1 Introduction	1
1.1 Background	1
1.2 Impact of DG on Power System Stability	2
1.2.1 Definition and classification of power system stability	2
1.2.2 Influencing factors	3
1.3 Problem Definition	4
1.4 Objective and Research Questions	6
1.5 Research Approach	7
1.5.1 Time domain simulations	7
1.5.2 Analytical description	8
1.5.3 Sensitivity analysis	8
1.5.4 Presentation of results	8
1.6 Outline of the Thesis	9
2 State of the Art & Discussion	11
2.1 Introduction	11
2.2 Impact of DG on Power System Stability	12
2.2.1 Impact on frequency stability	12
2.2.2 Impact on large disturbance voltage stability	13
2.2.3 Impact on transient stability	16
2.2.4 Summary of impact on power system stability	23
2.3 Network Fault Response Requirements for DG	25
2.3.1 Grid codes	25
2.3.2 Evolution	25
2.3.3 Quasi-stationary voltage control and dynamic reactive support	26
2.3.4 Disturbance voltage support	27
2.3.5 Summary of network fault response requirements for DG	30
2.4 Discussion of effectiveness of voltage support	31
2.5 Conclusions	38

3	Modelling of System Elements	39
3.1	Introduction	39
3.2	Distributed generation (DG) models	40
3.2.1	Wind power generating facilities	41
3.2.2	Photovoltaic power generating facilities	44
3.2.3	Micro-CHP generating facilities	48
3.3	Load models	48
3.4	Aggregation and Equivalencing of DG	49
3.4.1	State of the Art	49
3.4.2	Limitations of existing approaches	50
3.5	Proposed Methodology	50
3.5.1	Overview	50
3.5.2	Inputs and assumptions	51
3.5.3	Definition of detailed active distribution system models	53
3.5.4	Definition of equivalent active distribution system model	54
3.5.5	Validation method	56
3.6	Results and Validation	58
3.6.1	Case study	58
3.6.2	Study cases	61
3.6.3	Dynamic equivalents	61
3.6.4	Simulation results	62
3.6.5	Discussion	65
3.7	Conclusions	66
4	Network Fault Response during Reverse Power Flow Situations	67
4.1	Introduction	67
4.2	Challenges under Reverse Power Flow Situations	68
4.3	Methodology	68
4.3.1	Test system definition	69
4.3.2	Sensitivity analysis for system impact of LVRT modes	72
4.3.3	System performance criteria	75
4.4	System impact with LVRT and ‘blocking mode’	75
4.4.1	Impact of loads	75
4.4.2	Impact of PCC and transformer tap changer positions	79
4.4.3	Impact of pre-fault reactive power exchange	81
4.5	System impact with LVRT and fast voltage control	83
4.5.1	Impact with state-of-the-art requirements and $k_{RCI} = 6$ p.u.	83
4.5.2	Impact with state-of-the-art requirements and $k_{RCI} = 0$ p.u.	85
4.5.3	Impact with new robust control mode	88
4.6	Impedance adjusted control mode	92
4.6.1	Switching between operating modes during fault period	93
4.6.2	Impedance magnitude adjusted control mode	94
4.6.3	Impedance angle adjusted control mode	96
4.7	Conclusions	102

5	Network Fault Response Requirements for LV Connected DG	105
5.1	Introduction	105
5.2	Stability Simulation on a HV-MV-LV Power System	106
5.2.1	Test system overview	107
5.2.2	Test system DG penetration	108
5.2.3	Integration of ADSs into the transmission system	109
5.2.4	DG modelling	110
5.2.5	Load modelling	111
5.3	Study Cases	112
5.3.1	Operational Scenarios	112
5.3.2	Low Voltage Photovoltaic Systems Control Modes	114
5.4	Results	115
5.4.1	Case 1: year 2022 and OS2	115
5.4.2	Case 2: year 2022 and OS3	118
5.4.3	Discussion	120
5.5	Proposed Network Fault Response Requirements	122
5.6	Implications	122
5.6.1	Photovoltaic power generating facilities	122
5.6.2	Micro-CHP generating facilities	123
5.6.3	Distribution network protection	124
5.7	Conclusions	127
6	Conclusions and Future Research	129
6.1	Conclusions	129
6.1.1	Answers to research questions	129
6.1.2	Scientific Contributions	134
6.2	Recommendations for Future Research	135
A	Definitions and classifications	139
A.1	Power system transformation	139
A.2	Distributed generation	140
A.3	Active distribution systems	142
A.4	Definition and classification of power system stability	142
A.5	Network fault response	143
A.6	DG penetration levels	143
A.7	Current angle stability	145
A.8	DG grid connection interfaces	146
A.9	DG location	146
A.10	Grid connection requirements	147
A.11	Ancillary services	150
A.12	The ‘strength’ of a power system	152
A.13	Fault-induced delayed voltage recovery	153
A.14	Voltage funnel	155
B	Test system data	157
B.1	Simple test system for chapter 4	158
B.2	IEEE New England test system for chapter 5	160

C	DG modelling and control	163
C.1	Network fault controls	163
C.1.1	Voltage dependent direct-axis current reduction	163
C.1.2	Additional Reactive Current Injection	164
C.1.3	Additional Reactive & Active Current Injection	165
C.2	Wind power park modules	167
C.2.1	Type 3: Doubly fed asynchronous generator (DFAG)	167
C.2.2	Type 4: Full converter interface units (FC)	168
C.3	Photovoltaic power park modules	171
C.4	Combined heat and power plants	174
D	Load modelling	177
D.1	Exponential load model	177
D.2	Detailed induction motor load model	178
E	Active Distribution Systems for chapter 5	179
E.1	Statistical Analysis of German Grid Data	179
E.1.1	Typical DG Installation Size	180
E.1.2	Typical DG penetration	181
E.2	DG legacy performance analysis	185
E.2.1	Evolution of German grid connection requirements	185
E.2.2	Pre-2012 Installation Capabilities	190
E.3	Distribution Network expansions	192
E.3.1	Network Planning Criteria	192
E.3.2	Actual expansions	195
E.4	Equivalent Models	200
E.4.1	Low Voltage Distribution	200
E.4.2	Medium Voltage Distribution	205
E.4.3	Sub-transmission System: Ring Network	211
E.5	Network Data	215
E.5.1	Low Voltage Network Data	215
E.5.2	Medium Voltage Network Data	216
E.5.3	High Voltage Network Data	217
F	Additional results	219
F.1	Additional simulation results for chapter 4	219
F.1.1	Impact with state-of-the-art requirements and $k_{RCI} = 6$ p.u.	219
F.1.2	Impedance angle adjusted control mode	220
F.2	Operational scenarios for chapter 5	223
F.2.1	Generation and Load	223
F.2.2	Power Flows	224
	References	227
	List of Publications	245
	Acknowledgements	247
	Curriculum Vitae	249

Chapter 1

Introduction

This chapter presents the background and motivation for the research presented in this thesis. Relevant terms that will be used throughout the thesis are introduced. Definitions are collected in appendix A and referred to in a superscript when the term is used for the first time in the text. The problem of network fault response and stability of transmission and distribution systems with high penetration of distributed generation is defined, the objective is formulated, and related research questions are presented. The research approach is explained in detail and an outline of the thesis is given.

1.1 Background

Electrical power systems are being transformed: renewable power generating facilities, excluding large hydro power plants, accounted for 48 % of new generation capacity added worldwide in 2014 [Fra15]. In Europe, the drivers for this sustained change are among others: policies to reduce emissions of greenhouse gases that cause climate change [Eur09b], efforts to decrease the dependency on fuel imports and to maintain the security of supply in the long-term [Eur09a], and the liberalisation of the electricity sector, including the formation of electricity markets [Eur09c]. Some authors even notice a public movement towards a ‘democratisation’ of power generation [Fec10].

Consequently, power systems are nowadays undergoing an unprecedented *structural* and *technological* transformation^{A.1}. The increase of distributed generation (DG)^{A.2}, primarily wind power park modules (WPPMs) and photovoltaic power park modules (PVPPMs), is already changing the way power systems are structured and operated. Power systems are being transformed from vertically-designed systems with unidirectional transmission-to-distribution power flows to horizontally-designed systems with bidirectional power flows between all voltage levels. Distribution systems are turning from ‘passive’ into ‘active’ distribution systems (ADS)^{A.3}. Conventional (thermal) power plants with synchronous generators are being replaced by power park modules that are connected to the network non-synchronously and/or via power electronic converters.

In Germany, the transformation has been accelerated by the Federal Government proclaiming their *Energiewende* project (i.e., phase-out of nuclear power until the year 2022 [Deu09]), following the nuclear disaster at the Japanese Fukushima Dai-ichi nuclear power plant on 11 March 2011 [Str11]. While the German term ‘Energiewende’ is establishing itself as a global leitmotif, it is of particular interest to this thesis that the transformation of the German power system is heavily leaning on a massive, decentralised deployment of distributed generation, such as distribution system (DS) connected, medium-size wind farms and micro- to small-scale photovoltaic systems.

This thesis will help the reader to better understand the stability^{A.4} of sustainable power systems. The research focuses on the network fault response^{A.5} of transmission systems with very high penetration^{A.6} of distributed generation.

1.2 Impact of DG on Power System Stability

The *structural* transformation influences the network fault response, for example, because DG are connected ‘deep’ into the distribution system at a high impedance network. Consequently, DG are less exposed to faults at transmission system level but also contribute less to the subtransient short-circuit power (S_k'') of the transmission system. The *technological* transformation influences the network fault response, for example, because the reaction of DG connected to the network via power electronic converters to sudden changes of their terminal voltage is determined to a large extent by their control systems, chosen parameter settings and rating.

1.2.1 Definition and classification of power system stability

In this thesis, power system stability is understood in line with the definition given in [IEE04] as

the ability of an electric power system, for a given initial operating condition, to regain a state of operating equilibrium after being subjected to a physical disturbance, with most system variables bounded so that practically the entire system remains intact.

From a physical viewpoint, ‘stability’ is a condition of equilibrium between opposing forces [IEE04]. When these opposing forces experience sustained imbalance, this leads to different forms of *instability*.

The network topology, system operating condition, and the form of disturbance determine *which* sets of opposing forces may experience sustained imbalance. In order to better understand and effectively mitigate certain forms of instability, it is useful to differentiate between various classes of power system (in)stability, rather than studying them as a single problem. Figure 1.1 shows the different classes of power system stability as proposed by [IEE04]. From these, the three stability classes which are of particular interest for this research are:

- Transient stability (of synchronous generators in conventional power plants with an interconnected transmission system);
- large disturbance voltage stability; and

- frequency stability (resulting from the above).

The classification from [IEE04] may have some shortcomings when it comes to the introduction of power park module (PPM) based distributed generation. For example, the network fault response is a problem of the transient stability class for synchronous generators, whereas it may be classified a problem of the large disturbance voltage stability class for distributed power park modules. Furthermore, the concept of ‘current angle stability’^{A.7} is primarily a question of adequate current control of inverter-based DG. Nevertheless this stability class is important for this research.

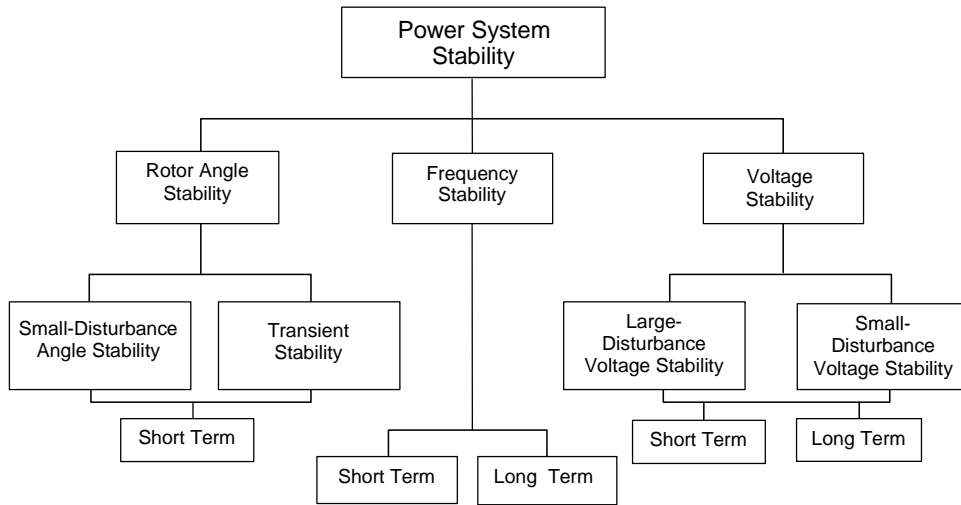


Figure 1.1: Classification of power system stability [IEE04]

1.2.2 Influencing factors

The impact of DG on power system stability is ambiguous and one cannot label it as ‘negative’ or ‘positive’ without further specification and discussion of the case study assumptions. The integration of large amounts of DG into distribution systems has been found in [Ant08] not to show significant ‘global’ stability problems, except for the disconnection of large amounts of DG during transmission faults, unless prevented by low voltage ride-through (LVRT). But transient and frequency stability were regarded by [MF10] as two major stability issues related to high DG penetration levels. On closer inspection, however, previous studies have shown that the impact of DG on power system stability depends primarily on these five characteristics of DG:

- Technology & grid connection interface^{A.8}.
- Penetration & operating point.
- Location (vertical & horizontal)^{A.9}.
- Protection & parameter settings.
- Control & parameter settings.

1.3 Problem Definition

This thesis investigates the network fault response of integrated transmission and distribution systems with very high penetration of distributed renewable and conventional generation. Network fault response is the dynamic response of the whole or of parts of the power system during and shortly following sudden faults in the network. The response is calculated in terms of changes in system variables over a time frame of interest, such as bus voltage magnitudes and angles, generator rotor angles, and fundamental system frequency. In other words, the impacts of DG on transient stability, large disturbance voltage stability, and frequency stability are analysed in this thesis. Network faults can be short-circuits on a line or a substation busbar. The analysis focuses on symmetrical, three-phase transmission network faults. Other classes of power system stability problems and unbalanced faults are not in the scope of this thesis.

The impact of DG on the aforementioned power system stability classes has been investigated in the literature extensively. It was found that this impact is influenced by five factors, i.e. (1) the technology and grid connection interface, (2) the penetration & operating point, (3) the location (vertical & horizontal), (4) the protection & parameter settings, and (5) the control & parameter settings of distributed generation. While the former three variables cannot or should not be influenced by the grid operator acting in a deregulated environment, stipulations about the protection and control with their respective parameter settings are defined in grid connection requirements (GCRs)^{A.10}. The GCRs form the technical basis for current and future ancillary services (ASs)^{A.11} that active distribution systems may provide to the system.

The massive insertion of DG into DSs leads to new challenges like the regular occurrence of reverse power flow (RPF) situations from the distribution to transmission level, the potential increase of the inductive reactive power demand when DG control their terminal voltage, and local stability problems with the connection of DG to ‘weak’^{A.12} points of common coupling (PCCs). Furthermore, with DG being located very close to the loads, it is more likely to be exposed to fault-induced delayed voltage recovery (FIDVR)^{A.13} events than transmission and sub-transmission connected generating facilities. This leads to the identification of the following *shortcomings in the state of the art*:

—Current modelling approaches to study the impact of DG on transient stability, large disturbance voltage stability, and frequency stability fall short with very high penetration of DG.— GCRs were originally studied and specified in simple system configurations where either the transmission or the distribution system level was highly simplified. In these studies, the accuracy of the integrated power system model may be significantly reduced, especially for the periphery region (‘annulus’) of a voltage funnel^{A.14} in which the retained voltage is very close to the undervoltage protection threshold of DG that do not have low voltage ride-through capability. These studies also have, so far, neglected the interaction of transmission and distribution systems with large amounts of DG with advanced control features, such as dynamic voltage support.

— Hence, grid connection requirements (GCRs) currently in force have undergone insufficient technical impact assessment for systems with reverse power flow situations and ‘weak’ points of common coupling (PCCs).— The existing GCRs for DG have been developed under the implicit assumption of a ‘strong’ transmission system and exclusively exporting power flow from active distribution systems with DG. The need for stability analysis and specification of GCRs for DG connected to ‘weak’ power systems was identified in [Ant08, MF10]. Such power systems are characterised by a low short-circuit ratio at the point of common coupling and with potentially low inertia. Furthermore, if the analysis of GCRs did not consider the characteristics of all devices connected to an active distribution system, including its loads, adverse effects on power system stability from the dynamic interactions between the transmission and distribution system levels would remain undetected. For example, if dynamic voltage support from DG were only required during the fault period, the voltage support that it can provide in the post-fault period to mitigate FIDVR would be left unexploited. Other issues that warrant investigation and quantification are reverse power flow situations and the influence of R/X ratio of the DS on the effectiveness of dynamic voltage support.

—Furthermore, the actual implementation of these grid connection requirements by distribution system operators (DSOs) for DG connected at medium voltage level can have undesired consequences for system stability under certain conditions.— Modern control systems of DG allow for a variety of possible responses to network faults. While this can be beneficial for power system stability, such freedom brings up the new challenge to choose adequate controls and their parameters. In previous works, the research objective was to determine which response of DG to network faults is *possible at plant level*. In this thesis, the main question will be which response is actually *desirable from a system perspective* to maintain power system stability. If current DSO practices continue and dynamic voltage support remains deactivated for the majority of medium voltage (MV) connected DG (as is the case in Germany), the likelihood of prolonged LVRT operation caused by FIDVR may increase. Hence, significant benefits of DG controllability for power system stability would be left unexploited.

—After all, state of the art requirements regarding network fault response of DG have so far been implemented insufficiently at low voltage (LV) levels.— LV connected DG, such as roof-top photovoltaic systems, has gained significance in recent years. Yet these units are currently not required to ride through voltage dips. The need for investigations of LVRT and related requirements for LV connected DG have been identified worldwide [Geo09, IEE13, For12]. Draft requirements have been proposed in [CEN15b] for Europe and [JEA13, Kob12] for Japan. If network fault response related GCRs for LV connected DG units are not changed, these units may become a risk for power system stability.

Ultimately, analysis of the identified problems is crucial and will help avoid expensive retrofitting actions similar to the ones taken to prevent massive disconnection of PVPPMs in Germany and other member states in the Continental Europe (CE) region due to unfavourable frequency protection settings [BBZ⁺11, EE14].

1.4 Objective and Research Questions

Ensuing from the previously given problem definition, the **overall objective** of this thesis is:

To critically review current and proposed grid connection requirements with regard to the network fault response of transmission systems with very high penetration of distributed generation, and to propose changes to the specifications where needed.

Requirements to be considered are fault ride-through, post-fault active power recovery, and fast voltage control (i.e. additional reactive and/or active current injection).

Subordinate objectives can be described that are intermediate steps in the research to reach the overall objective. These subordinate objectives and a number of related research questions that can be derived are presented in the following paragraphs.

Subobjective 1: *To develop a technique to derive sufficiently accurate dynamic equivalent stability models for active distribution systems (ADSs) that allow for the analysis of the stability of evolving sustainable power systems in a system-wide, accurate, and computational-efficient way in order to study dynamic interactions between the transmission and distribution system levels.*

1. What is the minimum level of detail that is necessary to accurately model ADSs in bulk power system stability studies with very high penetration of DERs? (chapters 3, 4, and 5)

Modelling aspects to evaluate here are whether sub-transmission and distribution system transformers' on load tap changer controllers and DG's quasi-stationary voltage controllers should be considered when initialising the integrated dynamic transmission and distribution system model? And how to adequately aggregate sub-transmission and distribution system impedances?

2. How can equivalent models of active distribution systems be validated? (chapter 3)

Subobjective 2: *To develop a comprehensive understanding of the challenges and the opportunities of very high penetration^{A.6} of distributed generation with regard to the network fault response of transmission and distribution systems.*

1. How does the 'effectiveness' of a 'full dynamic voltage support' depend on the DG penetration level and the network characteristics? (chapter 2)
2. How important are the load characteristics for the network fault response of DG? (chapter 4)
3. Would a combined additional reactive/active current injection (aRACI) be more effective for LV connected DG than a pure additional reactive current injection (aRCI)? (chapters 4 and 5)

4. How much in-feed from distributed generation connected at the LV distribution system level of a test system would a transmission network fault potentially trip in a hypothetical 2022 case study using input data specific for the German power system? (chapter 5)

Subobjective 3: *To justify and to specify future grid connection requirements per voltage level for distributed generation that have an impact on the network fault response of transmission systems and distribution systems.*

1. Should LV connected DG be capable of low voltage ride-through (LVRT)? (chapter 5)
2. What are the opportunities and challenges of a current injection by LV connected DG during faults? (chapter 5)
3. Which amendments to grid connection requirements for DG connected at low voltage (LV) and at medium voltage (MV) distribution system levels are recommended? (chapters 4 and 5)

When all three subordinate objectives have been reached, the overall objective will be reached and the following **research question** can be answered:

Which of the current and proposed grid connection requirements that have an impact on the network fault response of transmission systems are necessary from a system-wide stability perspective and what changes are needed, if any, to maintain the stability of a sustainable power system with very high penetration of distributed generation?

The conclusions should differentiate between the grid connection requirements for the low voltage (LV) and medium voltage (MV) levels and be valid for foreseeable power flow situations between these voltage levels.

1.5 Research Approach

The research approach that is taken to achieve the overall objective and find answers to the related research questions is a combination of time domain simulations (rms, positive sequence) and fundamental circuit analysis.

1.5.1 Time domain simulations

For the time domain simulations, assumptions are taken that permit tracking the dynamics in the rms values of selected circuit variables. The time frame of interest is related to short-term stability phenomena, i.e., one tenth of a second to tens of seconds. While transient stability falls into this time frame, frequency stability is usually related to the mid-term time frame (tens of seconds to minutes) and large disturbance voltage stability falls in both short- and mid-term time frames. Mid term phenomena and control actions such as change of transformer OLTC positions during the simulation time frame and conventional power plants' secondary frequency control actions, are not considered in this thesis. Automatic voltage regulators (AVRs), power system stabilisers (PSSs), governors for primary

frequency control of synchronous power generating modules (PGMs) as well as outer and inner control loops of distributed PPMs are modelled. For the modelling of the benchmark systems and the time domain simulations, the commercially available software DIgSILENT PowerFactory© v15.1 is used in rms (stability) mode.

1.5.2 Analytical description

Important results obtained from the time domain simulations are verified and explained analytically by use of quasi-stationary circuit theory and phasor diagrams showing the relationships between voltages, currents, and impedances based on Kirchhoff's current (KCL) and voltage (KVL) laws. The quasi-stationary approach is justified due to the very small time constants of the power electronic converters in power park modules in relation to the time frame of interest.

1.5.3 Sensitivity analysis

System and network values — In order to reach robust answers to the research questions, several sensitivity analyses are performed, both by use of time domain simulations (rms, positive sequence), as well as fundamental circuit analysis. The parameters to be adjusted in the sensitivity analysis are

- power flow cases, based on load and generation; values for the initial steady-state operating point;
- short-circuit power S_k'' at transmission & distribution system (TS/DS) interface;
- equivalent impedance between transmission and distribution system;
- load mix and load model coefficients;
- fault location in the transmission system.

Transmission network faults are always assumed to be symmetrical three-phase faults.

Protection, controls and their parameters — The network fault response of transmission and distribution systems with very high penetration of DG is investigated for protection settings that either allow or disallow low voltage ride-through (LVRT)^{A.10}, as well as a number of variants for DG control strategies and parameter settings, such as the quasi-stationary voltage control and the disturbance voltage support control mode^{A.10}.

1.5.4 Presentation of results

The results from the time domain simulations are presented in voltage magnitude vs. time (V-t) plots, voltage & rotor angle vs. time ($\arg(y)$ -t) plots, and active & reactive power vs. time (P-t/Q-t) plots.

The results from the fundamental circuit analysis are presented in phasor diagrams showing the relationships between voltages, currents, and impedances in the complex domain.

1.6 Outline of the Thesis

Chapter 2 — This chapter consists of two sections that summarise the state of the art. The first section reviews existing knowledge on the impact of distributed generation on power system stability. The impact on frequency stability, large-disturbance voltage stability, and transient stability is discussed separately. The second section describes the grid connection requirements related to network fault response of distributed generation. It presents the requirements for fault ride-through, additional current injection during fault, and active power recovery after fault. The third section discusses the effectiveness of dynamic voltage support based on fundamental circuit theory.

Chapter 3 — This chapter describes the power system element models used throughout the thesis. It reviews the state of the art and specifies model types, parameters and major assumptions taken. A comprehensive methodology of DG aggregation and dynamic equivalencing is proposed to derive highly accurate, equivalent dynamic models of ADSs. The contribution of this chapter is to define the minimum level of detail that is necessary to accurately model ADSs in bulk power system stability studies with very high penetration of DGs (i.e., more than approx. 50 % system-wide instantaneous penetration, regional reverse power flows from distribution to bulk system level).

Chapter 4 — This chapter contributes to the understanding of the stability of the power system with reverse power flow (RPF) situations. The system impact of the state-of-the-art DG network fault response requirements is studied by time domain simulations of an HV-MV benchmark system. The differences between the (sub-)transmission and distribution levels with regard to the impact of these requirements are discussed. The relevance of loads in active distribution systems and transformer tap-changers is then considered. The chapter concludes with the proposition of a new methodology that allows a distribution system operator (DSO) to choose the optimal parameters for an additional current injection during network fault control as a function of the network impedance at the point of common coupling (PCC) of a MV connected DG. Optimality is considered from a power system-wide stability viewpoint.

Chapter 5 — This chapter contributes to the (ongoing) discussion on network fault response requirements for distributed generation connected to low voltage networks. It investigates the network fault response of large amounts of LV connected distributed generation and its impact on post-fault active power balance following transmission system faults. Photovoltaic (PV) installations in low voltage networks are the focus of this chapter. A test system is constructed with DG penetration representative of a 2022 scenario for Germany. The test system comprises all voltage levels from LV to extra-high voltage (eHV), with the low and MV levels simplified by means of aggregation as described in chapter 3.

Chapter 6 — The final chapter summarises the main conclusions and scientific contributions from each of the previous chapters of the thesis. It identifies remaining knowledge gaps and gives recommendations for future research related to the stability of sustainable power systems.

Chapter 2

State of the Art & Discussion

This chapter describes the existing knowledge on the impact of distributed generation (DG) on power system stability, as well as the the grid connection requirements related to network fault response of distributed generation at the time of the writing of the thesis (state of the art). The impact on power system stability is discussed separately for the stability classes of frequency stability, large disturbance voltage stability, and transient stability. Grid connection requirements for fault ride-through, additional current injection during fault, and active power recovery after fault are then presented together with operating practices of distribution system operators (DSOs) that may be exceptions to these requirements. In the last part of the chapter, the effectiveness of dynamic voltage support with increasing penetration levels of DG is discussed by use of fundamental circuit theory.

2.1 Introduction

As long as the rated penetration of distributed generation was small^{A.6}, i.e. $\rho_{DG,r} < 20\%$, network planners and operators regarded DG as a ‘negative load’. The particular dynamical response of DG towards transmission network faults had an undetectable influence on the network fault response of distribution and transmission systems. It was mainly determined by the characteristic response of synchronous power generating modules (sPGM) and load behaviour.

The paradigm of the past was to disconnect DG as fast as possible in case the system went into an abnormal state. This paradigm led to very conservative settings of DG under-/overfrequency and under-/overvoltage protection relays. With DG rated penetration having reached significant levels, and with these levels likely to further increase to more than 400 % in some regions and voltage levels in Germany, a paradigm shift was needed. The paradigm intended to increase system stability, then turned into a reliability risk within less than a decade.

In the following section, the impact of DG on power system stability for medium to high rated penetration scenarios is presented. However, minimal analysis has been performed for very high penetration scenarios^{A.6}, i.e. $\rho_{DG,r} > 50\%$, including reverse power flows. It will be shown that the impact of DG on power system stability depends almost entirely on the protection and control systems with their respective parameter settings.

The control systems and their settings are primarily defined by grid connection requirements that have been stipulated by network operators in recent years. Grid connection requirements (GCRs) are the rules and regulations with which grid-connected components have to comply. These requirements are usually not compensated for in monetary terms. They provide a framework of compatibility and quality for the power system.

2.2 Impact of DG on Power System Stability

2.2.1 Impact on frequency stability

Frequency stability is understood in this thesis based on the definition given in [IEE04] as

the ability of a power system to maintain steady frequency following a severe system upset resulting in a significant imbalance between generation and load.

A ‘severe system upset’ could be the tripping of a large power generating facility or load due to an internal electrical fault but also the tripping of multiple loads or distributed generators, whose aggregated power would be considered ‘significant’, following a network fault in the transmission system. Significance is always specific to a given power system. It is important to note that for frequency stability the system-wide (global) power imbalance is the determining factor.

The impact of DG on frequency stability is mostly related to the reduction of the total inertia in the power system resulting from the technological transformation and is, therefore, highly dependent on the DG controls, their protection and the related parameter settings. Compared to large SG with high inertia, DG have either low inertia (e.g. small to medium size CHP facilities) or are connected to the network via power electronic converters that decouple the interaction of any rotating mechanical parts (if present) with the network (e.g. PVPPM and some WPPM). The latter makes these types of DG behave passively towards frequency changes and, as a result, the total system inertia is decreased and the rate of change of frequency (ROCOF) following system upsets is increased [LMO05, Muh06, Eco10]. Consequently, the risk that the system frequency leaves the acceptable frequency band becomes larger. The relationship between the ROCOF and DG penetration level is inversely proportional. The location of DG is less relevant for the impact on frequency stability.

Unfavourable frequency protection settings of DG can cause disconnection of massive amounts of DG following abnormal frequency excursions (common mode failure). This called for national regulatory authorities to request plant operators to re-adjust protection settings retrospectively [EE13a]. While such negative impact on frequency stability will be easy to avoid in future, it is a good example for the challenges related to combining the past and future in the context of the transformation of power systems.

Negative impact of DG on frequency stability that is related to the reduction of the total system inertia can be mitigated by implementation of adequate DG control systems and parameter settings. The provision of positive and negative reserve capacity by operating a WPPM in part load mode and dynamically controlling the pitch angle of the rotor blades was proposed, for example, in [EW10]. A supplementary control loop to provide an inertial response similar to a synchronous generator that was added to a wind turbine generator control system proved to be beneficial in [LMO05]; however, in case of type 3 (DFAG) and type 4 (full converter) WPPM the provision of inertia was considered limited by the

converter rating. A drawback of providing an inertial response by WTG is that the rotational speed of the wind turbine decreases and, therefore, the in-feed from the WTG will drop considerably when the frequency support is ended [MHKF06]. This can be prevented by an ‘inverse’ inertial response control mode, as proposed in [EW10], that means the WTG would accelerate first, and then decelerate by discharging energy during the phase of the disturbance in which the frequency is approaching its minimum.

In the context of this thesis, frequency stability is concerned with regard to the response of DG to transmission network faults. By all means, a common mode failure resulting into a permanent loss of large amounts of DG following those faults has to be avoided. Furthermore, the active power recovery in the short period after fault clearance is of importance [Wei13a, Wei15]. Given the very high penetrations of DG studied in this thesis and the related reduction in total system inertia, a deviation of the system frequency due to a post-fault power imbalance caused by too slow active power recovery should be avoided. The latter proved to be a key limiting factor for system non-synchronous penetration (SNSP) in the Irish All Island power system and it was expected that anticipation of new technological concepts, e.g. for ‘fast active power recovery after faults’, would allow for a relaxation of this limit [Eco10].

For the frequency stability studies performed in this thesis this means that the period shortly after a network fault has been cleared is of interest. Thus, in the terms of the definitions given in [IEE04], *short-term* frequency stability is considered. This allows for *neglecting long-term* phenomena related to slow processes such as conventional thermal power plant’s prime mover energy supply systems and boiler dynamics. The aerodynamic torque of wind turbine generators is also assumed to be constant although recent publications recommend otherwise when studying ‘weak’ power systems [For13]. The short-term phenomena considered relevant for the frequency stability studies in this thesis are the inertial response of synchronous generators, active power recovery of DG and frequency protection settings, including underfrequency load shedding. The time frame of interest extends to tens of seconds but not minutes.

2.2.2 Impact on large disturbance voltage stability

Large disturbance voltage stability is understood in this thesis based on the definition given in [IEE04] as

the system’s ability to maintain steady voltages following large disturbances such as system faults, loss of generation, or circuit contingencies.

Although voltage instability is regarded a local phenomenon—in contrast to frequency stability which is a global phenomenon—the consequences of voltage instability may have a widespread impact [Kun94]. This cause-and-effect chain becomes even more relevant for transmission systems with very high amounts of DG regarding their ability to maintain equilibrium between load demand and supply during reverse power flows (see section 4).

The ability of DG to ride through transmission faults (FRT capability) is assigned to the large disturbance voltage stability class in this thesis. Fault ride-through of DG is not considered a *transient stability* problem for distributed PPM in this thesis because of the special nature of power electronic converters. Although it *can be* a transient stability problem for DG with directly connected synchronous generators, e.g. distributed combined heat and power (CHP) generating facilities, the impact of FRT of the latter will still be discussed

in the present section on large disturbance voltage stability because of the similar effect on the voltages in the fault and post-fault period.

Impact of distributed synchronous power generating modules

Stability studies performed in [SK02b] had found a large voltage drop at some nodes in the transmission system following a transmission fault due to the disconnection of DG units that were not able to perform LVRT. However, a study focussing on distributed CHP generating facilities has shown for a Dutch benchmark network and a particular case [Cos10] with DG instantaneous penetration level resulting in a (local) reversal of the power flow over the HV/MV substation pre-fault, that disconnection of a significant part of these DG units would *not* cause the voltage to fall below the allowable lower voltage limit. While the disconnection of DG units led to an additional reversal of the power flow over the substation post-fault, i.e. from export back to import of active power by the distribution system, the resulting voltage drop was such that it could still be corrected by the tap changers of the HV/MV transformers [Cos10]. This finding, of course, would have to be revisited if the DG penetration level were increased substantially. This will be shown, among others, in the case study in chapter 5.

The same study [Cos10], however, found that the particular distribution system with numerous CHP generating facilities that *were* able to perform LVRT interacted strongly with the (sub-)transmission system in terms of active power swings and the consumption of reactive power in the post-fault period which caused a delayed voltage recovery; the latter effectively caused the LVRT-able DG units to disconnect in the post-fault period. As a mitigation measure, the application of a static synchronous compensator (STATCOM) in the distribution system was proposed to improve the voltage recovery. STATCOM was also found to support the voltage during the fault significantly and, therefore, improve the (transient) stability of DG with a directly coupled synchronous generator, too. The study also confirmed that the distributed synchronous PGM were able to support the voltage during a voltage dip. [Cos10]

From above findings one can conclude that the impact of DG with directly connected SG on large disturbance voltage stability will depend on the DG penetration level as well as the location of DG inside the power system in relation to the respective network fault.

Impact of distributed power park modules

Power park modules can also support the voltage during a voltage dip, as they have similar characteristics to a STATCOM, by adding a reactive current component to their pre-fault reactive current injection in proportion to the voltage dip depth at their terminal [BEW06]. This ability is limited by the PEC rating of the respective PPM and can be increased by giving the reactive current component priority over the active current component.

In a strong network the impact of voltage support from PPM on the network voltage is only marginal [ESE⁺09]. Moreover, the impact of reactive current injection on the network voltage for close-up faults with a retained voltage below 0.1 p.u. was found to be negligible [EE13d]. However, for DG connected to ‘modest’ and ‘weak’ networks and, hence, a short-circuit ratio at the PCC of less than 10 (see table A.5 in section A.12), the effect of voltage support can be substantial [MPR⁺11].

For the power system of Continental Europe (CE) simulations have shown that voltage support from WPPM reduces the risk of widespread simultaneous disconnection of wind

power in the event of a transmission system fault and, therefore, allows for integrating more wind power than otherwise [EE10].

All of the above leads to the conclusions that also the impact of distributed PPM on large disturbance voltage stability is dependent on the DG penetration level and location. Furthermore, the differences between DG technologies are obvious since fault ride-through of PPM does not lead to delayed voltage recovery.

Stability problems related to current grid connection requirements

FRT is state of the art for power generating facilities connected to eHV, HV, and MV networks nowadays; its positive impact on large disturbance voltage stability and, consequently, frequency stability is beyond dispute. But for LV connected DG the necessity of FRT has not been proved yet.

Also, the pros and cons of voltage support by additional reactive current injection (aRCI) at distribution system level and especially the details of the control system and the adequate parameter settings are still under debate. This thesis will contribute to further understanding of these discussions (see section 1.3).

Two examples for potential problems related to aRCI are the extreme values for parameter setting, i.e. (a) a very high reactive current gain $k_1 = 5 \dots 10 \text{ p.u.}$ on the one hand and (b) a zero reactive current gain $k_1 = 0 \text{ p.u.}$ on the other hand.

For a very high gain, simulations and practical experience showed undesired voltage and power oscillations at the PCC of a WPPM when connected to a ‘modest’ or ‘weak’ network, i.e. a short-circuit ratio of ≤ 10 [SKL12].

For a very low gain, [ESE⁺09, SKL12, Wei13b, Wei15] showed a risk of violation of the steady state stability limit for a WPPM: in an alternating current (ac) system, the voltage angle between sending and receiving nodes should be less than 90 degrees and this limits the active power that a PPM can transfer to the network during voltage dips in a quasi stationary situation. A related stability phenomenon observed when PPM that use voltage source converters are connected to a network with a small short circuit power, was studied in [DBB⁺12]. The so-called ‘loss of synchronism’ of VSC started like a voltage collapse and ended like a loss of angle stability phenomenon. The critical short circuit power ratio (SCR) was found to be below 2...4.

The problem was solved in [ESE⁺09] by adding a voltage dependent active current injection limitation to the control system. It was reported that this would significantly reduce the risk of network fault related ‘loss of synchronism’ of PPM. Control systems were also proposed in [DBB⁺12] and allowed to maintain stable operation of the VSC down to SCR of approximately SCR = 1.5.

What is missing is a system-wide analysis of these potential problems. This thesis will contribute such a system-wide analysis.

Summary

The impact of DG on large disturbance voltage stability is technology, penetration level, and location dependent but foremost subject to the respective protection and control and their parameter settings.

All phenomena that are considered relevant for the impact of DG on large disturbance voltage stability occur during the fault or within the few seconds following the fault

clearance. According to [IEE04] this study period of interest relates to *short-term* large disturbance voltage stability; this involves the dynamics of fast acting load components such as induction motors and electronically controlled loads as well as the dynamics of the power electronic converters applied in DG units. Action of on load tap changers (OLTC) of HV/MV transformers are, therefore, only to be considered if they act very fast. This is the case for some transformer models if the voltage deviation is large [A. 09]. Pre-fault OLTC position must always be considered.

2.2.3 Impact on transient stability

Transient stability is understood in this thesis based on the definition given in [IEE04] as

the ability of the power system to maintain synchronism when subjected to a severe disturbance, such as a short circuit on a transmission line. [IEE04]

Transient stability is a special class of rotor angle stability and, therefore, also called ‘large-disturbance rotor angle stability’.

[IEE04] relates rotor angle stability to the ability of all *synchronous machines* of an interconnected power system to remain in synchronism after being subjected to a disturbance. Hence, if only one or even a group of synchronous machine(s) would lose synchronism, the power system would be called ‘transient unstable’.

The transient stability of a power system is dominated by the dynamic behaviour of synchronous machines and generators in large conventional (thermal) power plants connected to the transmission system to transmission network faults.

Loss of synchronism of synchronous PGM in distribution systems

Loss of synchronism of synchronous power generating modules (type 1) in the distribution system, however, mainly occurs for faults near their terminals in the distribution system (close-up faults) which are out of the scope of this thesis. Given the typical clearance time of transmission network faults of 90...120 *ms* and the fact that distant faults lead to less severe voltage dips at distribution system level, [Cos10] showed for a typical Dutch network that transmission network faults do not lead to loss of synchronism of medium voltage connected CHP plants with directly coupled SG. The studies in [Ant08] quantified the threshold of the retained voltage at the HV/MV substation above which MV connected small-scale microturbines connected via conventional asynchronous generators (type 1 DG) would not become transient unstable to 0.6 *p.u.* . In case of distributed synchronous PGM with very low inertia however, such as LV connected micro-scale microturbines of type 1, loss of synchronism following transmission network faults might be a problem. Hence, the PGM protection systems have to be designed adequately in order to prevent their loss of synchronism [Ant08], for example by reducing the reaction time of the undervoltage relay. Alternatively, the stability of the PGM has to be improved [AE05], for example by increasing the DG’s inertia via a fly wheel [BGK09].

Loss of synchronism of PPM

Due to the absence of (rotor) angular excursions in power park modules (which are connected to the network non-synchronously or through PEC), disconnection of PPM following

severe disturbances is not considered a ‘transient stability’ problem of the power system in this thesis.

Some authors, however, discuss ‘transient stability’ of PPM, such as WPPM [ESE⁺09], but the underlying effects of their studies are related to the maximum active power that a PPM can transfer to the network during voltage dips in a quasi stationary situation. Such limiting factors are classified in the thesis as large disturbance voltage stability issues (see section 2.2.2).

Indicators to assess the impact of DG on transient stability

Different indicator exist to assess the impact of DG on transient stability. The overspeeding of the SG indicates how close these machines get to a rotor pole slip (rotor angle $\theta > \pi$) which would cause unacceptable mechanical stress. The higher the overspeeding, the less transient stable is the system. The critical clearance time (CCT) of a power system for a three-phase fault at a specific location defines the maximum duration of the respective fault before at least one synchronous generator would have a pole slip. A small CCT may indicate a transient stability issue for a given system. The oscillation duration of voltages, angles, and powers indicate the damping of transients in the system and is more related to small disturbance (or small signal) rotor angle stability. The longer the oscillation duration, the less is the system damped. The dynamic response of motor loads in the area of interest may serve as another indicator. As an ultimate transient stability indicator the maximum rotor angle difference between any two synchronous generators in the power system can be used. A gradual loss of synchronism can be expected when the maximum rotor angle difference approaches or exceeds 180° which would cause voltages at an intermediate point of the network to drop rapidly [Kun94, MF10]. An absolute loss of synchronism is defined in pragmatic terms once the maximum rotor angle difference between any two generators exceeds 360° [RKTB94, RERV⁺02]. Operational practices may vary between system operators with respect to acceptable limits for the maximum rotor angle difference during contingencies.

Technology dependent impact

The impact of DG on transient stability is very much dependent on the DG technology. A systematic comparison of the impact on transient stability of different DG technologies and standard controllers, based on a limited set of simulations, was discussed in [SK02b] for the dominant DG technologies in the year 2002, i.e. directly coupled synchronous generators, conventional asynchronous (type 1) generator WPPM, and full converter interface units (type 4) WPPM. A discussion based on this reference follows. This work was later extended to doubly fed asynchronous generator (type 3) WPPM by [ESPM05, MBPE07, QH08].

DG based on directly coupled synchronous generators improves the transient stability in terms of decrease of the overspeeding of the synchronous generators in transmission connected conventional (thermal) power plants but seems to decrease the transient stability in terms of increasing the oscillation duration. The former was explained in [SK02b] by the contribution of distributed SG to the short circuit current which effectively supports the network voltage and that, in turn, increases the synchronising torque for transmission connected SG. However, the total impact of distributed synchronous PGM on transient stability remains limited.

Similar, DG based on type 1 generators apparently does not have much impact on the transient stability as well. This finding was explained in [SK02b] by two opposite effects

related to generators near and remote of network faults which counterbalance (see section 2.2.3) and this effect was confirmed in [Muh06]. However, DG of type 1 is very vulnerable to network faults regarding its own ability to stay in synchronism and can cause voltage instability due to consumption of large amounts of reactive power in the fault and post-fault period [SK02a].

Modern DG of type 3 and type 4 were found to improve transient stability if their undervoltage protection settings allowed them to ride through faults and if their very fast and flexible control systems were designed to support the voltage by an aRCI or even by a closed-loop fast voltage control [ESPM05, QH08]. This finding also holds true for weak transmission systems [MBPE07].

Penetration level dependent impact

The impact of DG on transient stability for different penetration levels depends very much on the properties of the respective power system and the controls of DG. An exhaustive analysis of the impact of DG on transient stability, based on a large number of simulations and sensitivities, was carried out in [Muh06]. The DG penetration level was varied between 0 % and 33 % for the same unit commitment and up to 100 % by successively taking conventional (thermal) power plants out of operation. The impact of a very high DG penetration on transient stability was also analysed in [MF10] and a dependency on the pre-fault operating point was found in [MNP08]. The impact of ac connected offshore WPPM was studied in [SER09].

A modest increase of the DG penetration, while keeping the load constant, results into an improved transient stability of the power system [Muh06, Eir10, MF10]. The reason for this finding is that the in-feed from DG changes the pre-fault operating point of the power system beneficially, i.e. it reduces the loading of transmission connected SG and potentially also the power flows on transmission lines. In both cases, reduced loading leads to a wider rotor angle stability margin [MNP08].

Once the DG penetration increases to a level that transmission connected SG are shut-down, the transient stability can be affected adversely [Muh06]. However, while [Muh06] and [MF10] have identified a DG penetration level of 30 % to 40 % as a turning point from which the transient stability starts to decrease, [Eir10] has identified 60 % as that point.

For such high DG penetration levels, transient stability depends on the total kinetic energy remaining in the system and the reactive power support scheme adopted [Muh06, ESB08]. Insufficient dynamic reactive power supply may lead to transient instability [ESB08]. System damping is significantly reduced at high penetration levels for type 3 and 4 DG, unless these provide an inertial response and damping capability [MF10]. De-commitment of transmission connected SG also increases the electrical distances between the remaining SG which reduces their electromechanical coupling [BGK09].

Therefore, the impact of DG on transient stability for high penetration levels remains very dependent on the properties of the respective power system, since reactive power support depends on the network topology, the sequence in that conventional power plants are de-committed, the strategy whether and how their corresponding reactive power support is substituted, and the controls of DG [Muh06, ESB08, Eir10].

From a long-term investment perspective, increased levels of DG may require more flexibility in the conventional power plant portfolio. That could result in the installation of highly flexible peak load power plants which usually have a lower rating than base load

power plants. Hence, the synchronous generators of future power plants might become 'smaller' relative to the impedance of the grid which in turns strengthens the mutual electromechanical coupling between the large and improves the transient stability [SK03].

Pre-fault operating point dependent impact

The dependency of the impact of DG on transient stability on the pre-fault operating point of DG is very complex and not straight forward. A general relationship cannot be defined, except for the trivial effect on the loading of transmission connected SG and potentially transmission lines mentioned above. The dependency varies with the DG type and its controllers. While [MBPE07, MNP08] did not find any non-trivial effect of type 3 WPPM pre-fault loading on transient stability, the following examples illustrate the complex dependencies.

The network fault response of a type 3 WPPM with rotor circuit crowbar protection depends on the WPPM's pre-fault operating point and the distance to the fault. For close-up faults, an ignition of the crowbar becomes more likely the higher the pre-fault WPPM loading is; crowbar operation is likely to occur for close-up faults and WPPM loading of 50 % of rated power and above [MF10]. Crowbar ignition turns the doubly fed asynchronous generator (DFAG) into a conventional asynchronous generator. As a result, the WPPM consumes significant reactive power and at the same time the active power in-feed is reduced significantly. The consumption of reactive power by DFAG during crowbar operation has a negative impact on the power system transient stability. What is more, [MF10] argues that for high-load conditions close to the WPPM's rated capacity, the wind turbine pitch angle controller would reduce the wind power extraction significantly to limit the rotor speed during crowbar operation. This action is confirmed and justified in [For13] by the fact that the length of a network fault cannot be known at the moment it occurs and that, therefore, action must always be taken to avoid excessive acceleration. [MF10] shows that the effect of this action would be a delayed active power recovery after the fault is cleared and the crowbar is deactivated. For medium and low-load conditions pre-fault, the pitch angle is not changed as much and active power would recovery faster. The authors in [MF10] argue that maintenance of high active power in-feed from WPPM improves the transient stability of the power system.

Support of the network voltage during and after a voltage dip, on the other hand, can improve the transient stability of the power system because synchronising torques between transmission connected SG are better maintained. Such voltage support can be provided to a certain extent also by distributed synchronous PGM and distributed PPM by additional reactive current injection. The reactive current injected into the network, however, is limited by the power electronic converter rating and any active current that is injected simultaneously. In absence of a control that would give the reactive current priority over the active current, the pre-fault DG loading would directly determine how much reactive current can be injected during and after the fault.

The limited voltage support, i.e. the limited positive impact on transient stability, due to the PEC rating is partly relaxed by the smaller capacity credit of DG based on variable energy resources such as wind and solar compared to conventional (thermal) power plants [SER09]. The actual in-feed from WPPM and PVPPM can typically vary between zero and the maximum coincidence factor times their total rated capacity. As a consequence, the total rated DG capacity in operation will often exceed the total rated capacity of transmission

connected synchronous generators whose generation is replaced. Thus, the total reactive currents injected by WPPM and PVPPM during faults can be substantial.

Location dependent impact

The impact of DG on transient stability can depend significantly on the vertical and horizontal location of the DG in the power system. In general, the impact of DG on transient stability depends on the ‘relative electrical location’ of the DG to the fault location and the transmission connected SG in the power system.

For WPPM (horizontally) located far away from load centres and, therefore, leading to significantly changed power flows, i.e. increased tie-line flows, critical fault clearance times were found to be considerably reduced and transient stability affected adversely [ESPM05, SER09, MF10]. This finding can be explained by increased voltage angle differences pre-fault and reduced dynamic reactive power availability close to the transmission connected SG remaining in the system.

For WPPM (vertically) located at sub-transmission and distribution network level, a negative impact on transient stability was found [ESPM05, Muh06]. In [Muh06] the location of the DG was accounted for by varying the magnitude of the distribution network impedance between 0.035 *p.u.* and 0.08 *p.u.* and including a case with a high resistance value. The finding was especially pronounced when such placement of DG would lead to reverse power flows, i.e. very high penetration of DG in (parts of) the transmission system, and no mitigation measures were taken [BvR⁺11b]. The observed deterioration in transient stability is partly explained by the limited dynamic reactive power contribution from DG and, thus, reduced short-circuit power at transmission system level. The limitation stems from reactive power losses in sub-transmission and distribution systems and between the network levels, due to increased equivalent impedances between the transmission network and the DG connected ‘deeper’ into the sub-transmission and distribution networks [BvR⁺11b].

A related finding—which is of much interest for this thesis—is the influence of the impedance angle, i.e. R/X ratio, of either the DG’s network connection line or the equivalent impedance of the network ‘seen’ at the PCC. In [Muh06] a further decrease of transient stability was found for the case with high resistance value ($R/X = 0.33$) in the distribution network impedance. The analysis in [SER09] found that the injection of a real current can impede the voltage support by reactive current injection for R/X ratios of higher than 0.25, if no voltage dependent active current injection limitation control would be implemented. Again, as a result, the transient stability of the power system would be reduced. The cited reference, however, investigated the impact of large ac connected offshore WPPM and not of DG on transient stability of power systems. Whether similar effects can be observed for DG connected ‘deep’ inside the distribution system remains to be shown by this thesis.

With regard to the ‘relative electrical location’ of DG to transmission connected SG, an analysis of the previously mentioned ambiguous impact of type 1 (conventional asynchronous) generators on transient stability allows for a deeper understanding as follows. If these are located near SG and many of the latter accelerate during a fault, the stator frequency of the conventional asynchronous generators increases. As a result of this, the slip frequency is reduced and thereby also the DG’s active power in-feed. The reduced active power in-feed from DG inhibits the further acceleration of the SG. Hence, the transient stability is improved. On the other hand, if the type 1 DG is located more distant to SG and are, therefore, more weakly coupled to the latter, acceleration of the DG itself during a fault increases the

slip frequency and thereby leads to an increased DG reactive power consumption. The increased reactive power flows result in lower terminal voltages at the remote SG and thus in a decrease of synchronising torque and a faster increase in rotor speed. Thus, the transient stability is impaired. [SK02b]

Similar to the finding regarding the influence of the pre-fault operating point of type 3 WPPM with rotor circuit crowbar protection, the ‘relative electrical location’ of network faults to those WPPM determines whether or not the crowbar is triggered and the DFAG temporarily turns into a conventional asynchronous generator. For faults distant to type 3 WPPM that do not trigger the crowbar protection of numerous WPPM transient stability is improved due to the capability of those WPPM to support the network voltage during and after the fault [MF10]. However, if these faults are close to transmission connected SG and then again cause the latter to lose synchronism, WPPM are not able to uphold, let alone improve, the transient stability of the power system [MNP08, MF10].

Protection dependent impact

The impact of DG on transient stability is very much dependent on the DG protection and its parameter settings. The most important protection device in this context is the undervoltage protection relay that disconnects the DG if the voltage at its PCC or terminal falls below a defined threshold, e.g. 0.8 *p.u.*. DG that disconnects at the quoted undervoltage threshold are not able to run through low voltage events. The research in [Cos10] studied a part of the Dutch transmission system that included a sub-transmission and distribution network in a horticultural area to which CHP generating facilities were connected to at MV level. The study showed that especially three-phase and two-phase-to-earth faults trigger the undervoltage protection of the latter when applying the above mentioned threshold. Phase-to-earth faults were found to lead only in a significantly smaller area of the transmission system to a disconnection of CHP-plants.

In [SK02b] it was found that the disconnection of non-LVRT distributed generation has a positive impact on transient stability: it decreases the overspeeding of transmission connected synchronous generators. This was explained by the reduced active power in-feed from DG, hence, a reduction of the SGs acceleration.

Similarly, [Muh06] found that if distributed PPM would perform LVRT but without further supporting the voltage during and after the fault, the transient stability is decreased compared to when these units disconnected during low voltage events. However, once the disconnection of DG resulted in large voltage drops at some nodes in the transmission system (as mentioned in section 2.2.2) transient stability would be reduced instead. Moreover, disconnection of large amounts of DG would not be acceptable from a frequency stability viewpoint (see section 2.2.1).

Control systems dependent impact

The previous discussion has already indicated that the impact of DG on transient stability is very much dependent on the DG control and its parameter settings.

For distributed synchronous PGM as well as distributed PPM, the impact on the duration of the rotor speed oscillations depends on whether or not the DG is equipped with voltage and frequency control [SK02b, Muh06]. By implementing adequate control systems it was shown, for example for type 3 WPPM in [HALJS05, For13], that DG can match

the performance of SG regarding voltage control and the provision of network damping and even improve on them. Similarly, for weak power systems as discussed in [MBPE07], it was found that type 3 WPPM, equipped with PEC and LVRT capability, can be integrated without reducing transient stability.

Power park modules can improve transient stability if they positively influence the voltage magnitude and the active power balance in the system during and after faults. Higher terminal voltages create higher electrical torque at synchronous generators and, thereby, decreases their acceleration. Reduced active current injection from PPM during and after faults shifts the supply of system load to the synchronous generators which also decreases their acceleration during a network fault and increases their deceleration after the fault.

On the contrary, too slow active power recovery after faults bears the risk of swing back pole slip, especially in power importing areas [Wei13b]. It is important to note that transient stability is not only about the change in rotor angle of a single generator but also about the speed changes of the other synchronous generators in the power system that any generator would swing against.

While control systems of distributed generation tend to improve the transient stability of the power system, they require an appropriate choice of parameters to do so. If parameters are not well chosen, the control systems of DG—as any other controls in the power system—bear the risk to have adverse effects on power system stability. In the following, examples are given for adverse effects on transient stability caused by DG control systems.

Impact of a deadband in the fast voltage controller—Simulations in [SER09, For13] revealed that a deadband of $v_{DB} \neq 0$ in the fast voltage controller of DG that would operate during and shortly after network faults can cause oscillations in the post-fault voltage, real and reactive power traces. The authors concluded that the power system performs better without the deadband in the controller, i.e. $v_{DB} = 0$. [For13] explained that the motivation for using a deadband originated from the wish of distribution system operators (DSO) to keep DG's network fault related fast voltage control in distribution systems compatible with the power factor control that DG use during steady state operation when the network voltage is within the standard operating range.

With regard to additional reactive current injection, simulation in [SER09, Wei13b] have also shown that increasing the reactive current gain k_1 to values up to $7.5 p.u.$ —and thereby far beyond the standard value of $k_1 = 2.0 p.u.$ —would significantly improve the transient stability. Especially in case of less severe voltage dips caused by distant faults such high reactive current gains would allow distributed PPM to support the network voltage stronger than SG would do [FEK⁺09]. However, the question remains why such strong voltage support would actually be necessary for these faults.

Prioritising and limiting the reactive current component at the same time—The total reactive current injection from distributed PPM remains limited to the physical PEC rating, in case of type 4 WPPM to $1.2...1.4 p.u.$ (depending on the WPPM configuration) [Ene13] and in case of type 3 WPPM to $1.4...1.6 p.u.$ in over-excited mode (i.e. worst case), depending on the network voltage [FEK⁺09]. Similar to the effect mentioned in section 2.2.2, limiting the total reactive current to a value smaller than the physical limits, either by choosing a very low value for the reactive current gain, e.g. $k_1 = 0.0 p.u.$ or by introducing a maximum reactive current limit, e.g. $i_{Q,max} \leq 1.0 p.u.$, may have a negative effect on the transient stability of the power system, depending on the control structure and the R/X ratio of the equivalent network impedance. If the control is designed such that the remaining current

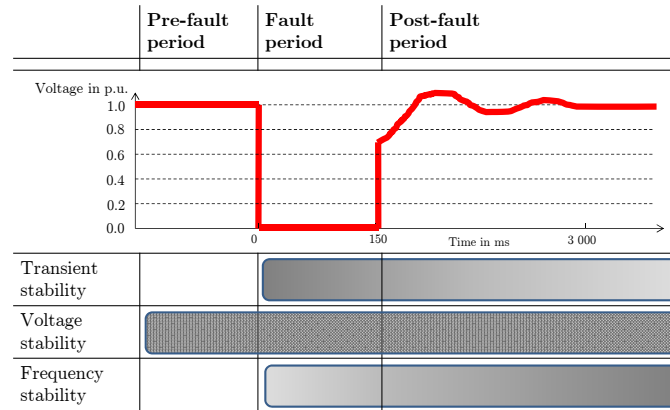


Figure 2.1: Classification of drivers related to the impact of DG on the network fault response by time period.

margin is used to feed in an active current, the positive effect on transient stability achieved by reactive current injection may be reversed for R/X ratios above 0.25 *p.u.* [SER09].

In order to overcome the adverse effect of active current injection during fault, a voltage dependent active current control is proposed in [SER09]. The proposed control reduces the active current reference set-point quadratically to the voltage dip depth once the voltage at the DG terminals falls below 90 % of the pre-fault voltage. The simulations in [SER09] showed that transient stability of the power system, in terms of rotor angle deviation and oscillation duration, can be significantly improved by this measure. On the other hand, in case of WPPM, the increased difference between electrical and mechanical torque causes an increase of the rotational speed of the wind turbine. This calls for careful consideration of speed limits or the dissipation of excess energy in a direct current (dc) chopper.

2.2.4 Summary of impact on power system stability

Figure 2.1 relates the classes of power system stability in the focus of the thesis to the time periods: pre-fault, fault, and post-fault. Transient stability relates to the fault period but stretches slightly into the post-fault period. Voltage stability relates to all periods, the pre-fault, the fault, and post-fault period. Frequency stability relates to the post-fault period but can also become relevant in the fault period for certain cases.

Based on this literature review, gaps in the existing state of the art have been identified and the research questions for this thesis have been derived and presented in section 1.4.

Table 2.1 summarises the main findings on the impact of DG on power system stability in a high-level tabular overview. If distributed generation leads to a decrease in short-circuit power levels or if DG even consumes reactive power, voltage and transient stability are negatively impacted. Frequency stability worsens if DG leads to reduced system inertia or a loss of active power in the post-fault period, either from not performing FRT or due to a slow active power recovery after a fault. On the other hand, the proximity of DG to loads and a reduced loading of transmission lines at low and medium penetration levels will improve voltage and transient stability of a power system. Both are improved even further, if DG

injects a reactive (short-circuit) current during and after a fault because this supports the voltage profile in the transmission and distribution system. If DG can ride through network faults and their active power recovers sufficiently fast enough for the specific remaining inertia in the system, frequency stability will be improved.

Table 2.1: High-level overview on negative and positive impact of distributed generation on power system stability

Stability class	Negative impact	Positive impact
Frequency stability	<ul style="list-style-type: none"> • if reduced system inertia • if DG without FRT • if slow P recovery post-fault • if reduced reserves 	<ul style="list-style-type: none"> • if synthetic or additional inertia • if DG with FRT • if fast P recovery post-fault • if primary reserves from DG
Voltage stability	<ul style="list-style-type: none"> • if reduced S_k'' • if increased Q consumption 	<ul style="list-style-type: none"> • if i_q injection • if Q injection post-fault • if close to loads
Transient stability	<ul style="list-style-type: none"> • if (very) high penetration • if de-commitment of SG • if reduced S_k'' • if increased Q consumption 	<ul style="list-style-type: none"> • if low to medium penetration • if reduced loading of SG or lines • if i_q injection • if Q injection post-fault

2.3 Network Fault Response Requirements for DG

2.3.1 Grid codes

Grid connection requirements, also known as interconnection requirements, are the rules and regulations with which grid-connected components have to comply. They provide a framework of compatibility and quality for the power system. They place requirements on important factors such as acceptable voltages and frequencies in different situations. Equipment vendors have to make sure that their products comply with grid connection requirements, otherwise they are not allowed to sell them.

Grid connection requirements have evolved with increasing DGs penetration and as a consequence of this, a number of DG classes with very different dynamic behaviour exist in the power system ('legacy'). Grid connection requirements are differentiated by individual DG's rated capacity in North America and by DG's connection voltage level in Europe.

For power system stability studies, GCRs determine a *performance framework* for the network fault response of individual DGs depending on their commissioning period, connection level or size, and sometimes technology type.

2.3.2 Evolution

With regard to network fault response, the 'get-out-of-the-way' principle, used for example in [Ver98, Ger01] for Germany and in [IEE03b] for North America, was first changed by introducing low voltage ride-through (LVRT) requirements at transmission and sub-transmission level as, e.g., in [E.O01, Ver03, U.S05]. DGs were later required to actively support the network voltage during faults by additional reactive current injection (aRCI) as in [E.O03, VDN04, Ger09] for Germany. This was meant to improve voltage stability at distribution system level and potentially help older installations without LVRT capability to stay connected during shallow voltage dips [BEW06]. Finally, requirements related to the post-fault real power recovery were found to be necessary in order to maintain frequency stability after transmission network faults [Eir10, Wei13a, Wei15]. The evolution of network fault response requirements are shown in Fig. 2.2 for Germany as one example jurisdiction.

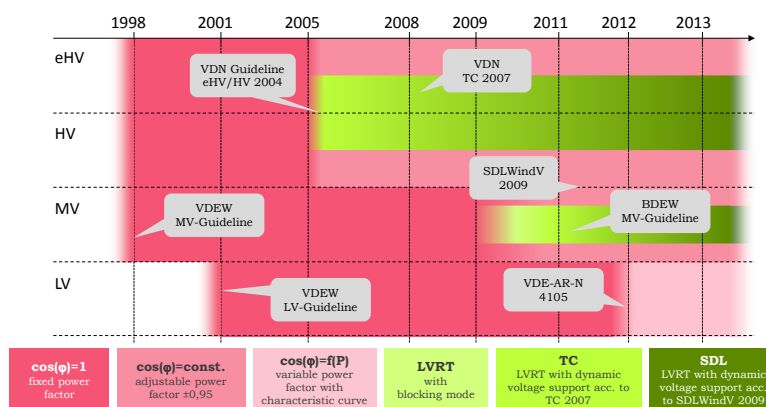


Figure 2.2: Historical overview of grid connection requirements in Germany for network fault response [Ver07] [Ger09].

Current grid connection requirements can be classified into the four categories (1) quasi-stationary voltage control, (2) dynamic reactive support, (3) disturbance voltage support, and (4) disturbance frequency support. A large variety of terms are used around the world to describe these requirements. Table A.4 in appendix A.10 gives an overview of terms that are widely used in the European and the North American context. From the four listed above, disturbance frequency support is out of the scope of this research.

2.3.3 Quasi-stationary voltage control and dynamic reactive support

Quasi-stationary voltage control and dynamic reactive support requirements determine the reactive power distributed generation may exchange with the network in order to control the voltage at its point of common coupling (PCC). Control modes include:

- a fixed power factor $\cos(\varphi) = const.$;
- a fixed reactive power $Q = const.$ set-point in MVar;
- a reactive power/active power characteristic $Q(P)$;
- a variable power factor/active power characteristic curve $\cos(\varphi) = f(P)$, see Fig. 2.3; or
- a reactive power/voltage characteristic $Q(U)$.

Quasi-stationary voltage control is a slow, often step-wise control with typical time frames of 1 min to 10 min. Dynamic reactive support controls voltage fast and smoothly, typically within the 1 s to 10 s time frame.

Figure 2.3 shows the characteristic of the control for low voltage (LV) and medium voltage (MV) connected distributed generation. For the MV networks, substation connected DG may have a reversed characteristic to provide capacitive reactive power to downstream distributed generation.

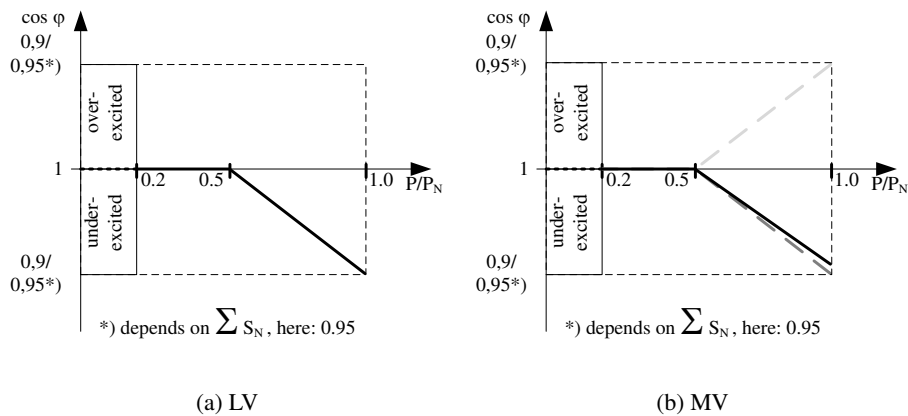


Figure 2.3: Dynamic power factor control characteristics [For11]

2.3.4 Disturbance voltage support

Low voltage ride-through

Low voltage ride-through is the ability for distributed generation to remain connected to the network and able to quickly restore current output after a voltage disturbance. Figure 2.4 visualizes the most stringent LVRT curves for MV connected DG as they are defined by [EE13c, CEN15c] in Europe (dashed lines). Such requirements are nowadays regarded as the state of the art for DG connected at MV level and above. However, most GCR around the world do nowadays not require LVRT capabilities from LV connected DG. European and North American standards, such as the European EN 50438:2013 [CEN15a], the German VDE-AR-N 4105 [For11] and the North American IEEE Std. 1547 [IEE03b, IEE14a], require (or allow) that small-scale LV connected DG trips if its terminal voltage drops below the normal voltage band (solid line in Fig. 2.4).

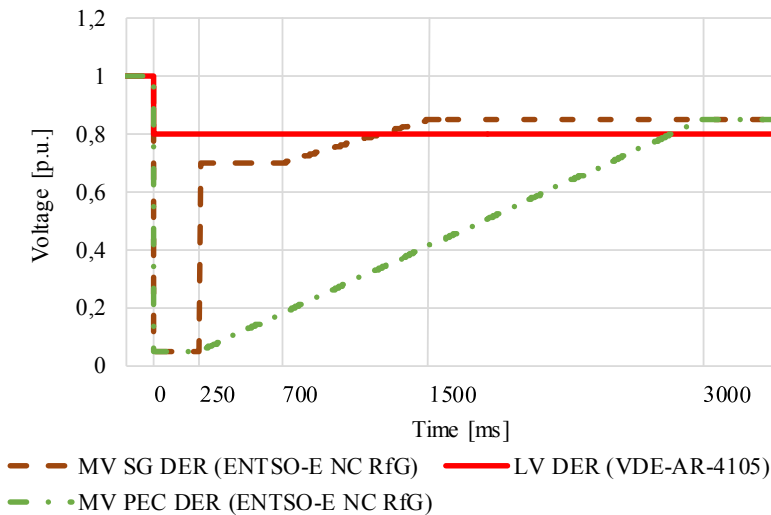


Figure 2.4: Low voltage ride-through (LVRT) curves based on [EE13c, CEN15c, For11]. New-to-be-installed synchronous generator (SG) and power electronic converter (PEC) based DGs at medium voltage (MV) level (dashed lines) as well as existing and new-to-be installed DGs at low voltage (LV) level (solid line)

With continued increase of LV connected DG installations, such as distributed photovoltaic (PV) systems, the discussion about LVRT requirements at LV level has started a few years ago [IEE, ENT12b, For12]. The concern is that voltage dips caused by transmission network faults would propagate to the LV grids in a wide area where they would potentially lead to massive tripping of LV connected DG (common mode failure).

This risk of a significant post-fault active power imbalance motivated ENTSO-E to include LVRT capability requirements in the final version of the Network Code for Requirements for Grid Connection Applicable to all Generators (NC RfG) that was published in March 2013 [EE13c]. However, these requirements were limited to ‘Type B’ generators, which are medium-scale DGs with a capacity between 1 MW and 50 MW and that are

typically not connected at LV level.

For LV connected, small-scale DG larger than 6 kVA, only Italy [Com14] and a recently issued European equipment standard [CEN15b] require LVRT. Only in Japan micro-scale DG, including LV single-phase connected PV systems, are soon to be required to ride through voltage dips [Kob12, JEA13]. Notably, all of these LVRT requirements for LV connected DG either allow the units to block the inverter current ('momentary cessation') or do not further specify their fault response at all.

A detailed overview on the evolution of grid codes requirements related to the network fault response of DG for the example of Germany is given in appendix E.2.1.

Low voltage ride-through with blocking mode

The distributed generation unit remains connected to the network and able to quickly restore current output after a disturbance, but blocks the current output when the voltage drops below a pre-defined threshold. This LVRT mode is commonly requested by distribution system operators from distributed generation connected downstream of a feeder, so that the LVRT operation of distributed generation does not interfere with the protection schemes of the distribution system. This mode is sometimes referred to as 'limited dynamic voltage support' or 'momentary cessation'.

Low voltage ride-through with additional reactive current injection

The distributed generation unit remains connected to the network and injects a reactive current component in proportion to the voltage deviation in addition to the pre-fault current output. The DG unit can operate in additional reactive current injection (aRCI) mode during the fault as well as in a pre-defined period shortly following a fault. Requirements for aRCI have been justified in the past by:

- support PCC voltage to ensure voltage stability;
- providing short-circuit current to ensure fast and reliable operation of protection schemes at HV and extra-high voltage (eHV) level;
- helping the DG themselves to ride through voltage dips, especially when these would otherwise be prolonged due to fault-induced delayed voltage recovery (FIDVR);
- improving transient stability under certain conditions;
- support distribution system voltage to maintain other devices online, like loads and DG that cannot ride through voltage dips.

Appendix C.1.2 describes the aRCI control mode mathematically and with block diagrams. Since the function adds a reactive current component to the pre-fault current set-point, it may initially reduce the total reactive current magnitude if the DG had operated with inductive power factor prior to the fault. Once the total current limit of the DG is reached, priority is given to the reactive current and active current is reduced accordingly.

Most grid connection requirements require an additional reactive current injection in the positive-sequence only. Recent requirements in Germany, like the VDE-AR-N 4120 for

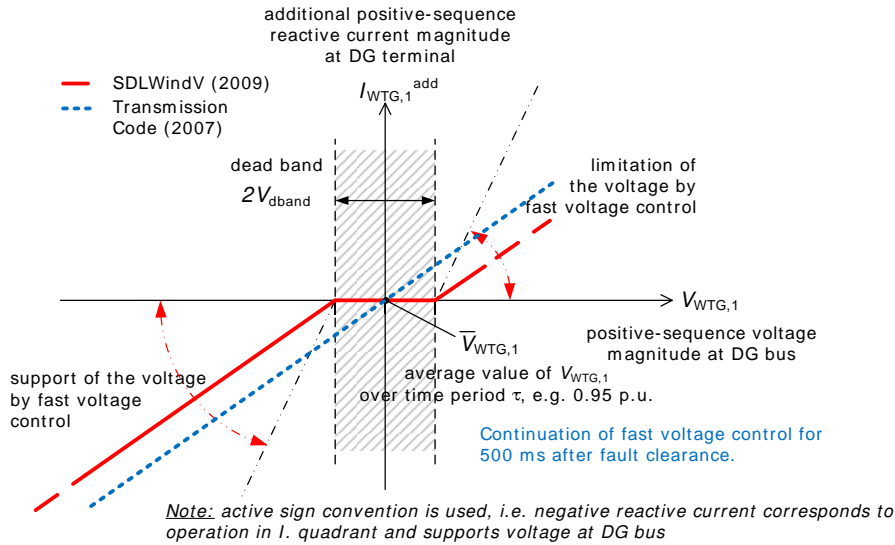


Figure 2.5: Additional reactive current injection according to TransmissionCode (2007) [Ver07] and SDLWindV (2009) [Ger09]

HV connected generation units [For15b], also require an injection in the negative-sequence. This aims at preventing undesired overvoltage conditions in healthy phases as well as contributing sufficient short-circuit current during unbalanced faults [NWDE15]. Negative-sequence control aspects are out of the scope of this research.

Figure 2.5 shows the characteristics of the LVRT with additional reactive current injection requirements as they were defined in the German TransmissionCode (2007) [Ver07] and the ancillary service ordinance SDLWindV (2009) [Ger09]. The deadband has typically been set to $\pm 10\%$ of the pre-fault voltage magnitude and the reactive current gain typically equals $k = 2$ p.u. although it must be adjustable within $k = [0 \dots 10]$ p.u..

A variation of the additional reactive current injection control mode is the less commonly described additional reactive/active current injection control mode [SBv⁺14, Ska14]. Refer to appendix C.1.3 for a mathematical description and control block diagrams.

Active power recovery after fault

Part of LVRT requirements is the specification of how fast DG should restore active power shortly after sudden network fault. Depending on system size this requirement can range from 0.5 s in island systems [Eir13] to 5 s in interconnected systems [Ver07]. Recent grid connection requirement, like in the German VDE-AR-N 4120, require DG to restore active power output 'as fast as possible' in order to stabilise system frequency shortly after network faults [For15a]. Simulations from [Wei15] even recommend a restoration with 200 % to 1 000 % per second.

The active power recovery of DG also depends on the disturbance voltage support strategy: whether priority is given to reactive over active current, the chosen reactive current gain, and whether disturbance voltage support is continued over a pre-defined period after

the voltage returns to the normal operating region.

For power system stability studies the most conservative assumption for the active power recovery should be considered based on existing GCRs if details about the actual performance of DG are unknown.

High voltage ride-through

Overvoltage conditions may arise in a power system due to load shedding or unbalanced faults [FEK⁺08] or at the instance when a fault is cleared due to tripping of induction motor loads following a FIDVR event [NER09, LSS⁺15, NER15]. Short overvoltage conditions may also occur at fault clearance if DG was injecting reactive current into the grid in order to support the voltage during a fault. Nodes behind long radial lines or cables show a higher risk for over-voltages than nodes in meshed networks.

The impact of overvoltage conditions on wind turbines and related high voltage ride-through (HVRT) features of wind power park module (WPPM) have been discussed in detail in [FEK⁺08]. Overvoltage conditions may lead to the reversal of the power flow in the line-side converter (LSC) of DFIGs which eventually may increase the dc-link voltage in the rotor circuit to an unacceptable value. All in all, HVRT requirements are becoming more important.

To date, several countries have established HVRT. Most recently, the German VDE-AR-N 4120 for customer installations connected to the 110 kV network specifies a HVRT capability which will enter into force in the year 2017. For inverter-based DG, the high voltage ride-through profile prescribes immunity against an overvoltage in the highest phase-to-phase voltage of up to 130 % of nominal voltage for a period of 100 ms as well as of up to 125 % of nominal voltage for a period of 60 s [For15b]. Besides Germany, other countries like Australia, South Africa and Italy have HVRT requirement for DG. Other countries, for example the U.S. are currently considering an inclusion in future GCRs [EPR15b].

A further discussion of HVRT is out of the scope of this thesis.

2.3.5 Summary of network fault response requirements for DG

Grid connection requirements determine a *performance framework* for the network fault response of individual DGs depending on their commissioning period, connection level or size, and sometimes technology type. In particular, network fault response requirements for distributed generation have been evolving over time and therefore, a number of DG classes with very different dynamic behaviour exist in the power system ('legacy'). These performance classes need to be adequately considered in power system stability studies.

From the disturbance voltage support requirements presented in this section, the opportunities and challenges related to requirements for LVRT with additional reactive current injection are the least understood. The next section will discuss the theoretical limits of how effective DG can support the distribution system voltage during and shortly after voltage disturbances.

2.4 Discussion of effectiveness of voltage support

The effect of wind power park module (WPPM) current injection during faults on the network voltage has been quantified in [Mor06,ESE⁺09,REvD12] as a function of short-circuit ratio and X/R ratio at the PCC. The following discussion closes the gap between these two electrical parameters on one side and the DG rated penetration level $\rho_{DG,r}$ and the related network expansion on the other side.

In the following, the analysis of the fundamental relationships that quantify the effectiveness of voltage support presented in [ESE⁺09] are extended to multi-level active distribution systems (ADSs). In step 1, the voltage at the PCC for a certain fault and *with* the current injection by the WPPM will be derived in polar coordinates, see (2.4). In step 2, the combined fault and load impedance is expressed as a function of the retained voltage during the fault and the equivalent (Thevenin) impedance of the external network, see (2.5). In step 3, the relationship between the latter and the WPPM penetration level will be derived, see (2.8)–(2.10). That finally allows, in step 4, to express the effectiveness of voltage support from WPPM as a function of the WPPM rated penetration at different system levels, see (2.17).

The *rated* penetration level is defined in (2.1) as

$$\rho_{DG,r} = \frac{P_{DG,r}}{P_{Ld,p}} \quad (2.1)$$

with $P_{DG,r}$ and $P_{Ld,p}$ being the total *rated* DG and *peak* load active power within the stated boundaries of the power system under study. For a definition of the *instantaneous* penetration level, see equation (A.2) in appendix A.6.

Figure 2.6a presents a basic circuit diagram to quantify the effectiveness of voltage support from WPPMs at distribution system (DS) level. With the PCC of a WPPM being the only node in the system, the external network is represented by its Thevenin equivalent ($\underline{V}_0 = V_0 \cdot e^{j\phi_0}$, $\underline{Z}_G = Z_G \cdot e^{j\phi_G}$). Generator-oriented sign convention is used for the current injected by the WPPM into the system at its PCC, i.e. $I_{WP} = I_{WP} \cdot e^{j\phi_{WP}}$. It is further assumed that \underline{Z}_{Flt} represents the combined fault and load impedance which leads to a certain retained voltage at the PCC. Since a large part of \underline{Z}_{Flt} is determined by the network quantities itself, it can be assumed that \underline{Z}_{Flt} and \underline{Z}_G have the same phase angle $\phi_G (= \arctan(X_G/R_G))$.

Step 1: Have

$$\begin{aligned} \underline{V}_{Flt} &= I_{Flt} \cdot \underline{Z}_{Flt} \\ I_{Flt} &= \frac{\underline{V}_0 + \underline{Z}_G \cdot I_{WP}}{\underline{Z}_G + \underline{Z}_{Flt}} \end{aligned}$$

according to voltage divider theory, then (2.2) gives the voltage at the PCC for a certain fault *without* the current injection by the WPPM

$$\underline{V}_{Flt,0} = \frac{\underline{Z}_{Flt}}{\underline{Z}_G + \underline{Z}_{Flt}} \underline{V}_0 \quad (2.2)$$

and (2.3) gives the voltage *with* the current injection by the WPPM:

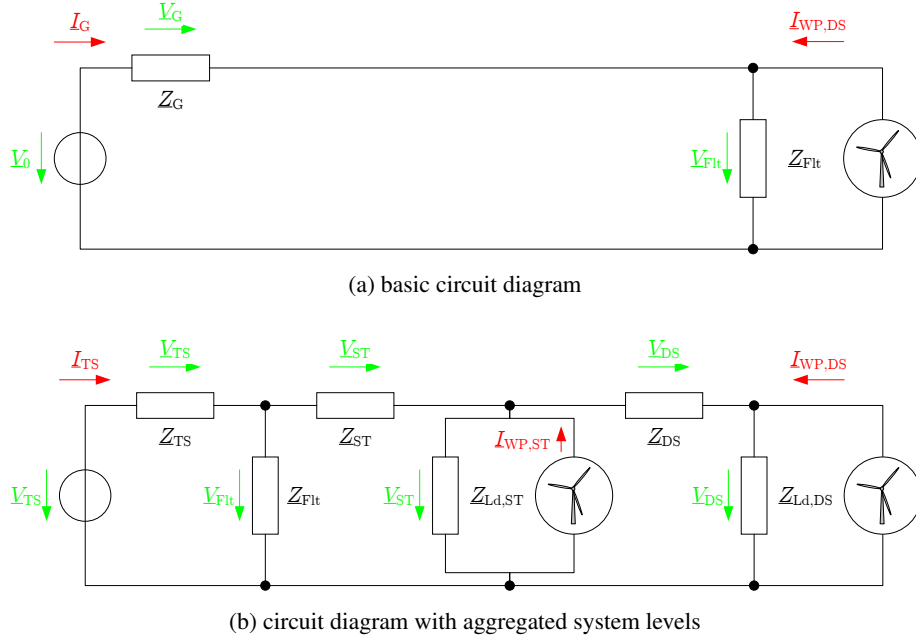


Figure 2.6: Circuit diagrams to quantify the effectiveness of voltage support

$$\underline{V}_{\text{Flt}} = \underline{V}_{\text{Flt},0} + \underbrace{\frac{Z_G \cdot Z_{\text{Flt}}}{Z_G + Z_{\text{Flt}}} I_{\text{WP}}}_{:=\Delta V_{\text{Flt}}} \quad (2.3)$$

$\underline{V}_{\text{Flt},0}$ is arbitrarily taken as the phase reference, hence $\underline{V}_{\text{Flt},0} = V_{\text{Flt},0}$. With Z_{Flt} and Z_G having the same phase angle ϕ_G , then (2.2) gives also $\phi_0 = 0$. Expressing (2.3) in polar coordinates gives

$$\underline{V}_{\text{Flt}} = V_{\text{Flt},0} + \underbrace{\frac{Z_G \cdot Z_{\text{Flt}}}{Z_G + Z_{\text{Flt}}} I_{\text{WP}}}_{:=\Delta V_{\text{Flt}}} \cdot e^{j(\phi_{\text{WP}} + \phi_G)} \quad (2.4)$$

which is visualised in Fig. 2.7. It becomes clear that the maximum effectiveness of voltage support is achieved for $\Delta \underline{V}_{\text{Flt}} = \Delta V_{\text{Flt}}$, i.e. when I_{WP} has a phase angle of $\phi_{\text{WP}} = -\phi_G$. The minimum effectiveness results if $\phi_{\text{WP}} = \pi - \phi_G$. In the following, the maximum voltage support during fault is named $\Delta V_{\text{Flt},\text{max}}$.

Step 2: Under the assumptions above, the combined fault and load impedance Z_{Flt} is a function of the (retained) voltage at the PCC during the fault period without the current injection by the wind power park module $V_{\text{Flt},0}$, the Thevenin voltage V_0 , and the Thevenin impedance Z_G according to (2.5):

$$Z_{\text{Flt}} = \frac{V_{\text{Flt},0}}{V_0 - V_{\text{Flt},0}} \cdot Z_G \quad (2.5)$$

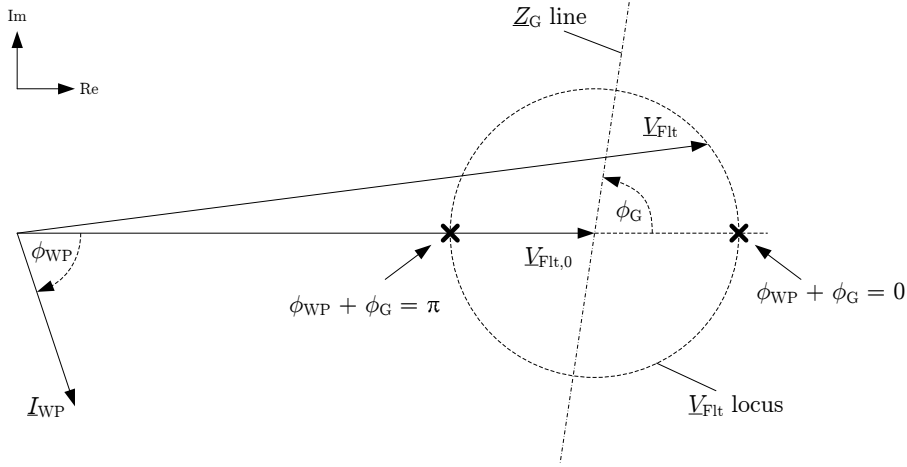


Figure 2.7: Phasor diagram to visualise the effectiveness of voltage support by current injection from WPPM

Step 3: In order to derive the relationship between the Thevenin impedance Z_G and the WPPM rated penetration level $\rho_{WP,r}$, one has to take into account the network planning criteria as outlined in appendix E.3 as well as the ratio between minimum and peak load (2.6):

$$\gamma_{Ld} = \frac{P_{Ld,min}}{P_{Ld,p}} = 0.5. \quad (2.6)$$

Line impedances are chosen to comply with voltage quality standards and for simplicity are assumed to be uprated by the same factor as transformers when necessary.

Combined with the impedance of the transformers used in the test system (see table B.1) and the distribution transformer overrating factor for load supply which is here assumed to be

$$\frac{1}{\eta_{Tr/Ld}} = \frac{S_{Ld,DS,p}}{S_{Tr,DS,r}} = \frac{P_{Ld,DS,p}}{\cos(\varphi)_{Ld,DS,p} \cdot S_{Tr,DS,r}}, \quad (2.7)$$

Z_G can be derived from the transmission network's short-circuit power at the TS/DS interface $S''_{k,TS}$, and the equivalent system level impedances Z_{ST} and Z_{DS} as follows:

$$Z_{TS} = \frac{(V_{TS})^2}{S''_{k,TS}} \quad (2.8)$$

$$Z_{ST} = \frac{1}{n_{Tr,ST}} \cdot (Z_{Tr,ST} + Z_{Ln,ST}) \quad (2.9)$$

$$Z_{DS} = \frac{1}{n_{Tr,DS}} \cdot (Z_{Tr,DS} + Z_{Ln,DS}) \quad (2.10)$$

with $n_{Tr,x}$ being the number of parallel transformers and lines based on the transformer's thermal rating calculated by

$$n_{Tr,ST} = \max_1 \left(\left[\frac{S_{DG,ST,r} + S_{DG,DS,r} - S_{Ld,ST,min} - S_{Ld,DS,min}}{S_{Tr,ST,r}} \right] \right)$$

$$n_{Tr,DS} = \max_1 \left(\left[\frac{S_{DG,DS,r} - S_{Ld,DS,min}}{S_{Tr,DS,r}} \right] \right)$$

and with (2.1), (2.6), and (2.7) rewritten to

$$n_{Tr,ST} = \max_1 \left(\left[\frac{\rho_{WP,ST,r} - \gamma_{Ld}}{\langle \cos(\varphi)_{ST} \rangle \cdot \eta_{Tr/Ld,ST}} \right] \right) \quad (2.11)$$

$$n_{Tr,DS} = \max_1 \left(\left[\frac{\rho_{WP,DS,r} - \gamma_{Ld}}{\langle \cos(\varphi)_{DS} \rangle \cdot \eta_{Tr/Ld,DS}} \right] \right) . \quad (2.12)$$

Step 4—With (2.1), (2.7), (2.11)–(2.12), and the split of total rated WPPM capacity installed at sub-transmission (ST) and DS level being $\xi_{WP,ST} + \xi_{WP,DS} = 1$, then I_{WP} becomes in per unit on the respective transformer base $S_{b,ST} = S_{Tr,ST,r} \Rightarrow I_{b,ST} = I_{Tr,ST,r}$ and $S_{b,DS} = S_{Tr,DS,r} \Rightarrow I_{b,DS} = I_{Tr,DS,r}$:

$$I_{WP,ST} = \frac{\rho_{WP,ST,r}}{\eta_{Tr/Ld,ST}} \cdot (\xi_{WP,ST} \cdot e^{j\phi_{WP,ST}} + \xi_{WP,DS} \cdot e^{j\phi_{WP,DS}}) - \frac{I_{b,DS}}{I_{b,ST}} \cdot I_{WP,DS} \quad (2.13)$$

$$I_{WP,DS} = \frac{\rho_{WP,DS,r}}{\eta_{Tr/Ld,DS}} \cdot e^{j\phi_{WP,DS}} . \quad (2.14)$$

Neglecting the system load impedances $Z_{Ld,ST}$ and $Z_{Ld,DS}$ but considering any ‘intermediate’ current injection from WPPMs, then (2.4) gives for multi-level active distribution systems

$$\Delta V_{Flt,ST} = \left[\frac{Z_{TS} \cdot Z_{Flt}}{Z_{TS} + Z_{Flt}} + Z_{ST} \right] (I_{WP,ST} + I_{WP,DS})$$

$$\Delta V_{Flt,DS} = \Delta V_{Flt,ST} + Z_{DS} \cdot I_{WP,DS} .$$

Placing (2.5), (2.8)–(2.10), and (2.11)–(2.12) into (2.4) gives

$$\Delta V_{Flt,ST} = \left[\underbrace{\frac{(V_{TS})^2}{S''_{k,TS}} + \frac{1}{n_{Tr,ST}} \cdot (Z_{Tr,ST} + Z_{Ln,ST})}_{1^{st} \text{ term}} \right] \cdot \frac{\rho_{WP,ST,r}}{\eta_{Tr/Ld,ST}} \cdot e^{j\phi_{WP,ST}} \quad (2.15)$$

$$\Delta V_{\text{Flt,DS}} = \Delta V_{\text{Flt,ST}} + \frac{1}{n_{\text{Tr,DS}}} \cdot \left(Z_{\text{Tr,DS}} + Z_{\text{Ln,DS}} \right) \cdot \frac{\rho_{\text{WP,DS,r}}}{\eta_{\text{Tr/Ld,DS}}} \cdot e^{j\phi_{\text{WP,DS}}} . \quad (2.16)$$

The latter can be further simplified as follows. For ‘strong’ transmission systems, the 1st term in (2.17) is ≈ 0 . It is also assumed that $\phi_{\text{DS}} \approx \phi_{\text{ST}}$ —which is reasonable for MV networks only but not so much for LV networks—hence $\phi_{\text{WP,DS}} \approx \phi_{\text{WP,ST}}$. A special case is considered where $\rho_{\text{WP,ST,r}} = \rho_{\text{WP,DS,r}}$ —i.e. all WPPMs installed at DS level and as many equivalent DS networks as required to reach the same penetration value in the ST network—hence $S_{\text{b,ST}} = S_{\text{b,DS}}$. Then (2.17) and (2.16) can be combined into the final result of:

$$\Delta V_{\text{Flt,ST}} = \left[\left(Z_{\text{Tr,ST}} + Z_{\text{Ln,ST}} \right) + \left(Z_{\text{Tr,DS}} + Z_{\text{Ln,DS}} \right) \right] \cdot \frac{\rho_{\text{WP,DS,r}}}{\eta_{\text{Tr/Ld,DS}} \cdot n_{\text{Tr,DS}}} \cdot e^{j(\phi_{\text{WP,DS}} + \phi_{\text{DS}})} \quad (2.17)$$

with

$$n_{\text{Tr,ST}} = n_{\text{Tr,DS}} = \max_I \left(\left[\frac{\rho_{\text{WP,DS,r}} - \gamma_{\text{Ld}}}{\langle \cos(\phi)_{\text{DS}} \rangle \cdot \eta_{\text{Tr/Ld,DS}}} \right] \right)$$

Typical values for the impedances in (2.17) are given in table 2.2. It is assumed that the line impedances comply with the network planning criteria in order to maintain voltage quality. In this special case where $\phi_{\text{DS}} \approx \phi_{\text{ST}}$, the maximum voltage support $\Delta V_{\text{Flt,max}}$ is achieved when for the phase angle holds $\phi_{\text{WP,DS}} = -\phi_{\text{DS}}$.

Table 2.2: Typical values for the impedances in (2.17)

Impedance	Typical value [p.u.]
$Z_{\text{Tr,ST}}$	0.12
$Z_{\text{Ln,ST}}$	0.05*
$Z_{\text{Tr,DS}}$	0.12
$Z_{\text{Ln,DS}}$	0.04*

*Note: these values are based on network planning criteria, in order to maintain voltage quality.

Based on the values given in table 2.2 and $\gamma_{\text{Ld}} = 0.5$, $\eta_{\text{Tr/Ld,DS}} = 0.6$, then Fig. 2.8 gives exemplary results for I_{WP} , ΔV_{FltWP} , and n_{Tr} as a function of the rated penetration level $\rho_{\text{WP,DS,r}}$. Note that I_{WP} is given on the base of total transformer rating $I_{\text{b,DS}} = n_{\text{Tr,DS}} \cdot I_{\text{Tr,DS,r}}$ and it is assumed that the current injection by the WPPMs is limited to their rated current $I_{\text{WP,r}}$.

It can be seen that the number of transformers is upgraded only when the penetration level $\rho_{\text{DG,DS,r}}$ exceeds 210%. Just before this first transformer upgrade, the voltage support reaches its highest effectiveness of $\Delta V_{\text{FltWP}} \approx 0.4$ p.u.. Whenever an additional transformer is added, the effectiveness is reduced significantly due to the step-wise decrease of that

impedance. For very high penetration levels, the current injected by the WPPMs is approaching a value of 1 p.u. on the total transformer's rated current base $I_{b,DS}$. The reason is that the active distribution system is being more and more transformed into a collecting network that exclusively exports the WPPMs power. At these penetration levels, the voltage support is approaching a value of $\Delta V_{FitWP} \approx 0.33$ p.u..

The relationship between the effectiveness of fast voltage control and network extension is presented in Figure 2.8 as a function of the rated penetration level $\rho_{WP,DS,r}$. A major assumption in the derivation of this relationship was to neglect the system load impedances $Z_{Ld,ST}$ and $Z_{Ld,DS}$. Considering these load impedances at different voltage levels in the system would likely reduce the effectiveness of a fast voltage control compared to the values shown in Fig. 2.8. Furthermore, the assumption that WPPMs would inject rated current $I_{WP,r}$ to support the distribution system voltage only holds for predominantly inductive systems. For these systems, priority would be given to reactive current injection which is independent from a WPPM's available wind resource. Especially for distribution-connected WPPMs where the X/R ratio at the PCC was smaller than one and a combined additional reactive/active current injection would support the voltage better than a pure additional reactive current injection, the effectiveness of fast voltage control may then be limited by the WPPM's available wind resource. These superimposing factors make it difficult to quantify the relationship between the effectiveness of fast voltage control and network extension as a function of the instantaneous penetration level $\rho_{WP,DS,i}$ in general terms. Eventually, the quantitative results presented in Fig. 2.8 should be regarded as the upper boundary of expected effectiveness of fast voltage control.

From the derivation of the fundamental relationships and calculations this exemplary calculation it can be concluded that the voltage support is highest for rated penetration levels that result into a maximum reverse power flow but do not yet trigger distribution network extensions. A voltage support from DS level connected WPPMs of more than 0.3 p.u. to 0.4 p.u. should not be expected as long as the existing network planning criteria are applied. Voltage support for similar values of instantaneous penetration levels are expected to be smaller than the ones presented here for rated penetration levels.

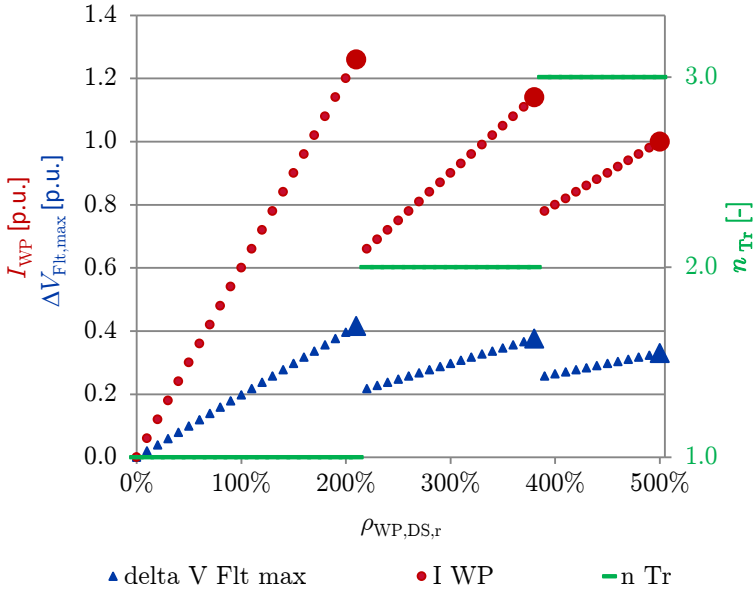


Figure 2.8: Relationship between the effectiveness of fast voltage control and network extension under the assumptions outlined in the text

2.5 Conclusions

The impact of distributed generation (DG) on transient stability, large disturbance voltage stability, and frequency stability has been investigated in the literature extensively. It was found that this impact is influenced by five factors, of which the network fault response related protection and control with their respective parameter settings are the most important ones. These are stipulated in grid connection requirement.

The existing grid connection requirements (GCRs) for distributed generation have been developed under the implicit assumption of a ‘strong’ transmission system. The massive insertion of DG into distribution systems leads to new challenges like the regular occurrence of reverse power flow (RPF) situations from the distribution to transmission level, the potential increase of the inductive reactive power demand when DG control their terminal voltage, and local stability problems with the connection of DG to ‘weaker’ points of common coupling (PCCs). With DG being located very close to the loads, it is also more likely to be exposed to fault-induced delayed voltage recovery (FIDVR) events^{A.13} than transmission and sub-transmission connected generating facilities. Hence, nowadays GCRs may have undergone insufficient technical impact assessment for these new system conditions.

Furthermore, common practices among distribution system operators, like the ones in Germany, do often not exploit the full potential of the existing GCRs. For example, the majority of the MV connected WPPMs are required to ride through voltage dips in blocking mode although modern WPPMs are capable of a LVRT with additional reactive current injection.

Even though the effectiveness of disturbance voltage support at distribution system level is limited by basic circuit theory, as it was shown in the last part of this chapter, its potential opportunities and challenges deserve further investigation for power systems with very high penetration of distributed generation.

Chapter 3

Modelling of System Elements

This chapter describes the power system element models used throughout this thesis. It reviews the state of the art and specifies model types, parameters and major assumptions taken. A comprehensive methodology of distributed generation (DG) aggregation and dynamic equivalencing is proposed to derive highly accurate, equivalent dynamic models of active distribution systems (ADSs). The contribution of this chapter is to define the minimum level of detail that is necessary to accurately model ADSs in bulk power system stability studies with very high penetration of DGs (i.e., more than approx. 50 % system-wide instantaneous penetration, regional reverse power flows from distribution to bulk system level). The proposed methodology considers the ADSs' composition of DG classes not only in terms of technology but also grid connection requirement (GCR) performance.

The methodology presented in this chapter can inform ongoing activities in a IEEE/PES/PSDP Task Force that seeks the contribution of DG connected at the distribution network to the control and stability of the bulk transmission system [IEE14b]. It can also inform ongoing activities in CIGRÉ JWG C4/C6.35/CIREN that strive for recommendations on developing equivalent dynamic electrical simulation models of clusters of same and different types of DG technologies [YC13].

The methodology presented was developed under the umbrella of a research project [Del14] by the German Forum network technology / network operation in the VDE (FNN). It can serve as a practical guideline for transmission system planning engineers as well as software vendors to include modular ADS elements into their planning tools. The proposed method has also been successfully applied for dynamic stability analysis of the German power system considering all voltage levels [AW15].

3.1 Introduction

Modelling modern bulk power systems with a detailed dynamic representation of a large number of DGs at distribution system level would increase the complexity and dimension of stability models beyond practical limits in terms of computational time, operability, and data availability [RMM13]. Therefore, a certain degree of simplification is needed. Defining the best trade-off between model accuracy and simplicity calls for deriving a thorough understanding of the critical success factors for derived equivalent models of ADSs.

One of these success factors is the accurate representation of the dynamic behaviour of ADSs in the *periphery region* (annulus) of a voltage funnel^{A.14} at transmission system level. Here, the retained voltage is very close to the undervoltage protection threshold of DG, see Fig. 3.1.

The annulus can have a very large geographic extension. The number of DG units in the annulus can be very large compared to the number of DG units that will obviously trip because they are located near the fault.

The accurate modelling of the voltage contour that delineates all system nodes where the retained voltage is smaller than the DG's undervoltage protection threshold will determine significantly the bifurcation point of the system-wide stability response: the aggregate MW-value of DG units that trip (power at risk) will be quite sensitive in high DG penetration scenarios to the modelling assumptions, network representation, and network fault response of individual DG units.

The dynamic behaviour of DGs, e.g., the (in-)capability for low voltage ride-through (LVRT) and full dynamic voltage support, significantly influences the voltage values at DG terminals at distribution system level. As illustrated in Fig. 3.1, the post-fault active power imbalance due to undervoltage tripping of DG will be larger in the case shown in subfigure 3.1a than in the case shown in subfigure 3.1b.

Without the right minimum level of modelling detail for the ADSs models and their included DGs, DG power at risk would be easily over- or underestimated.

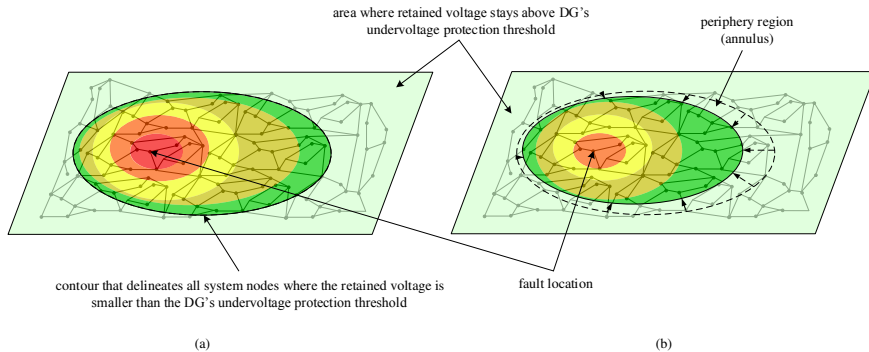


Figure 3.1: Voltage funnel with periphery region (annulus)

3.2 DG models

For power system dynamic studies, explicit distributed energy resource (DER) models determine the *performance details* for the network fault response of specific DERs technology classes.

After almost a decade of scientific research and discussion on wind turbine generator (WTG) models [P6l03,NWJ03,SHPK03] and [CIG07,EI109,WEC10], common agreement on generic models of WTG suitable for power system stability studies has been reached in [IEC15].

Generic stability models of photovoltaic (PV) systems have not yet been standardised at IEC level but are still under scientific debate. Various generic PV models have been pro-

posed, among others in [SED⁺12, NE12, YDG⁺11, NP14]. Reaching consensus is getting closer with notable publications like [WEC11, WEC12, FGW14]. Accurate modeling of undesired behavior such as tripping of single-stage PV systems at fault clearance as reported in [Kob12] needs further research.

Modelling of large-scale directly-coupled synchronous generator (SG) and their excitation systems in power system stability studies is a well-known exercise for which widely accepted recommendations exist [Kun94, IEE06]. Modelling of medium to small-scale, low-inertia, distributed combined heat and power (CHP) plants is a less investigated field [Cos10] although some older publications exist [EDML00, Gut02, TQLA⁺06]. A relevant publication from recent years, [Kli09], models the network fault response of a medium-scale diesel-driven synchronous generator.

The following sections describe in more detail how the various DGs are modelled in this thesis.

3.2.1 Wind power generating facilities

Positive-sequence, fundamental frequency, rms models are used to simulate the dynamic behaviour of the wind power park modules (WPPMs) in the time domain. The WPPM models used in this study are based on standard PowerFactory models [DIg11b], [DIg11a]. The models are capable of capturing system behaviour in the stability time frame, with the aim of identifying transient and voltage instability issues. Further details on the WPPM models can be found in appendix C.2. Two types of wind turbines are used:

- Full converter interface units (FCs)
- Doubly fed asynchronous generators (DFAGs)

For the study performed in chapter 5, turbines of both types have the same rating within each voltage level, and if possible there are equal amounts of DFAG and FC generators in the system. In case of an uneven number of turbines, the remaining turbine is a FC. On the MV level, the realistic size of a wind park was used as installation size (5 MW). These wind parks are represented by two 2.5 MW turbines.

Full converter interface unit

These models are used for the studies described in chapter 4 as well as in chapter 5.

The WPPM models are generic models of type 4 wind turbine generators included in the DIgSILENT PowerFactory software package [DIg11b]. The control systems of the full converter have been extended with additional LVRT control modes.

Doubly fed asynchronous generator

These models are used only for the study described in chapter 5.

The WPPM models are generic models of type 3 wind turbine generators included in the DIgSILENT PowerFactory software package [DIg11a]. The control system of the doubly fed asynchronous generator have remained unchanged.

WPPM operating mode

The response of the WPPM is studied by considering different settings for the operating modes in the pre-fault, fault, and post-fault period. A state machine determines which operating mode is active at a certain moment and a set of rules specifies the transition between the states. In order to design a control mode that is robust for a wide range of pre-fault power flow situations as well as variations of control parameters, the control characteristics, parameters, and transition rules are identified based on some theoretical considerations. The state diagram presented in Fig. 3.2 summarises the states and transition rules of the control systems for an LVRT with blocking mode and an LVRT with fast voltage control. Details and justifications are given below.

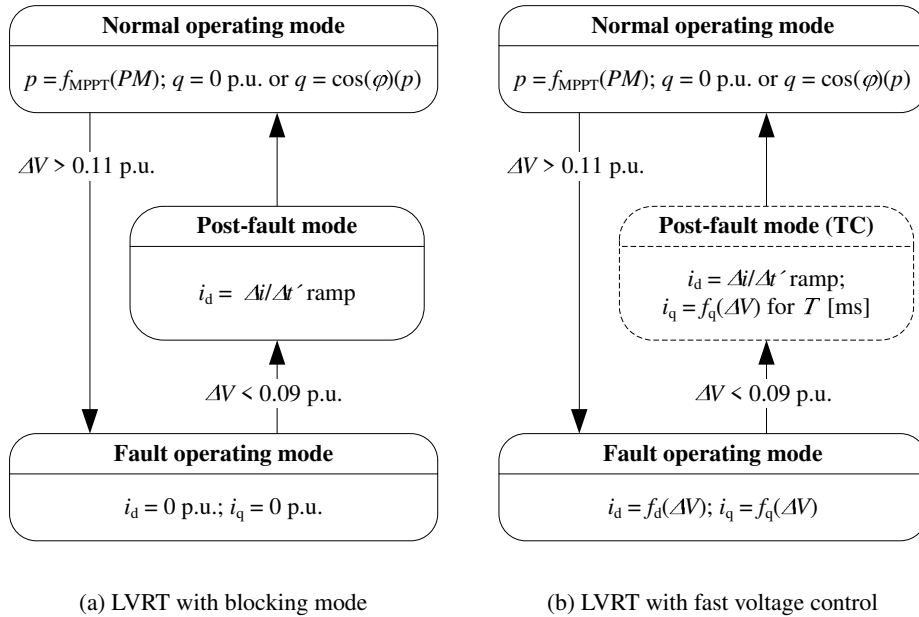


Figure 3.2: State diagram with used operating modes and transition rules. Notes: lower case quantities in per unit value on machine base, dashed post-fault state only in TC mode. Abbreviations: maximum power point tracking (MPPT), prime mover (PM).

—*Pre-fault period*— The GCR for the quasi-stationary voltage control determines pre-fault the operating point of a WPPM in normal state. In this thesis, the following two control modes based on the German GCR [BDE08, For11] are investigated:

- a fixed power factor $\cos(\varphi) = 1$;
- a variable power factor/active power characteristic curve $\cos(\varphi) = f(P)$, see Fig. 2.3 in section 2.3.3.

In the $\cos(\varphi)(P)$ control mode, WPPMs operate in underexcited mode whenever their active power output exceeds 0.5 p.u.. The exchange of inductive Vars with the network

requires the reactive power to be generated at higher voltage levels. This causes substantial additional reactive power flows. Depending on the voltage control scheme of the distribution system, this changes the initial transformer tap-changer positions pre-fault.

—**Fault period**— The transition from normal to fault operating mode occurs when the voltage deviation at the WPPM terminals ΔV is larger than 0.11 p.u. In fault mode, the performance is determined by the functions $f_d(\Delta V)$ and $f_q(\Delta V)$. These functions vary for different GCRs and are not necessarily exhaustively defined. In the following, three different fault modes will be tested:

- blocking mode (BM): a common distribution system operators (DSOs) practice fault mode labelled ‘blocking mode’ during which the set-points for \underline{I}_d and \underline{I}_q are set to zero;
- additional reactive current injection (aRCI): a state-of-the-art fault mode with two variants for fast voltage control according to TransmissionCode (2007) [Ver07] or SDLWindV (2009) [Ger09]; and
- additional reactive/active current injection (aRACI): a new fault mode that combines a voltage-dependent active current reduction as proposed in [ESE⁺09] and recommended in [Wei13b], and a reduced voltage deadband as suggested in [For13].

The fast voltage control of the state-of-the-art fault mode variants is realised by an aRCI. The function $f_d(\Delta V)$ is fully specified by (3.1) and the function $f_q(\Delta V)$ depends on the current limitation strategy etc. The additional reactive current $\Delta \underline{I}$ is added to the pre-fault 1-minute-average current value \bar{I}_0 ($T = 1$ min). Further details are given in appendix C.1.2.

$$\underline{I}_{\text{Flt}} = \bar{I}_0 + \Delta \underline{I}(\Delta V) \quad (3.1)$$

with

$$\Delta \underline{I}(\Delta V) = e^{j(\phi_G + \frac{\pi}{2})} \cdot \begin{cases} 0 & , |\Delta V| \leq V_{\text{DB}} \\ k_{\text{RCI}} \cdot [\Delta V \mp V_{\text{DB}}] & , |\Delta V| > V_{\text{DB}} \end{cases}$$

$$\Delta V = V - \bar{V}_0$$

$$\bar{I}_0 = \frac{1}{T} \int_{t'-T}^t \underline{I}(t') dt'$$

$$\bar{V}_0 = \frac{1}{T} \int_{t'-T}^t V(t') dt'$$

—**Post-fault period**— The transition from fault to normal operating mode occurs when the voltage deviation at the WPPM terminals ΔV is smaller than 0.09 p.u. Whether or not a specific post-fault mode is used, depends on the respective grid connection requirements (see Fig. 3.2):

- Cease the reactive current injection after the clearance of a fault has been detected (SDLWindV 2009 mode) or continue it for a time T (TransmissionCode 2007 mode), here $T = 500$ ms;
- Restore the active power instantly after the clearance of a fault has been detected (SDLWindV 2009 mode) or restore it with a delay, e.g. with a pre-defined linear ramp of $\Delta i/\Delta t'$ (blocking mode and TransmissionCode 2007 mode), here $\Delta i/\Delta t' = 2$ p.u./s.

The setting of $\Delta i/\Delta t' = 2$ p.u./s chosen for the post-fault active power ramp in the blocking mode and TransmissionCode 2007 mode restores the active power ten times faster than it is required in the respective GCRs [Ver07]. This is motivated by the relatively small inertia of the test system and allows for scaling the time axis of the result figures to a few seconds.

Grid code performance classes

In compliance with table E.10, all MV WPPMs are able to ride through faults. They however do not provide full dynamic support, i.e. they do not inject additional reactive current during the fault.

Installation capabilities depend on historic installation dates and the upgrading of turbines which has taken place as a result of the ‘SDL-bonus’ [EDBI13] (see appendix E.2.2). With the exception of the oldest turbines in the HV network, all machines have LVRT capability. The old turbines use an undervoltage relay that disconnects them from the network 100 ms after the voltage has dropped below 0.8 pu.u. Table 3.1 gives an overview of the naming convention and characteristics of the wind turbines used in the test system.

	Type	PF control	LVRT capability	aRCI capability and P recovery
MV	LVRT	dynamic	yes	no
	NEW	dynamic	yes	yes, no
HV	OLD	constant	no	no
	EEG	constant	yes	yes, acc. [Ver07]
	SDL	constant	yes	yes, acc. [Ger09]
	NEW	constant	yes	yes, acc. [Ger09]

Table 3.1: Wind turbine types.

3.2.2 Photovoltaic power generating facilities

The PV model used in this thesis is based on the stability-type (root mean square (rms)) model described in [SED⁺12]. The model was validated in comparison with an PSCAD instantaneous-values (electro-magnetic transient value (emt)) model. The PLL algorithm and the MPPT are included in the original model, as well as active and reactive power control.

To simplify the PV model, the DC link dynamics are removed and the DC voltage is kept at a constant value. This simplification is reasonable for the stability-type simulations and time-frame considered in this thesis.

The PV model has four types of network fault control as shown in the state diagram of figure 3.3. The nLVRT and three LVRT modes are described below. Mathematical descriptions of the control modes are provided in appendix C.1.

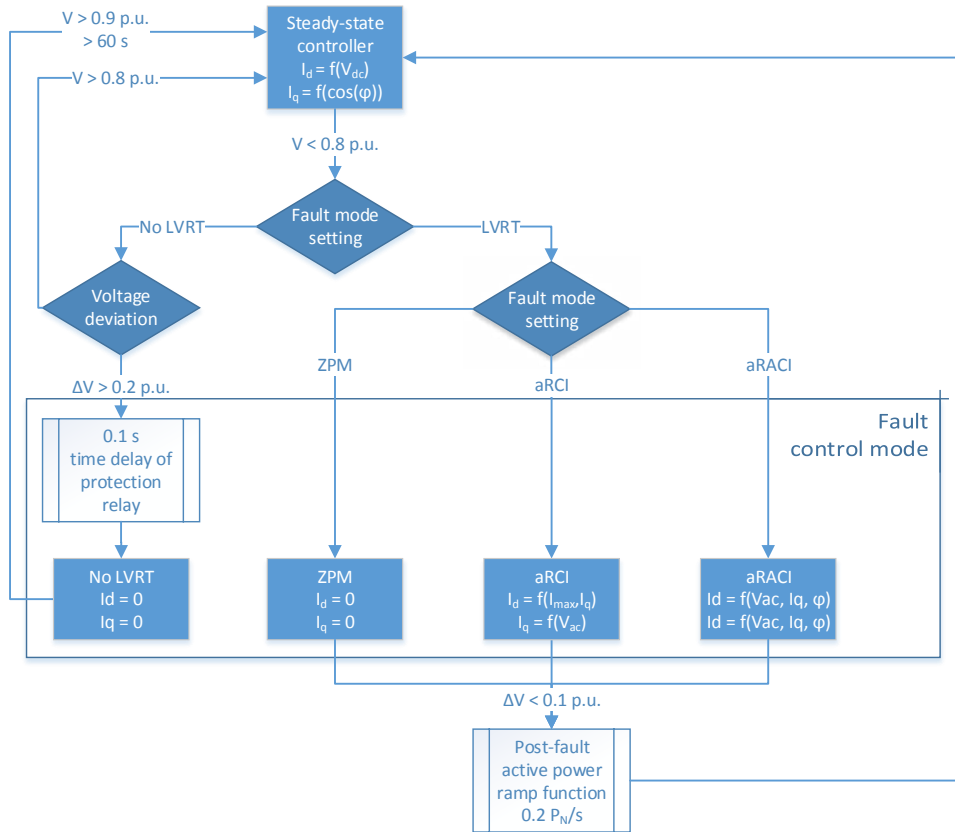


Figure 3.3: State diagram of PV system control [Ska14]

No low-voltage ride through

The nLVRT control mode reflects the status quo. In this control mode, PVs disconnect when the voltage drops below 0.8 p.u. (see section 2.3). GCR demand that the PVs disconnect within 200 ms. To comply with this requirement, the relay opens 100 ms after the voltage drops below the threshold. If the voltage returns above the threshold and stays there for 60 s, the PVs reconnect. This mode represents the current practice.

Figure 3.4a shows the PV behaviour with nLVRT mode during a fault (i_d current in red, i_q current in blue). The fault occurs at 0 s, and the PV disconnects 100 ms later.

Blocking mode

In BM, the PV system remains connected to the system, but stops exchanging any (active or reactive) power with the network as soon as possible after a fault is detected. This behaviour does not interfere with the protection schemes that are implemented in the distribution networks. As soon as the voltage at the PCC is restored, power infeed is restored.

Figure 3.4b shows the i_d and i_q currents for the BM. When the fault occurs at 0 s, both currents are driven to zero. They stay there until the fault is cleared and voltage is restored. At fault-clearance, there is a spike in the i_q current as the controller switches operation mode, and the pre-fault operating point is restored with a delay. As per GCR, the delayed active power recovery (dAPR) post-fault occurs at 20 percent of rated power per second. The reactive power follows later, according to the reactive power characteristic. It should be noted that due to the lack of relay response time, the BM reaches zero power output much quicker than the nLVRT mode.

Additional reactive current injection

The aRCI mode actively aims to raise the voltage during the fault by injecting additional reactive current into the network. This injection of additional reactive current during a fault was introduced in the MV network in [BDE08]. Since HV and MV networks tend to have low R/X ratios, reactive current has the strongest impact on voltage. The additional reactive current infeed is achieved by adding an additional reactive current component to the pre-fault operation point. Equations are given in appendix C.1.2.

Figure 3.4c shows that at the occurrence of the fault, the converter starts injecting reactive current instead of consuming it. When the fault is cleared and voltage is restored, the pre-fault operating point is restored.

Additional reactive & active current injection

The last network fault control mode is the additional reactive & active current injection (aRACI) mode. Its operation is similar to the aRCI mode, but adds an additional active current injection component. In the LV networks, R/X ratios are usually higher than in the higher voltage levels. This means that active power has a larger effect on voltage in the LV network than it does elsewhere. The angle at which the additional current is injected is adjustable. In this thesis the angle is set at the impedance angle at the point of common coupling (PCC). Equations are found in appendix C.1.3.

Figure 3.4d shows how during the fault, less reactive current is injected into the network than in the aRCI case. It also shows clearly the additional injection of active power during the fault.

Table 3.2 gives an overview of the naming convention and the characteristics of each PV installation type present in the test system.

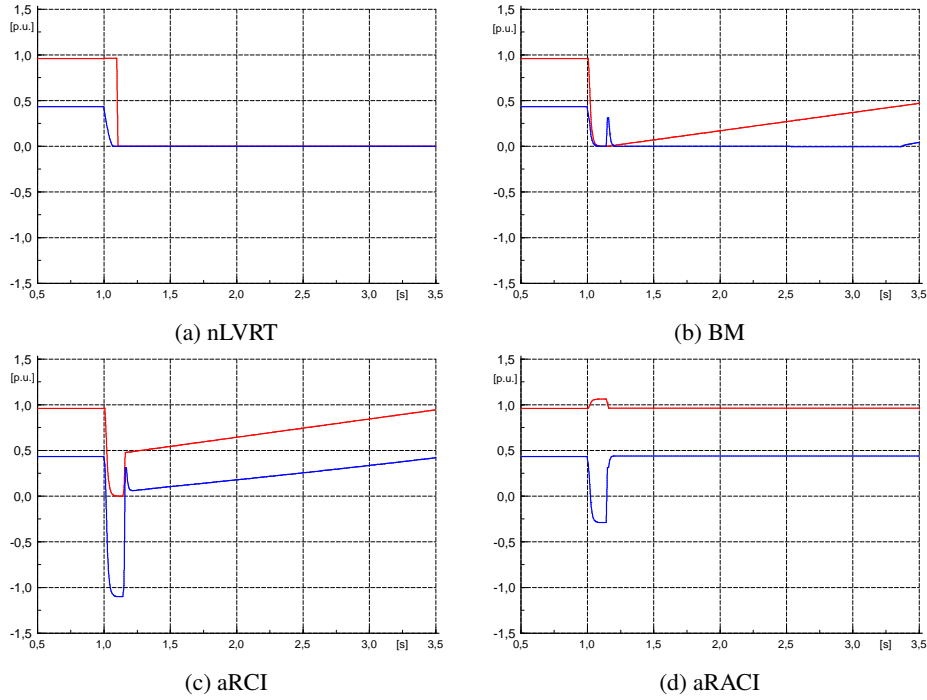


Figure 3.4: 2022 LV connected PV fault control modes (active power infeed to network is positive, capacitive reactive power infeed to network is negative).

	Type	PF control	LVRT cap- ability	aRCI capability and P recovery
LV	PF100	constant	no	no
	PFPOW	dynamic	no	no
	NEW	dynamic	yes	yes, $P_{rec} = 20\%/s$
MV	PF100	constant	no	no
	LVRT	dynamic	yes	no, $P_{rec} = 20\%/s$
	aRCI	dynamic	yes	yes, $P_{rec} = 20\%/s$
	NEW	dynamic	yes	yes, $P_{rec} = 20\%/s$

Table 3.2: PV system types.

3.2.3 Micro-CHP generating facilities

Modelling of large-scale directly-coupled SG and their excitation systems in power system stability studies is a well-known task for which widely accepted recommendations exist [Kun94, IEE06]. Modelling of medium to small-scale, distributed and mostly CHP plants, however, is a less investigated field [Cos10] although some older publications exist [EDML00, Gut02, TQLA⁺06]. Relevant publications from recent years are notably [Kli09, Erl13].

In this study, all CHP generators are modelled as directly coupled synchronous generators. The dynamic model developed by Coster (2010) is used [Cos10], which includes a governor and an automatic voltage regulator (AVR). These are modelled with standard DEGOV1 and EXAC1A respectively. Due to the time frame of interest, the governor is deactivated in the simulations, i.e. the prime mover stays constant. Generator parameters are taken as much as possible from commercially available machines with ratings close to the used generator ratings. Detailed non-standard parameters can be found in appendix C.4.

Table 3.3 lists the power factor control and LVRT capabilities of the CHP models which are later used in the test system presented in chapter 5.2.4. Only the latest and future CHPs installed at the MV level have LVRT capability. These generators do not have an undervoltage protection, but care must still be taken so that they do not become transiently unstable. To this end, a simple out of step (OOS) relay model was developed. The model allows for the disconnection of a generator when the voltage angle between the generator and its PCC becomes too large. The tripping angle is set to 120 degrees, because early simulations showed that generators become unstable shortly after this angle is reached.

All other CHP types use the same undervoltage protection as the photovoltaic power park modules (PVPPMs) and WPPMs without LVRT capability. A voltage drop below 0.8 p.u. at the PCC causes disconnection of a CHP 100 ms later.

	Type	PF control	LVRT capability
LV	PF100	constant	no
	NEW	constant	no
MV	PF100	constant	no
	PF095	constant (=1)	no
	LVRT	constant	yes
	NEW	constant	yes
HV	PF100	constant	no

Table 3.3: CHP installation types.

3.3 Load models

The importance of load behaviour in identifying the correct dynamics for the voltage recovery after network faults is well known [Nav05]. Therefore, two different load models are used in the analysis. The static load model considers the voltage and/or frequency at any

point in time to determine the active and reactive power consumption at that instant. The dynamic load model also takes into account the time history of voltage and/or frequency and is, therefore, a state-space model.

The static part of the load is represented in the exponential form, see equations D.1 and D.2 in appendix D. A voltage deviation causes a change in power from the initial value. The parameter values used in the test system are listed in table D.1 in appendix D. With the exponents chosen as $e_{aP} = e_{aQ} = 2.0$, the static part effectively becomes a constant impedance load model. Because no representative data was found for the frequency dependency of the loads, this dependency is ignored.

The dynamic part of the load is either represented in a simplified way in the DIGSILENT general (composite) load model [DIg08] with a linear representation or in a more detailed way by a standard single cage induction motor model [DIg12a] and a motor-driven machine model [DIg12b]. See equation D.3 in appendix D for the torque-speed characteristic. Parameters are given in tables D.2 and D.3 in appendix D. The time constant for the simplified linear dynamic loads is chosen to be 0.1 s.

3.4 Aggregation and Equivalencing of DG

The review of existing models of DERs shows that a number of sophisticated stability models are available for WPPMs, PVPPMs and CHP plants. However, modelling modern bulk power systems with a detailed dynamic representation of a large number of DERs at distribution system level would increase the complexity and dimension of stability models beyond practical limits in terms of computational time, operability, and data availability [AE04, RMM13]. Therefore, a certain degree of simplification is needed.

Defining the best trade-off between model accuracy and simplicity calls for deriving a thorough understanding of the critical success factors for derived equivalent models of ADSs.

3.4.1 State of the Art

Until a few years ago, only little research has been published on dynamic equivalencing of stability models of active distribution systems that comprise significant amounts of DERs [BGK09]. Notable publications in early years were [MWA01, AE03, MY03, GILM03, PHS05]. Publications from recent years include an analytical method of equivalencing the collector system of large DERs [MBE⁺06, SKMC14] into a single equivalent impedance, an analytical system reduction method of distribution systems with PV systems for transient stability studies [CTN⁺14] and a reduced stability model of DERs in distribution systems considering partial loss of DER in-feed [SKN⁺10, WEC12] as well as a CIGRÉ Technical Brochure on the development and operation of ADSs [CIG11]. Parallel informative activities have been performed in the field of microgrids as summarised in [Ce14, RL07].

An ‘equivalent impedance’ can be used to represent the propagation of a voltage dip from the transmission to the distribution level [WEC11]. This voltage difference is dependent on multiple factors, including the types of ADSs (rural, suburban, urban, residential, commercial, industrial, etc.), the dominant type of DERs (solar PV, CHP, etc.), spatial distribution of DERs and loads along a given distribution feeder as well as the highly non-linear nature of the DERs responding to voltage a voltage dip (undervoltage tripping of ‘legacy’ DERs versus modern DERs with LVRT and dynamic reactive support (DRS), etc.). The

equivalent impedance can, therefore, not be computed analytically as it was possible in the simpler case of a collector system in [MBE⁺06] or when DERs tripping and DRS were neglected as in [CTN⁺14]. It may rather be determined by the use of parameter identification techniques based on dynamic simulations. While the existing literature suggests some default values for equivalent impedances (see top line of Table 3.7), a systematic analysis that derives values to adequately model the weighted average voltage difference between a substation and the terminals of all DERs located in different types of ADSs is missing.

Western Electricity Coordinating Council (WECC)'s distributed PV model does model the uneven voltage dip propagation in an ADS by use of a special protection block but it is currently not widely applied in the practice and lacks further validation.

Publication [RMM13] summarizes the state of the art for the application of dynamic equivalencing methods to derive aggregated models of ADSs: Classic approaches such as modal analysis and coherency based methods [IMK07, FLB07] are nowadays regarded as unsuitable for this exercise. Modal analysis is based on linear models that cannot adequately capture nonlinear power system dynamics following major disturbances, e.g. network faults. And coherency based methods are restricted to conventional power systems, comprised of a number of large-scale synchronous generators that are concentrated within a few areas. Instead, nonlinear system identification techniques in measurement based approaches have shown promising results with artificial neural networks (ANNs) being the most prevalent method, as for example used in [AE04]. Such black box modeling based on artificial neural networks is applicable especially when physical insights are too limited for selecting a suitable model structure based on physical insight. But training an ANN can be very time consuming.

Therefore, a consensus is evolving that grey box modelling is recommended for equivalent modelling of ADSs when sufficient physical knowledge is available [RMM13]. Not only the computational challenges are significantly reduced but these composite models can also be easily integrated in dynamic simulation tools.

3.4.2 Limitations of existing approaches

The review of the state of the art shows that stability models for different DERs technologies are available and that these can accurately model the evolving grid code (GC) related performance requirements. Further research, however, is needed to enhance existing grey box model structures and parameter identification techniques as proposed and validated in [MM13a, MM13b] by explicitly considering the ADS's composition with regard to the grid code related performance framework and the explicit modeling of the low voltage (LV) and medium voltage (MV) equivalent impedances. The methodology described in this chapter is intended to fill these gaps.

3.5 Proposed Methodology

3.5.1 Overview

Figure 3.5 gives a high-level overview on the proposed six-step methodology to derive validated equivalent models of ADSs. This approach is limited to networks that are radially operated (unmeshed) such as LV and MV networks and should not be used for meshed high

voltage (HV) networks. After defining a set of representative inputs and assumptions, *detailed* ADS models are created bottom-up (1). An *equivalent* ADS model is then constructed by clustering of DERs which are represented by equivalent generator models including their control systems (2). The equivalent impedance is then estimated based on the input data (3) and iteratively adapted until the equivalent ADS performance is satisfactory (4).

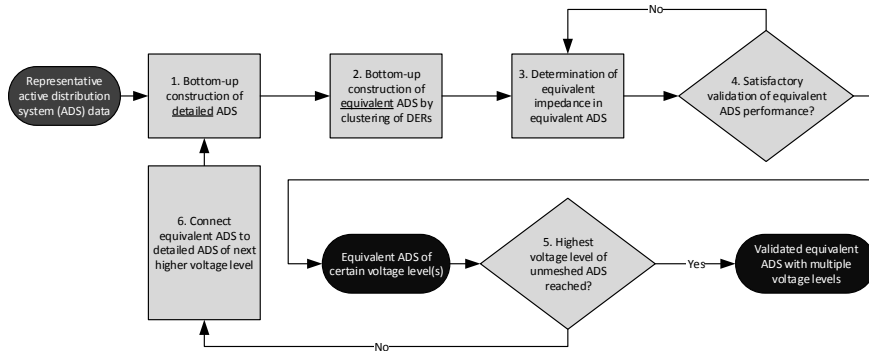


Figure 3.5: Overview on the proposed six-step methodology to derive validated equivalent models of ADSs

The dynamic ADS equivalent of each voltage level is validated against its corresponding detailed ADS model with time-domain simulations for a number of relevant voltage dips resulting from short-circuits in the bulk power system. Validation for other kind of responses can be performed as needed. As long as the highest voltage level, below which all networks are operated radially (unmeshed) is not reached (5), the obtained equivalent ADS is connected to the detailed model of the ADS of the next higher voltage level (6). This bottom-up approach is repeated until a validated equivalent ADS with multiple voltage levels is obtained.

3.5.2 Inputs and assumptions

Figure 3.6 gives a more detailed insight into the required inputs and assumptions to create the detailed ADSs models.

—Analysis of existing datasets and information— Datasets of structural information on the existing DERs in the power system are used to derive technology classes, DER rated capacity classes, connection point classes (voltage level, substation or feeder) and commissioning dates.

The relevant past and present GCs are differentiated regarding the voltage level or DER rated capacity they are applicable to, and their dates of entry into force. To these classes the corresponding requirements for normal operation (e.g., quasi-stationary voltage control, see Fig. 3.7) and fault operation (e.g. LVRT, aRCI, and post-fault real power recovery, see Table 3.5 and Fig. 3.11) are attributed.

The quasi-stationary voltage requirements shown in Fig. 3.7 refer to a real power-dependent power factor control [For11] with settings that depend on the DER location in

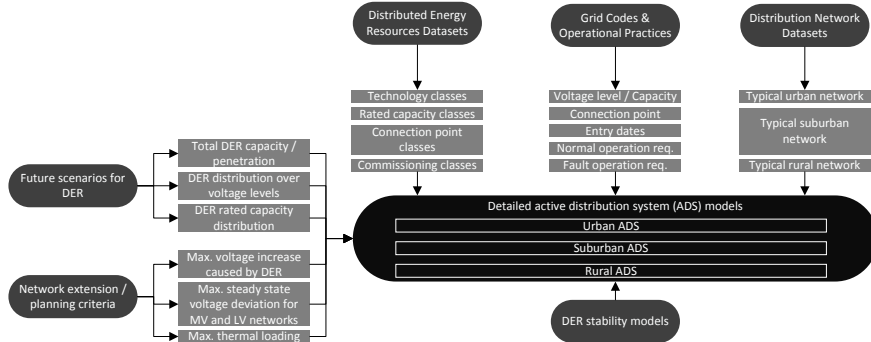


Figure 3.6: Inputs and assumptions for building detailed models of active distribution systems

the network as well as the DER's rated apparent power S_r . They determine the pre-fault operating point of DERs and must be considered.

Distribution network datasets contribute information on network topology and parameters of network elements. The latter comprise line, load, and transformer parameters and also operating data of the transformers' on load tap changers. In order to reduce the number of different distribution networks that have to be modeled, clustering techniques, such as *k-means* may be applied, based on DER penetration [Ger12a], distance between houses and transformer rating [KW08] or other characteristics [CIG14], to derive representative distribution networks, e.g., an urban network, suburban network, and rural network.

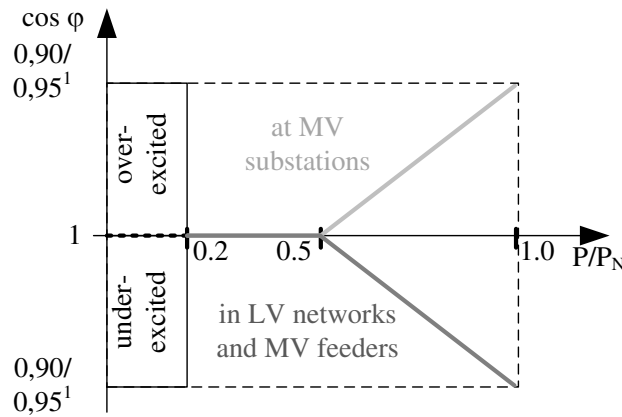


Figure 3.7: Quasi-stationary voltage control requirements [For11].

¹Note: $\cos(\varphi) = 0.95$ applies to DERs with rated apparent power $S_r > 13.8$ kVA and $\cos(\varphi) = 0.90$ applies to DERs with $S_r \leq 13.8$ kVA

—*Definition of future scenarios for DER*— Future scenarios define the technology-specific distribution of new DER capacity among the voltage levels. The system region's *rated* DER capacity $P_{DG,r}$ and the system region's *peak* load $P_{Ld,p}$ determine the system

region's future DERs *rated* penetration level (3.2) per voltage level. Anticipated changes in the typical rated capacity classes may have to be considered as necessary.

$$\rho_{DG,r} = \frac{P_{DG,r}}{P_{Ld,p}} \quad (3.2)$$

—*Network extension / planning criteria*— The future detailed ADSs are extended according to pre-defined planning criteria and voltage quality standards as defined, for example, in [Ger12a, Eur08]. Voltage deviation and quality issues are the primary constraints at distribution level whereas equipment thermal loading is less stringent. The network may have to be reinforced to limit the voltage increase caused by DER to 2–3 % or to keep the steady state voltage deviation caused by MV and LV lines and MV/LV transformers for different generation/load situations below ± 10 %.

3.5.3 Definition of detailed active distribution system models

The detailed ADSs can now be defined based on the previously described inputs and assumptions. If detailed information is missing, individual DER systems that are connected along the feeder are distributed homogeneously among the network (Fig. 3.8a). Each DER system is represented by its own stability model and respective controller for normal and fault operating mode. The transition between the control states is determined by the local voltage at either the point of common coupling (PCC) or generator terminal, depending on the grid code requirement.

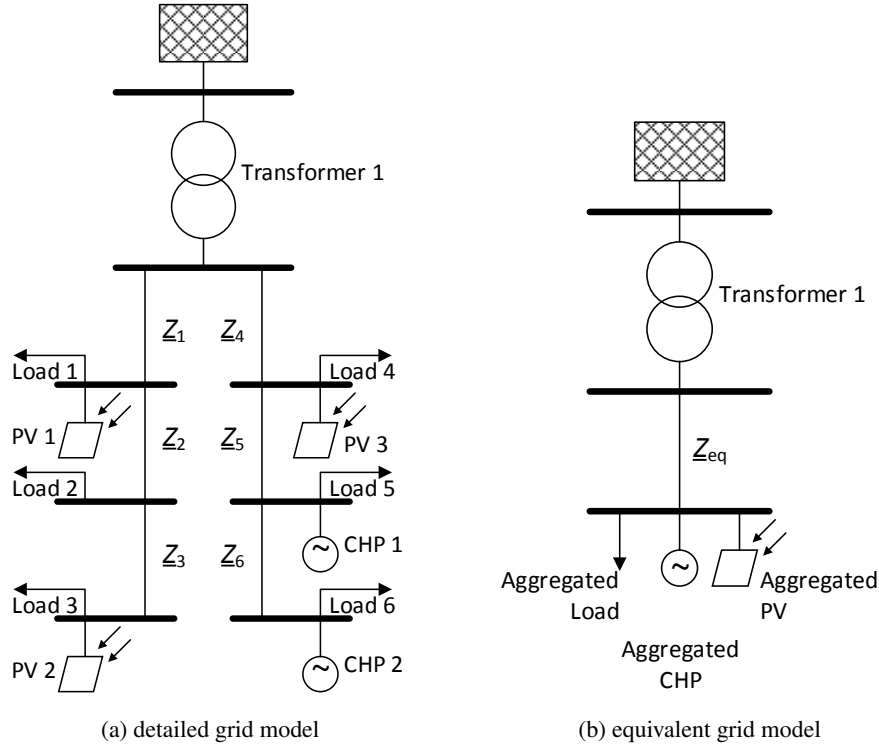


Figure 3.8: Determination of the equivalent distribution network impedance Z_{eq} by clustering of loads and DERs

3.5.4 Definition of equivalent active distribution system model

—*Clustering of loads and DERs*— The loads and DERs of similar class at each voltage level of the network are aggregated behind a single ‘equivalent’ impedance and modelled as described in section 2.3 (Fig. 3.8b). The transformers between the voltage levels are kept unchanged for the equivalent network.

—*Determination of equivalent impedance for each of the voltage levels*— The value of the ‘equivalent’ impedance in Fig. 3.8b represents the lines in the detailed network of a specific voltage level. It is determined by using an optimization based technique such that the equivalent ADS would respond to an *external* network fault similarly to the detailed network model. Optimization techniques, either classical such as the Gauss-Newton method or Levenberg-Marquardt algorithm, or heuristical can be used to minimize the error values for the model validation described in subsection E. In this thesis, the equivalent impedances are determined for a set of typical distribution systems that represent different topologies. Due to the non-linear nature of DG responding to a voltage dip, general rules or analytical calculations cannot be applied for typical distribution systems.

—*Bottom-up construction of multiple voltage levels*— The equivalent ADSs are constructed from the lowest to the highest voltage level:

- An equivalent version of the detailed LV network is constructed and validated (see below);
- In the detailed MV system, the equivalent LV network is used to substitute the original LV (distribution) loads;
- An equivalent version of the detailed MV network (including a single LV network equivalent) is constructed and validated.

The equivalent MV networks are then connected to a HV sub-transmission network. The HV network is not reduced, as this is often a meshed system with multiple connections to the extra-high voltage (eHV) level.

—*Final result*— As the final result, an equivalent model of the ADS with technology and grid code performance related equivalent models of DERs is obtained as illustrated in Fig. 3.9.

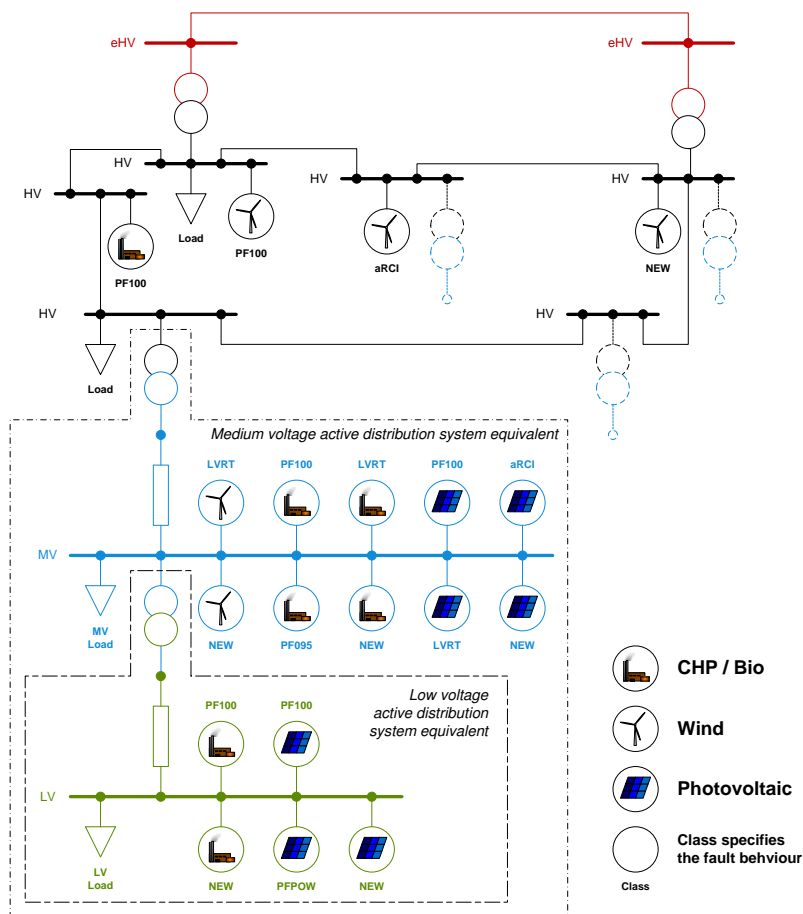


Figure 3.9: Example equivalent model of an ADS comprising of different technology and grid code performance related equivalent models of DERs

3.5.5 Validation method

The response of an ADS equivalent is compared with the response of its detailed representation to a number of *external* network faults. Voltage dips with a retained voltage at the high voltage side of the ADS transformer (i.e. HV/MV transformer for the medium voltage ADS and MV/LV transformer for the low voltage ADS in Fig. 3.9) of $V_{DS} = 0.75$ p.u., 0.5 p.u., 0.25 p.u. and 0 p.u. are recommended to represent a wide range of transmission network faults.

The validation method presented in [FGW14] is used to quantify the accuracy of the equivalent ADSs models for network fault studies. That method is typically used to validate DER stability models against measurements from real machines. Here, the measurement input is replaced by the modeled network fault response of a detailed ADS. Two metrics are used to compare the response of the systems at the high voltage terminal of the respective ADS transformer:

1. real power, P ;
2. reactive power, Q ;

Each of these metrics is assessed for the pre-fault (A), fault (B) and post-fault (C) period by the calculation of corresponding error values F_1 , F_2 , F_3 , and F_G as defined in (3.3)–(3.5) and illustrated in Fig. 3.10. Within each of the periods A, B and C, there may be a further distinction between transient and (quasi-)steady state sub-periods. While periods A, B and C are determined by the voltage curve (plot at the top of Fig. 3.10), the distinction between transient and (quasi-)steady state periods is made for each measured value separately.

For the stability studies investigated in this study, determining the largest loss of generation contingency, the validation can be limited to the following periods and sub-periods:

A consists of only a stationary part (A1 in Fig. 3.10);

B consists of a transient part (B1) and may contain a (quasi-) stationary part (B2), based on conditions;

C consists of only a stationary part (C1).

The unlabeled, transient part in the post-fault period (C) in Fig. 3.10 is disregarded because only the post-fault real power balance is of concern.

Three error values are defined as follows with time steps i , ‘measurement’ values from the detailed ADS indicated by subscript m , and ‘simulation’ values from the equivalent ADS indicated by subscript s :

F_1 is the error for the average value in a (quasi-) stationary period and

F_2 is the error for the average value in a transient period, both of which are defined by (3.3):

$$F_{1,2} = \left| \frac{1}{k_{m,End} - k_{m,Begin}} \sum_{i=k_{m,Begin}}^{k_{m,End}} x_m(i) - \frac{1}{k_{s,End} - k_{s,Begin}} \sum_{i=k_{s,Begin}}^{k_{s,End}} x_s(i) \right| \quad (3.3)$$

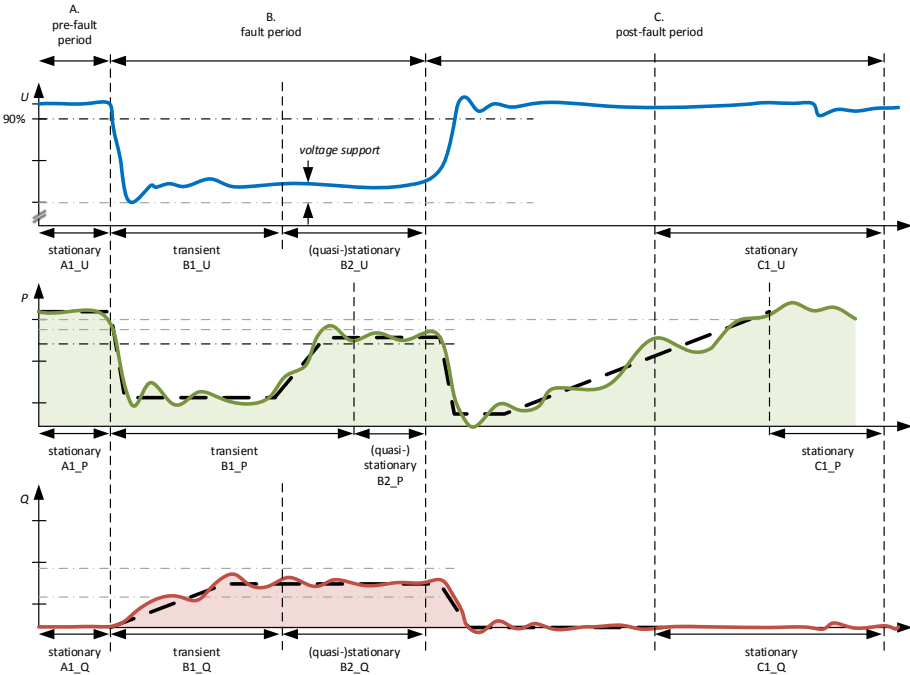


Figure 3.10: Used classification of real and reactive power in transient and (quasi-)stationary areas for measurement and simulation, based on [FGW14].

F_3 is the maximum instantaneous error for positive sequence values in a (quasi-)stationary period:

$$F_3 = \max_{i=k_{Begin}, \dots, k_{End}} |x_m(i) - x_s(i)| \quad (3.4)$$

In case there are multiple (transient and/or (quasi-) stationary) sub-periods within each of the periods A, B or C, errors F_1 and F_2 are weighed according to the duration of each sub-period to obtain the error for the complete period. For the overall error F_G , the errors in all periods are weighted:

$$F_G = 0.1F_A + 0.6F_B + 0.3F_C \quad (3.5)$$

The allowable maximum error values for a successful validation of the equivalent ADS models are given in table 3.4 according to [FGW14].

Table 3.4: Allowable maximum error values [FGW14].

	F_1	F_2	F_3	F_G
Real power $\Delta P/P_N$	0.10	0.20	0.15	0.15
Reactive power $\Delta Q/Q_N$	0.07	0.20	0.10	0.15

3.6 Results and Validation

3.6.1 Case study

In this section, the proposed methodology to derive equivalent models of active distribution systems is applied to example future rural and suburban ADSs comprising of MV and LV networks, loads and DERs. These distribution grids have been based on an extensive analysis of grids in Germany. Results for the equivalent impedances are shown for all grids while result from the validation with time-domain, rms, stability-type, positive-sequence simulations are only shown for the rural grids due to space restrictions.

The grid code performance composition of the rural system is shown in Fig. 3.11 with the classes defined in table 3.5. The peak load of the combined rural LV and MV networks is 12.6 MW. The installed DERs reflect penetration levels expected for the year 2022. For rural networks, a regional analysis suggests a median penetration at MV level of about $\rho_{DG,r} = 300\%$ [vBR⁺14]. Further details on the installed DERs are provided in table 3.6 including the DER technology classes considered.

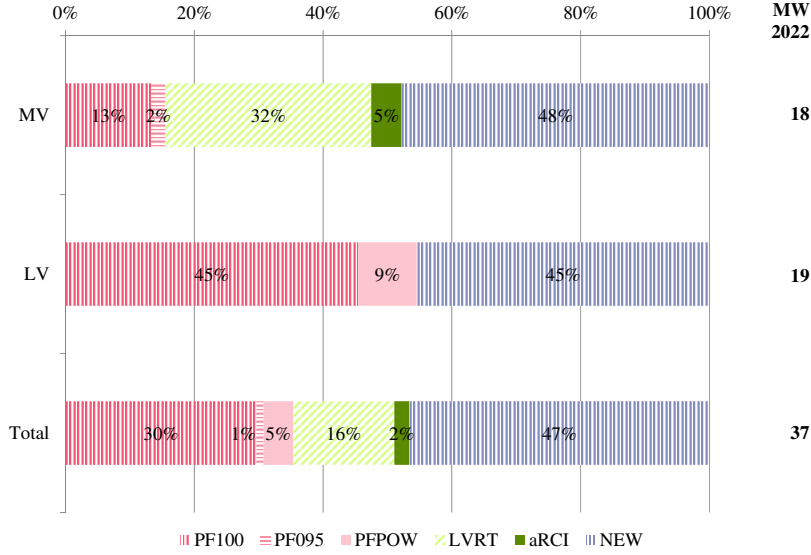


Figure 3.11: Grid code performance framework composition of the example rural active distribution test system. For the performance of new to be installed DER (*NEW*) refer to Table 3.5 and the text.

Table 3.5: grid code classes performance shown in Fig. 3.11

Class name	Pre-fault control mode	Fault control mode
PF100	fixed power factor $\cos(\varphi) = 1$	no LVRT
PF095	fixed power factor $\cos(\varphi) = 0.95$ (underexcited)	no LVRT
PFPOW	variable power factor/real power characteristic curve $\cos(\varphi) = f(P)$, see Fig. 3.7	no LVRT
LVRT	fixed power factor $\cos(\varphi) = 0.95$ (underexcited)	LVRT in BM ¹
aRCI	fixed power factor $\cos(\varphi) = 0.95$ (underexcited)	LVRT with aRCI
NEW at MV	same as PF095	LVRT with aRCI
NEW at LV	same as PFPOW	nLVRT/BM/ aRCI ²

¹ DER ceases to energize for PCC voltages below 0.8 p.u.

² fault control mode depends on study case, refer to subsection B.

Table 3.6: Installed DERs in rural active distribution test system.

Voltage level	DG type	PF100	PF095	PFPOW	LVRT	aRCI	NEW	Total	Typical Size [kW]	Capacity [MW]	Peak Load [MW]	$\rho_{DG,r}$ [%]		
MV (1x)	PV	1			1	2	4	8	430	3.4				
	Wind				1		1	2	5,000	10.0				
	CHP	5	1		1		5	12	400	4.8				
Total												18.2	2.5	728
LV (171x)	PV	855		171			684	1,710	10	17.1				
	CHP						171	171	10	1.7				
Total												18.8	10.1	186
Total												37.1	12.6	294

3.6.2 Study cases

The model validation is performed for a number of voltage dips of different severity at the HV side of the 110/20 kV transformer. In this section, special attention is given to the validity of the models around the 0.8 p.u. disconnection threshold of existing LV-connected DERs (Fig. 2.4).

DERs at MV level to be installed between the base year (2012) and the target year (2022) are assumed to comply with the latest MV performance requirements, i.e. low voltage ride-through (LVRT) with additional reactive current injection (aRCI). The accuracy of the models to reflect the particular behavior of different network fault control strategies for new to be installed DERs at LV level is analyzed for three cases:

1. nLVRT mode ('tripping'): No LVRT, permanent disconnection of the DER for PCC voltages below 0.8 p.u.
2. BM mode ('momentary cessation'): LVRT with BM, i.e. the DER ceases to energize for PCC voltages below 0.8 p.u. but stays connected and ready to resume service post-fault.
3. aRCI mode ('smart LVRT'): DER rides through faults with additional reactive current injection.

The in-feed of the DERs is chosen to be high (0.8 p.u. on their rated power base) in the cases with nLVRT and BM mode. This requires the LV-connected DER, thus the ADS, to consume reactive power pre-fault, according to the GCs introduced in section 2.3 and presented in Fig. 3.7. In the case with aRCI mode the in-feed of the DERs is chosen to be low (0.4 p.u.). Thus, the LV-connected DER do not consume reactive power prior to the fault and the effect of the aRCI mode can be studied independently.

3.6.3 Dynamic equivalents

The heuristically computed values for the equivalent impedances for the equivalent ADSs are shown in table 3.7.

Table 3.7: Equivalent impedances computed for the equivalent active distribution systems.

Voltage level	R [p.u.]	X [p.u.]	Z [p.u.]	R/X [-]
Rural network, solar PV dominated				
MV	0.03325	0.03325	0.04725	1.0
LV	8.18750	0.87500	8.18750	9.4
Suburban network, solar PV dominated				
MV	0.00625	0.00625	0.00885	1.0
LV	5.18750	0.81250	5.25000	6.4
Suburban network, CHP dominated				
MV	0.01375	0.01375	0.01925	1.0
LV	2.43750	1.00000	2.62500	2.4

Per unit values based on $S_{\text{base}} = 100 \text{ MVA}$ and $V_{\text{base}} = 20 \text{ kV}$ for MV and $V_{\text{base}} = 0.4 \text{ kV}$ for LV networks.

3.6.4 Simulation results

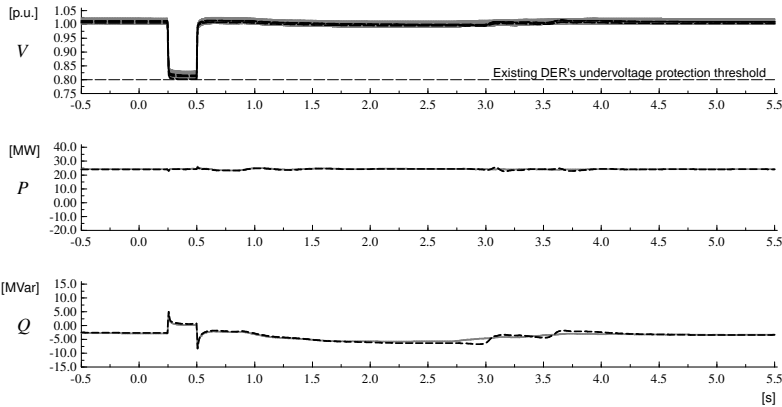
The result plots at the top of the subfigures in Fig. 3.12 show the voltages (V) at the 20 kV side of the 110/20 kV transformer and, for further insight, also shows the downstream end of the equivalent MV and LV impedances of the equivalent ADS (dashed black lines) as well as at the individual PCCs of MV and LV connected DERs in the detailed ADS (solid gray lines). The plots in the middle show the real power (P) and the plots at the bottom show the reactive (Q) power at the 110 kV side of the 110/20 kV transformer.

First, the response of the ADS for an ‘uncritical’ voltage dip with 80 % retained voltage and the nLVRT mode is shown in Fig. 3.12a. The results for the detailed and the equivalent network are almost in perfect alignment.

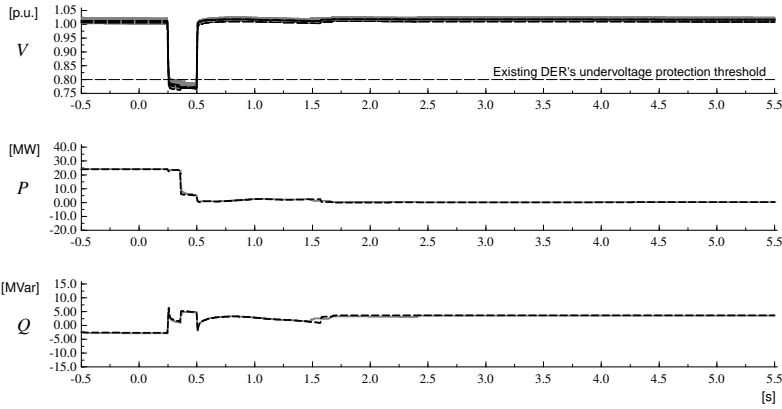
For this voltage dip, no in-feed from DER is lost after the network fault is cleared. The DERs with power electronic converters (PECs) are able to keep their real power output constant during this shallow voltage dip by increasing the value of their direct-axis current. The voltage dip leads to a temporary increase in reactive power in-feed during the fault, due to the dynamic behavior of the integrated CHP plants.

Second, the response of the ADS is shown for a ‘critical’ voltage dip with 76 % retained voltage and the nLVRT mode in Fig. 3.12b. The results for the detailed and the equivalent network again match very well. This voltage dip triggers the loss of about 65 % of the pre-fault in-feed from DERs immediately after the fault is cleared. With regard to the temporary increase of reactive power in-feed the results show an additional increase about 100 ms into the fault. In that moment, the existing LV-connected DERs with PECs disconnect. Because they had been required to consume reactive power in the pre-fault period (see Fig. 3.7), this reactive power becomes ‘suddenly’ available and leads to an ‘indirect’ voltage support in the remaining fault period.

Third, the response of the ADS is shown for the same ‘critical’ voltage dip with 76 % retained voltage but now with the BM mode in Fig. 3.12c. Again, the results for the detailed and the equivalent network match very well. As in the previous case, the voltage dip triggers the loss of about 65 % of the pre-fault in-feed from DERs immediately after the

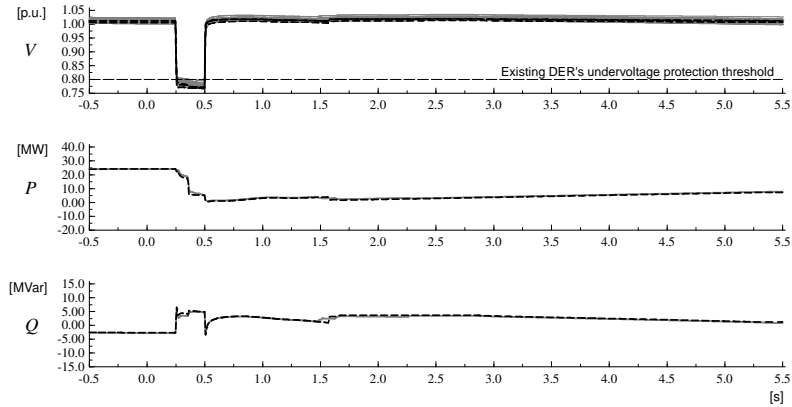


(a) 0.80 p.u. retained voltage and nLVRT mode

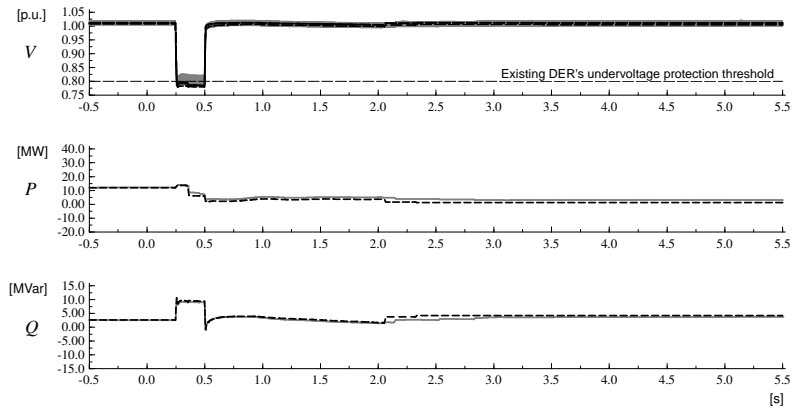


(b) 0.76 p.u. retained voltage and nLVRT mode

detailed model (— solid grey) equivalent model (— dashed black)



(c) 0.76 p.u. retained voltage and BM mode



(d) 0.76 p.u. retained voltage and aRCI mode

detailed model (— solid grey)	equivalent model (— dashed black)
-------------------------------	-----------------------------------

Figure 3.12: Validation results for 2022 MV rural network for various sensitivity cases

fault is cleared. Because the DERs reduce their d- and q-axis currents in BM mode to zero within about 30 ms after the fault occurs, the ‘indirect’ voltage support occurs much faster compared to the nLVRT case. Most importantly, the real power export from the ADS ramps up within a 5-second period after fault clearance. At the end of the post-fault recovery period, only 45 % of the pre-fault in-feed from DERs remains lost. That is an improvement by 31 % compared to the nLVRT case.

Fourth, the response of the ADS is shown once again for the same ‘critical’ voltage dip with 76 % retained voltage in Fig. 3.12d. But this time the new LV-connected DERs operate at a low real power output of 0.4 p.u. and unity power factor prior to the fault and operate in aRCI mode during the fault. The equivalent model is less accurate than in the previous cases. The closer the simulated retained voltage gets to the threshold of 0.8 p.u., the less accurate the equivalent model becomes. This is attributed to the ‘active’ behavior of the DERs during the fault period and the induced error when combining different DERs on a feeder into a single equivalent. In this case, the voltage dip triggers a loss of about 35 % of the pre-fault in-feed from DERs for the detailed model and 44 % for the equivalent model. In the former, the terminal voltage of some of the DERs is increased by the aRCI just above the disconnection threshold. Thus, the behavior of the equivalent ADS models can be considered as conservative.

3.6.5 Discussion

The simulation results allow for a discussion of the strength and limitations of the proposed methodology. First, the performance-driven approach to explicitly model DERs at each voltage level behind an equivalent impedance can produce highly accurate results for the dynamic response of active distribution systems to external faults. Second, the method is modular in the sense that DERs can be differentiated 1) per resource type in order to derive meaningful dispatch scenarios, 2) per applicable interconnection requirement in order to consider the dynamic response to abnormal voltage and frequency conditions, and if necessary 3) per connection interface type, e.g., inverter-based DER versus directly-coupled synchronous generator-based DER, in order to represent the technology-specific dynamic response. Third, without compromising modelling accuracy, computational performance is improved and data requirements with regard to distribution system properties are minimised. These strengths make the proposed methods particularly suitable for commercially-available power system analysis tools.

On the other hand, the proposed methodology has the following limitations. First, the method loses accuracy for distribution systems that are operated non-radially but meshed because reactive power loop flows may change the voltage magnitude in the detailed ADS compared to the equivalent ADS. Additional research is required to quantify this effect. Second, the method is more computationally challenging than other reduced-order dynamic equivalent approaches such as WECC’s distributed PV (*PVDI*) model [WEC14] which disregards the dynamic behaviour during the fault period or the generic ADS model proposed in [MM13a, MM13b]. Despite the significant reduction in the order of the derived ADS models by aggregation of loads and DG behind a single equivalent impedance, the simulation runs for the IEEE 39-bus, 10-machine New England test system over a study period of approximately ten seconds presented in chapter 5 may take several hours on a standard workstation.

The proposed method would still work for non-radial distribution systems but lose accur-

acy given reactive power loop flows that will change the voltage magnitude in the detailed ADS compared to the equivalent ADS.

3.7 Conclusions

In bulk power system stability studies, the dynamic behavior of active distribution systems (ADSs) has to be accurately accounted for to properly reflect their influence on the overall dynamic performance of the system. This thesis proposes an improved methodology of dynamic equivalencing of ADSs for bulk system stability studies using grey box modeling. This methodology can contribute to ongoing activities in IEEE/PES/PSDP [IEE14b] and CIGRÉ JWG C4/C6.35/CIREN [YC13].

For stability studies of bulk systems with more than approx. 50 % system-wide instantaneous penetration, it is recommended to explicitly model the equivalent impedances of for radial low voltage and medium voltage ADSs and to consider the evolving grid code (aka interconnection) requirements ('legacy') by explicitly modelling dedicated performance classes of DERs. Based on this approach, the derived equivalent ADS models were validated against detailed models of ADSs and showed a high accuracy. The validation was performed for very high regional DER penetration levels that caused pre-fault reverse power flows, i.e. export from the ADS.

The derived models confirmed the expectation that requiring LV-connected DERs to ride through voltage dips significantly improves the post-fault real power balance and that an 'active' voltage support from DERs during the fault period can further reduce the post-fault real power imbalance. It should be noted that for the latter operating mode the accuracy of the models reduces slightly but shows a conservative behavior which is regarded as suitable for bulk system reliability studies.

Chapter 4

Network Fault Response during Reverse Power Flow Situations

This chapter contributes to the understanding of the network fault response of (parts of) the power system during reverse power flow situations (RPFs). The first part describes the simple test system used and the sensitivity analyses performed in this study. In the results parts, the first sensitivity analysis focuses on the system impact with low voltage ride-through (LVRT) in ‘blocking mode’. The second sensitivity analysis investigates the system impact with fast voltage control and proposes a new fault control mode that shows robust performance under a large number of system conditions and control parameter variations. The third sensitivity analysis finally tests the new control modes for shallower voltage dips and further develops it into an adjusted fault control mode to mitigate the impact of a point of common coupling (PCC) with smaller short-circuit ratio (SCR) and/or a lower X/R ratio.

The methodology section 4.3 and section 4.4 that presents the results for the first sensitivity analysis are based on a journal paper published by IET Renewable Power Generation [BRG⁺15].

4.1 Introduction

Wind power park modules (WPPMs) are the dominating distributed generation technology at medium voltage (MV) level and, therefore, in the focus of this chapter. While the network fault response has been studied in the past for individual WPPM and other power electronic converter (PEC) coupled distributed generation (DG), this chapter adds a comprehensive analysis at system level for very high penetration scenarios. The fundamental principles discussed in this chapter are also valid when distributed generation (DG) is connected at low voltage (LV) level. These will actually be analysed in detail in the next chapter by taking photovoltaic systems as the dominating DG technology at that level.

Common practices of distribution system operators (DSOs) with regard to network fault response requirements are investigated and critically reviewed in this chapter. The influence of induction motor loads and transformer tap-changers on the WPPM’s network fault response is studied. A new robust fast voltage control during faults is proposed that performs well for a large number of realistic sensitivity cases from a system-wide stability viewpoint.

An additional improvement is trying to be achieved by adjusting the current injection to the magnitude and angle of the network impedance at the PCC of a MV connected DG. The results are obtained from time domain simulations of a HV-MV benchmark system. For an analytical discussion of the effects by use of phasor diagrams and circuit analysis it is referred to the previous chapter 2.

4.2 Challenges under Reverse Power Flow Situations

The previous chapter has described the state-of-the-art network fault response requirements for distributed generation. Many of the latter have been thoroughly assessed only for ‘strong’ (sub-)transmission systems and ‘normal’ power flow scenarios. Furthermore, common practices among distribution system operators—for example in Germany [RWE14]—may often diverge from these requirements, for example when WPPMs are required to ride through low voltages in ‘blocking mode’. All of these practices have not shown any noticeable negative effects when the WPPMs penetration is small.

With wind power serving a large share of load, however, the control systems of wind power park modules for normal (quasi-stationary) and abnormal (transient) states increasingly influence the power system response to transmission network faults. In order to understand in what way they influence the system response, one must consider the following effects which are related to the distributed nature of future WPPM:

- The regular occurrence of reverse power flow (RPF) situations from the distribution to transmission level [Tho00, LKP05, CT07];
- The increase of the inductive reactive power demand of a distribution system due to some quasi-stationary voltage control requirements for distributed generation in order to maintain the distribution system’s operating voltage limits [BAL09]; and
- The connection of WPPMs to ‘weaker’ points of common coupling (PCCs), i.e. reduced short-circuit power ratios (SCRs) [MBPE07, SSS13], and also to networks with a lower X/R ratio [DBB⁺12, GTB⁺14].
- the potential exposure of WPPM to fault-induced delayed voltage recovery, especially in North American distribution systems [NER12]. FIDVR events are known as a depressed voltage for 5 s to 30 s following a network fault and are caused by the presence of large amounts of induction motor loads at distribution level.

The objective of this chapter is to investigate the network fault response of wind power park modules in sub-transmission and distribution systems during reverse power flow situations and to quantify the impact on power system stability.

4.3 Methodology

Time domain analysis (positive-sequence, rms) is carried out with WPPM models integrated into a simplified test system. The description of the models for the various power

system components is given in the following subsections. A solid, three-phase short-circuit at the transmission system load's busbar occurs at $t' = 0.2$ s and is cleared 200 ms later. A sensitivity analysis is performed to understand the differences in the system response seen between normal and reverse power flow scenarios, the impact of the WPPM's pre-fault, fault and post-fault control modes and their settings, the impact of the initial positions of transformer tap-changers, and the load modelling. The performance of the test system is assessed by its frequency response, the voltage magnitudes and voltage angles. The voltage magnitude is measured at the WPPM terminals which is the reference for the fast voltage controller. The voltage angles are measured at the WPPM PCC which is located inside of the sub-transmission or distribution system. Also synchronous generator (SG) internal rotor angles δ_i are shown.

Simulation results for selected cases are presented in comparative time domain graphs for system frequency, voltage magnitudes, the WPPM's active and reactive power output. Frequency quality defining parameters for the Continental Europe (CE) Area are used according to Table 4.1 and indicated as horizontal (grey) lines in the frequency plots. The simulations are carried out with DIgSILENT PowerFactory.

Table 4.1: ENTSO-E Frequency Quality Defining Parameter for Continental Europe Area

Frequency Quality Defining Parameter	Abbreviation	Value in CE
Standard Frequency Range	F_STD	± 50 mHz
Maximum Instantaneous Frequency Deviation	F_INST	800 mHz
Maximum Steady State Frequency Deviation	F_STEAD	200 mHz

Source: ENTSO-E Network Code on Load-Frequency Control and Reserves (2013) [EE13b]

4.3.1 Test system definition

The simple test system used represents a regional sub-transmission network (110 kV) with very high penetration of distributed generation connected to a part of a 'weak' transmission system (220 kV). The external network is represented by a 1,315 MVA/1,050 MW constant-voltage-behind-transient-reactance model that includes the mechanical equations of an equivalent synchronous generator with $T_a = 10$ s. It provides frequency containment reserve of 15 % of its nominal active power at 49.8 Hz. A 6th order model is used to represent the one synchronous generator which is connected to that 'weak' part of the transmission system and provides no reserves.

The medium and low voltage distribution networks (20 kV and 0.4 kV) connected to the sub-transmission network, including their respective WPPMs, are represented in an aggregate way with a single machine per case. The WPPMs are modelled as described in section 3.2.1 and a load model as described in section 3.3 is used.

The WPPM's rated penetration at sub-transmission (ST) or distribution system (DS) level (ratio of installed generating capacity to ST or DS peak load) was chosen to 285 % which is in line with mid- to long term scenarios for DG in some parts of Germany [Deu13, Ger12b]. The distribution network has been upgraded to incorporate this high amount of

DG. The respective planning criteria were based on [Ger12a]:

1. Thermal overloading (max. loading depends on voltage level and power flow);
2. Voltage deviation from the situation without any DG installed;
3. Voltage quality at end-user.

The single line diagram of the resulting test system is shown in Fig. 4.1. The system data is given in Table B.1 in the appendix.

Four different scenarios are investigated. The feeder in Fig. 4.1a (indice ‘ST’) represents large-scale wind parks that are connected to a ‘weak’ sub-transmission network. The feeder in Fig. 4.1b (indice ‘DS’) represents medium-scale wind parks connected to ‘weak’ distribution networks. The scenarios indicated with ‘EXP’ represent a typical setup where the wind parks exclusively export their power to the (sub-)transmission system; here, the load in the sub-transmission or distribution system is set to zero. The scenarios indicated with ‘RPF’ represent a realistic setup where the power generated by the wind parks is partly consumed locally.

Table 5.4 lists the two load cases that are used in the analysis and their respective composition.

Case	Static load	Dynamic load
Zstat	100 %	0 %
Zdyn	80 %	20 %

Table 4.2: Load composition for the two load cases.

The results have been confirmed with validated, manufacturer-specific models. Because those models were provided as a black box for confidentiality reasons and did not allow for an adaptation of the control systems, the validation results are not shown.

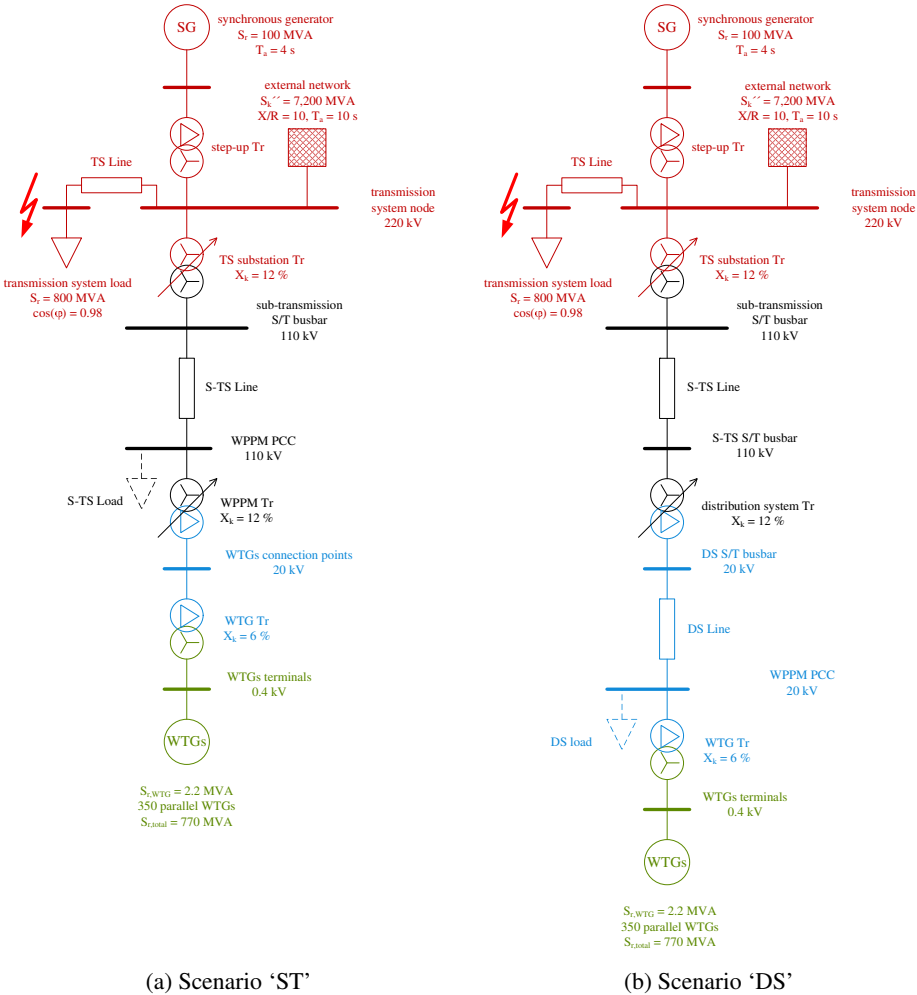


Figure 4.1: Simple test system used for different scenarios and the 'EXP'/'RPF' cases (dashed loads)

4.3.2 Sensitivity analysis for system impact of LVRT modes

The system impact of LVRT modes is investigated by means of a sensitivity analysis. The sensitivity parameters are described in the following and table 4.3 gives an overview on the sensitivity cases. The corresponding case numbers are given in brackets:

Three different scenarios are investigated

- ‘ST_NPF’ (1–2): sub-transmission connected WPPM and normal power flow situation
- ‘ST_RPF’ (3–4, 9–17): sub-transmission connected WPPM and reverse power flow situation
- ‘ST_EXP’ (5): sub-transmission connected WPPM and exporting power flow situation;
- ‘DS_RPF’ (6–8, 18–23): distribution connected WPPM and reverse power flow situation.

Two different cases for the load behaviour are investigated:

- ‘Zstat’ (3): an exclusive static load case;
- ‘Zdyn’ (4–16): a mixed static and dynamic load case.

Also, two different quasi-stationary voltage control modes are investigated:

- $\cos(\varphi) = 1$ (2–7, 9–16): a fixed unity power factor case;
- $\cos(\varphi) = f(P)$ (8, 18–23): a variable power factor case.

The fast voltage control reactive current gain is varied for:

- $k_{RCI} = 0$ p.u. (11–13): deactivation of fast voltage control;
- $k_{RCI} = 2$ p.u. (21–23): standard gain according to grid connection requirements (GCRs);
- $k_{RCI} = 6$ p.u. (9–10, 14, 16, 18–20): high gain for strong voltage support even for distant faults.

Further, two different transformer tap changer cases are studied:

- ‘Tap0’ (6): taps being unchanged from normal power flow situations;
- ‘Tap1’ (3–5, 7–23): taps adapted to keep the WPPM PCC voltage at 1.0 p.u. pre-fault.

Finally, the system impact with LVRT and four different fault control modes will be analysed:

- ‘BLOCK’ (3–8): ‘blocking mode’;

- ‘TC’ (9, 11): fast voltage control mode according to TransmissionCode (2007);
- ‘SDL’ (10, 12): fast voltage control mode according to SDLWindV (2009);
- ‘NEW’ (13–15): a new robust fast voltage control mode;
- ‘ADJ’ (16–23): an adaptation of the new robust fast voltage control mode adjusted to the local network conditions at the PCC.

While this potentially makes several hundreds of different cases, only a subset of 23 cases is presented to explain the main effects of interest. Table 4.3 lists the presented cases, their sensitivity parameters and the related figures the results are presented in.

Table 4.3: Presented sensitivity cases

Case	Scenario	Fault mode	Load	Trf. taps	$\cos(\varphi)$	Figure(s)
1	ST_NPF	BLOCK	Zstat	Tap1	1	Fig. 4.2
2	ST_NPF	BLOCK	Zdyn	Tap1	1	
3	ST_RPF	BLOCK	Zstat	Tap1	1	Fig. 4.3
4	ST_RPF	BLOCK	Zdyn	Tap1	1	/
5	ST_EXP	BLOCK	Zdyn	Tap1	1	Fig. 4.4
6	DS_RPF	BLOCK	Zdyn	Tap0	1	Fig. 4.5
7	DS_RPF	BLOCK	Zdyn	Tap1	1	/
8	DS_RPF	BLOCK	Zdyn	Tap1	$f(P)$	Fig. 4.6
9	ST_RPF	TC, k=6	Zdyn	Tap1	1	Fig. 4.7
10	ST_RPF	SDL, k=6	Zdyn	Tap1	1	
11	ST_RPF	TC, k=0	Zdyn	Tap1	1	Fig. 4.8–
12	ST_RPF	SDL, k=0	Zdyn	Tap1	1	Fig. 4.10
13	ST_RPF	NEW, k=0	Zdyn	Tap1	1	Fig. 4.11 &
14	ST_RPF	NEW, k=6	Zdyn	Tap1	1	Fig. 4.12
15	ST_RPF	NEW, k=10	Zdyn	Tap1	1	Fig. 4.15
16	ST_RPF	ADJ, k=10, dAPR	Zdyn	Tap1	1	
17	ST_RPF	ADJ, k=10, STAB	Zdyn	Tap1	1	
18	DS_RPF	ADJ, k=6, $\psi_{aRACI} = 90$	Zdyn	Tap1	$f(P)$	Fig. 4.17
19	DS_RPF	ADJ, k=6, $\psi_{aRACI} = 75$	Zdyn	Tap1	$f(P)$	
20	DS_RPF	ADJ, k=6, $\psi_{aRACI} = 45$	Zdyn	Tap1	$f(P)$	
21	DS_RPF	ADJ, k=2, $\psi_{aRACI} = 90$	Zdyn	Tap1	$f(P)$	Fig. 4.18 & Fig. 4.19
22	DS_RPF	ADJ, k=2, $\psi_{aRACI} = 75$	Zdyn	Tap1	$f(P)$	
23	DS_RPF	ADJ, k=2, $\psi_{aRACI} = 45$	Zdyn	Tap1	$f(P)$	

4.3.3 System performance criteria

The criteria, according to which the performance of the control modes is compared to, are presented in Table 4.4. The maximum system frequency deviation ΔF_{\max} is assessed using the ENTSO-E frequency quality defining parameters [EE13b] shown in Table 4.1 (horizontal grey lines in Fig. 4.3a and subsequent frequency plots). The time until the voltage recovers into the voltage deadband T_{FIDVR} as well as the occurrence of voltage oscillations i_{VO} are used as an indicator for the voltage stability. The maximum deviation of the synchronous generator’s rotor angle $\Delta \delta_{i,\max}$ indicates the effect on the system’s transient stability. And the deviation of the local voltage angle at the WPPM PCC $\Delta \phi_{\max}$ hint at the synchronism between the transmission and distribution system.

Table 4.4: Control modes performance criteria

Criterion	Symbol	Unit
System frequency deviation (max.)	ΔF_{\max}	[Hz]
Fault-induced delayed voltage recovery	T_{FIDVR}	[s]
Voltage oscillations	i_{VO}	[YES/NO]
Voltage angle deviation (max.)	$\Delta \phi_{\max}$	[degree]
Rotor angle deviation (max.)	$\Delta \delta_{i,\max}$	[degree]

Note: For frequency quality defining parameters see also Table 4.1.

The system frequency is derived from the speed of the equivalent generator that represents the external network. Due to its simplified representation and the high penetration of WPPM, its speed does not increase during the fault.

4.4 System impact with LVRT and ‘blocking mode’

The following section describes the impact of a low voltage ride-through control with ‘blocking mode’ on the system frequency response. This control mode means that the WPPM ceases any exchange of active and reactive power with the network during the fault period. This mode is actually a very common requirement of distribution system operators in Germany [RWE14] since the injection of a short-circuit current would impact the existing distribution network protection scheme. Hence, only those medium voltage connected WPPM which are connected directly to a substation ride through low voltages and activate a fast voltage control. Their installed capacity equals about 10 percent of the total capacity installed at MV level. The ‘blocking mode’ (‘BM’) is used by the other 90 percent. The full set of controller parameters can be found in table C.3 in appendix C.2.2.

4.4.1 Impact of loads

The impact of dynamic loads on the response of WPPMs to transmission network faults during *normal* and *reverse* power flow situations and the resulting system performance is studied for the sub-transmission connected WPPM (scenarios ST). First, the relevance of

dynamic loads at transmission and distribution system level is studied for the normal and the reverse power flow situations by comparison of results for a 100 % constant impedance load model ('Zstat') and a dynamic load model (20 % induction motors, 'Zdyn'). Then, the difference whether local distribution system load is present or not is shown for the dynamic load model by comparing the two cases with exclusive export ('ST_EXP') and with reverse power flow ('ST_RPF').

Simulation results for the system frequency, the WPPM terminal voltage, active and reactive power are presented. The WPPM is assumed to ride through a voltage dip in blocking mode. This assumption is consistent with common DSO practice in Germany. The pre-fault operating point of the WPPM is set to $\cos(\varphi) = 1$. The transformer tap-changer positions are adapted to keep the WPPM PCC voltage at 1.0 p.u. ('Tap1').

Impact of dynamic loads

Simulation results for the normal power flows cases for the sub-transmission connected WPPM and either static or dynamic load model are presented in Fig. 4.2. From these, the impact of dynamic loads at transmission and sub-transmission system level can be observed for the normal power flow situation.

The results show only very minor differences between the static and the dynamic load cases in normal power flow situations. In both load cases, the WPPMs switch into fault operating mode and block active and reactive current exchanges as long as the voltage stays below the deadband of 0.1 p.u., indicated by grey horizontal lines in Fig. 4.2b. Once the fault is cleared and the WTG terminal voltages return into the deadband, the pre-fault operating point is restored while respecting the active power ramp rate.

Simulation results for the same system variables are presented comparing the static (grey solid line) against the dynamic (dashed black line) load model case during reverse power flow situations in Fig. 4.3.

The results show a significant frequency drop below the lower maximum steady-state frequency deviation limit in both cases. This results from an active power deficit in the fault and post-fault period, due to the very high penetration scenario and the blocking mode of WPPM during faults which result in ceasing their active power in-feed. As this active power deficit is the net sum of reduced WPPM output and reduced load consumption during and following the fault, this deficit would be even higher if the load was not voltage dependent.

During the fault period, the rate of change of frequency (ROCOF) is higher and the frequency drops lower in the static load case than in the dynamic load case (49.65 Hz versus 49.75 Hz). This is attributed to the inertia that dynamic loads add to the system in the latter case. The frequency, however, stays well above the lower maximum instantaneous frequency deviation limit. Hence, there is little risk of load-shedding in both cases.

When the loads at transmission and at distribution system level are 100 % static loads, the voltage at the WTG terminals recovers immediately at the fault clearing into the deadband and the WPPMs transition to normal operation with a pre-set active power ramp of $\Delta i/\Delta t' = 2$ p.u./s. The maximum frequency deviation in the static load case is $\Delta F_{\max} = -0.4$ Hz. However, when the load at the transmission and distribution levels includes 20 % of induction motors, the voltage recovers about $T_{\text{FIDVR}} = 200$ ms later into the deadband than in the static load case (grey solid line). The transition from the WPPM's fault into normal operating mode is delayed by the same time. Thus, in the dynamic load case

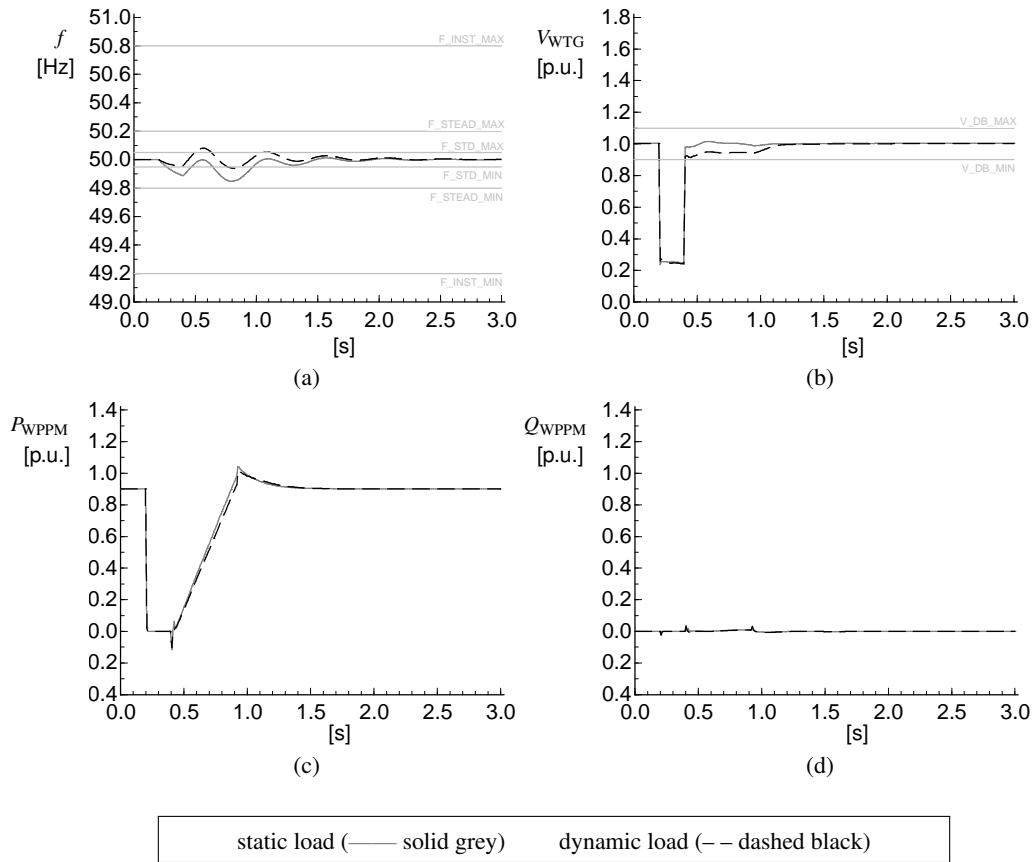


Figure 4.2: Impact of load type during normal power flow situations. Sub-transmission connected scenario and WPPM control with blocking mode (ST_NPF).

(black dashed line), the results show a prolonged low voltage ride-through operation of the WPPMs.

The prolonged LVRT operation in the dynamic load case results in a sustained active power deficit in the post-fault period. That drives down the system frequency in the post-fault period to a lower value than for the static load case. In this particular system setup, the frequency drops to 49.5 Hz ($\Delta F_{max} = -0.5$ Hz). Hence, the relative increase of the maximum frequency deviation from the static to the dynamic load cases is 25 %.

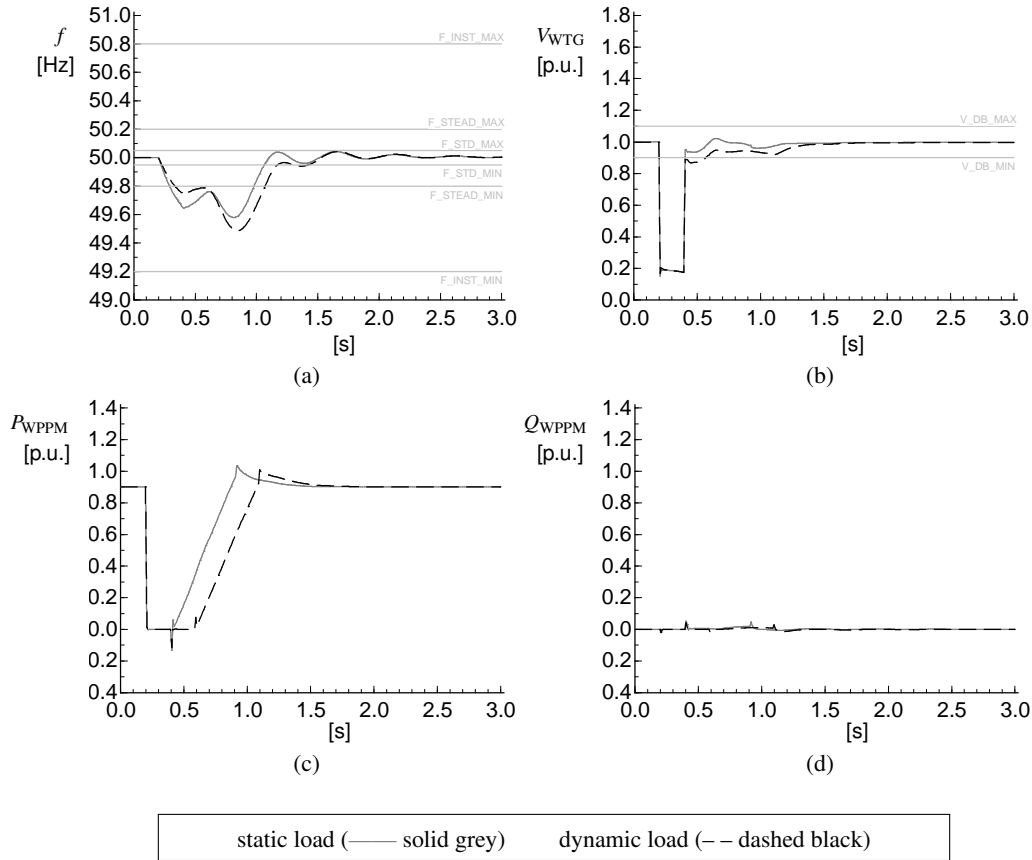


Figure 4.3: Impact of load type during reverse power flow situations. Sub-transmission connected scenario and WPPM control with blocking mode (ST_RPF).

Impact of local distribution system loads

The impact of local distribution system loads on the response of WPPMs to transmission network faults during reverse power flow situations and the resulting system performance is studied for the sub-transmission connected WPPMs (scenarios ST).

Simulation results are presented in Fig. 4.4 for the previously presented reverse power flow (RPF) case (RPF, dashed black line) as well as for the exclusive export case (EXP, solid grey line) case.

The results are similar to the ones previously presented in Fig. 4.3. Again, there is little risk of load-shedding in both cases. However, the results also show that the prolonged LVRT operation of the WPPMs only occurs when the loads with 20 % of induction motors are located close to the WPPMs as in the reverse power flow case. When the induction motor loads are located in the transmission system only, as in the exclusive export case, the WPPMs are less exposed to fault-induced delayed voltage recovery.

From the results, one can conclude that the presence of local induction motor loads can cause a prolonged LVRT operation of DG. While the delay was only $T_{FIDVR} = 200$ ms in the

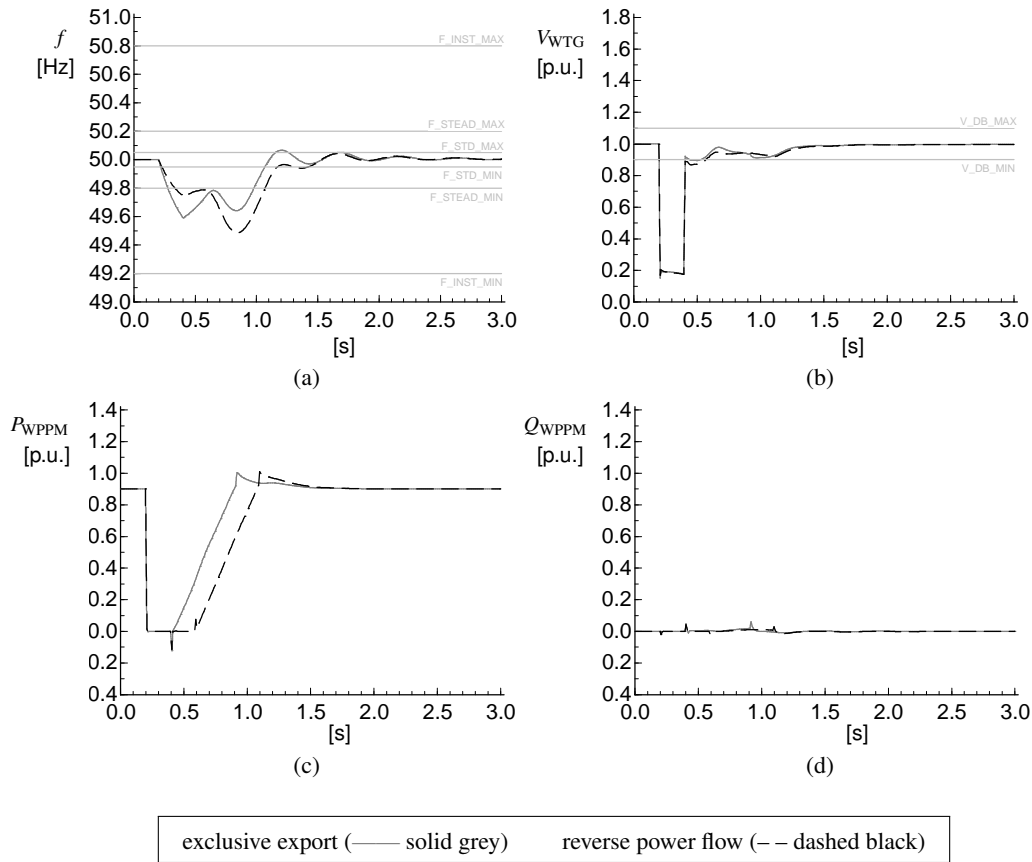


Figure 4.4: Impact of local dynamic sub-transmission load. Sub-transmission connected scenario and WPPM control with blocking mode (ST_Zdyn).

presented cases, a much longer delay of active power recovery could occur in combination with a fault-induced delayed voltage recovery (FIDVR) event.

4.4.2 Impact of PCC and transformer tap changer positions

The impact of the point of common coupling and the transformer tap changer position on the response of WPPMs to transmission network faults during reverse power flow situations and the resulting system performance is studied for the sub-transmission and distribution connected WPPMs and the 80 % static/20 % dynamic load case (scenario DS_RPF, Zdyn cases). The X/R ratio of the equivalent network impedance at the point of common coupling is smaller in this case than for the previously studied sub-transmission connected WPPMs. Simulation results are presented in Fig. 4.5 for the sub-transmission connected WPPMs (grey line) and the distribution connected WPPMs (black lines) with two different tap-changer cases where the taps are either unchanged from their position in normal power flow situations (‘Tap0’) or where taps are adapted to keep the WPPM PCC voltages at 1.0 p.u. pre-fault (‘Tap1’). The WPPM fault mode is kept as ‘blocking mode’ and all

other parameters are kept unchanged from the previously presented cases. The pre-fault operating point of the WPPMs is set to $\cos(\varphi) = 1$.

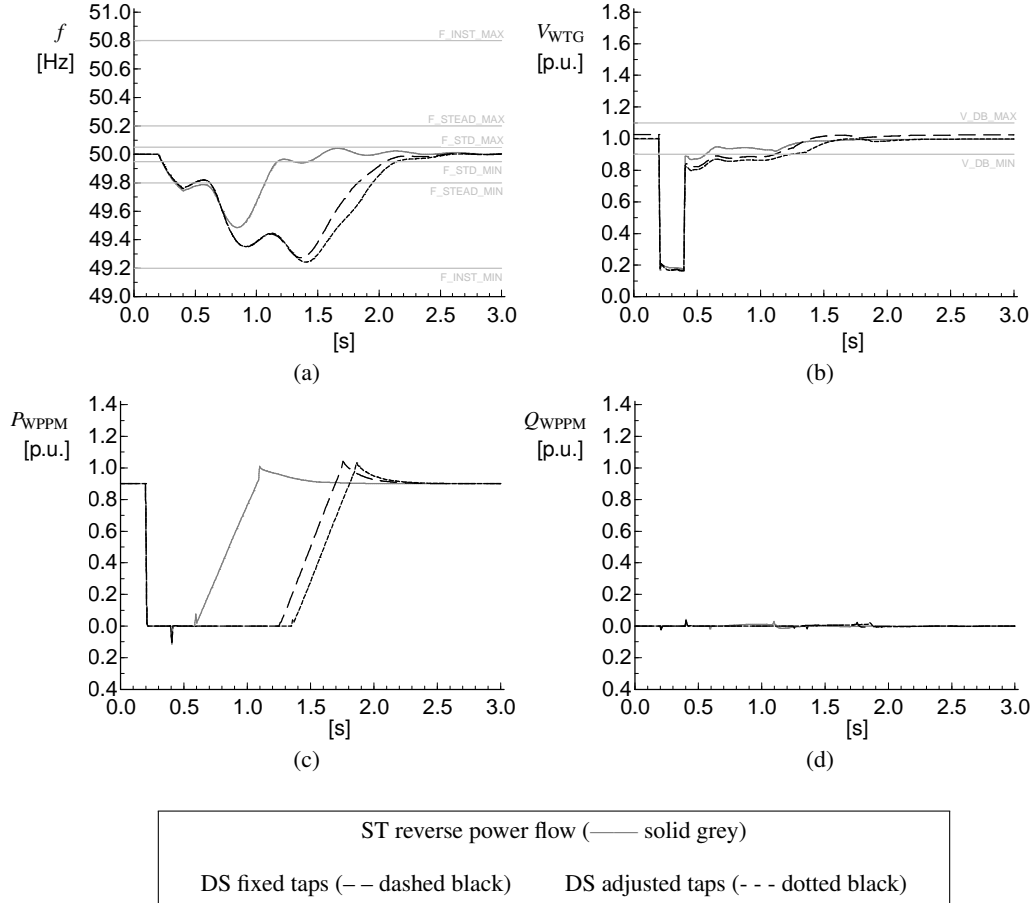


Figure 4.5: Impact of connection location (scenario ST vs. scenario DS) and distribution transformer tap-changer positions (Tap0 vs. Tap1) during reverse power flow situations. WPPMs control with blocking mode (ST_RPF_Zdyn and DS_RPF_Zdyn). Pre-fault operating point of the WPPM was in both cases set to $\cos(\varphi) = 1$.

The results for the distribution connected WPPMs (black lines) show a more severe frequency drop than for the previously presented sub-transmission connected WPPMs (grey line). The system frequency drops close to the lower maximum instantaneous frequency deviation limit of 49.2 Hz (49.24 Hz to 49.28 Hz). That stems from an even more prolonged LVRT operation of the distribution connected WPPMs compared with the sub-transmission connected WPPMs. The risk of load shedding is high in these cases.

The longer delay can be explained by the lower X/R ratio of the equivalent network impedance at the PCC in the distribution system compared to the one in the sub-transmission system. In the former, the blocking of active power during the fault leads to a longer depression of the WTG terminal voltages than in the sub-transmission connected WPPM cases.

The results further show a small difference in the amount of time when the WPPMs transition from fault to normal operating mode depending on the initial transformer tap-changer positions (see Table B.2 in appendix B.1). This effect is particular in RPF situations; however, it is much smaller than the influence of the X/R ratio at the PCC. When the taps are kept unchanged from a normal power flow situation, this causes a small increase of the initial voltage to 1.03 p.u. In that case, the WTG terminal voltages reach the deadband at $t = 1.25$ s and the WPPMs start to ramp up their active power at the same time. When the taps are adapted to keep the WTG terminal voltage at 1.0 p.u., the results show that the WPPM terminal voltage recovers about 1 s later into the deadband.

From the results, one can conclude that the LVRT operation of MV-connected WPPMs would be substantially prolonged if they were set to ride through faults in ‘blocking mode’ in very high penetration scenarios. Furthermore, a LVRT with ‘blocking mode’ would have to be coordinated with the voltage control by transformer tap-changers present in the distribution system. For example, power electronic assisted on load tap changer (OLTC) with very short response times in the order of 200 ms [CBW⁺14] should be used, if a substantial amount of WPPMs ride through faults in ‘blocking mode’ in a certain network area.

4.4.3 Impact of pre-fault reactive power exchange

The impact of the reactive power exchange determined by different quasi-stationary voltage control modes is studied for the same distribution connected WPPMs cases as in the previous section (scenario DS_RPF with Zdyn cases). Simulation results are presented in Fig. 4.6 for the previously presented unity power factor case ($\cos(\varphi) = 1$, solid grey line) as well as for the underexcited operation case ($\cos(\varphi) = f(P)$, dashed black line). The WPPMs fault mode is kept as ‘blocking mode’ and all other parameters are kept unchanged from the previously presented cases. The transformer tap-changer positions are adapted to keep the WPPM PCC voltage at 1.0 p.u. (case ‘Tap1’).

The results show that the pre-fault reactive power exchange has a high impact on the response of MV-connected WPPMs to transmission network faults. The frequency performance is much better when the WPPMs exchange inductive Vars with the network prior to the fault ($\cos(\varphi) = f(P)$) because the transition from fault to normal operating mode occurs almost immediately, as compared with a duration of $T_{fidvr} = 1.05$ s in the $\cos(\varphi) = 1$ case. The WPPMs start to ramp up their active power output earlier so that the post-fault active power deficit remains smaller and the system frequency stays within the allowable steady-state deviation limits. The observed overfrequency at $t' = 1$ s is caused by the fast active power recovery of the WPPMs and the active power swings of the transmission system (TS)-connected synchronous generator that have not damped out by that time and create a temporary surplus of active power in the system.

This finding can be explained by an ‘indirect’ voltage support that results from a combination of the ‘blocking mode’ during the fault with this specific pre-fault reactive power control mode. However, this positive impact on system performance can only be exploited if the controller responsible for the fault mode acts fast enough to change the reactive power set-point to zero before the fault is cleared. Therefore, it is recommended to choose a small time constant in the range of $T_{q,RCI} = 30$ ms to 60 ms.

From the results, one can conclude that the prolonged LVRT operation of MV-connected WPPMs in ‘blocking mode’ will be reduced if WPPMs exchange inductive Vars with the

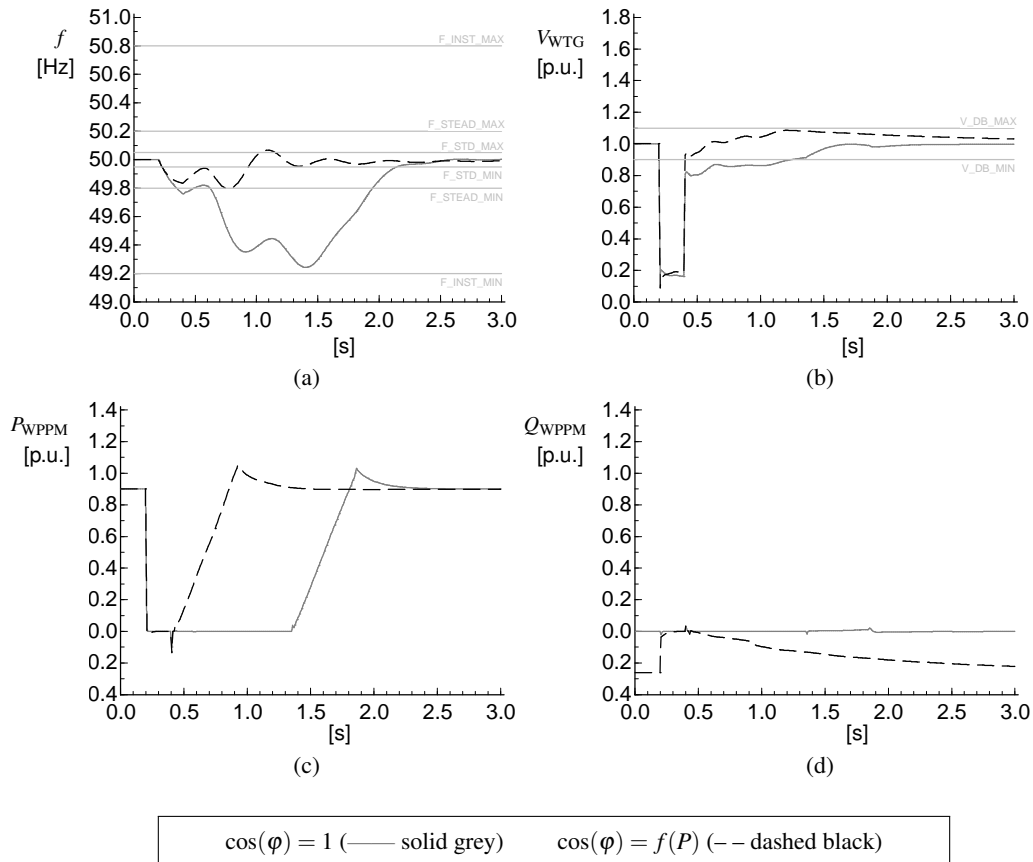


Figure 4.6: Impact of pre-fault reactive power exchange ($\cos(\varphi) = f(P)$ vs. $\cos(\varphi) = 1$) during reverse power flow situations. Distribution connected scenario and WPPM control with blocking mode (DS_RPF_Zdyn). Taps were in both cases adapted to keep WPPM terminal voltage at 1 p.u. (Tap1).

network prior to the fault ($\cos(\varphi) = f(P)$).

4.5 System impact with LVRT and fast voltage control

The impact of the fault control mode and its parameter settings on the response of WPPMs to transmission network faults during reverse power flow situations and the resulting system performance is studied for the sub-transmission connected WPPM (scenario ST). The ‘ST’ scenario is used in this section to illustrate the key pros and cons of the state-of-the-art fast voltage control modes and propose improvements. In the following section 4.6 additional adjustments will be analysed for distribution connected WPPMs. Simulation results are presented in the following for the reverse power flow case in combination with the following three fault modes:

1. state-of-the-art control mode TransmissionCode 2007 (TC);
2. state-of-the-art control mode SDLWindV 2009 (SDL); and
3. a new robust control mode (NEW).

First, results for two different settings for the reactive current gain (standard value of $k_{RCI} = 2$ p.u. according to [Ver07, Ger09]) are presented for the two state-of-the-art control modes ($k_{RCI} = 6$ p.u. and $k_{RCI} = 0$ p.u.) and related effects are analysed. The latter represents an *alternative* practice of German DSOs to ‘mimic’ a LVRT with ‘blocking mode’ if the respective WPPM does not provide such mode. As will be seen, that approach can have adverse effects on the WPPM’s PCC voltage angles. Based on the analysis, a new robust control mode (NEW) is proposed that performs well for a large number of realistic sensitivity cases, including normal and reverse power flow situations and any value of $k_{RCI} = [0...6]$ p.u. The transformer tap-changer positions are adapted to keep the voltage at the WPPM’s PCC at 1.0 p.u. (‘Tap1’) and the pre-fault operating point of the WPPM is set to $\cos(\varphi) = 1$. While the latter is a simplification from reality, it was chosen to eliminate any impact of pre-fault reactive power exchange from this analysis. The full set of controller parameters can be found in table C.3 in appendix C.2.2.

4.5.1 Impact with state-of-the-art requirements and $k_{RCI} = 6$ p.u.

The impact of the fault control mode (‘TC’ vs. ‘SDL’) on the response of sub-transmission connected WPPMs to transmission network faults during reverse power flow situations and the resulting system performance is studied for a reactive current gain of $k_{RCI} = 6$ p.u. Simulation results are presented in Fig. 4.7 for the reverse power flow case. The fast voltage control is realised by an additional reactive current injection (aRCI), see (3.1) and appendix C.1.2 for further details.

The results show that the fault control mode can have a significant impact on the system performance. For both control modes, the frequency deviation is smaller than in the reverse power flow case with dynamic loads at transmission and sub-transmission level (ST_RPF_Zdyn) and an LVRT with ‘blocking mode’ (Fig. 4.4). In the TC mode case, the system frequency drops just below the lower maximum steady state frequency deviation limit due to the delayed active power recovery in that control mode. In the SDL mode case, the active power is restored immediately at fault clearance and the system frequency increases quickly with an overshoot close to the upper maximum steady state frequency deviation limit of 50.2 Hz. The latter is regarded as a critical threshold at which distributed

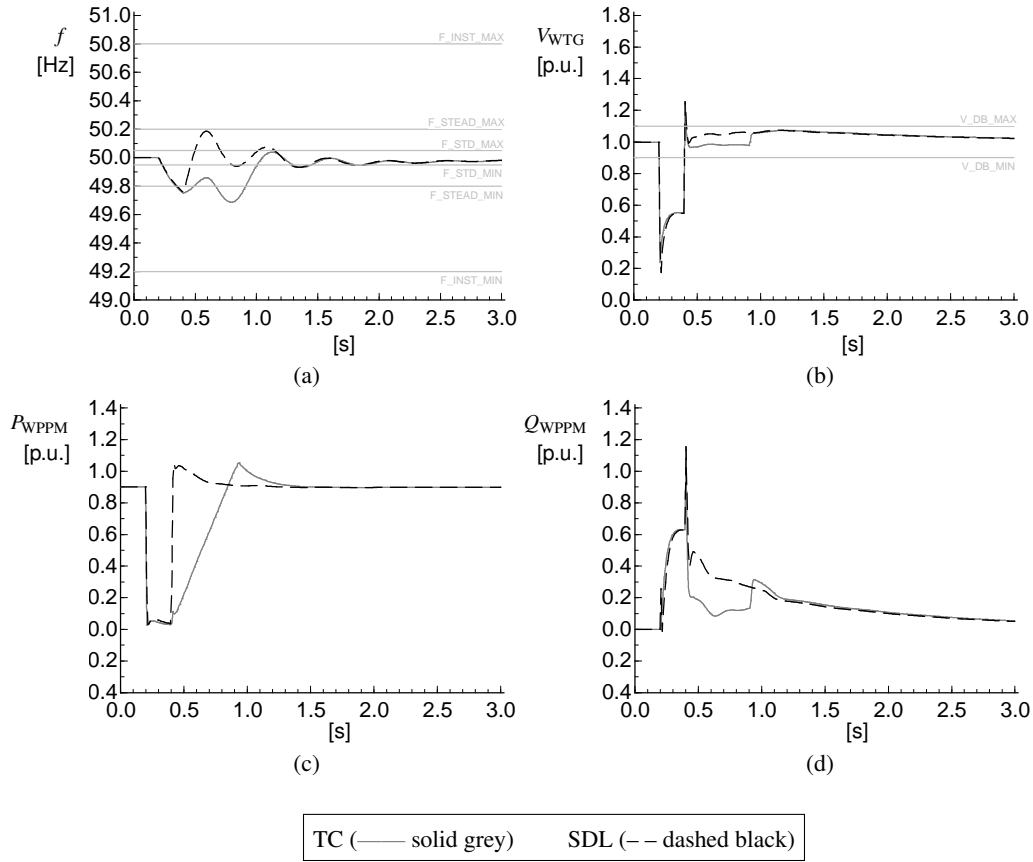


Figure 4.7: Impact of fault control mode (TC vs. SDL) during reverse power flow situations on sub-transmission connected WPPM control and system performance (ST_RPF_Zdyn) with reactive current gain $k_{RCI} = 6$ p.u. Taps were in both cases adapted to keep WPPM terminal voltage at 1 p.u. and the pre-fault operating point of the WPPM was in both cases set $\text{tocos}(\varphi) = 1$.

generation in the German power system might trip [Eco11, EDBI13] and should, therefore, not be surpassed.

The results further show that if the WPPM supports the local voltage via a fast voltage control, the transition from fault to steady-state operating mode occurs immediately at the fault clearance ($t' = 0.4$ s) for the SDL mode and, as required, $T = 500$ ms later at $t' = 0.9$ s for the TC mode (Fig. 4.7c–d). Interestingly, for the chosen steady-state reactive power control time constant $T_q = 0.5$ s, the voltage support in the post-fault period is higher for the SDL than the TC mode. This is attributed to the fact that the internal state value of that controller increases substantially during the fault period and decreases only slowly in the post-fault period. Since this has a positive effect on the voltage, a large reactive power control time constant is recommended. In the TC mode, however, the large time constant results in a jump of the voltage at the WPPM terminals at the instance when the WPPM switches from the continued fault control mode to the steady-state control mode ($t' = 0.9$ s,

Fig. 4.7b). As long as the voltage stays within the deadband of $V_{DB} = \pm 0.1$ p.u., this behaviour is acceptable.

The results also show an undesired transient overvoltage at the WPPM terminals in the moment of fault clearance for both fault control modes that exceeds 1.1 p.u. in this very high penetration scenario. A closer look reveals that the transient overvoltage is slightly lower for the TC mode than SDL mode (1.245 p.u. vs. 1.254 p.u.) due to the delayed active power ramp in the former. The only way to mitigate such transient overvoltage effectively is to make the detection of the fault clearance or the controller for the fast voltage control faster. A detection time of $T_{FRT_detect} < 10$ ms (half a period in 50 Hz power systems) or a reactive current control rise time $T_{q,RCI} < 30$ ms both seem technically infeasible. Thus, a fast transition between fault and normal operating mode can only be achieved at the cost of a 30 ms to 40 ms transient overvoltage at the WPPM terminals following the instance of fault clearance.

From the results one can conclude that a fast voltage control during fault successfully mitigates the risk of a prolonged LVRT operation of sub-transmission connected WPPM. Consequently, the risk of load shedding is significantly reduced for high penetration scenarios. However, the described system benefit comes at the cost of a 30 ms to 40 ms local transient overvoltage at the WPPM terminals following the instance of fault clearance. Given the importance of the overall system performance and the transient nature of the overvoltage, this drawback seems to be acceptable. The power quality standard EN 50160:2008-04 [Eur08] allows for such transient overvoltages.

The conclusions drawn from the presented results also hold for distribution connected WPPM. The main difference is that the transient overvoltage can reach even higher values for a LVRT operation with fast voltage control. But these will still be acceptable from a power quality viewpoint.

4.5.2 Impact with state-of-the-art requirements and $k_{RCI} = 0$ p.u.

The impact of the fault control mode (TC vs. SDL) on the response of sub-transmission connected WPPMs to transmission network faults during reverse power flow situations and the resulting system performance is studied for a reactive current gain of $k_{RCI} = 0$ p.u. The latter represents an *alternative* practice of German DSOs to ‘mimic’ a LVRT with ‘blocking mode’ if the respective WPPM does not provide such mode. Simulation results are presented in Fig. 4.8 and Fig. 4.9 for the reverse power flow case.

The results show that a reactive current gain of $k_{RCI} = 0$ p.u. can have a negative impact on the system performance in the post-fault period under the given conditions. The system frequency is driven above the upper maximum steady state frequency deviation limit of 50.2 Hz. While this is acceptable from a frequency quality viewpoint [EE13b], this could trigger distributed generation in the German power system to trip [Eco11, EDB113] and should, therefore, be avoided. The results further show no substantial differences in the impact on the system performance between the two fault control modes.

In both fault control modes, the WPPMs restore their pre-fault active power set-point within 30 ms to 40 ms from fault clearance. The active current (I_d) was not significantly reduced during the fault period because the reactive current (I_q) remained small due to $k_{RCI} = 0$ p.u. The changes in the active and reactive power shown in Fig. 4.8c–d are attributed to the change of the WPPM terminal voltage magnitude V_{WTTG} and voltage angle at PCC

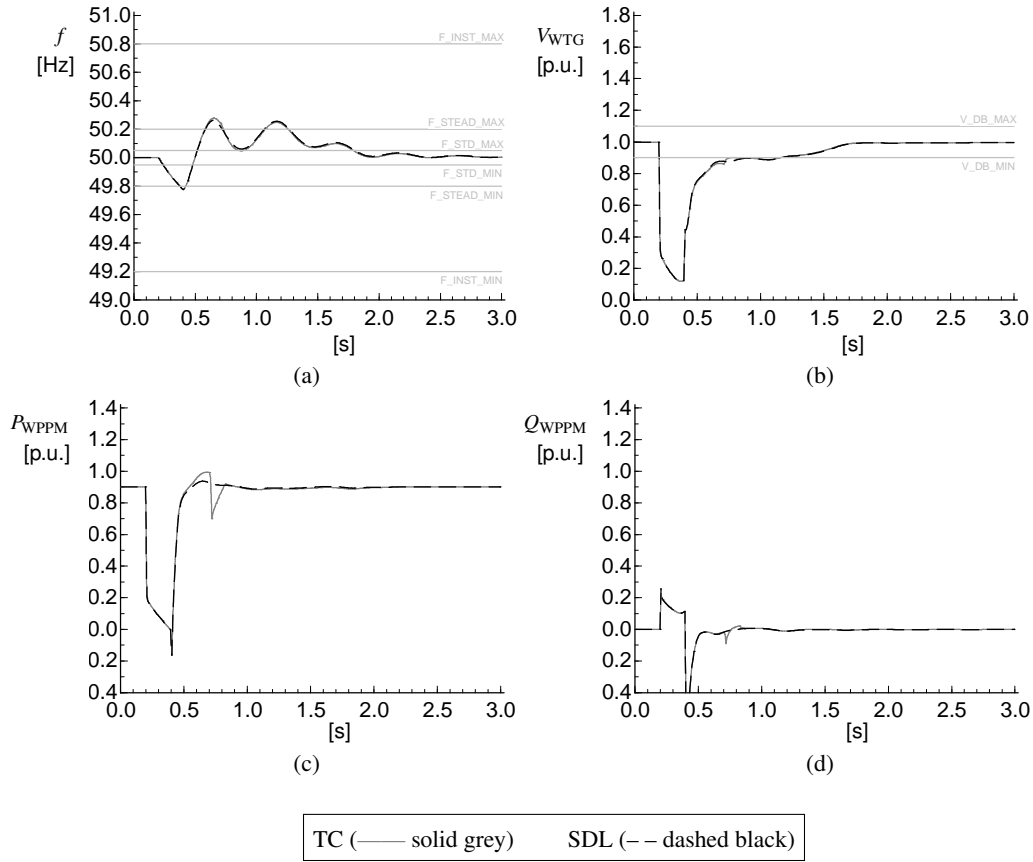


Figure 4.8: Impact of fault control mode (TC vs. SDL) during reverse power flow situations on sub-transmission connected WPPM control and system performance (ST_RPF_Zdyn) with reactive current gain $k_{RCI} = 0$ p.u. Taps were in both cases adapted to keep WPPM terminal voltage at 1 p.u. and the pre-fault operating point of the WPPM was in both cases set to $\cos(\varphi) = 1$.

ϕ_{WP} . Furthermore, the sub-transmission system voltage recovers slowly in the post-fault period and enters the deadband not earlier than $t' = 300$ ms after fault clearance ($t' = 0.7$ s, Fig. 4.8b). The slow voltage recovery can be explained with extraordinarily high reactive power consumption by the sub-transmission connected induction motors in the post-fault period.

As Fig. 4.9b reveals, the active power injected by the WPPM during the fault of initially $P_{WPPM} = 0.2$ p.u. (see Fig. 4.8c) caused an large excursion of the voltage angles in the sub-transmission system. As a consequence, the steady state stability limit for the power transfer from the sub-transmission connected WPPMs to the transmission system is violated during the fault period ($\phi_{WP} > \frac{\pi}{2}$). One could say that the sub-transmission system with WPPMs loses its synchronism with the transmission system and the sub-transmission voltage collapses (declining slope in Fig. 4.8c during the fault). Therefore, the electrical torque of the sub-transmission connected induction motors is heavily decreased during the fault period

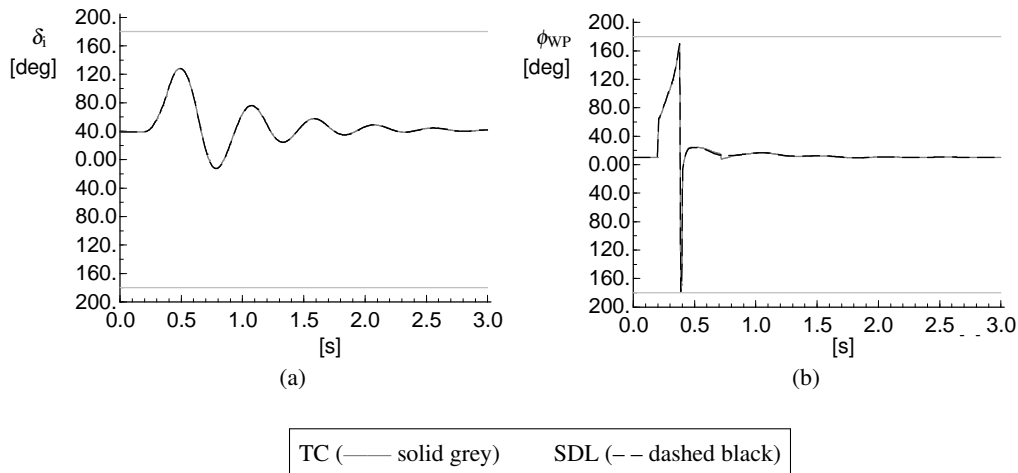


Figure 4.9: Impact of fault control mode (TC vs. SDL) with reactive current gain $k_{RCI} = 0$ p.u. during reverse power flow situations on the transient stability of the transmission connected synchronous generator and the excursion of the voltage angle at the WPPM PCC.

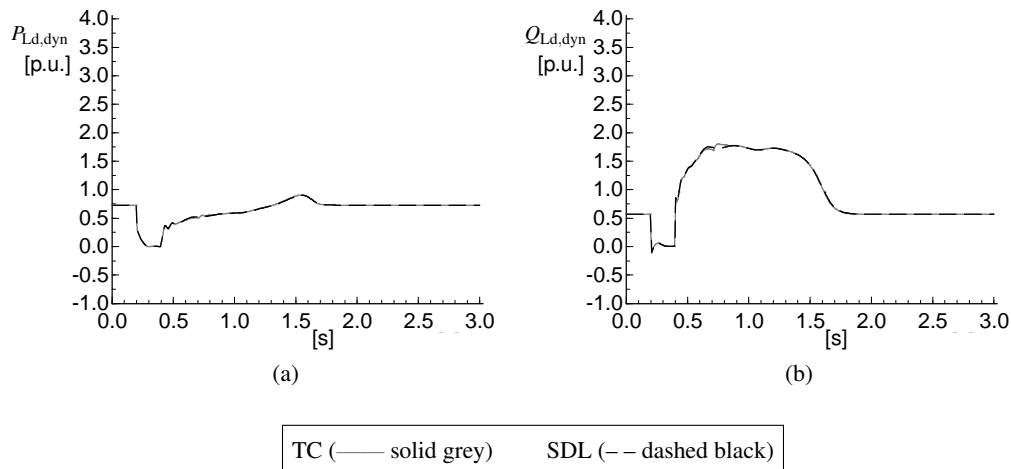


Figure 4.10: Impact of fault control mode (TC vs. SDL) with reactive current gain $k_{RCI} = 0$ p.u. during reverse power flow situations on the response of sub-transmission connected induction motor load.

which causes them to decelerate further than in the case with $k_{RCI} = 6$ p.u. where the sub-transmission voltage is supported by the WPPMs. The heavy slow-down of the induction motors increases their slip s and causes them to consume almost four times as much reactive power $Q_{Ld,dyn}$ for a period of 1 s after the fault ($t' = 0.4$ s to 1.4 s, Fig. 4.10b). This period is twice as long as in the case with $k_{RCI} = 6$ p.u. ($t' = 0.4$ s to 0.8 s, Fig. F.2b in appendix F).

The active part of the sub-transmission system load remains below its pre-fault value as long as the post-fault undervoltage subsists (see Fig. 4.10a). Combined with the fast recovery of the WPPM's active power P_{WPPM} and the active power swings of the TS connected synchronous generator that have not damped out by that time, the surplus in the system's active power balance leads to an overfrequency in the period of $t' = 0.6$ s to 1.2 s after the fault.

For the fault period, a comparison of these results with the ones previously presented (for $k_{\text{RCI}} = 6$ p.u.) shows an almost similar system frequency response. That already hints at a finding that a fast voltage control at distribution system level has only a small effect on the system frequency *during* the fault period, especially when compared to the influence of the load. As will be shown in section 4.6.3, however, the fast voltage control can influence the transient stability of transmission connected synchronous generators positively. Both control modes result in the same response of the rotor angle δ_i of the transmission connected SG present in the studied area (in relation to the reference machine) as seen in Fig. 4.9a.

The results confirm previous works presented in [ESE⁺09, REvD12, SKL12]. These works also showed a large excursion of the local voltage angle at the PCC of the WPPM for inductive networks with a high X/R ratio if the active current injection during the fault was high. However, no system wide effects were analysed in these previous works as it has been the case in the presented case study. Recommendations on how to mitigate the observed voltage angle excursion will be presented in section 4.5.3.

From the results one can conclude that 'deactivating' the fast voltage control of WPPM during fault by setting the reactive current injection gain to $k_{\text{RCI}} = 0$ p.u. could cause undesired effects both at distribution and transmission system level. While an increased risk of load shedding was identified for cases where a prolonged LVRT operation would occur (section 4.4), the risk of an overfrequency above 50.2 Hz that could potentially trigger the tripping of distributed generation in the German power system [Eco11, EDBI13] was identified in the present case of sub-transmission connected WPPMs with a state-of-the-art fault operating mode and $k_{\text{RCI}} = 0$ p.u. One should, therefore, refrain from setting $k_{\text{RCI}} = 0$ p.u. If really necessary, an appropriate 'blocking mode' should be used during LVRT operation as analysed in section 4.4 and the resulting impact on the system performance should be studied by the relevant transmission system operator.

4.5.3 Impact with new robust control mode

The impact of the new robust fault control mode (NEW) on the response of sub-transmission connected WPPM to transmission network faults during reverse power flow situations and the resulting system performance is shown for two different reactive current gains of $k_{\text{RCI}} = 6$ p.u. and $k_{\text{RCI}} = 0$ p.u. Simulation results are presented in Fig. 4.11 and Fig. 4.12 for the reverse power flow case. This new control mode was designed heuristically based on the previous analysis of the state-of-the-art control modes.

Table 4.5 shows the modifications regarding control characteristics, parameters, and transition rules implemented for this control mode.

In the following analysis, the fast voltage control is set to be continued over a period of $T = 500$ ms after fault clearance and the voltage deadband is reduced from $V_{\text{DB}} = \pm 0.1$ p.u. to ± 0.05 p.u.. The I_d current is reduced to a value proportional to the square of the retained voltage, i.e. $I_d = \bar{I}_{d,0} \cdot (V_{\text{Fit}} \mp V_{\text{DB}})^2$. The active power recovery after fault is delayed with a

Problem	Solutions
voltage jump for high $k_{\text{RCI}} \geq 6$ at operating mode transition ($t' = t'_{\text{Flt}} + T$)	<ul style="list-style-type: none"> • use SDL instead of TC curve
poor post-fault voltage recovery for SDL curve	<ul style="list-style-type: none"> • continue fast voltage control over period of T post-fault • reduce deadband
voltage angle instability for $k_{\text{RCI}} = 0$ p.u.	<ul style="list-style-type: none"> • use voltage dependent I_d reduction
transient overvoltage at fault clearance	<ul style="list-style-type: none"> • continue fast voltage control over period of T post-fault • delayed active power recovery with $\Delta i/\Delta t'$

Table 4.5: Overview and motivation of modifications in NEW mode

ramp of $\Delta i/\Delta t' = 2$ p.u./s which is about ten times faster than the standard ramp given for the TC mode in [Ver07] but significantly slower than the instantaneous recovery requested for the SDL mode in [Ger09].

The results show that the new fault control mode overcomes some of the problems that were found for the state-of-the-art control modes during reverse power flows. The system performance is enhanced for both values of $k_{\text{RCI}} = 6$ p.u. and $k_{\text{RCI}} = 0$ p.u. The new fault control mode also performs well for normal power flow and exporting power flow situations (not shown here).

In both cases, the frequency deviation stays almost completely within the upper and lower maximum steady state frequency deviation limits. For $k_{\text{RCI}} = 0$ p.u. the frequency drops two times below the lower maximum steady state frequency deviation limit for a small period at $t' = 0.4$ s and $t' = 0.8$ s. For $k_{\text{RCI}} = 6$ p.u. it stays above this limit and then increases much faster than in the previous case. In both cases, the system frequency recovers into the standard frequency range within 1.3 s after the fault clearance ($t' = 1.7$ s). The critical threshold of 50.2 Hz is not surpassed for neither of the reactive current gain values studied. In conclusion, the new fault control mode performs better than the state-of-the-art control modes from a system frequency performance viewpoint in this test system.

The results further show that the restoration of active power in-feed starts immediately at the fault clearance ($t' = 0.4$ s) for both values of the reactive current gain. The reason is the implemented voltage dependent I_d reduction. This controller reduces the I_d current in proportion to the square of the retained voltage. Whenever the terminal voltage V_{WTG} increases again, the controller will also increase the WPPM's direct-axis current again. With the combination of the SDL characteristic curve and a reduced deadband of $V_{\text{DB}} = \pm 0.05$ p.u., the fault control mode continues until $t' = 1.17$ s to 1.25 s in both cases and then for an additional $T = 500$ ms. For that whole period, the WPPM continues the fast voltage control in the case with $k_{\text{RCI}} = 6$ p.u. by injection of a small amount of reactive power into the network. No voltage jump at the time of transitioning from fault to steady-state operating mode ($t' = 1.67$ s to 1.75 s) can be observed. Compared to the previously shown

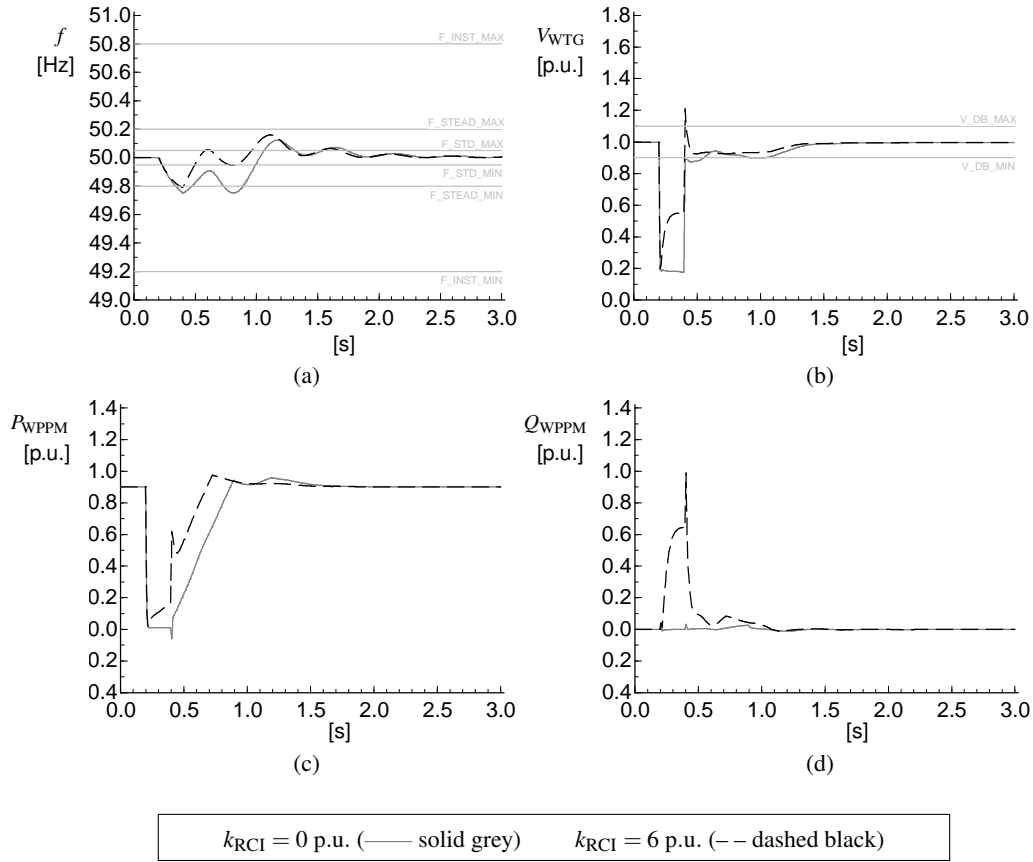


Figure 4.11: Impact of fault control mode (NEW) and reactive current gain ($k_{RCI} = 0$ vs. 6) during reverse power flow situations on sub-transmission connected WPPM control and system performance (ST_RPF_Zdyn). Taps were in both cases adapted to keep WPPM terminal voltage at 1 p.u. and the pre-fault operating point of the WPPM was in both cases set to $\cos(\varphi) = 1$.

results for the TC and SDL control modes, the improved transition between the operating modes comes at the cost of a slightly poorer voltage recovery at the WPPM terminals.

While most of the former are improvements over the state-of-the-art fault control modes, the new control mode still causes a local transient overvoltage at the WPPM terminals at the time of the fault clearance for $k_{RCI} = 6$ p.u. As stated earlier, technical limits do not allow for fully mitigating that transient overvoltage. Therefore, a fast transition between fault and normal operating mode can be achieved only at the cost of a 30 ms to 40 ms transient overvoltage at the WPPM terminals following the instance of fault clearance. As stated earlier, such transient overvoltage is deemed acceptable from a power quality viewpoint.

With regard to the excursion of the voltage angle at the WPPM PCC Fig. 4.12b proves that the new control mode does not cause a large excursion of the voltage angle even for the $k_{RCI} = 0$ p.u. case.

As Fig. 4.11a reveals, an overfrequency can be observed at $t' = 1$ s. However, compared

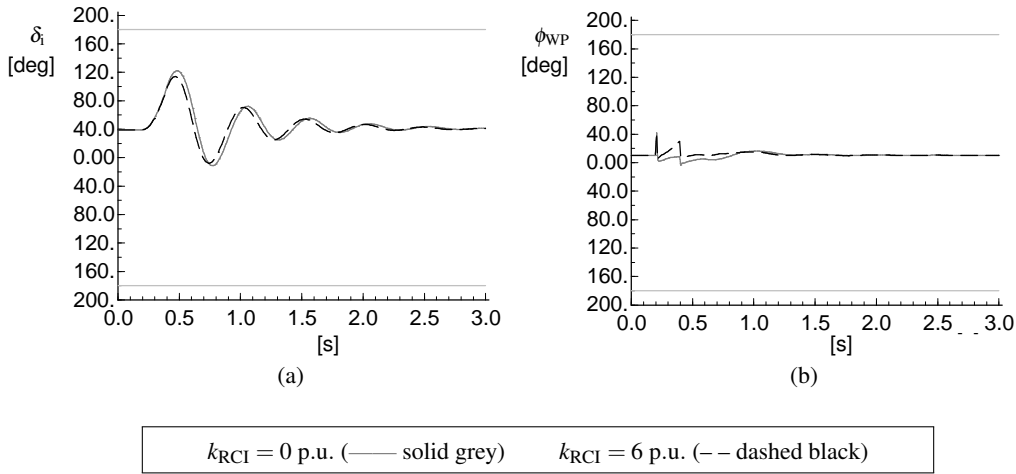


Figure 4.12: Impact of fault control mode (NEW) and reactive current gain ($k_{RCI} = 0$ p.u. vs. 6 p.u.) during reverse power flow situations on the transient stability of the transmission connected synchronous generator and the excursion of the voltage angle at the WPPM point of common coupling.

to the overfrequency observed for the state-of-the-art control modes with $k_{RCI} = 0$ p.u. as presented in Fig. 4.8a, the new control mode leads to a smaller frequency overshoot. This is due to the delayed active power recovery after fault which reduces the active power surplus in the power system that would have otherwise occurred when interacting with the active power swings of the TS connected synchronous generator.

The benefit of a fast voltage control ($k_{RCI} > 0$) for the transient stability of transmission connected synchronous generators can be observed in Fig. 4.12a. For the present control mode, a higher value for the reactive current gain k_{RCI} results into a slightly smaller excursion of the rotor angle δ_i of the transmission connected SG present in the studied area (in relation to the reference machine). This confirms findings from previous works in [SER09, Wei13b].

From the results one can conclude that the new fault control mode performs better for both low and high reactive current gains k_{RCI} in terms of system frequency and local voltage angle than the two state-of-the-art control modes. In terms of local voltage magnitude, the improved transition between the operating modes comes at the cost of a slightly poorer voltage recovery at the WPPM terminals in the post-fault period. Due to the reduced voltage deadband V_{DB} used for the control following the SDL characteristic curve, the post-fault voltage still recovers into the normal operating range of $V = (1 \pm 0.1)$ p.u. and is, therefore, acceptable. The main disadvantage of the new control mode is a risk of local transient overvoltage at distribution system level over a duration of 30 ms to 40 ms which can actually be of substantial value in the range of 1.2–1.4 p.u. Therefore, a reactive current gain k_{RCI} close to the standard value of $k_{RCI} = 2$ p.u. should be used for WPPM at a PCC with a small short-circuit ratio.

4.6 Impedance adjusted control mode

In this section the previously introduced new fault control mode (NEW) is tested against the state-of-the-art fault control modes for shallower voltage dips and further developed into an adjusted fault control mode (ADJ) to mitigate the impact of a PCC with smaller SCR and/or a lower X/R ratio. The objective is to further justify some of existing control schemes and to further improve the response of WPPMs to transmission network faults during reverse power flow situations with the ADJ fault control mode. The focus is put on the ‘effectiveness’ and the ‘stability’ of supporting the WTG terminal voltage (which is similar to the WPPM’s PCC voltage). Impacts on the other performance criteria listed in table 4.4 are highlighted where necessary.

The resulting system performance is first studied for sub-transmission connected wind power park modules (scenario ST) for high values of the reactive current gain k_{RCI} . Then, the performance is studied for distribution connected WPPMs (scenario DS) with an additional reactive/active current injection (aRACI) fault control mode. This is believed to lead to higher effectiveness and stability than a pure reactive current injection due to the lower X/R ratio at the PCC of the latter.

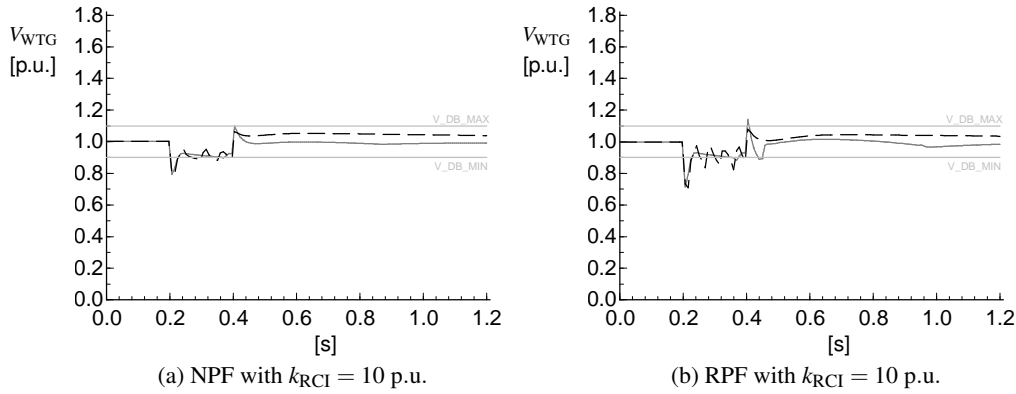
Results for three faults that lead to different values of the retained voltage V_{Flt} are presented ($V_{Flt} = 0.25$ p.u., 0.5 p.u., and 0.75 p.u.). Simulation results are presented for normal and reverse power flow cases in comparative voltage plots. The adjustments are outlined and motivated in table 4.6. For block diagrams and a mathematical description of the adjustments in the controller refer to appendix C.1.3.

Problem	Solutions
switching between normal and fault mode during fault period, see Fig. 4.13	<ul style="list-style-type: none"> • use SDL instead of TC curve • use hysteresis • continue fast voltage control over period of T post-fault
voltage oscillations during fault period for shallow voltage dips and high $k_{RCI} > 6$, see Fig. 4.14 and Fig. 4.15	<ul style="list-style-type: none"> • delayed active power recovery with $\Delta i/\Delta t'$ • use voltage dependent I_d reduction
limited effectiveness of voltage support at PCC with low X/R ratio, see Fig. 4.17	<ul style="list-style-type: none"> • injection of additional reactive/active current dependent on the angle ψ_{aRACI} of the equivalent network impedance at PCC

Table 4.6: Overview and motivation of controls in ADJ mode

4.6.1 Switching between operating modes during fault period

Figure 4.13 shows the WTG terminal voltage response for a normal and reverse power flow situation with certain modifications of the state-of-the-art fault control modes for a very high reactive current gain of $k_{RCI} = 10$ p.u. and a shallow voltage dip with $V_{Fit} = 0.75$ p.u. The TC mode was modified by deactivating the hysteresis, i.e. setting $\Delta V_{FRT_DB_FAULT} = \Delta V_{FRT_DB_CLEAR} = 0.1$ p.u., and the continuation of voltage support after fault, i.e. setting $i_{FRT_CI_CONT} = 0$. The SDL mode was modified by changing the characteristic curve to the TC curve, i.e. setting $i_{FRT_CI_MOD} = 0$.



TC mode without hysteresis and $i_{FRT_CI_CONT} = 0$ (— solid grey)

SDL mode with TC curve, i.e. $i_{FRT_CI_MOD} = 0$ (--- dashed black)

Figure 4.13: WTG terminal voltage [p.u.] impact of pre-fault power flow direction (NPF vs. RPF) for modified TC and SDL fault control modes for sub-transmission connected WPPM (ST_RPF_Zdyn) and $V_{Fit} = 0.75$ p.u. Taps were in both cases adapted to keep WPPM terminal voltage at 1 p.u. and the pre-fault operating point of the WPPM was in both cases set to $\cos(\varphi) = 1$.

The results show oscillations of the WTG terminal voltage for both the normal and reverse power flow situation. These oscillations are more pronounced in the SDL variant. In the normal power flow situation, they are hardly noticeable in the TC variant.

An analysis of the internal states of the WPPM fault mode controller showed that the observed oscillations result from a switching between fault and normal operating mode during the fault period. The high reactive current gain of $k_{RCI} = 10$ p.u. lifts the WTG terminal voltage for a shallow voltage dip back into the voltage deadband $V_{DB} = (1 \pm 0.1)$ p.u. Due to the fault controller's design, it erroneously detects a fault clearing and switches to normal operating mode. The voltage support is ceased, the voltage drops out of the deadband and the controller switches to fault operating mode again. That process is repeated until the actual end of the fault.

From the results one can conclude on the importance of the three settings varied. The continuation of the voltage support after fault prevents the WPPM from switching from fault to normal operating mode too early. The SDL characteristic curve ensures that the voltage

is not lifted into the deadband. As an additional safety measure, the hysteresis creates an additional security margin between the voltage threshold for the fast voltage support and the transition from fault to normal operating mode. The proposed new control mode considers these factors. This is explained in the next section.

4.6.2 Impedance magnitude adjusted control mode

Figure 4.14 shows the WTG terminal voltage response for a normal and reverse power flow situation for the SDL fault control mode with a very high reactive current gain of $k_{RCI} = 10$ p.u. The voltage plots compare the response of the sub-transmission connected WPPM for different voltage dip depths, i.e. $V_{Flt} = 0.25$ p.u., 0.5 p.u., and 0.75 p.u.

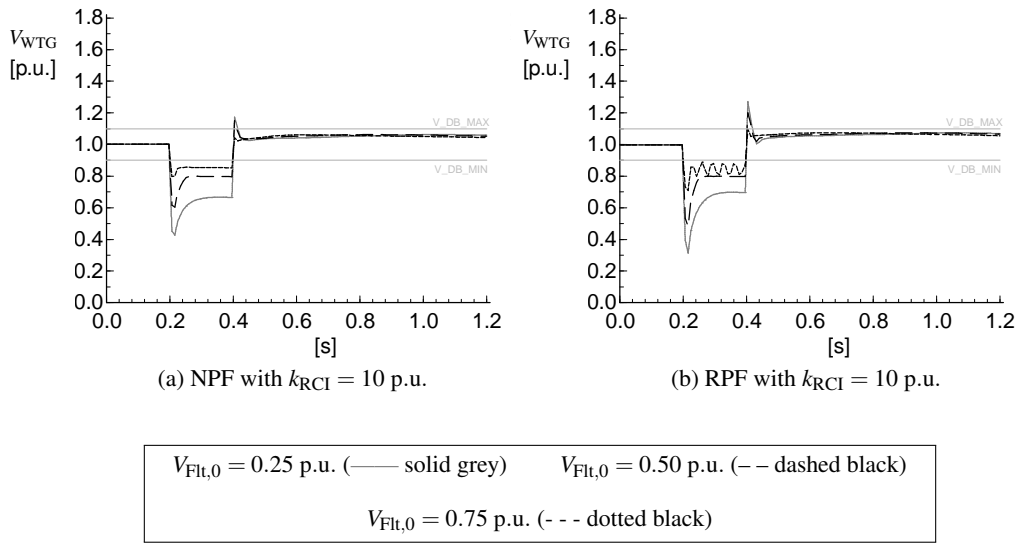


Figure 4.14: WTG terminal voltage [p.u.] impact of pre-fault power flow direction (NPF vs. RPF) for SDL fault control mode for sub-transmission connected WPPM (ST_RPF_Zdyn). Different voltage dip depths $V_{Flt} = 0.25$ p.u., 0.5 p.u., and 0.75 p.u. Taps were in both cases adapted to keep WPPM terminal voltage at 1 p.u. and the pre-fault operating point of the WPPM was in both cases set to $\cos(\varphi) = 1$.

The results show oscillations of the WTG terminal voltage for a shallow voltage dip with $V_{Flt} = 0.75$ p.u. in the reverse power flow situation. For deeper voltage dips or in the normal power flow situation, these oscillations do not occur.

An analysis of the internal states of the WPPM fault mode controller showed that the observed oscillations *do not result* from a switching between fault and operating mode during the fault period. In order to identify the underlying reasons and to develop potential solutions, further modifications to the SDL fault control mode were applied. These results are presented in Fig. 4.15.

Fig. 4.15b indicates that reducing the reactive current gain from $k_{RCI} = 10$ p.u. to $k_{RCI} = 6$ p.u. can mitigate the observed voltage oscillations in reverse power flows. Fig. 4.15c suggests that activating the delayed active power recovery (dAPR) in the SDL mode by setting $i_{FRT_CL_dAPR} = 1$ can mitigate the voltage oscillations even for a very high reactive current

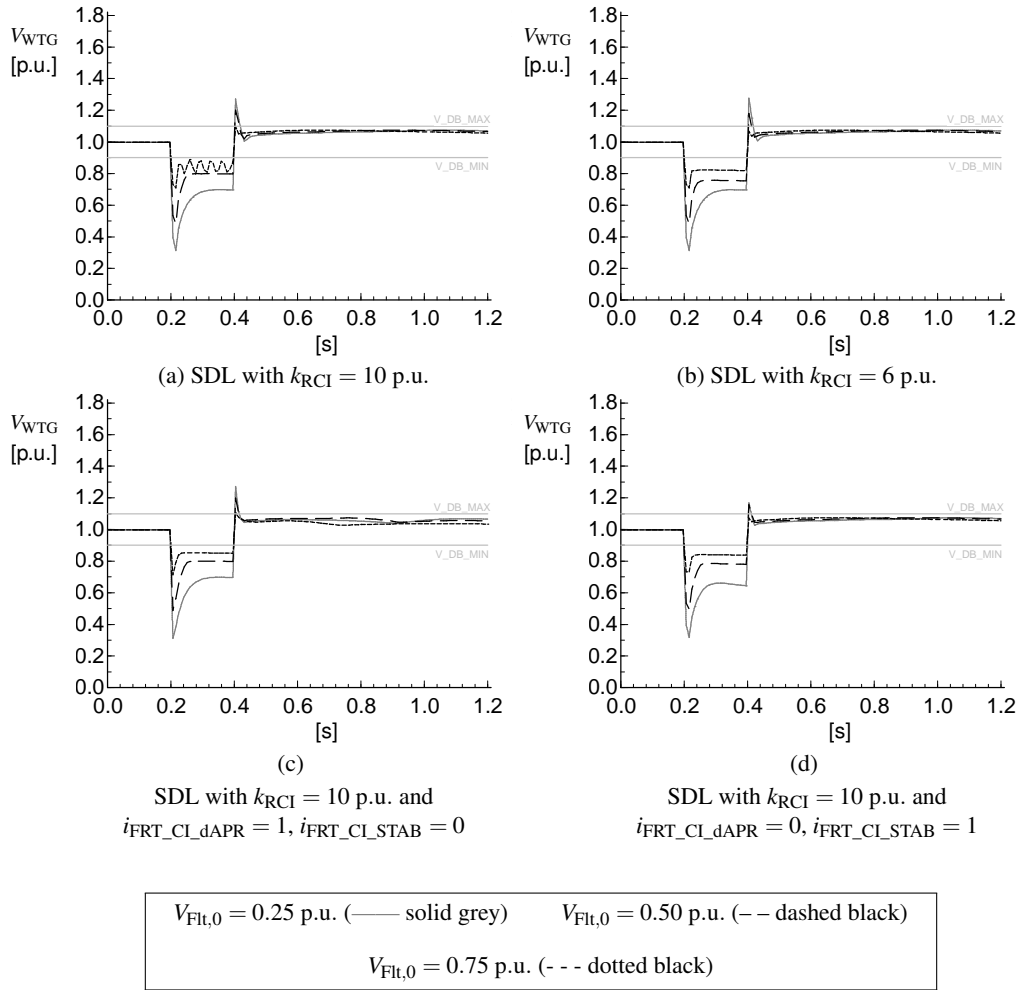


Figure 4.15: WTG terminal voltage [p.u.] impact of reactive current gain ($k_{RCI} = 10$ p.u. vs. 6 p.u.) and active current control strategy ($i_{FRT_CI_dAPR}$, $i_{FRT_CI_STAB}$) during reverse power flow situations for sub-transmission connected WPPM (ST_RPF_Zdyn). Taps were in both cases adapted to keep WPPM terminal voltage at 1 p.u. and the pre-fault operating point of the WPPM was in both cases set to $\cos(\varphi) = 1$.

gain of $k_{RCI} = 10$ p.u. Finally, Fig. 4.15d suggests that activating the voltage dependent direct-axis I_d current reduction can also mitigate the voltage oscillations for a very high k_{RCI} .

The identified mitigation measures suggest the finding that the voltage oscillation results from an interaction between the two controllers for the reactive current and the active current during the fault mode. The oscillations always seem to occur when a very high k_{RCI} causes large changes of the reactive current I_q and the active current I_d is adjusted very quickly thereafter. The fault controller is designed such that the I_q current has a rise time of 30 ms whereas the I_d current has a rise time of only 2 ms. An additional analysis has shown that

the oscillations did not occur when the rise time of the I_q current was reduced to 2 ms.

From the results one can conclude that very high values of the reactive current gain such as $k_{\text{RCI}} = 10$ p.u. in the SDL fault control mode may result in local voltage oscillations at the WTG terminals in case of shallow voltage dips during reverse power flows. With the design of the adjusted fault control mode these voltage oscillations do not occur, because the active current I_d is reduced during the fault depending on the retained voltage V_{Fit} and its recovery is delayed by a ramp of $\Delta i/\Delta t'$. Strictly speaking, only one of these two measures would already be sufficient to prevent the voltage oscillations.

4.6.3 Impedance angle adjusted control mode

—*Influence of X/R ratio*— The X/R ratio at the WPPM PCC determines for which angle ψ_{aRACI} between current and voltage at the WTG terminals the highest voltage support can be achieved (see also section 2.4). The X/R ratio of the equivalent network impedance at a given PCC in the distribution system is determined by all upstream network elements as well as the X/R ratio of and the position on the adjacent network line (Fig. 4.16). Typical values for the X/R ratio of line elements at different voltage levels are given in table 4.7.

Table 4.7: Ranges for the X/R ratio of line elements at different voltage levels

Voltage level	X/R ratio	Ψ
HV	> 10	> 84°
MV	0.7...3.3	35°...73°
LV	0.4...0.5	22°...27°

Typical values for the X/R ratio at the PCC are given in table 4.8. Compared to values of 10 in high voltage (HV) networks, the X/R ratio of a PCC in the German MV distribution system can be as low as 3.3 ($\psi_{\text{G,MV}} = 73^\circ$) and in the LV distribution system as low as 0.5–1 ($\psi_{\text{G,LV}} = 27^\circ$ to 45°). Further analytical considerations on the influence of the X/R ratio ($= \tan(\phi_{\text{G}})$) on the effectiveness of disturbance voltage support can be found in section 2.4.

Table 4.8: Ranges for the X/R ratio of the equivalent network impedance at the PCC for different voltage levels

Voltage level	X/R ratio	ψ_{G}
HV	> 10	> 84°
MV	3.3	73°
LV	0.5...1	27°...45°

—*Control mode*— The proposed control mode from section 4.5.3 is adjusted such that the angle ψ_{aRACI} of the *additional* current injection in the fault operating mode can be chosen. Equation (3.1) is replaced by (4.1)–(4.2) and the resulting total current I_{Fit}° is scaled by a factor F_{max} that maintains the resulting total current angle. Further details are given in appendix C.1.3.

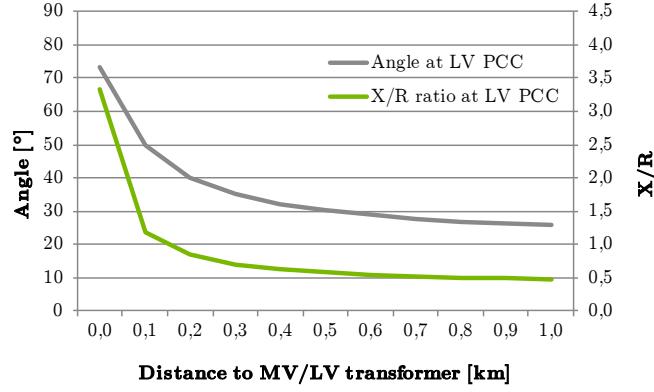


Figure 4.16: Dependence of X/R ratio of the equivalent network impedance at the PCC on the position on the adjacent network line

$$\underline{I}_{\text{Flt}}^{\circ} = \bar{I}_0 + \Delta \underline{I}(\Delta V) = I_{d,\text{Flt}}^{\circ} + jI_{q,\text{Flt}}^{\circ} \quad (4.1)$$

$$\underline{I}_{\text{Flt}} = \underline{I}_{\text{Flt}}^{\circ} \cdot F_{\text{max}} = I_{d,\text{Flt}} + jI_{q,\text{Flt}} \quad (4.2)$$

with

$$\Delta \underline{I}(\Delta V) = e^{j(\phi_G + \psi_{a\text{RACI}})} \cdot \begin{cases} k_{\text{RACI}} \cdot [\Delta V \mp V_{\text{DB}}] & , |\Delta V| \leq V_{\text{DB}} \\ 0 & , |\Delta V| > V_{\text{DB}} \end{cases}$$

$$\Delta V = V - \bar{V}_0$$

$$\bar{I}_0 = \frac{1}{T} \int_{t'-T}^t \underline{I}(t') dt'$$

$$\bar{V}_0 = \frac{1}{T} \int_{t'-T}^t V(t') dt'$$

—**Results**— Figure 4.17 shows the WTG terminal voltage response for a medium voltage dip with $V_{\text{Flt}} = 0.50$ p.u. for the ADJ fault control mode with a reactive current gain of $k_{\text{RACI}} = 6$ p.u. in a reverse power flow situation. The angle of the additional reactive/active current injection $\psi_{a\text{RACI}}$ is varied for the distribution connected WPPM ($\psi_{a\text{RACI}} = 45^\circ$ vs. 75° vs. 90°). The angle of the equivalent network impedance at the WPPM's PCC is $\psi_{G,\text{MV}} = 73^\circ$ (see table B.1).

The results show that the 'effectiveness' of the fast voltage control depends on the additional reactive/active current injection angle $\psi_{a\text{RACI}}$. For a small value of $\psi_{a\text{RACI}} = 45^\circ$, the least voltage support is achieved. For a value of $\psi_{a\text{RACI}} = 90^\circ$ (exclusive reactive current injection) the maximum voltage support is achieved. The latter is a surprising finding since from the discussion in section 2.4 it was to be expected that the maximum voltage support would be achieved when $\psi_{a\text{RACI}} = \psi_{G,\text{MV}}$, hence $\psi_{a\text{RACI}} = 73^\circ$ in this case. The underlying reason for why this does not hold here will be analysed in the following by use of

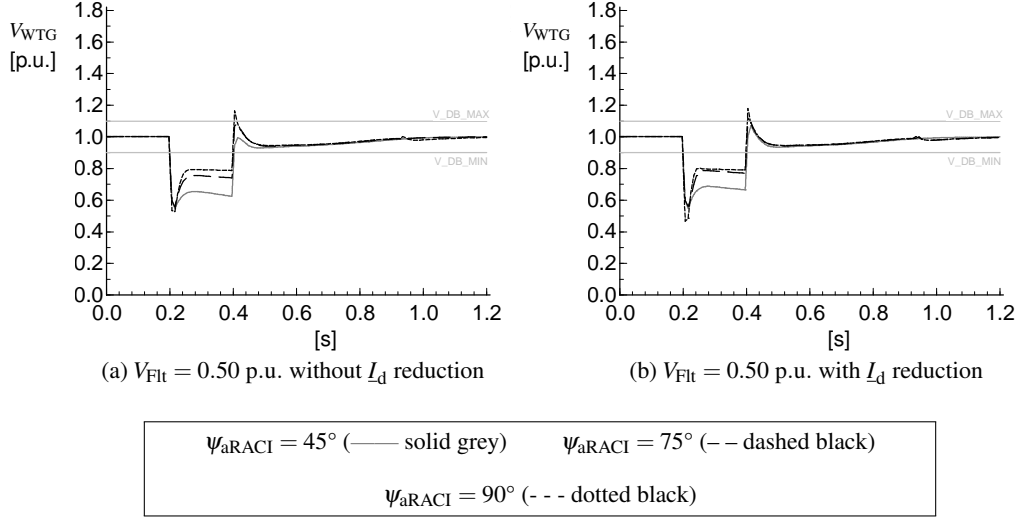


Figure 4.17: Impact of additional reactive/active current injection angle ($\psi_{aRACI} = 45^\circ$ vs. 75° vs. 90°) for $k_{RCI} = 6$ p.u. on WTG terminal voltage during reverse power flow situations for distribution connected WPPM (DS_RPF_Zdyn). Medium voltage dip with $V_{Flt} = 0.50$ p.u. Without (left column) and with (right column) voltage dependent direct-axis current I_d reduction. Taps were in both cases adapted to keep WPPM terminal voltage at 1 p.u. and the pre-fault operating point of the WPPM was in both cases set to $\cos(\varphi) = 1$.

Fig. 4.18. From Fig. 4.17 it can be further noted that the difference between $\psi_{aRACI} = 75^\circ$ and $\psi_{aRACI} = 90^\circ$ is negligible when the voltage dependent active I_d current reduction is activated.

Figure 4.18 shows the WTG terminal voltage response for a various voltage dip depths ($V_{Flt} = 0.25$ p.u., 0.5 p.u., and 0.75 p.u.) for the ADJ fault control mode with a reactive current gain of $k_{RCI} = 2$ p.u. (instead of $k_{RCI} = 6$ p.u.) in a reverse power flow situation. The angle of the additional reactive/active current injection ψ_{aRACI} is again varied for the distribution connected WPPM ($\psi_{aRACI} = 45^\circ$ vs. 75° vs. 90°). The angle of the equivalent network impedance at the WPPM's PCC is $\psi_{G,MV} = 73^\circ$ (see table B.1). The left column shows results *without* voltage dependent I_d reduction and the right column results where this function *is* activated. Additional results for the system frequency f , the transmission connected SG rotor angle δ_i and the WPPM's PCC voltage angle ϕ_{WP} are helpful for the further understanding and can be found in appendix F.

The results show that an exclusive additional reactive current injection, i.e. $\psi_{aRACI} = 90^\circ$, achieves the most effective voltage support in all fault cases and independent from the direct-axis current control strategy. For very deep voltage dips with a retained voltage of $V_{Flt} \leq 0.25$ p.u., the voltage angle instability described in section 4.5.2 can be identified for any $\psi_{aRACI} \leq 75^\circ$ without voltage dependent direct-axis I_d current injection. If that function is activated, the voltage angle instability only occurs for any $\psi_{aRACI} \leq 45^\circ$ (see also additional results in appendix F). Hence, the combination of voltage dependent direct-

axis I_d current reduction and aRACI improves the voltage stability significantly.

Having in mind that for RPF situations, any short-circuit current injection from WPPMs with a direct-axis I_d current component unequal to zero will inevitably increase the voltage angle of the WPPM's PCC, the unexpected results for medium and shallow voltage dips can be explained as follows. As has been reported in [Zho13], the tracking of the local voltage angle by a WPPM's phase locked loop (PLL) in a 'weak' system ($SCR < 5$) can be poor. Consequently, the I_d and I_q reference values do not correspond to the active and reactive part of the current any longer. Since the WPPM has only the local voltage as a phase reference, the pre-set aRACI angle ψ_{aRACI} will not result in the desired effectiveness of voltage support. Future research should investigate whether a reduction of the gains of the WPPM's PLL or a blocking of the PLL below a certain value of V_{Flt} can increase the effectiveness of an aRACI.

Results for the transmission connected SG's rotor angle δ_i shown in Fig. 4.19 indicate that for a deep voltage dip without voltage dependent direct-axis I_d current reduction (Fig. 4.19e), the transient stability of that SG is reduced for any $\psi_{aRACI} \neq 90^\circ$. This result confirms previous results from [SER09]. From a TS viewpoint, an aRACI is not a preferred control mode.

From the analysis of the results regarding an impedance angle adjusted control mode (aRACI) one can conclude that this should not be a preferred control mode in future GCR. First, its effectiveness in very high penetration scenarios and RPF situations is limited. Second, this mode bears the risk of a local voltage angle instability. And third, the aRACI mode can have a negative impact on the transient stability of transmission connected SG.

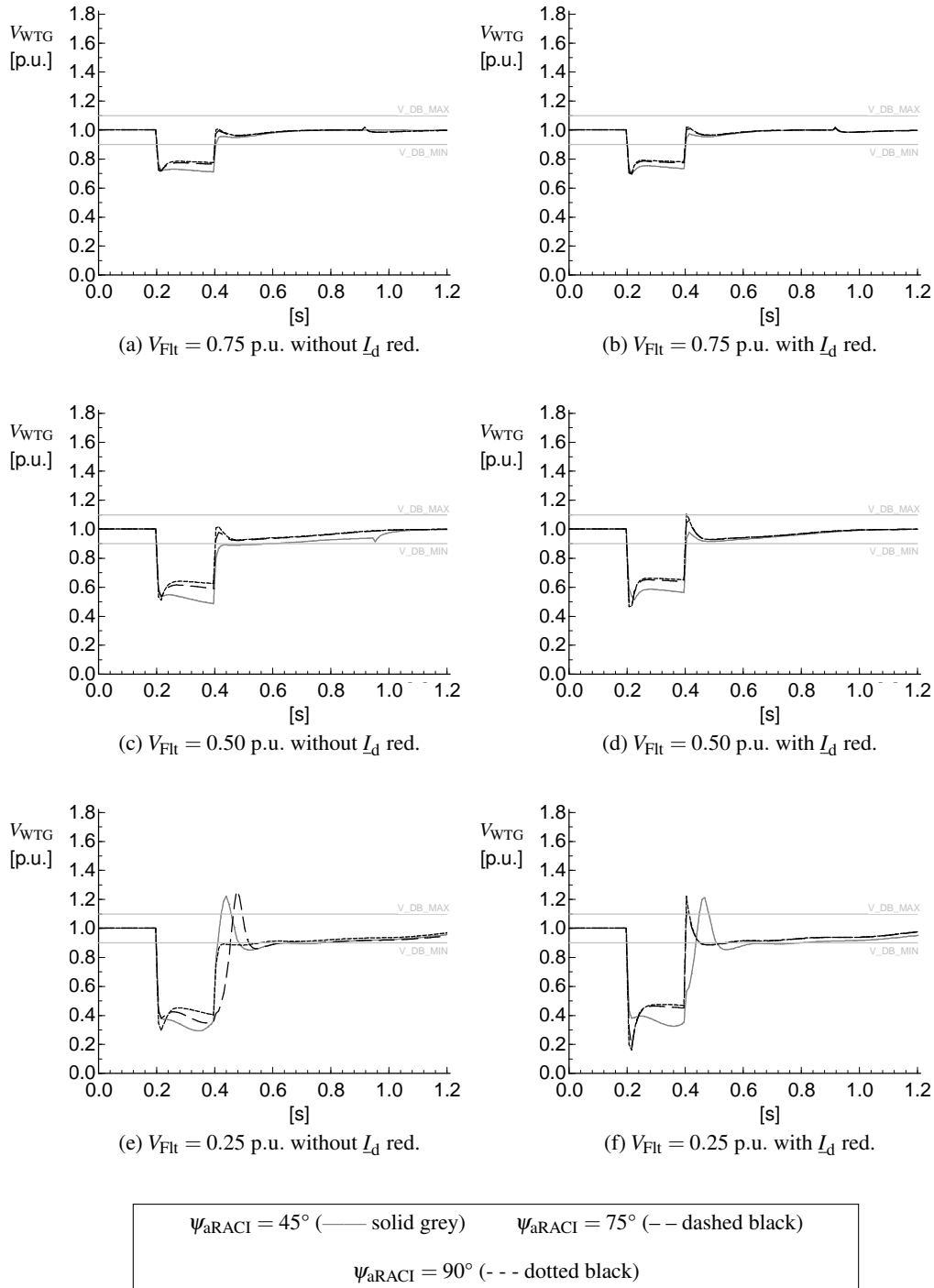


Figure 4.18: Impact of additional reactive/active current injection angle ($\psi_{aRACI} = 45^\circ$ vs. 75° vs. 90°) for $k_{RCI} = 2$ p.u. on WTG terminal voltage during reverse power flow situations for distribution connected WPPM (DS_RPF_Zdyn). Shallow (top row), medium (middle row) and deep (bottom row) voltage dip. Without (left column) and with (right column) voltage dependent direct-axis current L_d reduction. Taps were in both cases adapted to keep WPPM terminal voltage at 1 p.u. and the pre-fault operating point of the WPPM was in both cases set to $\cos(\varphi) = 1$.

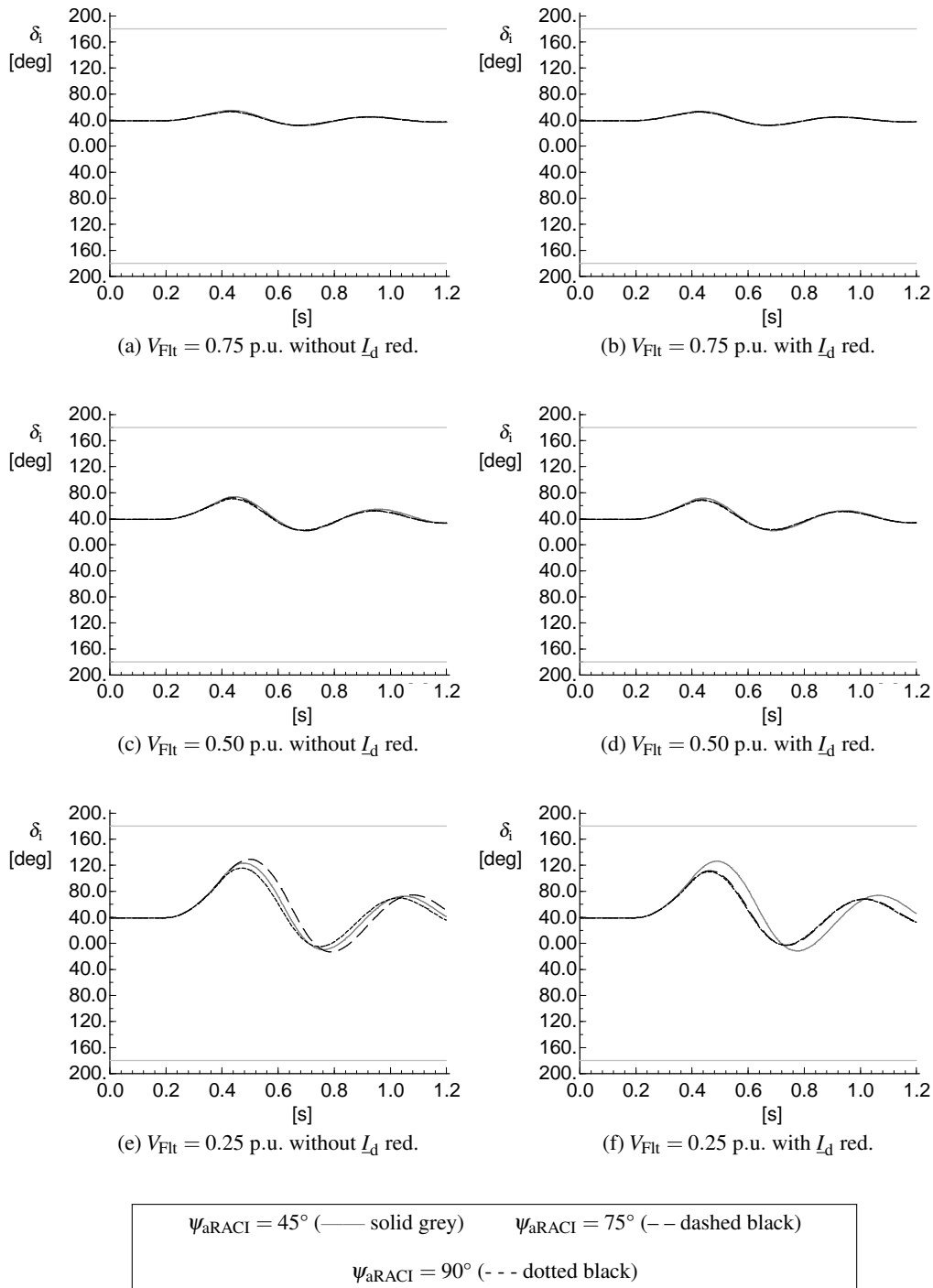


Figure 4.19: Impact of additional reactive/active current injection angle ($\psi_{\text{aRACI}} = 45^\circ$ vs. 75° vs. 90°) for $k_{\text{RCI}} = 2$ p.u. on transmission connected SG rotor angle δ_i during reverse power flow situations for distribution connected WPPM (DS_RPF_Zdyn). Shallow (top row), medium (middle row) and deep (bottom row) voltage dip. Without (left column) and with (right column) voltage dependent direct-axis current L_d reduction. Taps were in both cases adapted to keep WPPM terminal voltage at 1 p.u. and the pre-fault operating point of the WPPM was in both cases set to $\cos(\varphi) = 1$.

4.7 Conclusions

The objective of this chapter was to investigate the network fault response of wind power park modules connected to sub-transmission and distribution systems with a significant amount of induction motor loads during reverse power flow situations. The power system stability was assessed by using the system frequency as the major performance indicator. Local voltage stability was assessed by the local voltage angle at the WPPM's point of common coupling.

—Impact of pre-fault power flow direction— The results show significant differences between normal, exporting and reverse power flow situations (Fig. 4.2–4.4). Wind power park modules transition between normal and fault operating mode based on their terminal voltage. Fault-induced delayed voltage recovery, as it can be caused by large amounts of induction motor loads in an area, tends to be more pronounced in reverse than in normal power flow situations with high penetration of distributed generation.

—Prolonged LVRT operation with ‘blocking mode’— For reverse power flow situations, the simulation results suggest that the LVRT operation of sub-transmission and distribution connected WPPMs can be prolonged if they ride through low voltages below 0.9 p.u. in ‘blocking mode’. The effect does not seem to be specific of WPPMs and could potentially occur for any DG in an active distribution system that is prone to fault-induced delayed voltage recovery. Depending on the system inertia and frequency containment reserves available, the resulting sustained active power deficit in the power system can trigger a large frequency deviation in the post-fault period and, thereby, increase the risk of load shedding. Hence, these findings challenge current implementation practices of distribution system operators.

—New fast voltage control mode— A fast voltage control of WPPMs during the fault and post-fault period can mitigate their prolonged LVRT operation. A hysteresis for the transition between operating modes and a current injection ‘in addition to’ the pre-fault current set-point prevents undesired switching between the operating modes. An increase of the reactive current injection gain above its standard value of $k_{RCI} > 2$ p.u. further improves the post-fault voltage recovery. A reduction of the direct-axis current dependent on the retained voltage reduces the risk of violation of the WPPM's steady-state stability limit and a local voltage collapse. The robust performance of the new fault control mode was shown for a large number of system conditions and control parameter variations.

—Influence of WPPM's connection location— Wind power park modules connected to PCCs with low X/R ratio are more prone to the prolonged LVRT operation than WPPMs connected to PCCs with high X/R ratio. On the other hand, undesired voltage oscillations may occur when WPPMs that are connected to ‘weak’ PCCs^{A.12} ride through shallow voltage dips with fast voltage control and a very high reactive current gain ($k_{RCI} > 6$ p.u.). Delaying the active power response during the fault operating mode or activating a terminal voltage dependent reduction of the WPPM's direct-axis current may mitigate these oscillations.

—Combined active and reactive current injection during fault— For WPPMs connected to PCCs with low X/R ratio, a combined injection of reactive and active current aligned to the angle of the equivalent network impedance seen from the PCC was expected to show the most effective voltage support. This expectation, however, was not confirmed. The aRACI mode was found in reverse power flow situations to support the voltage less effectively than an exclusive reactive current injection, to bear a higher risk of violating the WPPM's steady-state stability limit, and also to negatively impact transmission connected synchronous generator's transient stability. Therefore, the aRACI mode should not be considered as a preferred option in future grid connection requirements.

The new fault control mode was adjusted according to these additional findings with terminal voltage dependent reduction and delayed recovery of the active current (I_d) and, therefore, shows a very good performance also for WPPMs connected 'deep' into the distribution system.

Chapter 5

Network Fault Response Requirements for LV Connected DG

This chapter investigates the network fault response of large amounts of low voltage (LV) connected distributed generation (DG) and its impact on post-fault active power balance following transmission system faults. Photovoltaic (PV) installations in low voltage networks are in the focus of this chapter. The main contribution of this chapter is to identify minimum grid connection requirements (GCRs) for LV connected DG and to analyse the opportunities and challenges of a full dynamic voltage support from distribution connected DG for system-wide stability.

In order to quantify this network fault response, a test system is constructed with DG penetration representative of a 2022 scenario for Germany. The test system comprises all voltage levels from low voltage to extra-high voltage (eHV), with the low and medium voltage levels simplified by means of aggregation as described in chapter 3.

The presented research was carried out in a research project funded by the German Forum network technology / network operation in the VDE (FNN) [Del14]. Parts of the results were published in a contribution to the International Solar Integration Workshop 2014 [vBR⁺14].

5.1 Introduction

Until today, most grid connection requirement around the world do not require low voltage ride-through (LVRT) capabilities from LV connected DG (see chapter 2 for more details). With continued increase of LV connected DG installations, such as distributed PV systems, the discussion about LVRT requirements at LV level has started a few years ago [IEE, ENT12b, For12]. The concern is that voltage dips caused by transmission network faults propagate to the LV grids in a wide area where they would potentially lead to massive tripping of LV connected DG.

For LV connected, small-scale DG larger than 6 kVA, only Italy [Com14] and a recently issued European standard [CEN15b] require LVRT. Only in Japan micro-scale DG,

including LV single-phase connected PV systems, are soon to be required to ride through voltage dips [Kob12, JEA13]. Notably, all of these LVRT requirements for LV connected DG either allow the units to block the inverter current ('momentary cessation') or do not further specify their fault response at all.

In-depth and system-wide stability studies of the network fault response of LV connected DG have been rare to date. Recent results have been published in [TGTB13] and [Ska14], primarily focusing on system voltage performance. The sensitivity of the retained voltage at LV distribution level to different power flow situations analysed by NationalGrid (UK) in 2005 [JT05, ENT12a]. Studies that adequately assess the 'legacy' of existing DG installations in the system and the opportunities that new-to-be connected DG installations can provide to the system are still missing. Hence, in order to prevent problems similar to those caused by unfavourable frequency protection settings [BBZ⁺11], [EE13a], the adequacy of current and recently proposed grid connection requirements with respect to the network fault response LV connected DG is investigated in the following.

The focus of this chapter lies on the impact of large amounts of PV installations in LV networks on post-fault active power balance following transmission system faults. The approach is based on representative modelling of real power systems. Two research questions are formulated:

1. How much active power in-feed from LV connected DG is lost due to a transmission system fault in a worst case scenario if current GCRs remain unchanged?
2. If a LVRT requirements for new LV connected DG proved necessary, should these units ride through voltage dips and block the inverter current ('limited dynamic voltage support') or should they support the voltage by feeding a reactive and/or active current into the grid ('full dynamic voltage support')?

5.2 Stability Simulation on a HV-MV-LV Power System

The research is conducted through time-domain simulations on a test system based on the IEEE New England (NE) 39-bus test system [Kun94, Mol12]. The test system is extended to include low voltage (0.4 kV), medium voltage (20 kV) and high voltage (110 kV) subsystems which are built based on current (2012) and forecasted (2022) data for the German network [Deu13], [Fed11]. Modelling the system in this new integrated way across all voltage levels allows for obtaining results that depend on interactions between the voltage levels and consider the response of active distribution system (ADS) at the *periphery region* (annulus) of a large-area voltage dip.

Modelling a complete power system would, however, lead to unacceptable computing burden for running time domain simulations. Therefore, the dynamic equivalencing technique proposed in chapter 3 is used for the LV and medium voltage (MV) levels. DG technologies included in the test system are photovoltaic power park modules (PVPPMs), wind power park modules (WPPMs) (full converter interface unit and doubly fed asynchronous generator) and combined heat and power plants. Details on the used ADSs are given in appendix E.

The problem is analysed in the time domain using positive-sequence, root mean square (rms) simulations for a transmission network fault that causes the retained voltage at transmission level to drop close to the existing DG's undervoltage protection settings. From a

modelling perspective, this is a case where accurate modelling of the network fault response of ADSs is very important as discussed in chapter 3. While a balanced three-phase transmission fault with a high fault impedance is assumed in this study, it may represent three-phase transmission faults distant to the analysed system area or (more common) phase-to-earth faults in reality.

Multiple operational scenarios (dispatches) are considered to study the effects of pre-fault operating point, LV connected DG fault control modes (CMs) and MV connected DG low voltage ride-through operation with additional reactive/active current injection ('full dynamic voltage support') settings. Results are compared by merit of their post-fault active power balance and voltage quality.

5.2.1 Test system overview

A high-level overview of the complete test system is given in Fig. 5.1.

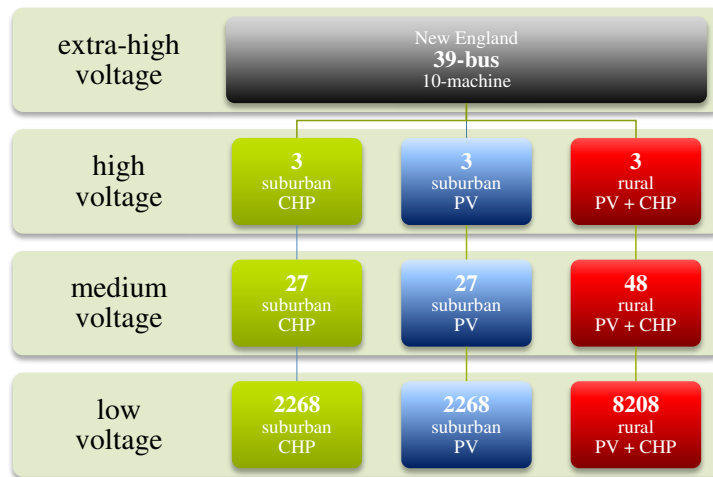


Figure 5.1: Overview of test system networks.

The used IEEE 39-bus, 10-machine New England test system model was developed for the IEEE Task Force on Benchmark Systems for Stability Controls in [Mol12]. The originally North American based model was adapted to operate at European nominal frequency (50 Hz) and eHV voltage level (380 kV).

A total of nine sub-transmission ring systems (110 kV) based on [BvR⁺11a] are connected to the transmission system in three different areas. These three areas represent a rural and two distinct suburban regions with their corresponding dynamic ADS equivalents connected to each sub-transmission ring system. The suburban distribution systems (DSs) differ in their dominant DG technology at LV level. This distinction is important because of the fundamentally different dynamic behaviour between PVPPMs and combined heat and power (CHP) units. Hence, a total of three ADS types are integrated into the test system at the locations illustrated in Fig. 5.2:

- in Area 1, suburban CHP networks integrate CHPs as the only DG technology on the LV network (green circles).

- in Area 2, suburban PV networks integrate PVPPMs as the only DG technology in the LV network (blue circles).
- in Area 3, rural networks integrate large amounts of PVPPMs and small amounts of CHPs in the LV network (red circles).

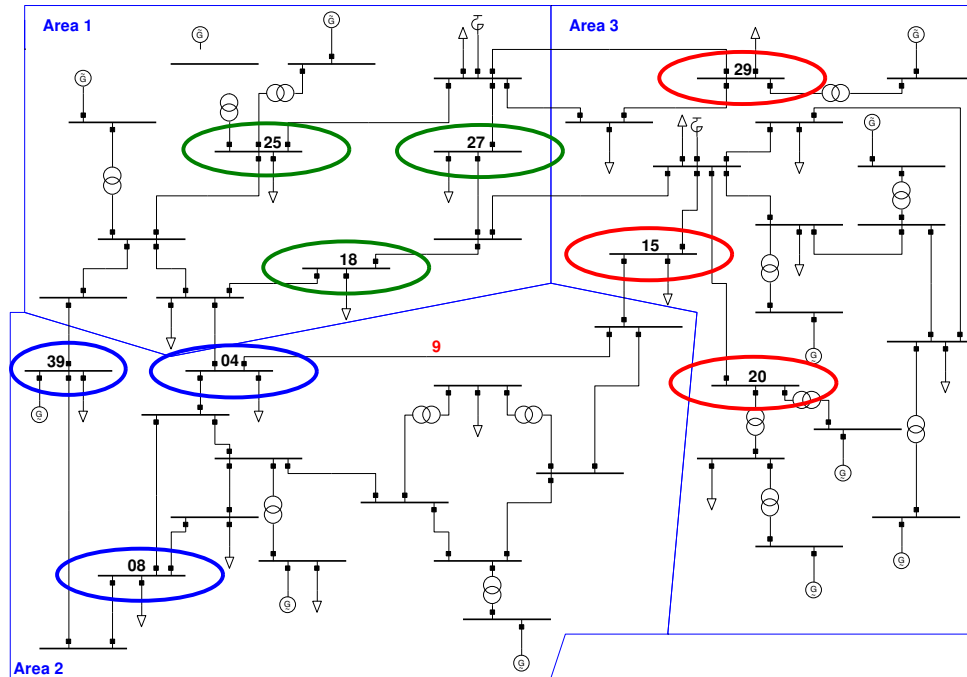


Figure 5.2: Schematic overview New England System, adapted from [Gal13].

The complete test system model represents approximately 12 500 LV systems with DG in an aggregated way, consists of about 950 (equivalent) DG models and 5 500 controllers. The simulations are performed with DIgSILENT PowerFactory© v15.1.

5.2.2 Test system DG penetration

The total capacity of transmission connected generation is 6 360 MW. With significant amounts of DG integrated into the test system, only a fraction of this capacity is used. Table 5.1 gives the rated DG penetration levels. These have been obtained from a statistical analysis based on [Deu13] as further explained in appendix E.1.

	Suburban PV			Suburban CHP			Rural			
	[%]	HV	MV	LV	HV	MV	LV	HV	MV	LV
All DG 2012	80	95	60	50	55	5	140	155	100	
All DG 2022	115	135	100	70	65	5	245	285	180	
PV 2012	35	50	60	5	10	0	65	95	100	
PV 2022	55	85	100	10	10	0	110	165	170	
Wind 2012	35	30	0	35	30	0	55	40	0	
Wind 2022	45	30	0	45	30	0	100	80	0	
CHP 2012	10	15	0	10	15	5	20	20	0	
CHP 2022	15	25	0	15	25	5	35	45	10	

Table 5.1: Test system penetration.

5.2.3 Integration of ADSs into the transmission system

The test system is divided into three areas. In the original NE test system, areas 1 and 2 import power, while area 3 exports power.

Area 1 has the highest power import in the original test system. Since the suburban CHP distribution system has the lowest penetration out of the three distribution networks, it is most suited to be connected in area 1. Similarly, the rural distribution system has the highest penetration and is thus connected at the power exporting area 3. Wherever a distribution system is connected to the transmission system, the original load at the transmission busbar is reduced by the total installed amount of load in the distribution system. This way, the installed load at the busbar is kept constant and power flows are minimally altered from the original New England transmission system.

An overview of the DS connection points is given in table 5.2 and illustrated in Fig. 5.2. It should be noted that theoretically, this method of placing the aggregated distribution systems would allow for a total of 23 (11 suburban PV, 5 suburban PV and 7 rural) networks. However, only nine systems are used to keep simulation times reasonable.

Any lack or excess of power in the test system is balanced by the generators in the NE system. Active power is balanced by distributed slack generators, whereby the original dispatch is optimised for cost. Each area has one fictitious slack generator that can represent interconnections with areas outside of the modelled power system.

Area	Busbars	Type
1	18, 25, 27	Sub_CHP
2	04, 08, 39	Sub_PV
3	15, 20, 29	Rural PV + CHP

Table 5.2: Sub-transmission system connection points.

The high in-feed of active and reactive power from the distribution networks causes overvoltages at the transmission level. These are mitigated by placing shunt reactors at the substations located at nodes 16 and 26. Each shunt reactor has a rated capacity of 300 Mvar and the number of shunts in operation is adjusted to keep the network voltage

within acceptable limits.

Further New England test system details are given in appendix B.2.

5.2.4 DG modelling

For power system dynamic studies, DGs models determine the *performance details* for the network fault response of specific DGs technology classes. In this case study, the PVPPMs, WPPMs, and CHP plants are modelled as described in section 3.2.

Existing DG is modelled according to their actual performance defined by GCR in place when they went into operation. This holds for fault response, as well as for (dynamic) power factor control. The only exception are the MV connected wind turbines, as 50 percent of these were retrofitted to give them LVRT capability to prevent massive disconnection of wind power in case of a transmission system fault [PKD⁺13]. This creates multiple ‘clusters’ of e.g. MV connected PVPPM, each with different settings. The resulting clusters and their installed capacities in the aggregated networks are presented in Fig. 5.3 with the performance classes as defined in Table 3.5 in chapter 3.

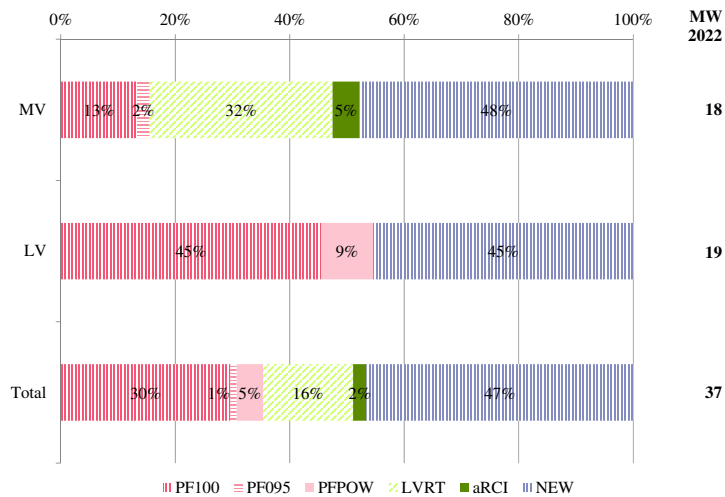


Figure 5.3: Grid code *performance framework* composition of the test system. Legend: PF100, PF095, PFPOW: various reactive power capabilities and steady state voltage control modes but no LVRT capability; LVRT, aRCI: low voltage ride-through capability with either inverter blocking or additional reactive current injection; NEW: fault response based on sensitivity case. Refer to Table 3.5 in Chapter 3 for further details.

In the base case, the reactive current injection gain (k-factor) of the MV connected PVPPMs and WPPMs is set to 0.2 p.u. This reflects current distribution system operator (DSO) operating practices that only allow MV connected DG connected at a substation to provide full dynamic voltage support through additional reactive current injection (aRCI). Those DG connected to a further downstream MV feeder are required to use the blocking mode (BM). According to the statistical analysis there is only very little substation connected DG in the ADSs.

5.2.5 Load modelling

The DIgSILENT general load model with an exponential representation of the static load and a linear representation of the dynamic load is used for representation of aggregated loads [DIg08]. The equations for the load model, D.1 and D.2, are given in appendix D. The parameter values used in the test system are listed in table 5.3.

Because no representative data was found for the frequency dependency of the loads, this dependency is ignored. In the time frame of interest of up to ten seconds, system frequency does not change significantly. The extra-high voltage loads in the New England system are of constant impedance.

	HV Loads		MV loads	LV loads	
	Mixed	Commercial/	industrial	Residential	Commercial
a_P	1.0		1.0	1.0	1.0
e_{aP}	1.0		1.4	1.7	1.4
a_Q	1.0		1.0	1.0	1.0
e_{aQ}	3.2		5.5	4.7	5.5

Table 5.3: Exponential load parameters [Ska14].

Table 5.4 lists where the different load types are used, as well as their respective dynamic parts. The time constant for the linear dynamic loads is assumed to be 0.1 s.

Type [-]		Dynamic [%]	Static [%]
LV	Residential	0	100
MV	Commercial/ industrial	20	80
HV	Mixed	20	80

(a) Suburban

Type [-]		Dynamic [%]	Static [%]
LV	Commercial	20	80
MV	Commercial/ industrial	20	80
HV	Mixed	20	80

(b) Rural

Table 5.4: Installed load types in representative networks.

5.3 Study Cases

In each of the study cases, a balanced three phase fault is introduced after 0.1 s, and cleared 150 ms later. The fault occurs in the middle of NE system line 9 and has an impedance of 12Ω .

Two study years, three operational scenarios (OSs) and, for 2022, four LV connected PVPPM fault control modes and two reactive current gains (k-factors) of MV connected DG are considered. In total 27 study cases were investigated. An overview of the study cases is provided in figure 5.4.

With this approach, the system impact of the different control settings in 2022 could be compared for three typical scenarios with very different instantaneous penetration levels. The 2012 cases serve as a base and show the ‘current’ state of the system.

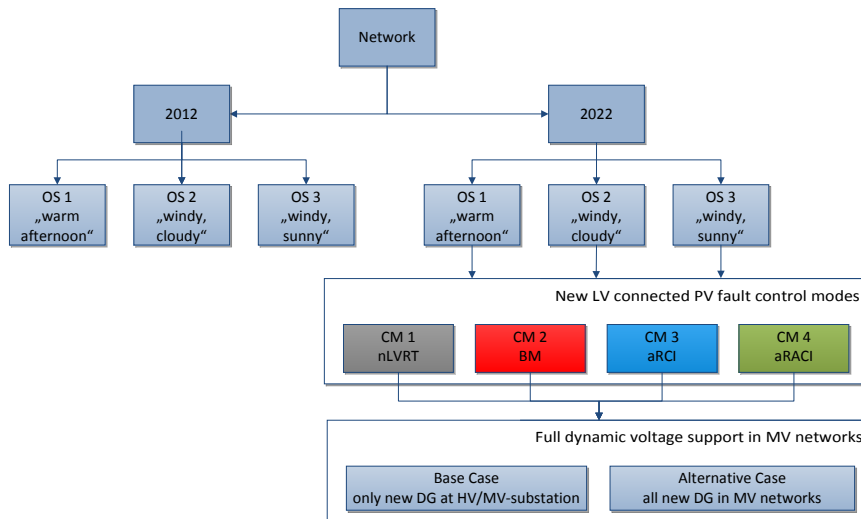


Figure 5.4: Overview of study cases. OS is operational scenario. nLVRT, BM, aRCI and aRACI denote no low voltage ride-through, blocking mode, additional reactive current injection and additional reactive and active current injection respectively.

5.3.1 Operational Scenarios

The three dispatches are selected to investigate the network in the extremes of its normal operating envelope. The dispatch for the three OSs are presented in figure 5.5.

Table 5.5 shows how the three OSs are set up. ‘H’ stands for high, ‘L’ stands for low in-feed from the respective DG. High and low are further quantified in table 5.6 for the suburban and rural networks.

$$P_{set} = P_{rated} \cdot Multiplier \cdot Coincidence\ factor \quad (5.1)$$

Since it is unlikely that all installations of a certain technology are at full generating capacity even in favourable conditions (some PV modules might be shaded by trees even if it is sunny), a coincidence factor is also applied for the generation (table 5.7). The active

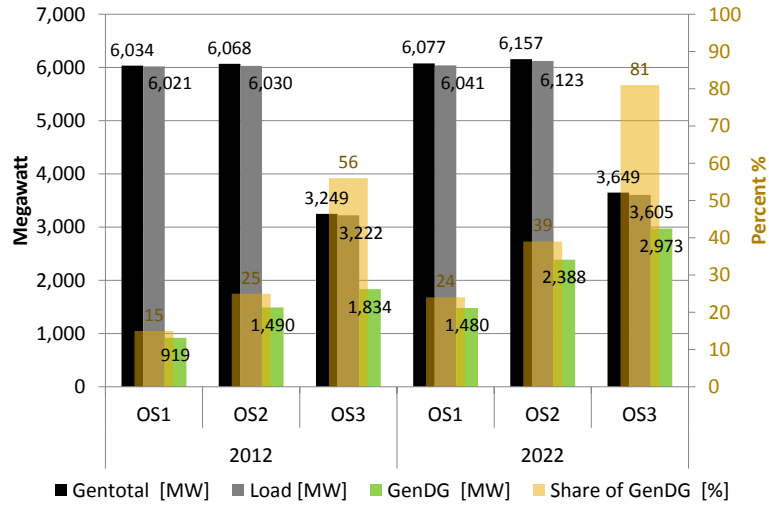


Figure 5.5: Dispatch settings for study cases (see figure 5.4).

	Load	PV	Wind	CHP
OS 1 warm summer afternoon	H	L	L	L
OS 2 windy, cloudy fall day	H	L	H	H
OS 3 windy, sunny spring day	L	H	H	H

Table 5.5: Operational scenarios.

	High	Low
Load	1.0	0.5
Generation	1.0	0.5

(a) Rural

	High	Low
Load	0.9	0.5
Generation	1.0	0.5

(b) Suburban

Table 5.6: Load and generation multipliers.

power setting of the installations are calculated by multiplying the appropriate coincidence factor and multiplier for each operational scenario:

Technology	Coincidence factor
PV	0.80
Wind	0.90
CHP	0.85

Table 5.7: Coincidence factor for different DG technologies [EDBI13].

Appendix F.2 gives a summary of total generation, load and generation share from DGs for each scenario. Additionally, it provides the active and reactive power flows for between all voltage levels per region type and for the complete test system.

5.3.2 Low Voltage Photovoltaic Systems Control Modes

The LV connected PVPPMs labelled as ‘NEW’ (installed between 2012 and 2022) can be set to four control modes:

1. nLVRT mode (‘tripping’)—grey colour: No LVRT, permanent disconnection of the PVPPM for point of common coupling (PCC) voltages below 0.8 p.u.
2. BM mode (‘momentary cessation’)—red colour: LVRT with BM, i.e. the photovoltaic power park module ceases to energize for PCC voltages below 0.8 p.u. but stays connected and ready to resume service post-fault.
3. aRCI mode (‘smart LVRT’)—blue colour: PVPPM rides through faults with additional reactive current injection.
4. aRACI mode (‘smarter LVRT’)—green colour: PVPPM rides through faults with additional reactive/active current injection

The reactive current gain of LV connected PVPPMs (proportional gain k_{RCI} for aRCI and k_{RACI} for aRACI modes) is set to 6 p.u. to increase the impact of the network support. All LVRT control modes for the PVPPMs use a delayed active power recovery (dAPR) according to GCRs, i.e. active power is restored post-fault with a ramp of 20 percent per second of the pre-fault value.

MV connected PVPPMs use a k-factor of 0.2 p.u. In practice only HV/MV substation connected PV systems provide full dynamic support during a fault with a k-factor of 2 p.u. These account for approximately 10 % of installed MV connected PV capacity. Simulations are performed with a k-factor of 0.2 p.u. and 2 p.u. to consider the consequences of operating all MV connected PVPPMs with full dynamic support.

5.4 Results

All simulations were run for 10 s which was deemed sufficient for the transient stability time frame. Results are presented for the first 5 s for sake of readability. No further transients occur after 5 s. The most important results for OSs 2 and 3 in 2022 are discussed here, as these represent moderate and very high instantaneous penetration of DG. Results will only be shown for these and all other results can be obtained from [van14].

Table 5.8 shows that in OS2, WPPM and CHP output are high, while PVPPMs output is low. Load consumption is also high. Large reverse power flows occur in OS3, with all DG output set high while load is low. Voltage profiles are shown for the LV busbar connected to high voltage (HV) busbar number 3, connected to eHV busbar 20 (see figure 5.2). At this busbar, different control modes lead to voltage dips either below or above 0.8 p.u., illustrating that they can make the difference between DG disconnecting or staying online.

Table 5.8: Multiplication factors for rated capacity (including coincidence factors) for operational scenarios 2 and 3.

	PV	Wind	CHP	Load _{suburban}	Load _{rural}
OS2	0.40	0.90	0.85	0.90	1.00
OS3	0.80	0.90	0.85	0.45	0.50

5.4.1 Case 1: year 2022 and OS2

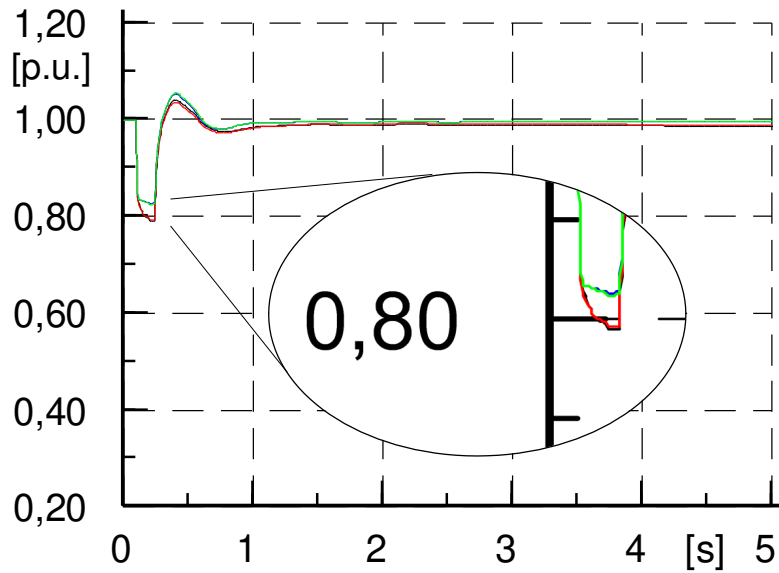
In OS2, the PVPPMs are set to a low power output and therefore any PVPPMs with dynamic power factor control do not exchange any reactive power with the network.

Figure 5.6a shows the voltage in the selected LV busbar for the four control modes of the new LV connected PVPPMs. Pre-fault voltage is 1.00 p.u.. The fault occurs at 0.1 s and is cleared after 150 ms. The voltage drop during the fault is virtually identical for the nLVRT and BM modes. During the first 100 ms of the fault, the voltage drops just below 0.80 p.u. After 100 ms, the nLVRT LV connected DGs disconnect and a further voltage drop occurs, down to 0.79 p.u.. This sudden voltage drop is caused by the lack of active power injection in the LV network upon disconnection of DG. To maintain the power balance, power has to be imported from the MV network, causing a voltage drop over the impedance between the networks. The aRCI and aRACI modes deliver full dynamic network support by injecting additional current during the fault. The purely reactive power injection by the aRCI mode results in a slightly higher voltage during the fault. Since the LV network has a high R/X ratio this is an unexpected result but confirms the findings from chapter 4. After 100 ms, the voltage with both modes is 0.83 p.u. The voltage then drops a further 0.01 p.u. for the aRACI mode. For the aRCI mode however, the voltage remains at 0.83 p.u. In this case the second voltage drop is caused by disconnection of old nLVRT LV connected DG in other LV networks, causing larger power flows in the higher voltage levels.

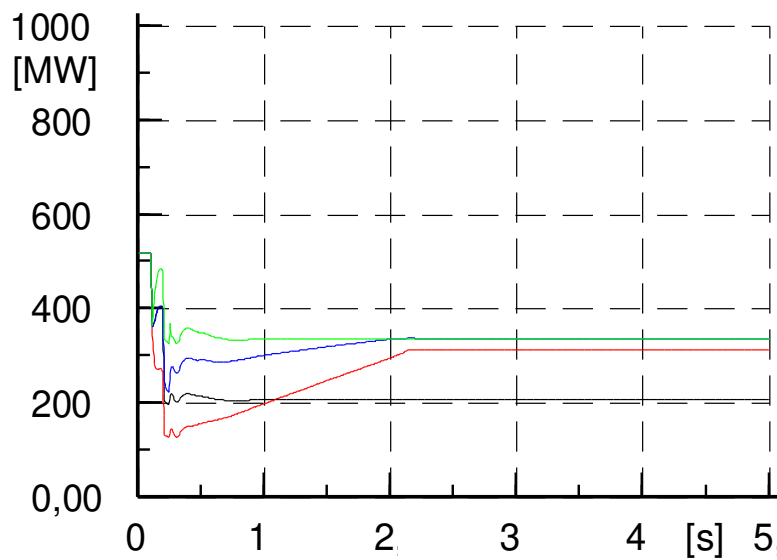
Post-fault, the voltage drops to 0.98 p.u. and 0.99 p.u. for the nLVRT and BM cases respectively. The voltage returns to 1.00 p.u. for the aRCI and aRACI modes. The differences are caused by the amount of disconnecting DGs in the system. The temporary overvoltage occurring immediately after fault clearance and subsequent undervoltage in the system is

caused by the behaviour of the large synchronous generators and their power system stabilisers in the eHV system. The slight slope in steady-state post-fault voltage for the nLVRT and BM modes is caused by the lack of governor models for central power plants and related frequency drop in the system.

The active power output by all LV connected DG (PV, CHP) is shown in figure 5.6b. Pre-fault power output is equal for all control modes at 519 MW. After the initial drop in power, the power output rises for all modes except the BM. For the nLVRT mode, this is caused by the increase of active current by LV connected PV systems. For the aRCI and aRACI modes, the injection of additional current in the LV network contributes as well since the PV systems were only loaded half pre-fault. The BM has the largest initial power loss as the active current setpoint is driven to zero almost immediately after fault occurrence. Post-fault however, the BM almost returns to the same value as the aRCI and aRACI modes. The difference arises from the fact that the voltage boosting by the aRCI and aRACI modes has kept some of the old nLVRT DG at the outskirts of the voltage dip online by keeping the voltage above 0.80 p.u. during the fault. The BM does not boost the voltage significantly in OS2 and thus not all old DGs inject power post-fault. The aRCI and BM show the post-fault active power ramp for the PV systems. The aRACI mode does not show a ramp in active power post-fault, as the setpoint during fault is even higher than in steady-state. The total power output post-fault by the LV connected DG is 208 MW for the nLVRT mode, 313 MW for BM and 338 MW for the aRCI and aRACI modes. This translates to a loss of power compared to the pre-fault condition of 60, 40 and 35 percent respectively.



(a) Voltage in busbar eHV-20_HV-03_MV-02_LV-02. nLVRT in black, BM in red, aRCI in blue, aRACI in green.



(b) Active power output by LV DG. nLVRT in black, BM in red, aRCI in blue, aRACI in green.

Figure 5.6: 2022 OS2 results

5.4.2 Case 2: year 2022 and OS3

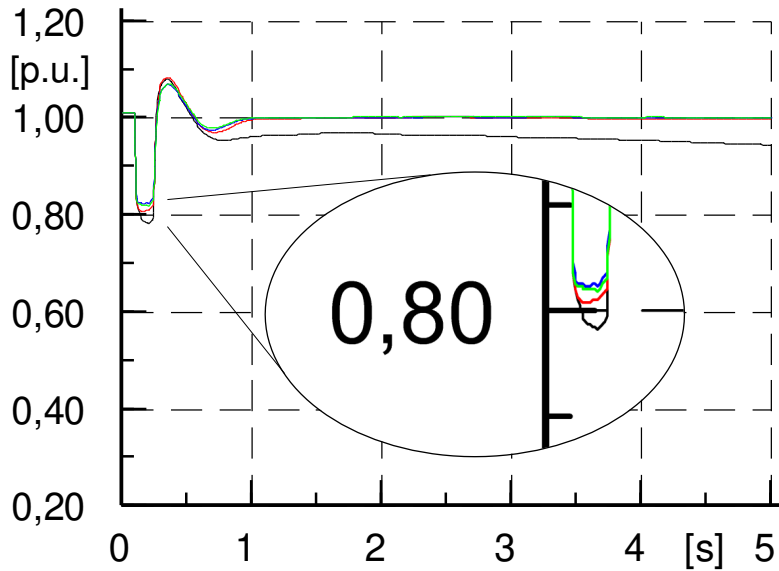
In OS3, PV system output is high, meaning all installations with dynamic power factor control are operated with an inductive power factor and thus consume reactive power pre-fault.

Figure 5.7a shows the voltage in the selected LV busbar. The lowest voltage reached in the nLVRT case is 0.78 p.u. The voltage rises at disconnection of nLVRT DG due to the pre-fault reactive power consumption of the DG and confirms findings from [SBv⁺14]. For the same reason, in OS3 the BM actually ‘indirectly’ boosts the voltage during the entirety of the fault, keeping the voltage above 0.80 p.u. As a result, fewer old nLVRT PV systems disconnect. The aRCI and aRACI modes again deliver maximum voltage boosting of 0.04 p.u.

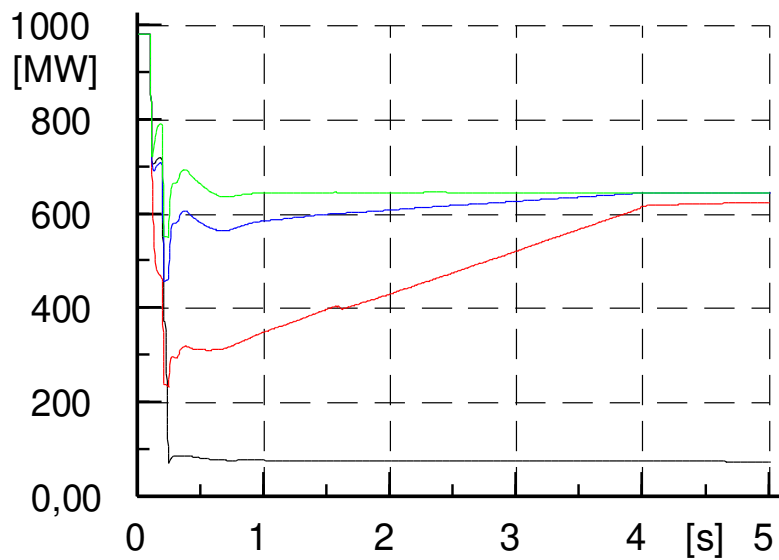
The temporary post-fault overvoltage for all modes is greater than in OS2 at 1.08 p.u. for the nLVRT and BM modes and 1.07 p.u. for the aRCI and aRACI modes. This is caused by the combination of large reverse power flows and the transformer tap-changer settings [BRG⁺15] as well as pre-fault reactive power consumption. Post-fault steady state undervoltage for the nLVRT mode is larger than in OS2 at 0.05 p.u. The LVRT modes manage to restore the voltage to 1.00 p.u. Again, the post-fault negative slope for the voltage in the nLVRT case is caused by the lack of governors in the central power plants and the related frequency drop.

Figure 5.7b shows that the pre-fault active power output by LV connected DG is 983 MW. In OS3, the remaining post-fault active power in nLVRT mode is even less than in OS2. The voltage now drops below 0.8 p.u. in all LV networks, whereas in OS2 the voltage remains above 0.8 p.u. in the rural LV networks connected to the NE system nodes 20 and 29. Post-fault only 75 MW remains in the nLVRT mode, meaning 92 percent of pre-fault LV power is lost. The voltage boosting by the BM in OS3 keeps the voltage above 0.8 p.u. in the affected distribution systems and thus post-fault power is higher than in the nLVRT case. After the active power is ramped up post-fault in the BM case, the output of LV connected DG is 639 MW. The aRCI and aRACI modes manage to keep even more old DG online and have a post-fault power output of 647 MW.

The active power ramp of the BM is paused at approximately 1.5 s, when the voltage in the LV networks connected to eHV busbar 39 drops below the threshold of 0.9 p.u. and the connected LVRT-capable PV systems return to their fault state for a short time. This is also the reason that there are still some PV systems ramping up their power after 4 s. Connected to eHV busbar 39 is an equivalent generator, which due to its large size causes larger voltage swings here than anywhere else in the system.



(a) Voltage in busbar eHV-20_HV-03_MV-02_LV-02. nLVRT in black, BM in red, aRCI in blue, aRACI in green.



(b) Active power output by LV DG. nLVRT in black, BM in red, aRCI in blue, aRACI in green.

Figure 5.7: 2022 OS3 results

5.4.3 Discussion

The simulation results suggest that if current grid connection requirements remain unchanged, voltage sags below 0.75-0.80 p.u. retained voltage at *transmission* level will cause the disconnection of non-LVRT compliant distributed generation. The range of the retained transmission voltage depends on the voltage support of other, LVRT-capable DG at distribution level which may keep the voltage at *distribution* level close to or above the DG's under-voltage protection threshold of 0.8 p.u.

For this test system and under the modelling assumption that distribution system loads and distributed generation can be aggregated at a single bus for each voltage level, a lack of LVRT capability of LV connected PV systems causes a loss of active power of 908 MW in the worst case scenario in 2022. Considering the active power output of *all* DG in the test system, approximately 1 400 MW is lost, equivalent to a large centralised power plant. Realising that the amount of 'active' distribution networks in the test system could be more than doubled considering the total number of distribution system loads in the eHV level, it can be concluded that the amount of active power lost in the system would be significantly higher if all distribution systems were 'active'.

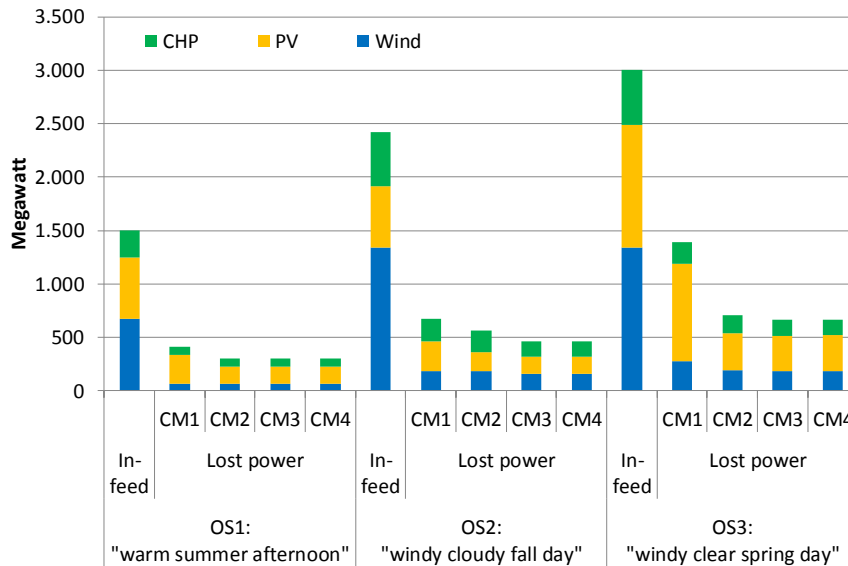
The frequency containment reserve of the Continental Europe region, 3 000 MW, has been designed for the loss of two large power plants of 1 500 MW capacity each. The modelling for the benchmark system used in this study suggests that loss of LV connected DG could become the largest contingency in future if current grid code requirements will not be changed.

Figure 5.8 shows the total generation by DG in the test system pre-fault and the lost power post-fault for all operational scenarios with a k-factor of MV DG of 0.2 p.u. It is clear that higher in-feed pre-fault leads to a larger loss post-fault. Furthermore, in each OS the power lost is greatest in the nLVRT (CM1) case. The BM (CM2) performs better than the nLVRT mode in all scenarios.

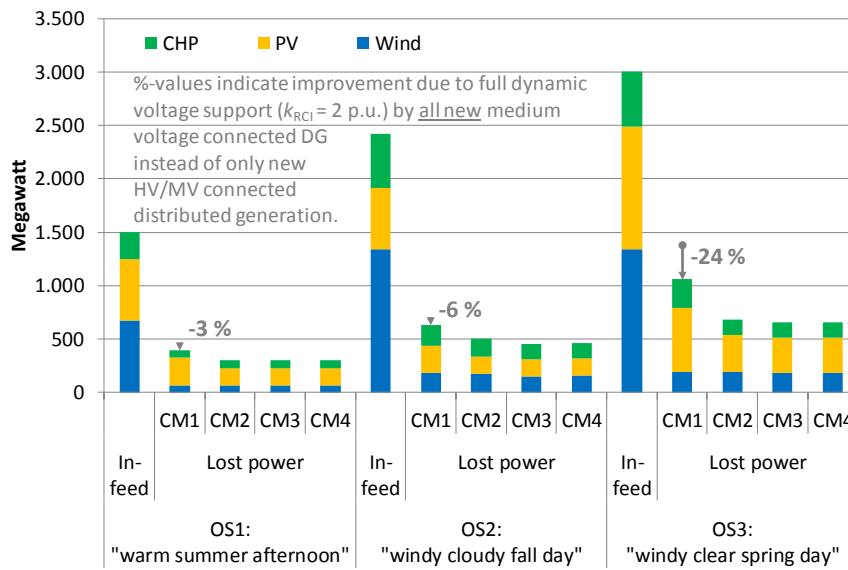
The aRCI and aRACI modes (CM3 and CM4 respectively) perform best and lead to identical amounts of power lost in this study. Increasing the k-factor of new MV connected DG to 2 p.u. in 2022 OS3 decreased the disconnected capacity in the nLVRT case the most, by 24 percent. The effect is greater at higher pre-fault in-feed of DG. Further reductions of lost active power can be expected when also existing MV connected DG would operate with aRCI at a k-factor of 2 p.u.. This could be of particular interest given that the revision of current LV grid connection requirements might take some time during which more LV connected DG will be connected that trips at 0.8 p.u. voltage.

However, it should be noted that even the aRCI mode has a limited capability of raising the voltage in the LV network during a fault. The penetration of new PV systems in the rural LV network is 70 percent, and voltage dips that would lead to a voltage below 0.75 p.u. would not be raised above 0.8 p.u. by the aRCI mode. Thus, unless penetration levels are increased significantly beyond 70 percent for new PV systems or old PV systems are retrofitted, no control mode is capable of keeping existing LV connected online. Future research must show whether this is acceptable.

LV connected CHP plants (synchronous generators) were found to be incapable of maintaining transient stability for the 150 ms faults below 0.6 p.u. For deeper voltage dips, SG are expected to consume large amounts of reactive power post-fault unless current controls are significantly changed. Since their penetration is low and consumption of reactive power could further delay voltage recovery, it is advised that LVRT capability is required of directly coupled generators in the LV network only at voltages above 0.6 p.u.



(a) $k = 0.2$ (represents current DSOs practice)



(b) $k = 2$ (diverges from current DSOs practice)

Figure 5.8: Active power lost in the test system due to the transmission system fault with two different reactive current gains k for all 'new' MV DG.

5.5 Proposed Network Fault Response Requirements

The limited amount of simulation results confirms theoretical considerations on the value of LVRT and aRCI from section 2.4 in chapter 2. The following network fault response requirements are proposed for LV connected DG:

- In the short term, a minimum requirement for new LV connected PV systems should be to ride through voltage dips caused by transmission system faults in blocking mode.
- In the mid-term, the aRCI mode should be used for all new MV connected DG, and not only those ones connected to the substation. The k-factor should be at least 2 p.u. Re-programming of existing DG connected in MV feeders and currently operating without aRCI should be considered.
- In the long term, the aRCI mode should be required from new LV connected PV systems as it is most successful at boosting the voltage at the connection point of the PV system. A high k-factor of 6 p.u. is recommended in areas where much non-LVRT capable DG is installed.
- If penetration levels of directly coupled generators in the LV network remain low, a LVRT requirement above voltages of 0.6 p.u is recommended.

5.6 Implications

Manufacturers of DG face challenges in offering their products in a competitive global market. They need to keep cost of equipment at competitive levels while complying with a broad range of technical requirements that may differ widely all over the world at the same time. This calls for standardization and harmonization of technical requirements, including voltage and frequency ride-through for synchronous generation- and inverter-based DG.

Network operators have traditionally designed their system under the assumption that LV-connected DG would trip for voltage dips below 0.8 p.u.. New LVRT requirements may have impact on network protection and anti-islanding detection.

5.6.1 Photovoltaic power generating facilities

A good overview on common functions for ‘smart’ inverters, as mostly used in solar PV and battery storage systems, has been published in [EPR14]. Many of these functions are already required by GCRs in many European member states [Brü14].

The recommended network fault response for LV-connected PVPPMs to ride through voltage dips of $V_{\text{ret}} = 0.3$ p.u. for a duration of 150 ms is state of the art. As a matter of fact, most inverters that are offered on the market today will be able to comply with these recommendations without any major adjustments. Hence, the impact on DG manufacturers is believed to be limited.

5.6.2 Micro-CHP generating facilities

Micro-CHP generating facilities use synchronous generators or induction generators that are directly connected to the network. For sake of simplicity, only CHP with synchronous generators are considered here. These DG generating facilities are very sensitive to voltage dips.

The prime mover of these units cannot change instantaneously. Depending on the engine and controller design, it can take 1–6 revolutions (0.5–3.0 s) [Kli09] to reduce the mechanical power by 40 %. This is much longer than the typical duration of transmission system faults, hence the DG accelerates significantly during the voltage dip.

The duration of a voltage dip that micro-CHP can ride through is limited by their transient stability. A DG loses stability once its electrical rotor angle δ_i surpasses the critical clearing angle δ_{CC} beyond which the post-fault electric energy is not large enough to prevent the rotor angle to exceed 180° (pole slip) in dynamic performance. Since these units have a small capacity rating and are designed very compact, their inertia constant H_P is much lower than for medium- and large-scale synchronous generators. Table 5.9 shows typical values for rated capacity and inertia time constant H_S of synchronous generation-based DG based on [Kli09, Bos14].

Equations 5.2–5.5 give the approximated relationship between inertia time constant H_P and voltage dip duration. Figure 5.9 plots traces for the electrical rotor angle $\Delta\delta_e$ for two different voltage dips with $V_{ret} = 0.3$ p.u. and $V_{ret} = 0.6$ p.u. caused by an inductive fault. Micro-CHP units can lose stability 2–5 times faster than large-scale power plants and 1–3 times faster than medium-scale DG that are connected to the MV networks. While LVRT for 150 ms at $V_{ret} = 0.3$ p.u. seems challenging for micro-CHP units, riding through low voltages at $V_{ret} = 0.6$ p.u. seems to be a feasible requirement.

For limited future penetration levels, a LVRT operation of 150 ms at $V_{ret} = 0.6$ p.u. is recommended for state-of-the-art technology of LV-connected synchronous generation-based DG. More stringent requirements may required for higher penetration levels in which case transient instability of low-inertia DG during or after a fault could be avoided by technical redesign. This could be achieved by one of these options [Kli09]:

- Adding inertia (e.g., flywheel).
- Increasing the speed of the engine controller and fuel supply.
- Decoupling of the synchronous generator from the network via a full-size converter.

$$H_P = \frac{\frac{1}{2} \cdot I_r \cdot \omega^2}{P_r} \quad (5.2)$$

$$\Delta\omega = \frac{1}{2} \omega_n \cdot \frac{1}{H_P} \cdot \frac{\Delta P}{P_r} \cdot t \quad (5.3)$$

$$\Delta\delta_m = \frac{1}{4} \cdot \frac{1}{H_P} \cdot \frac{180}{\pi} \cdot \frac{\Delta P}{P_r} \cdot t^2 \quad (5.4)$$

$$\Delta\delta_e = m \cdot \Delta\delta_m \quad (5.5)$$

DG connection level	Rated capacity P_r	Inertia time constant H_S
eHV/HV	> 100 MW	2.5–10 s
MV	400 kW – 20 MW	0.2–3.8 s
LV	10–230 kW	0.1–0.2 s

Table 5.9: Typical values for rated capacity and inertia time constant H_S of synchronous generation-based DG based on [Kli09, Bos14]

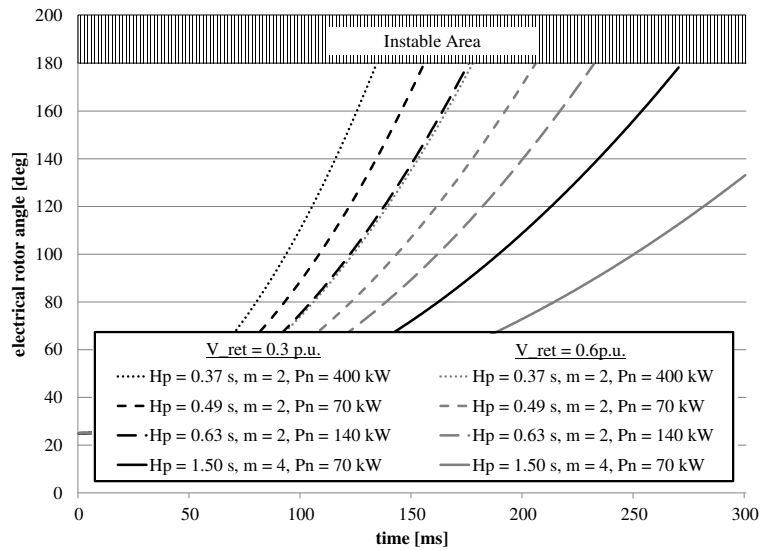


Figure 5.9: Electric rotor angle of small- and medium-scale synchronous generation-based CHP plants. (Calculations based on [Kli09] with values of [Bos14], $V_{ret} = 0.3$ p.u., $\delta_{e,0} = 25$ degree.)

5.6.3 Distribution network protection

The impact on the distribution system and DSOs varies significantly between LVRT in ‘blocking mode’ and aRCI. While the former is recommended as a minimum requirement for most DG installations, recommended minimum requirements for certain DG and advanced requirements to mitigate fault-induced delayed voltage recovery (FIDVR) [NER09, NER12] events may include a aRCI, during which the DG feed a short-circuit current at the PCC.

Depending on DG penetration level, the magnitude of the DG’s short-circuit current and the sensitivity of the DS protection scheme, the selectivity of the protection can be harmed. The DSO should therefore coordinate the setting of the DG’s undervoltage protection function with the responsible transmission system operator (TSO).

For illustration, Fig. 5.10 shows two examples for the potential impact of DG with aRCI on the DS protection [CMKK11].

- **Blinding of protection:** For short-circuits that occur on the feeder to which a DG is connected, the short-circuit current from the grid is decreased due to the contribution of the DG. This can either deteriorate the fault current detection or leave the short circuit undetected. This effect is also known as ‘protection under-reach.’
- **False tripping:** This may occur when a DG unit contributes to the fault in an adjacent feeder connected to the same substation. The generator contribution to the fault current can exceed the pickup level of the overcurrent protection in the DG feeder, causing a possible trip of the healthy feeder before the actual fault is cleared in the disturbed feeder. This effect is also known as ‘sympathetic tripping.’

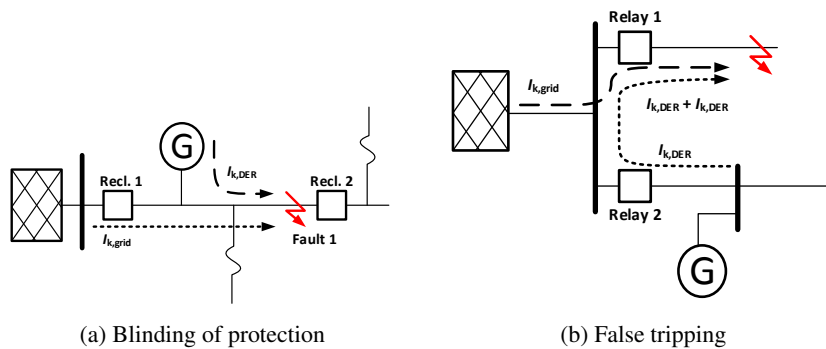


Figure 5.10: Potential impact of DG with LVRT and aRCI on distribution system protection. (Adapted from [CMKK11].)

Additional problems that may arise [CMKK11]:

- Prohibition of automatic reclosing.
- Fuse-recloser coordination.
- Anti-islanding problems.

—**Prohibition of automatic reclosing**— Coordination of the ride-through duration with distance protection and line reclosers might become necessary when considering an advanced requirement for aLVRT with aRCI. For example, if DG was not tripped before the recloser action takes place, the latter may be misled and regard the temporary fault as a permanent one, hence falsely switching off the line permanently. In addition, the LVRT with aRCI operation of the DG creates a temporary island and the DG might accelerate or decelerate and increase the risk for unsynchronized automatic reclosing, including serious equipment damage [CMKK11]. In the U.S., for example, the first attempt of automatic reclosing on distribution feeders may sometimes be close to instantaneous [EPR13] or is being delayed intentionally by 5 s to 15 s [Nat09] after the fault occurrence in order to allow for DG to securely trip off the grid. An alternative approach to coordinate distribution system protection with DG is to install voltage supervision of reclosing at the substation or feeder breakers.

—*Fuse-recloser coordination*— With regard to an intentional islanded operation of distribution systems (temporary microgrid operation), problems with unsynchronized reclosing have to be considered to avoid damage to utility and customer equipment as well as (synchronous) DG. For high DG penetration levels that cause reversed power flows, from distribution to sub-transmission level, a LVRT operation with aRCI should be taken into account when selecting the settings of distance protection elements. Distance protection is commonly used in meshed sub- and regional transmission grids.

—*Anti-islanding problems*— Anti-islanding detection has traditionally relied on voltage and frequency relays that would trip the DG during abnormal voltage or frequency conditions within specified clearing times. But frequency relays of DG are being de-sensitised in the course of revised GCR for new and retrofit programmes for existing installations [EE14]. If voltage relays would simultaneously be desensitised due to LVRT requirements, longer periods of unintended islanded operation could occur in cases where DG in-feed and load are balanced.

During unintentional islanded operation, the DSOs will be concerned with power quality (PQ) issues. Most controls of power park modules (PPMs) are currently not designed to operate in islanded mode. For example, the inverter continues to supply current to a load until either the overvoltage limit is reached or the anti-islanding protection is activated. Phase voltages may show heavily distorted run-on waveforms in certain cases.

These PQ-related concerns from DSOs stress the importance of identifying new effective anti-islanding techniques that would securely trip the DG or make the DG cease to energize the DS within a given time, say 2 s [IEE14a] to 5 s [For11]. Identifying such new anti-islanding techniques that do not rely on frequency can be a formidable task, as [EPR15a, HSU15] point out. Fig. 5.11 gives an overview of the problem and over various candidate solutions.

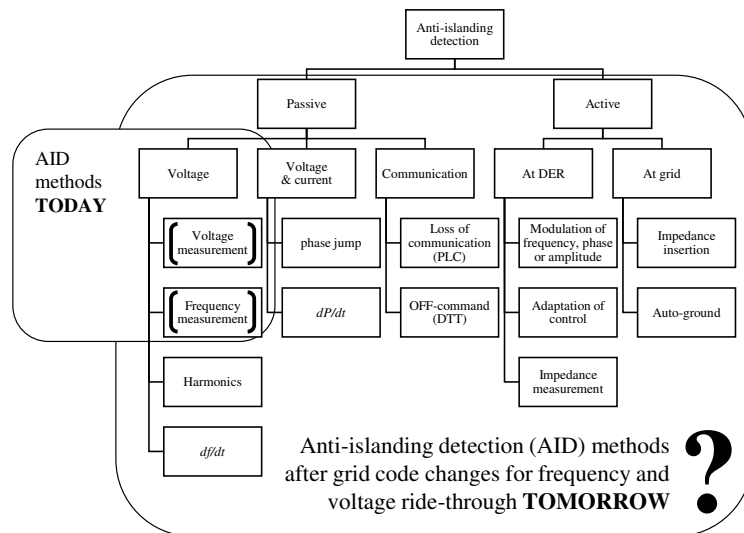


Figure 5.11: Problem definition and overview over various candidate solutions for anti-islanding detection. (Adapted translation from [Pal14].)

5.7 Conclusions

Current grid codes in Germany and most other European countries still mandate LV connected DG to disconnect in case of voltage dips below 0.8 p.u. For a critical review of this requirement, the impact of high penetration of PVPPMs in LV distribution systems following a distant transmission system fault has been investigated. Case studies were performed for pre-fault power flow levels and various LV connected PVPPM LVRT control modes with realistic composition of DG in active distribution systems.

It was demonstrated that nowadays undervoltage protection schemes for small- and medium-scale DG connected in LV distribution networks may become a risk for power system stability to the extent of ultimately causing blackouts. Hence, it is recommended that LV connected PVPPMs should ride through voltage dips caused by transmission system faults in blocking mode ('limited dynamic voltage support'). This control mode should be implemented in the short term. In the long term, the aRCI mode is advised ('full dynamic voltage support').

As long as penetration levels for directly coupled synchronous generators in the LV network are low^{A.6}, a LVRT requirement for shallow voltage dips above voltages of 0.6 p.u. is deemed sufficient.

Further, new MV connected DG should be required to perform LVRT with aRCI at a k-factor of 2 p.u. Re-programming of existing MV connected DG should be considered given that the revision of current LV grid connection requirement might take some time during which more LV connected DG will be connected that trips at 0.8 p.u. voltage.

However, a full dynamic voltage support for LV and MV connected DG systems would have a high impact on the protective system prevalent in the respective LV and MV networks. The protective system might have to be revised in order to prevent blinding and false tripping of protective devices. Additionally, anti-island detection would have to be revised. Given the limited voltage support found in this paper a requirement for voltage support through aRCI or aRACI remains questionable. Future research will have to assess its value.

Based on the outcomes of this study, future research should investigate different dynamic equivalencing methods, aim at a more realistic representation of the German power system, such as using a German transmission system model and differentiating for urban areas.

Chapter 6

Conclusions and Future Research

This chapter summarises the main conclusions and highlights the scientific contributions of the presented research. The research questions are answered and recommendations for future research are given.

6.1 Conclusions

6.1.1 Answers to research questions

A technique of dynamic equivalencing was developed that allows to derive high-accuracy dynamic equivalent stability models for active distribution systems (ADSs). The analysis based on this modelling approach allows to answer the following research questions:

1. What is the minimum level of detail that is necessary to accurately model ADSs in bulk power system stability studies with very high penetration of DERs? (chapters 3, 4, and 5)

When aggregating ADSs for stability studies of sustainable power systems, radial parts of distribution systems can be aggregated, i.e. feeders of medium voltage (MV) and low voltage (LV) system connected to the same substation respectively. Individual voltage levels should be explicitly modeled with their respective transformer impedance and an equivalent impedance that represents the average distance of distributed generation (DG) from the busbar. Any significant DG prevalent at a certain voltage level should be clustered into equivalent models of the same technology type and network fault response performance, including protection trip settings. On-load tap-changers of transformers and the steady state voltage control of DGs should be explicitly modelled in order to correctly initialize the ADS model, so as to correctly initialise the dynamic simulation. Positive-sequence, root mean square (rms) stability-type DG models are sufficient to perform transmission system reliability studies. Balanced connection of loads and DG in distribution systems can be assumed.

2. How can equivalent models of active distribution systems be validated? (chapter 3)

Equivalent models of ADSs can be validated against detailed ADS models. Accuracy is reduced if the retained voltage is close to the undervoltage protection setting of non-LVRT capable DG. Full dynamic voltage support from DG can further reduce the accuracy.

If less sophisticated equivalencing techniques are used to model DG in stability studies, the accuracy of the integrated power system model can be significantly reduced and results obtained would tend to be too conservative and underestimate the potential benefits of a full dynamic voltage support by DG. This holds especially for the annulus region of the system where the retained voltage is close to the undervoltage trip setting of DG that do not have low voltage ride-through capability. Hence, the proposed technique can help save operating reserves.

A comprehensive understanding of the challenges and the opportunities of very high penetration of distributed generation with regard to the network fault response of transmission and distribution systems was developed. This allows to answer the following research questions:

1. How does the ‘effectiveness’ of a ‘full dynamic voltage support’ depend on the rated DG penetration level and the network characteristics? (chapter 2)

It is proven that the support of the distribution system voltage by DG in the fault period will not exceed 0.3 p.u. to 0.4 p.u. even for a very high rated DG penetration level. The effectiveness is highest before the network has to be updated to integrate high levels of DG according to nowadays planning standards. With increasing penetration levels, the network gradually changes from a load serving to a generation collector system. However, small voltage increases in the post-fault period can already be very effective to improve power system stability.

2. How important are the load characteristics for the network fault response of DG? (chapter 4)

It was shown that, with DG being located very close to the loads, the network fault response of DG is even more influenced by the load characteristics than transmission connected generation. For a test system with 20 % induction motor loads in a region, simulations suggest that a low voltage ride-through (LVRT) operation in blocking mode (‘limited dynamic voltage support’) will be prolonged due to fault-induced delayed voltage recovery (FIDVR). This could trigger a large frequency deviation in the post-fault period, thereby increasing the risk of load-shedding and frequency instability.

3. Would a combined additional reactive/active current injection (aRACI) be more effective for LV connected DG than a pure additional reactive current injection (aRCI)? (chapters 4 and 5)

For points of common coupling (PCCs) with low X/R ratio, a combined injection of reactive and active current aligned to the angle of the equivalent network impedance seen from the point of common coupling (PCC) was expected to show the most effective voltage support. This expectation, however, was not confirmed. The aRACI mode supported the voltage less effectively than an exclusive reactive current injection, created a higher risk of violating the wind

power park module (WPPM)'s stability limit, and negatively impacted transmission connected synchronous generator's transient stability. The main benefit of aRACI was a higher active power in-feed from DG immediately after the fault clearance which could be of interest in low-inertia power systems, e.g. islands. Considering potentially negative effects of this control mode on anti-islanding detection of DG at distribution level, the use of aRACI is not recommended.

4. How much in-feed from distributed generation connected at the LV distribution system level of a test system would a transmission network fault potentially trip in a 2022 case study for Germany? (chapter 5)

The simulation results have shown that significant active power is lost in case of a transmission system fault in the studied power system which resembles the DG penetration levels and technologies expected for Germany in 2022. Under the modelling assumption that distribution system loads and distributed generation can be aggregated at a single bus for each voltage level, continuation of currently enforced LV grid connection requirements seems to result in a maximum loss of active power in the system of approximately 1 400 MW in the worst case scenario (high in-feed of all DG technologies in 2022). Approximately 880 MW of these are LV connected DG. Given that the amount of 'active' distribution networks in the test system could be more than doubled considering the total number of distribution system loads in the eHV level, the amount of active power lost in a real world power system could be significantly higher and become the largest contingency. If that was the case for the real German power system, the 3 000 MW frequency containment reserve of the Continental Europe region would have to be reconsidered.

If the analysis of grid connection requirements (GCRs) did not consider the characteristics of all devices connected to an active distribution system, including its loads, appropriately, adverse effects on power system stability from the dynamic interactions between the transmission and distribution system levels would remain undetected. For example, if dynamic voltage support from DG would only be required for the fault period, the voltage support that it can provide in the post-fault period to mitigate FIDVR would be left unexploited.

Current and future grid connection requirements for distributed generation that have an impact on the network fault response of transmission systems and distribution systems were justified and specified per voltage level. This allows to answer the following research questions:

1. Should LV connected DG be capable of low voltage ride-through (LVRT)? (chapter 5)
 - Yes, LVRT capability should be required from LV connected DG as soon as possible. In the short term, it is recommended that LV connected photovoltaic power park modules (PVPPMs) ride through voltage dips caused by transmission system faults in blocking mode ('limited dynamic voltage support'). In the long term, the aRCI mode is advised ('full dynamic voltage support').

- As long as penetration levels for synchronous generation-based DG are low^{A.6}, a LVRT requirement for shallow voltage dips is deemed sufficient.
2. What are the opportunities and challenges of a current injection by LV connected DG during faults? (chapter 5)
- In the fault period, full dynamic voltage support can increase the voltage at distribution level in the annulus of a voltage funnel and thereby move the voltage contour that delineates all system nodes where the retained voltage is smaller than the DG's undervoltage protection threshold. This reduces the aggregate MW-value of DG units that trip.
 - In the post-fault period, it can prevent a prolonged LVRT operation of DG units at all locations in the system where FIDVR occurs in ADSs with large amounts of induction motors (e.g., air conditioning systems). Increasing the reactive current injection gain above its default value of $k_{RCI} > 2$ p.u. as in current GCRs can significantly improve the voltage stability in the post-fault period.
 - However, injection of a short-circuit current may require a complete revision of the distribution system protection scheme and anti-islanding techniques.
3. Which amendments to grid connection requirements for DG connected at low voltage (LV) and at medium voltage (MV) distribution system levels are recommended? (chapters 4 and 5)
- Low voltage (LV): For synchronous generation-based DG, a minimum requirement of LVRT above voltages of 0.6 p.u. For inverter-based DG, in the short term, a minimum requirement of LVRT in blocking mode above voltages of 0.3 p.u.; also a reduction of the voltage threshold, below which this DG type ceases to energize, well below 0.9 p.u.. Consider introducing a sufficiently long LVRT capability for shallow voltage dips to prevent tripping during FIDVR events as well as introducing a maximum duration for the fault operating mode, e.g. 2–5 s. In the long term, the aRCI mode should be required from new LV connected PV systems. A high k-factor, of for example 6 p.u., is recommended in areas where much non-LVRT capable DG is installed.
 - Medium voltage (MV): In the mid term, new MV connected DG should be required to perform LVRT with aRCI at a k-factor of 2 p.u. Re-programming of existing MV connected DG should be considered given that the revision of current LV grid connection requirements might take some time during which more LV connected DG will be connected that trips at 0.8 p.u. voltage.

If grid connection requirements related to network fault response of LV connected DG units are not changed, these units may become a risk for power system stability. If new requirements for these units remain limited to LVRT in blocking mode ('momentary cessation') starting at high retained voltage values, the likelihood of prolonged LVRT operation caused by fault-induced delayed voltage recovery increases and significant benefits for power system stability will be left unexploited.

Now that the three subordinate objectives have been reached and all research questions have been answered, the overall objective is reached by answering the following research question:

- Which of the current and proposed grid connection requirements that have an impact on the network fault response of transmission systems are necessary from a system-wide stability perspective and what changes are needed, if any, to maintain the stability of a sustainable power system with very high penetration of distributed generation?

All of the current GCR that were studied intend to increase system stability and reliability when penetration levels of DG are further increasing. However, these requirements are not always adequately specified or may be easily misinterpreted to the detriment of reliable power system operation. Here are a few salient points:

1. Network fault response requirements from higher voltage levels will need to be carefully adapted to the distinct characteristics of LV and MV distribution levels.
2. A zero-voltage ride-through at distribution level is not required from a power system stability viewpoint.
3. Deactivation of the full dynamic voltage support of MV connected DG by setting the reactive current gain to $k_{RCI} = 0$ p.u. is not recommended. In order to maintain the stability of inverter-based DG, the active current should be reduced in proportion to the voltage dip.
4. The new robust fault mode proposed in this thesis shows better performance than the existing control modes over a wide set of power flow situations, including reverse power flow (RPF). The properties of the proposed control mode are a fast voltage control by dynamic reactive support with a deadband around the operating voltage, the use of an hysteresis for the transition between the operating modes and a reactive current injection 'in addition to' the pre-fault active and reactive current set-points.
5. Induction motors can cause fault-induced delayed voltage recovery at distribution level and that should be adequately considered in the choice of required depth and duration of LVRT curves for LV and MV connected DG as well as in their fault performance requirements.
6. To better manage the risk associated with implicit assumptions such as modest penetration levels for certain DG technologies and dominance of PVPPMs in inverter-based DG, a performance-based approach to network fault response requirements of DG could be considered to replace the technology-based approach of nowadays GCRs.

Regulatory authorities would then have to conduct impact assessments and attribute certain DG technologies to certain performance categories.

6.1.2 Scientific Contributions

This thesis contributes to the ongoing discussion on grid connection requirements for DG by analysing the dynamic interactions between the transmission and distribution system levels under various disturbance and DG penetration scenarios.

The major scientific contributions are summarised below.

—Analysis of the stability of evolving sustainable power systems in a system-wide, accurate and computational-efficient way that considers dynamic interactions between the transmission and distribution system levels.—

- Definition of the minimum level of detail that is necessary to accurately model active distribution systems in bulk power system stability studies with very high penetration of DERs, i.e., more than approx. 50 % system-wide instantaneous penetration leading to regional reverse power flows from distribution to bulk system level.
- Development of a methodology to derive and validate high-accuracy dynamic equivalents of realistic ADSs for bulk system stability studies using grey box modelling.

—Improved understanding of the effects of very high penetration of distributed generation, including renewable energy sources for electricity generation (RES-E), on power system stability.—

- Demonstration that nowadays undervoltage protection schemes for small-scale and medium-scale DG connected in LV distribution networks may become a risk for power system stability.
- Demonstration that a LVRT operation of small-scale and medium-scale inverter-based DG connected in LV and MV distribution networks with blocking of the inverter current (also known as 'momentary cessation', 'zero-power' mode, or 'limited dynamic voltage support') for terminal voltages immediately below the continuous operating region can compound fault-induced delayed voltage recovery and negatively impact power system stability.
- Mathematical formulation of the relationship between the 'effectiveness' of dynamic reactive voltage support and DG penetration level.

—Identification of minimum requirements for LV connected DG and improvement of existing grid connection requirements for MV connected DG to maintain power system stability.—

- Proposal of minimum requirements for the network fault response of LV connected DG.
- Justification of full dynamic voltage support from distribution connected DG through demonstration of related improvement of power system stability .
- Analysis of LVRT requirements for LV connected, low-inertia synchronous generator-based DG.
- Proposal of a new fault control mode that shows robust performance under a large number of system conditions and control parameter variations.
- Evaluation of both additional reactive/active current injection to achieve a dynamic voltage support optimised for the network impedance angle.

In addition, from a practical viewpoint, the findings of this thesis can support distribution system operators (DSOs) and national grid code committees as they define justified and effective grid connection requirements for fault ride-through and fast voltage control for distributed power park modules connected to low and medium voltage networks. The recommendations on modelling of DG in bulk power system stability studies can contribute to ongoing activities related to power system dynamic performance in IEEE/ PES/ PSDP [IEE14b] and CIGRÉ JWG C4/ C6.35/ CIRED [YC13].

6.2 Recommendations for Future Research

Based on the results of this study, future research should be carried on in the following topics:

—Further improvement of the proposed dynamic equivalencing technique—

- Comparison with Western Electricity Coordinating Council (WECC)'s simplified distributed photovoltaic (PV) model.

WECC recommends the use of a very simplified, distributed PV model based mostly on algebraic equations. The model considers protection settings and basic active and reactive current controls. It would be interesting to compare the system performance with this model and the proposed dynamic equivalents of ADS from this thesis.

- Innovative parameters identification techniques.

The parameter identification technique used in this research to identify the value for the equivalent impedance is not automated and requires manual work from the user. Future research should identify and implement innovative parameter identification techniques, such as heuristic optimisation techniques, to automatically derive equivalent models for ADS based on a sophisticated set of input data.

- Extension to sequence network models.

The DG models used in this research are positive-sequence, rms stability-type models that allow for the simulation of balanced conditions. Future research should extend these models in the negative-sequence to allow analysis of unbalanced conditions. Special attention would have to be given to the correct modelling of transformer vector groups.

—Further analysis of the developed aRACI control mode—

- Impact on ‘current angle stability’.

The research found that the active current injection during voltage dips based on LVRT operation with aRACI potentially increases the risk of ‘current angle stability’ of inverter-based DG connected to ‘weak’ distribution systems with low X/R ratio. This finding is contrary to findings from other research and will need further investigation. For example, it should be investigated whether a reduction of the gains of the WPPM’s phase locked loop (PLL) or a blocking of the PLL below a certain value of V_{Flr} can increase the effectiveness and stability of voltage support from the aRACI fault control mode.

- Impact on transient stability.

The research indicated that LVRT operation with aRACI could deteriorate the transient stability of the transmission system. Further research should be carried out based on real-world power system models. Future research should investigate the impact of this control mode for LV and MV connected DG explicitly, due to the different X/R ratio at each of these voltage levels.

- Online detection method of network impedance.

The simulations performed in this research assumed that the network impedance remains constant and that the setting for the angle of the current injected in the additional reactive/active current injection (aRACI) control mode could be precisely defined. However, this assumption does not hold for DG in the field. Future research should investigate methods for online detection of the network impedance, how impedance angle measurement errors impact the power system stability, and how aRACI settings could be adapted continuously.

—Further analysis of the implications of dynamic voltage support at distribution system level.—

- Islanded operation and detection methods.

The network fault response requirements proposed for distribution connected DG in the mid term would have a high impact on anti-islanding and related detection methods. Conventional anti-islanding techniques are less applicable and islanding conditions are more likely to occur with DG providing voltage support. Future research should investigate which of the additional reactive current

injection (aRCI) and additional reactive/active current injection (aRACI) control mode more likely keeps an unintentional island alive, identify robust anti-islanding techniques for DG with full dynamic voltage support as well as the safe operation of islanded power systems.

- Distribution system protection.

The selectivity of the distribution system protection may be negatively influenced by the recommendations from this research. Future research should investigate new protection schemes and their related costs. Differences in the impact of LVRT operation with additional reactive current injection and additional reactive/active current injection on system protection are also of interest.

- Improve LVRT capability of synchronous generation-based DG.

The research has shown that the state of the art technology of this type of DG has only limited capability to ride through voltage dips. New control concepts should be developed that allow for a better LVRT performance of these DG, for example through high-speed fuel injection or increased inertia with flywheels.

—Application of the research—

- Application of the proposed technique of dynamic equivalencing in real-world large-scale power system stability studies.

The research in this study was carried out with test systems obtained from literature and derived from a statistical analysis of a 2022 scenario of the German power system. By applying the proposed methodology on a real-world large-scale power system its practical value can be further analysed and more realistic values can be determined for the amount of ‘lost’ active power from LV connected DG.

Appendix A

Definitions and classifications

This appendix defines important terms that are used frequently within this thesis. It also introduces a classification of distributed generation (DG) grid connection interfaces which will be used later.

The definition and classification of ‘power system stability’, however, will be presented in the context of section 1.2 where it will be explained in detail.

A.1 Power system transformation

Nowadays power systems are undergoing a historic transformation that is unprecedented in their hundred year history. The key characteristic of this transformation process is that power system elements, control systems and operational strategies from the past coexist with new elements, new control systems and new operational strategies related to the integration of DG in the present and future. Figure A.1 visualises the ongoing transformation process and summarises some important characteristics of the vertically-operated power system of the past and the horizontally-operated power system of the future.

Two classes of transformation are distinguished: a *structural* transformation and a *technological* transformation of power systems.

The *structural transformation* means that power systems are being transformed from vertically structured systems with unidirectional power flows from the transmission to the distribution system to horizontally structured systems with ‘bidirectional’ power flows, i.e. where power flows among voltage levels may vary in magnitude and direction from one moment to the next depending on the in-feed from variable, RES-E based DG and consumption of loads. The *technological transformation* means that conventional (thermal) power plants with synchronous generators are continuously being substituted, often by power park modules (PPM) that are connected to the network non-synchronously via power electronic converters.

The time frames of the transformation process are classified in this thesis as shown in table A.1.

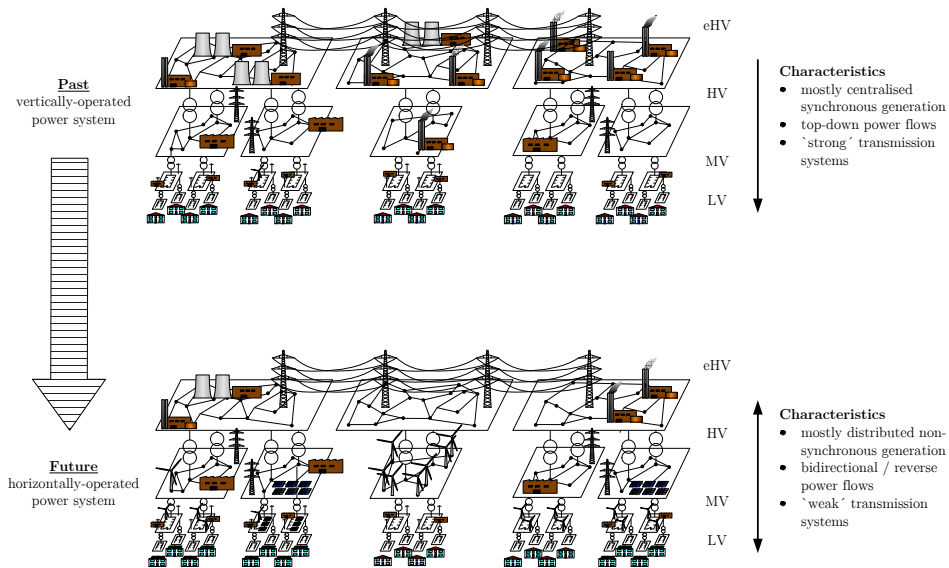


Figure A.1: Transformation of the power system from the past to the future

Table A.1: Time frames of the transformation process

Qualifier	Time frame
short term	1–5 years
mid term	6–10 years
long term	> 10 years

A.2 Distributed generation

Distributed generation (DG) can be defined as

an electric power source connected directly to the distribution system or on the customer site of the meter. [AAS01]

According to the same source, DG can be classified into micro DG (1 W ... 5 kW), small DG (5 kW ... 5 MW), medium DG (5 MW ... 50 MW), and large DG (50 MW ... 300 MW) [AAS01]. This classification is used in the thesis accordingly. Due to the special focus put on decentralised DG, large DG are less relevant for this thesis.

In the terminology of the Network Code for Requirements for Grid Connection applicable to all Generators by the European Network of Transmission System Operators for Electricity (ENTSO-E) (ENTSO-E NC RfG) [EE13c], distributed generation consists of one or more power generating modules (PGMs) which are either synchronous synchronous power generating modules (sPGMs) or power park modules (PPMs), depending on the grid connection interface used. Synchronous PGMs use synchronous generators (SGs) directly connected to the network while PPMs are units, or an ensemble of units, connected to the network non-synchronously or through power electronic converters (PECs). PPMs in

themselves can be further classified depending on the specific grid connection interface (see section A.8). Synchronous PGMs and power park modules can have very different dynamic behaviour and impact on power system stability as it is discussed in section 2.2.

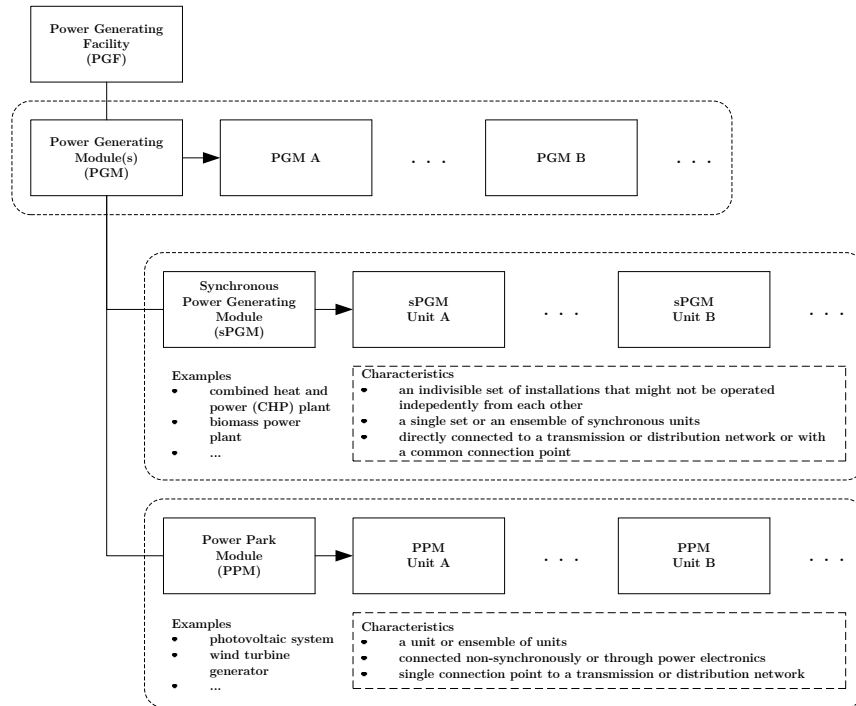


Figure A.2: Definitions based on the ENTSO-E Network Code for Requirements for Grid Connection applicable to all Generators [EE13c]

Different types of distributed generation use different primary energy sources: these can be either renewable energy sources such as wind, solar, biomass and biogas or fossil energy sources such as natural gas and oil as well as other sources such as hydrogen, sewage gas and landfill gas. From these energy sources, DG that use wind and solar energy showed the highest increase in Europe in the past decade due to the promotion of renewable energy sources for electricity generation (RES-E). Thus, DG based on these two sources are in the focus of this thesis:

- Wind power park modules (WPPM) consisting of an ensemble of wind turbine generators (WTG).
- Photovoltaic power park modules (PVPPM) consisting of an ensemble of PV systems.

A.3 Active distribution systems

This thesis follows in part the definition of Cigré Working Group C6.11 for ‘active distribution systems’ to

have systems in place to control a combination of distributed energy resources [...], defined as generators, loads and storage. [...] Distributed energy resources take some degree of responsibility for system support, which will depend on a suitable regulatory environment and connection agreement. [CIG11]

Especially the second part of this definition is important in the context of this thesis since it refers to the possibility for system-wide support from distribution system level. In order to facilitate this system support, adequate grid connection requirements or new ancillary services products are required.

A.4 Definition and classification of power system stability

In this thesis, power system stability is understood in line with the definition given in [IEE04] as

the ability of an electric power system, for a given initial operating condition, to regain a state of operating equilibrium after being subjected to a physical disturbance, with most system variables bounded so that practically the entire system remains intact.

From a physical viewpoint, ‘stability’ is a condition of equilibrium between opposing forces [IEE04]. When these opposing forces experience sustained imbalance this leads to different forms of *instability*.

The network topology, system operating condition, and the form of disturbance determine *which* sets of opposing forces may experience sustained imbalance. In order to better understand and effectively mitigate certain forms of instability, it is useful to differentiate between various classes of power system (in)stability rather than studying them as a single problem. Figure A.3 shows the different classes of power system stability as proposed by [IEE04]. Despite some shortcomings when it comes to the introduction of PPM based DG, this thesis follows the established classification. The three stability classes which are of particular interest for the network fault response of transmission systems with very high penetration of DG are:

- Transient stability (of synchronous generators in conventional power plants of an interconnected transmission system);
- large disturbance voltage stability; and
- frequency stability (resulting from the above).

Other classes of power system stability problems are out of the scope of this thesis.

One should bear in mind that the established classification has been derived from the physical relationships that determined the dynamic behaviour of the power system in the past decades. This behaviour was dominated by the response of synchronous generators. As

the response of a SG and of a PPM to a network fault differ substantially from each other it will sometimes be cumbersome to discuss the impact of DG on the before mentioned stability classes within sharp edges. For example, the network fault response is a problem of the transient stability class for synchronous generators whereas it is a problem, as will be shown, of the large disturbance voltage stability class for distributed power park modules.

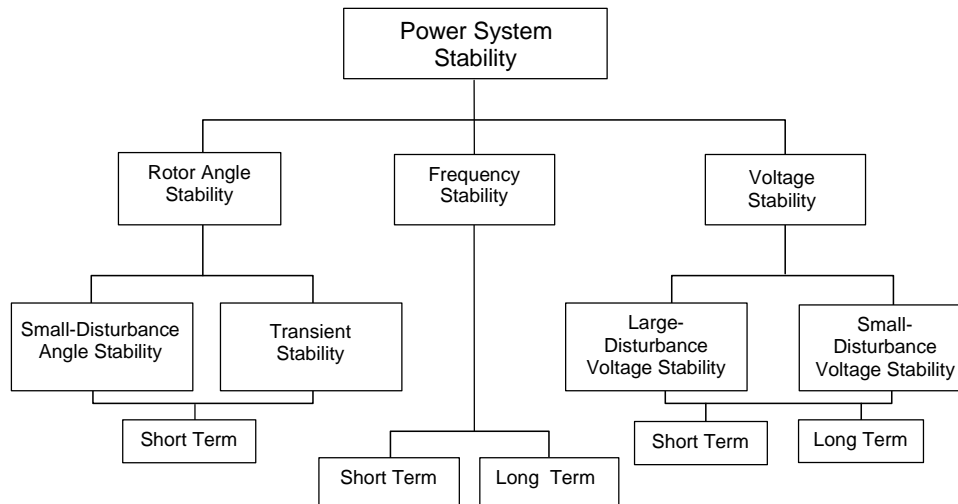


Figure A.3: Classification of power system stability [IEE04]

A.5 Network fault response

By ‘*network fault response*’ this thesis understands

the dynamic response of the whole or parts of the power system during and shortly following sudden faults in the network, such as short-circuits on a line or a substation busbar. The response is calculated in terms of changes in system variables over a time frame of interest, such as bus voltage magnitudes and angles, generator rotor angles, and fundamental system frequency.

Only symmetrical, three-phase network faults that would threaten overall power system stability are in the scope of this thesis while other faults are out of the scope.

A.6 DG penetration levels

Penetration levels of DG can vary significantly among the power system. They are also changing in time. Furthermore, it is almost impossible to derive general statements about what value of DG penetration level has a ‘high’ impact and what value has a ‘low’ impact on power system planning and operation. Such statements would always be very specific to a certain power system and a certain study type. For the sake of orientation, table A.2 qualifies the ranges of penetration level as considered in this thesis.

Table A.2: Ranges that qualify the DG penetration level of a power system in this thesis

Qualifier	ρ_{DG}
high	$> 50 \%$
medium	$20 \%\dots 50 \%$
low	$< 20 \%$

Care must be taken when DG penetration levels are defined: the system boundaries must be clearly stated and the reference values must be well chosen for the study purposes. In this thesis, two types of penetration level of DG based on *power* are defined. Both are defined for a certain part (or the whole) of the power system. The *rated* penetration level is defined in (A.1) as

$$\rho_{\text{DG,r}} = \frac{P_{\text{DG,r}}}{P_{\text{Ld,p}}} \quad (\text{A.1})$$

with $P_{\text{DG,r}}$ and $P_{\text{Ld,p}}$ being the total *rated* DG and *peak* load active power within the stated boundaries of the power system under study. The *instantaneous* penetration level is defined in (A.2) as

$$\rho_{\text{DG,i}} = \frac{P_{\text{DG,i}}}{P_{\text{Ld,i}}} \quad (\text{A.2})$$

with $P_{\text{DG,i}}$ and $P_{\text{Ld,i}}$ being the total *actual* DG and load active power *at a certain instant in time* in the studied part of the power system. Losses are neglected in these definitions. The differences between the two types of penetration levels are visualised in Fig. A.4a.

The boundaries of the (part of the) power system of interest depend, among others, on the voltage level. In this thesis, the penetration level at a certain voltage level always includes any installed DG capacity and load in the subsequent voltage level, see Fig. A.4b. For example, the DG rated penetration at medium voltage (MV) level also considers the low voltage (LV) level. That way, penetration level can be easily linked to the expected power flow direction with the overlaying voltage level and the superposition principle is always considered for linear circuits.

Apart from (A.1) and (A.2), DG penetration levels can be defined based on annual *energy*. Those are much lower than the ones based on power as PVPPM and WPPM operate at lower than rated output for large periods in a year (see table A.3).

Table A.3: Typical full load hours, capacity credit and country-wide coincidence factor for RES-E based DG in Germany [Fra13,EDBI13]

RES-E type	range of full load hours	range of capacity credit	coincidence factor
wind	1 300–2 700	15–31 %	90 %
solar	1 000–1 200	11–14 %	80 %
CHP & biomass	6 000–8 000	68–91 %	85 %

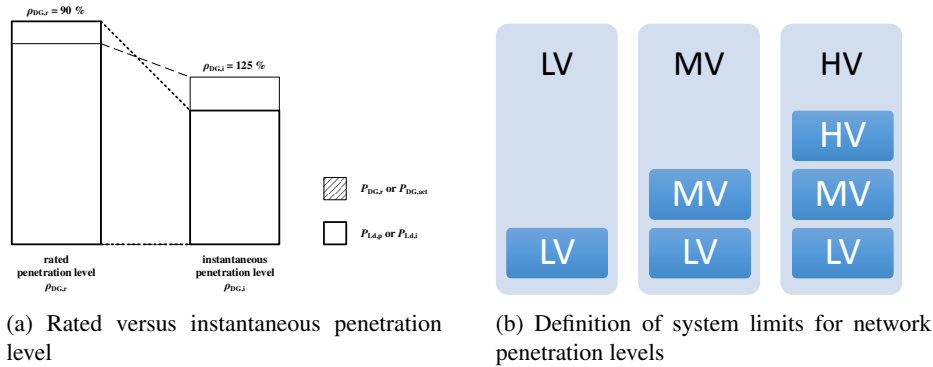


Figure A.4: Clarifications regarding the penetration level definition

A.7 Current angle stability

By ‘current angle stability’ this thesis understands

the ability of a generating unit which is grid-interfaced via a voltage source converter (VSC) and operated in parallel to the grid to inject current (magnitude, angle) for transiently changing grid conditions without violating the VSC synchronisation methods’s stability zone.

This definition is based on [Wei14] and has been edited to clarify that it does not apply to VSC that are operated as voltage sources and that both magnitude and angle of the injected current must be considered.

According to [Wei14], current angle instability is characterised by:

- Caused by inadequate current injection.
- Angles of current injection and of remaining voltage move.
- Loss of synchronism of VSC generating unit.
- VSC generating unit runs asynchronous to the grid.
- Frequency much higher or lower than steady-state system frequency.
- Resulting behaviour of VSC generating unit depends on design and parameter settings of phase locked loop (PLL) and current controller.
- Resynchronisation of VSC generating unit immediately after voltage recovery possible (no inertia).

The described instability is also known as ‘loss of synchronism’ [GTB⁺14], ‘loss of stability phenomenon’ [DBA11] or ‘steady state stability limit in quasi stationary operation’ [ESE⁺09].

Concerns about distribution system operator (DSO) general practices that can cause this instability for MV connected DG in practice have been reported in [SKL12].

A.8 DG grid connection interfaces

With respect to the grid connection interface, DG have undergone significant technological development in the past. Early WPPM used directly connected asynchronous generators whereas doubly fed asynchronous generators and different types of full converter interface units dominate in the market nowadays as they allow for improved controllability. Both of the latter WPPM types use, in one way or the other, power electronic converters (PEC), typically voltage source converters (VSC). VSC are also used in PVPPM. In contrast, combined heat and power (CHP) generating facilities often use synchronous PGMs but with much lower inertia compared to conventional generating units. Micro-CHP, however, are often coupled through a PEC as well [AE03, GPP08].

In this thesis, DG is classified with respect to the grid connection interface and disregarding their primary energy source as follows [EE13c, SAB⁺12]:

- distributed synchronous power generating modules (PGMs)
 - type 0: DG based on directly coupled synchronous generators, e.g. medium size combined heat and power generating facilities;
- distributed PPMs
 - type 1: DG based on conventional asynchronous generators (CAGs), e.g. fixed speed wind turbine generators, small CHP generating facilities, small microturbines;
 - type 2: DG based on variable rotor resistance asynchronous generators (VRRAGs), e.g. older variable speed wind turbine generators;
 - type 3: DG based on doubly fed asynchronous generators (DFAGs), e.g. modern variable-speed wind turbine generators;
 - type 4: DG based on full converter interface units (FCs), e.g. modern variable speed wind turbine generators, photovoltaic power park modules, and micro-CHP power park modules.

Out of these types of DG, only the types 0, 3, and 4 are modelled in this thesis.

A.9 DG location

The location of DG in the power system can be differentiated into ‘horizontal’ and ‘vertical’ location.

With ‘horizontal location’ the (often spatial) distribution of DG is described that determines (changes of) the power flows primarily at transmission system level. An example are large amounts of WPPM in a certain area of the power system that cause a large power transfer towards load centres.

With ‘vertical location’ the distribution of DG among voltage levels is described. This determines (changes of) the power flows between voltage levels, e.g. between transmission and distribution system level. An example are large amounts of PVPPM connected to the LV distribution network that may cause reverse power flows from the distribution to the transmission network.

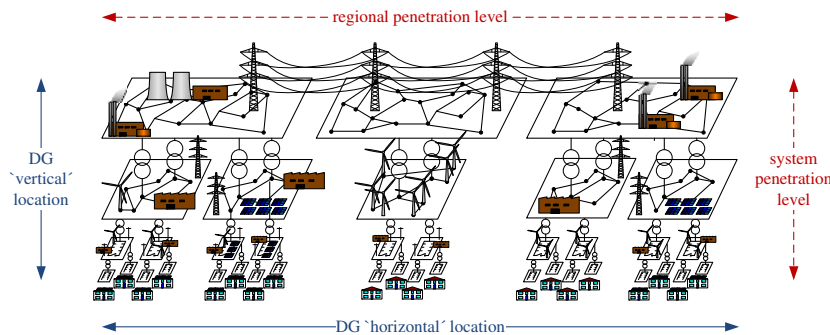


Figure A.5: Power system dimensions for DG location and penetration levels

A.10 Grid connection requirements

By ‘grid connection requirements’ (GCR) this thesis understands

a set of [legally binding] technical rules aiming at setting out clear and objective requirements for power generating modules for grid connection in order to contribute to non-discrimination, effective competition and the efficient functioning of the internal electricity market and to ensure system security [EE13c].

Together with safety standards which are, for example international (IEC, IEEE), European (CENELEC) or National (VDE, etc.) norms, grid connection requirements (GCR) are a mandatory part of the *connection services* a transmission system operator (TSO) or DSO provides to the users that want to be connected to the system (see Fig. A.6).

Some member states, e.g. the United Kingdom, have considered grid connection requirements to be an industry wide document and, consequently, have established already in the 1990’ies a so-called ‘Grid Code Review Panel’ to govern the document [JT05]. Other member states, however, followed a relatively closed, top-down approach until a few years ago, i.e. transmission system operators setting grid connection requirement without or with very little consultation of industry stakeholders. In Germany, for example, these requirements were for a long time defined by the national network operator association before a transparent procedure was introduced by the founding of the ‘Forum network technology / network operation in the VDE (VDEIFNN)’ [Eco08, For10].

Of particular importance is the capability of distributed generation to ride through faults. Fault ride-through (FRT) capability entails both low voltage ride-through (LVRT) as well as high voltage ride-through (HVRT), plus the ability to support the voltage during and after the fault. LVRT means that DG would stay connected during and after voltage dips caused by network faults. Similarly, HVRT means that DG stays connected during and after temporary overvoltages that may occur in a power system due to load shedding or unbalanced faults [FEK⁺08]. The alternative, a massive disconnection of DG due to a under- or over-voltage situation in large parts of the power system and the consequent protection actions can be regarded as a *common mode* failure.

Current grid connection requirements can be classified into the four categories (1) quasi-stationary voltage control, (2) dynamic reactive support, (3) disturbance voltage support, and (4) disturbance frequency support. A large variety of terms are used around the world

to describe these requirements. Table [A.4](#) gives an overview of terms that are widely used in the European and the North American context. The first two columns list the terminology used in this thesis.

Table A.4: Overview of grid connection requirement terms used in the European and the North American context

	Europe	North America	Characteristic
<ul style="list-style-type: none"> quasi-stationary voltage control 	<ul style="list-style-type: none"> $\cos(\theta)=\text{const.}$ Q(P) Q setpoint 	<ul style="list-style-type: none"> static network support [BDE08, For11] steady-state voltage support 	<ul style="list-style-type: none"> Static reactive support slow step control reactive power to control voltage at DG point of common coupling. Control loops typically operate in the 1 min ... 10 min. time frame.
<ul style="list-style-type: none"> dynamic reactive support 	<ul style="list-style-type: none"> $\cos(\theta)=f(P)$ Q(V) 	<ul style="list-style-type: none"> static network support [BDE08, For11] steady-state voltage support 	<ul style="list-style-type: none"> dynamic reactive capability [IVG12] smoothly controlled reactive power to control voltage at DG point of common coupling Control loops typically operate in the 1 s ... 10 s time frame.
<ul style="list-style-type: none"> disturbance voltage support 		<ul style="list-style-type: none"> dynamic voltage support dynamic network support [BDE08, For11] fault ride-through limited [BDE08, For11] zero power mode LVRT with BM mode LVRT with aRCI mode 	<ul style="list-style-type: none"> support during and after disturbances [IVG12] Ride through voltage disturbances Restore output after disturbance voltage ride-through momentary cessation [IEE16, CPU] cease to energize dynamic reactive current injection (DRC) [EPRI4] dynamic voltage support [IEE16] fast voltage control / fast-responding closed-loop voltage regulation [IVG12] injection of reactive power in direct proportion to the voltage decrease (open-loop) [IVG12] short-circuit capability n/a
<ul style="list-style-type: none"> disturbance frequency support 	<ul style="list-style-type: none"> LVRT with aRACI mode HVRT 	<ul style="list-style-type: none"> n/a n/a n/a high-voltage ride-through frequency ride-through frequency droop mode FRT with frequency-droop mode 	<ul style="list-style-type: none"> see above. very fast less accurately controlled or uncontrolled current that supports voltage at the resource's own terminals and nodes that are electrical close to the resource. Control loops, if prevalent, typically operate in the sub-second time frame, often within a few cycles. ride through frequency disturbances restore output after disturbance control active power output based on frequency deviation overfrequency response underfrequency response

A.11 Ancillary services

Independent system operators (ISO), transmission system operators (TSO) and distribution system operators (DSO) have to maintain the integrity and stability of the transmission or distribution system and deliver electric power with an adequate quality to users connected to the system. They achieve this objective by providing *system services* (ISO/TSO) or *network services* (TSO/DSO) to the connections.

In order to be able to provide these services, ISOs, TSOs and DSOs have to procure *ancillary services* from (some) system connections. By ancillary services (ASs) this thesis follows the definition in [Eur04] and refers to

all services required by the transmission or distribution system operator to enable them to maintain the integrity and stability of the transmission or distribution system as well as the power quality.

Ancillary services are further classified in this thesis based on the entity and the objective they are procured for (see Fig. A.6):

- ISO or TSO: Ancillary services *to system* are required to securely operate the whole power system.
- TSO or DSO: Ancillary services *to network* are required to securely operate the electrical power network.

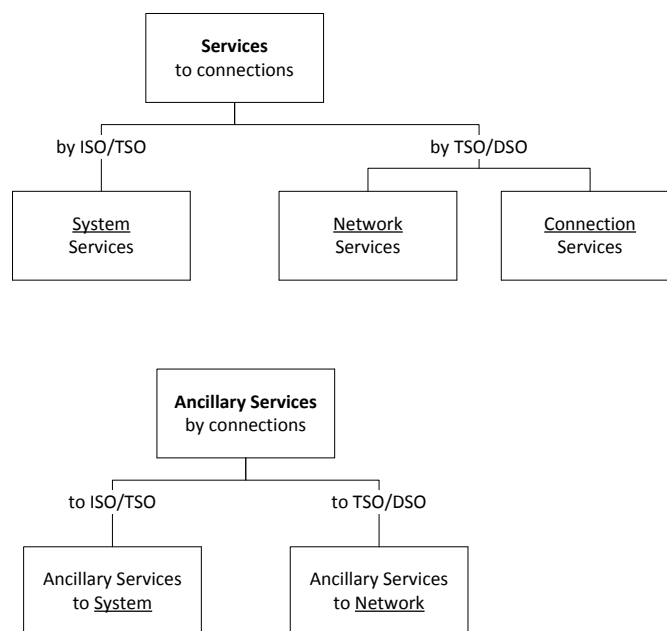


Figure A.6: Classification of services

As recommended in [CIG13], distributed generation will have to provide ancillary services at least in those hours of the year when substantial amount of conventional generation

is replaced. If this advice manifests itself in future, distribution systems will contribute actively to power system operation and stability. Figure A.7 presents the many ancillary services that such active distribution system respectively their connections can provide to the system or to the network.

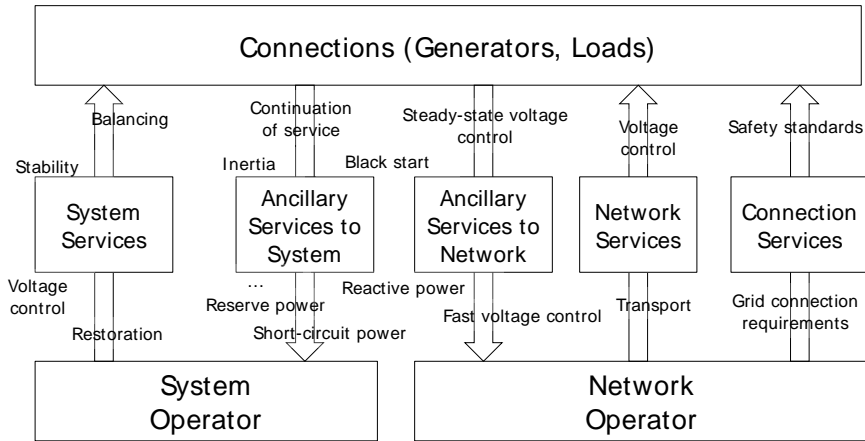


Figure A.7: Ancillary services to system and to network provided by connections

In the context of this thesis, the important ancillary services that active distribution systems would provide are:

- Ancillary services to system: continuation of service, short-circuit power
- Ancillary services to network: fast voltage control

Continuation of service—Instead of tripping in-feed from DG following transmission network faults, active distribution systems (ADSs) will be able to immediately restore their pre-fault active power in-feed to the transmission system and, thereby, increase power system frequency stability.

Short-circuit current—By help of distributed type 3 and type 4 power park modules, ADS will be able to contribute to short-circuit currents in the sub-transmission and transmission system level which preserves the ability of the protection scheme to detect and isolate a network fault. While this contribution should not be mistaken for short-circuit power contribution, the classic definition of s_k'' must be revised for power systems with very high penetration of distributed PPMs.

Fast voltage control—By help of distributed generation, ADSs will be able to control their system level voltage dynamically during and after transmission system faults within the range that their connection to the transmission system would allow. While this range may be limited during a transmission system fault, a significant improvement of the post-fault voltage recovery will be achieved.

A.12 The ‘strength’ of a power system

The ‘strength’ of a power system is considered too be a local variable and is defined in this thesis by the short-circuit ratio at the point of common coupling (PCC) of a distributed generator or a group of distributed generators. The PCC is

the point in the public network closest to the customer system to which further customer systems are connected or can be connected [For11].

The short-circuit ratio (SCR) is defined according to (A.3).

$$SCR_{PCC} = \frac{S''_{k,PCC}}{S_{DG,r}} \quad (A.3)$$

as the ratio of the subtransient short-circuit power levels at the PCC, $S''_{k,PCC}$, to the DG’s rated apparent power, $S_{DG,r}$.

Table A.5 shows the ranges that define the ‘strength’ of a power system in this thesis. A ‘weak’ power system has a SCR at the PCC of less than 5. Hence, either the DG’s rating $S_{DG,r}$ is high or the short-circuit power levels at the PCC $S''_{k,PCC}$ are low.

Table A.5: Ranges that define the ‘strength’ of a power system in this thesis

Strength	SCR_{PCC}
strong	> 10
modest	5...10
weak	< 5

The subtransient short-circuit power is defined by the product of the subtransient short-circuit current, i''_k , and the *pre-fault* voltage, v_0 , at the bus of interest:

$$s''_k = v_0 i''_k \quad (A.4)$$

At the same time, i''_k , is equivalent to the network impedance seen from the bus of interest according to:

$$s''_k = \frac{v_0^2}{z''_k} \quad (A.5)$$

However, it must be noted that the definitions of s_k and z''_k as well as the corresponding theory on short-circuit levels in a power system have been developed for power systems with synchronous generators as main sources. With respect to networks faults, the response of the latter can be modelled by voltage sources while this does not hold for power park modules that use power electronic converters. PPMs rather behave like current sources and, therefore, the presented theory is not applicable to power systems with very high penetration of distributed type 3 and type 4 PPMs.

Other sources define the total inertia of a power system as an indicator to assess its ‘strength’. This definition is not followed in this thesis because it aims at investigations of phenomena in longer time frames than the tens of a second to tens of seconds relevant for the short-term stability phenomena that are in the focus of this thesis.

A.13 Fault-induced delayed voltage recovery

By 'fault-induced delayed voltage recovery' (FIDVR) this thesis understands

a depressed voltage for 5 to 30 s following a network fault caused by the presence of large amounts of induction motor loads at distribution level. [NER12]

A.14 Voltage funnel

A voltage funnel (German: ‘Spannungstrichter’) is a time-variant, spatial voltage profile among the nodes of a power system that is caused by a network fault. The retained voltage at different nodes in a power system at a given time is a function of the location and type of the network fault and the propagation of the voltage dip through the network and across network levels. The voltage propagation depends on the relationship of system impedances, sources and loads according to Kirchhoff voltage law (KVL) and Kirchhoff current law (KCL).

Voltage funnels caused by transmission network faults can create low voltages at nodes in a wide geographical area. This can provoke a large contingency from a common-mode undervoltage trip of DG.

From a power system stability and modelling viewpoint it is noteworthy that each voltage funnel has a periphery region (annulus) in which the retained voltage is very close to the undervoltage protection threshold of distributed generation, see Fig. A.8. This annulus can have a very large geographic extension. The number of DG units in the annulus can be very large compared to the number of DG units that will obviously trip because they are located near the fault. The accurate modelling of the voltage contour that delineates all system nodes where the retained voltage is smaller than the DG’s undervoltage protection threshold will determine significantly the bifurcation point of the system-wide stability response: the aggregate MW-value of DG units that trip (power at risk) will be quite sensitive in high DG penetration scenarios to the modelling assumptions, network representation, and network fault response of individual DG units. As illustrated in Fig. A.8, the post-fault active power imbalance due to undervoltage tripping of DG will be larger in the case shown in subfigure A.8a than in the case shown in subfigure A.8b.

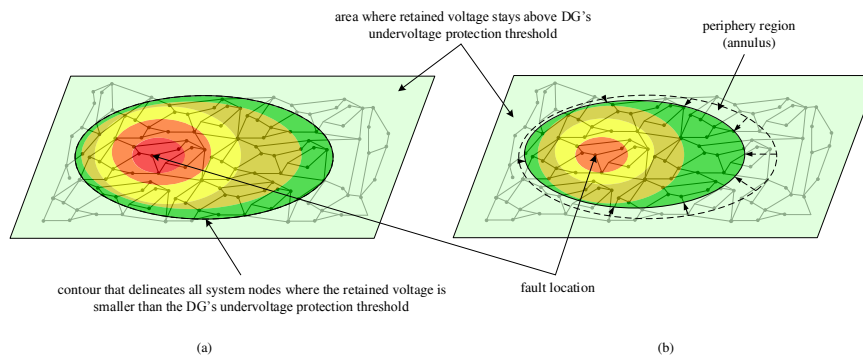


Figure A.8: Voltage funnel with periphery region (annulus)

Appendix B

Test system data

B.1 Simple test system for chapter 4

Table B.1: Simple test system data

Element	Info	Base	ST_NPF	ST_RPF	DS_RPF
Short-circuit power					
Ext. Network	X/R = 10, $T_a = 10$ s, $\Delta P/\Delta f =$ 800 MW/Hz	MVA	11,200	7,200	7,200
Rating					
Sync. Gen.	$T_a = 4$ s	MVA		100	100
Parallel machines					
TS Tr	YGy0 12%	250	1	3	3
S-TS Line	Overhead	150	2	5	5
WPPM Tr	YGd11 12%	50	5	16	./.
DS Tr	YGd11 12%	50	./.	./.	16
DS Line	Cable	34.6	./.	./.	100
WTG Tr	Dyn5 6%	2.3	100	350	350
WTGs		2.2	100	350	350
TS Load			800	800	800
S-TS Load	$\cos(\varphi) =$	MVA	250	250	./.
DS Load	0.98 ind.		./.	./.	250
P, Q flows over TS Tr	neg.: RPF	MW, Mvar	50, 85	-450, 165	-407, 372
Tap changer specifications					
TS Tr			$\pm 16, 0.625$ %		
WPPM Tr /			$\pm 16, 0.625$ %		
DS Trf			no tap changer modelled		
WTG Tr			no tap changer modelled		
S/C ratio at PCC		1	10	5	3
network angle at PCC		degrees	79	81	73

Table B.2: Tap changer positions

Case	TS Tr	WPPM Tr / DS Trf
1	3	2
2	4	2
3	3	3
4	3	-1
5	9	11

Note: bold numbers differ between cases

B.2 IEEE New England test system for chapter 5

Line	R [Ω]	X [Ω]	R/X [-]
eHV-01-02_LINE	0.1852	21.7443	0.009
eHV-01-39_LINE	0.5289	13.2226	0.040
eHV-02-03_LINE	0.6883	7.9945	0.086
eHV-02-25_LINE	0.5779	5.8572	0.987
eHV-03-04_LINE	0.6877	11.2678	0.610
eHV-03-18_LINE	0.5824	7.0423	0.083
eHV-04-05_LINE	0.4236	6.7775	0.063
eHV-04-14_LINE	0.4230	6.8211	0.062
eHV-05-06_LINE	0.1057	1.3743	0.077
eHV-05-08_LINE	0.4228	5.9195	0.071
eHV-06-07_LINE	0.3173	4.8650	0.065
eHV-06-11_LINE	0.3703	4.3372	0.085
eHV-07-08_LINE	0.2112	2.4285	0.087
eHV-08-09_LINE	1.2166	19.2018	0.063
eHV-09-39_LINE	0.5289	13.2226	0.040
eHV-10-11_LINE	0.2110	2.2683	0.093
eHV-10-13_LINE	0.2110	2.2683	0.093
eHV-13-14_LINE	0.4765	5.3475	0.089
eHV-14-15_LINE	0.9524	11.4815	0.083
eHV-15-16_LINE	0.4757	4.9687	0.096
eHV-16-17_LINE	0.3698	4.7012	0.079
eHV-16-19_LINE	0.8460	10.3110	0.082
eHV-16-21_LINE	0.4232	7.1409	0.059
eHV-16-24_LINE	0.1584	3.1156	0.051
eHV-17-18_LINE	0.3703	4.3372	0.085
eHV-17-27_LINE	0.6872	9.1445	0.075
eHV-21-22_LINE	0.4230	7.4025	0.057
eHV-22-23_LINE	0.3177	5.0831	0.063
eHV-23-24_LINE	1.1642	18.5218	0.063
eHV-25-26_LINE	1.6923	17.0817	0.099
eHV-26-27_LINE	0.7401	7.7712	0.095
eHV-26-28_LINE	2.2745	25.0719	0.091
eHV-26-29_LINE	3.0152	33.0617	0.091
eHV-28-29_LINE	0.7408	7.9898	0.093

Table B.3: Line parameters eHV network.

Load	Active power [MW]	Reactive power [Mvar]	Type [-]
eHV-03_STATLD	273.15	0	Constant Z
eHV-04_STATLD	293.15	150.2	Constant Z
eHV-07_STATLD	233.8	84	Constant Z
eHV-08_STATLD	315.15	142.2	Constant Z
eHV-12_STATLD	7.5	88	Constant Z
eHV-15_STATLD	25.4	99.8	Constant Z
eHV-16_STATLD	329	32.2	Constant Z
eHV-18_STATLD	0	-1.4	Constant Z
eHV-20_STATLD	333.4	49.8	Constant Z
eHV-21_STATLD	274	115	Constant Z
eHV-23_STATLD	247.5	84.6	Constant Z
eHV-24_STATLD	308.6	-92.2	Constant Z
eHV-25_STATLD	17.15	13.4	Constant Z
eHV-26_STATLD	139	17	Constant Z
eHV-27_STATLD	74.15	41.7	Constant Z
eHV-28_STATLD	194.9	1.3	Constant Z
eHV-29_STATLD	0	0	Constant Z
eHV-31_STATLD	9.2	4.6	Constant Z
eHV-39_STATLD	897.15	216.2	Constant Z

Table B.4: Load ratings eHV network.

	Active power rating [MW]	Local voltage setting [p.u.]	X_d [p.u.]	X_q [p.u.]
eHV-30_SG	800	1.0475	0.1	0.069
eHV-31_SG	1 250	1.04	0.295	0.282
eHV-32_SG	231.25	0.9831	0.2495	0.237
eHV-33_SG	250	0.9972	0.262	0.258
eHV-34_SG	781.25	1.0123	0.67	0.62
eHV-35_SG	987.5	1.0493	0.254	0.241
eHV-36_SG	873.75	1.0635	0.295	0.292
eHV-37_SG	1206.25	1.0278	0.29	0.28
eHV-38_SG	1312.5	1.0265	0.2106	0.205
eHV-39_SG	1 375	1.03	0.1	0.069

Table B.5: eHV synchronous generator parameters.

	T_w [s]	K_{pss} [p.u.]	T_1 [s]	T_2 [s]	T_3 [s]	T_4 [s]	u_{pss_min} [p.u.]	u_{pss_max} [p.u.]
eHV-30_SG_PSS	10	1	1	0.05	3	0.5	-0.2	0.2
eHV-31_SG_PSS	10	0.5	5	0.4	1	0.1	-0.2	0.2
eHV-32_SG_PSS	10	0.5	3	0.2	2	0.2	-0.2	0.2
eHV-33_SG_PSS	10	2	1	0.1	1	0.3	-0.2	0.2
eHV-34_SG_PSS	10	1	1.5	0.2	1	0.1	-0.2	0.2
eHV-35_SG_PSS	10	4	0.5	0.1	0.5	0.05	-0.2	0.2
eHV-36_SG_PSS	10	7.5	0.2	0.02	0.5	0.1	-0.2	0.2
eHV-37_SG_PSS	10	2	1	0.2	1	0.1	-0.2	0.2
eHV-38_SG_PSS	10	2	1	0.5	2	0.1	-0.2	0.2
eHV-39_SG_PSS	10	1	1	0.05	3	0.5	-0.2	0.2

Table B.6: eHV synchronous generator PSS parameters.

	T_r [s]	T_c [s]	T_b [s]	K_a [p.u.]	T_a [s]	E_{fd_min} [p.u.]	E_{fd_max} [p.u.]
All eHV SG_AVR	0.01	1	10	200	0.015	-5	5

Table B.7: eHV synchronous generator AVR parameters.

Transformer	Rated power [MVA]	Voltage levels [kV]	SC voltage [%]	Losses [kW]
eHV-02-30_TRF	100	380/22	1.81	0
eHV-06-31_TRF	100	380/22	2.5	0
eHV-10-32_TRF	100	380/22	2	0
eHV-12-11_TRF	100	380/380	4.35	160
eHV-12-13_TRF	100	380/380	4.35	160
eHV-19-20_TRF	100	380/380	1.38	70
eHV-19-33_TRF	100	380/22	1.42	70
eHV-20-34_TRF	100	380/22	1.80	90
eHV-22-35_TRF	100	380/22	1.43	0
eHV-23-36_TRF	100	380/22	2.72	50
eHV-25-37_TRF	100	380/22	2.32	60
eHV-29-38_TRF	100	380/22	1.56	80

Table B.8: Parameters of eHV network transformers.

Appendix C

DG modelling and control

C.1 Network fault controls

The mathematical and graphical descriptions of the proposed network fault control modes are provided in this section. The d-axis and q-axis quantities are aligned to the voltage at the distributed generation (DG)'s terminal. Superscripts for the reference frame are omitted.

C.1.1 Voltage dependent direct-axis current reduction

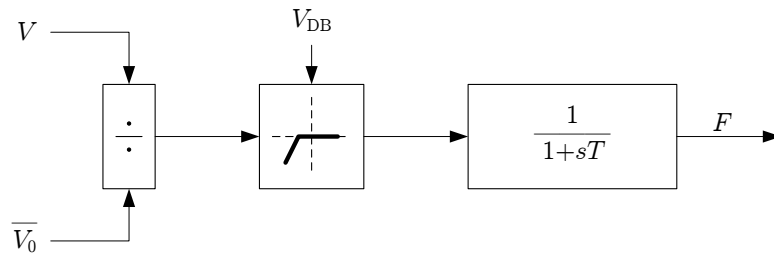


Figure C.1: Voltage dependent direct-axis current reduction block diagram [SER09]

$$I_{d,Flt} = \bar{I}_{d,0} \cdot (F)^2 \quad (C.1)$$

C.1.2 Additional Reactive Current Injection

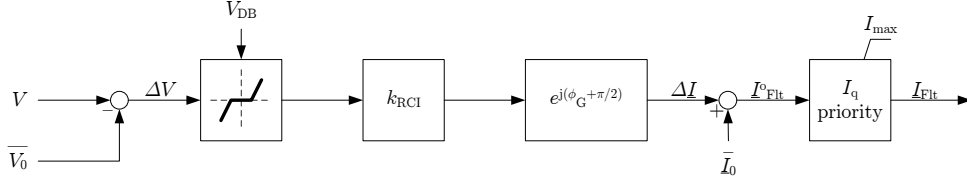


Figure C.2: Additional reactive current injection with I_q priority block diagram

$$\underline{I}_{\text{Flt}} = \bar{I}_0 + \Delta \underline{I}(\Delta V) = I_{d,\text{Flt}} + jI_{q,\text{Flt}} \quad (\text{C.2})$$

with

$$\Delta \underline{I}(\Delta V) = e^{j(\phi_G + \frac{\pi}{2})} \cdot \begin{cases} 0 & , |\Delta V| \leq V_{\text{DB}} \\ k_{\text{RCI}} \cdot [\Delta V \mp V_{\text{DB}}] & , |\Delta V| > V_{\text{DB}} \end{cases}$$

$$\Delta V = V - \bar{V}_0$$

$$\bar{I}_0 = \frac{1}{T} \int_{t'-T}^t \underline{I}(t') dt'$$

$$\bar{V}_0 = \frac{1}{T} \int_{t'-T}^t V(t') dt'$$

and with current limitation

$$I_{q,\text{Flt}} = \bar{I}_{q,0} + \Delta I_q = \min^{I_{\text{max}}} \left(\bar{I}_{q,0} + k_{\text{RCI}} \cdot [(\Delta V) \mp V_{\text{DB}}] \right)$$

$$I_{d,\text{Flt}} = \begin{cases} 0 & , \text{for } i_{\text{FRT_CL_PRIO_MOD}} = 0 \\ \min^{I_{\text{max}}} (I_{\text{max}} - I_{q,\text{Flt}}) & , \text{for } i_{\text{FRT_CL_PRIO_MOD}} = 1 \\ \min^{I_{\text{max}}} \left(\sqrt{(I_{\text{max}})^2 - (I_{q,\text{Flt}})^2} \right) & , \text{for } i_{\text{FRT_CL_PRIO_MOD}} = 2 \end{cases}$$

where

$$I_{\text{max}} = \begin{cases} I_{\text{max}} & , \text{for } i_{\text{FRT_CL_STAB}} = 0 \\ \bar{I}_{d,0} \cdot (V_{\text{DG}})^2 & , \text{for } i_{\text{FRT_CL_STAB}} = 1 \end{cases}$$

C.1.3 Additional Reactive & Active Current Injection

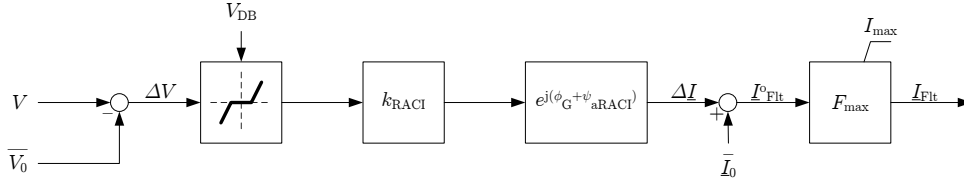


Figure C.3: Additional reactive & active current injection block diagram

$$\underline{I}_{\text{Flt}}^{\circ} = \bar{I}_0 + \Delta I(\Delta V) = I_{\text{d,Flt}}^{\circ} + jI_{\text{q,Flt}}^{\circ} \quad (\text{C.3})$$

$$\underline{I}_{\text{Flt}} = \underline{I}_{\text{Flt}}^{\circ} \cdot F_{\text{max}} = I_{\text{d,Flt}} + jI_{\text{q,Flt}} \quad (\text{C.4})$$

with

$$\Delta I(\Delta V) = e^{j(\phi_G + \psi_{\text{aRACI}})} \cdot \begin{cases} 0 & , |\Delta V| \leq V_{\text{DB}} \\ k_{\text{RACI}} \cdot [\Delta V \mp V_{\text{DB}}] & , |\Delta V| > V_{\text{DB}} \end{cases}$$

$$\Delta V = V - \bar{V}_0$$

$$\bar{I}_0 = \frac{1}{T} \int_{t'-T}^t I(t') dt'$$

$$\bar{V}_0 = \frac{1}{T} \int_{t'-T}^t V(t') dt'$$

and with current limitation

$$I_{\text{q,Flt}} = I_{\text{q,Flt}}^{\circ} \cdot F_{\text{max}}$$

$$I_{\text{d,Flt}} = I_{\text{d,Flt}}^{\circ} \cdot F_{\text{max}}$$

$$I_{\text{q,Flt}}^{\circ} = \bar{I}_{\text{q},0} + \Delta I_{\text{q}} = \bar{I}_{\text{q},0} + [k_{\text{RACI}} \cdot [\Delta V \mp V_{\text{DB}}] \cdot \sin(\psi_{\text{aRACI}})]$$

$$I_{\text{d,Flt}}^{\circ} = \bar{I}_{\text{d},0} + \Delta I_{\text{d}} = \bar{I}_{\text{d},0} + [k_{\text{RACI}} \cdot [\Delta V \mp V_{\text{DB}}] \cdot \cos(\psi_{\text{aRACI}})]$$

where

$$\bar{I}_{\text{d},0} = \begin{cases} \bar{I}_{\text{d},0} & , \text{for } i_{\text{FRT_CI_STAB}} = 0 \\ \bar{I}_{\text{d},0} \cdot (V_{\text{DG}})^2 & , \text{for } i_{\text{FRT_CI_STAB}} = 1 \end{cases}$$

$$F_{\text{max}} = \max_1 \left(\frac{I_{\text{max}}}{|I_{\text{Flt}}^{\circ}|} \right)$$

Figure C.4 gives the graphical representation of the additional reactive/active current injection (aRACI) scaling scheme. It should be noted that an increase of the active current during the voltage dip does not necessarily result into an increase of active power. Also, the active sign convention is used, meaning:

- Injection of positive active power $\underline{S} = V \cdot \underline{I}^* = P + jQ = (V \cdot I_d - jV \cdot I_q)$;
- Pre-fault current: exchange of negative reactive power (positive reactive current, $I_q > 0$) causes voltage decreases (inductive power factor);
- Full dynamic network support: exchange of positive reactive power (negative reactive current, $I_q < 0$) causes voltage increase (capacitive power factor).

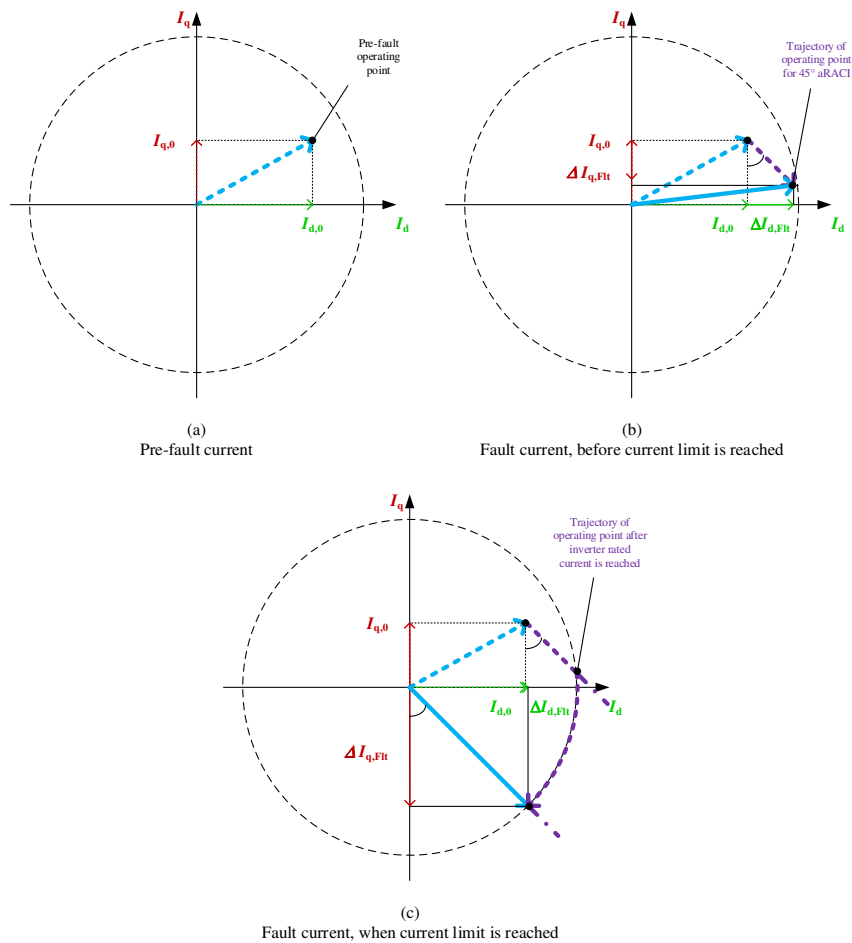


Figure C.4: Scaling of d-axis and q-axis currents in additional reactive/active current injection control mode, own drawing based on [Ska14]

C.2 Wind power park modules

This appendix shows the network fault control modes and parameters for the wind power park modules. The doubly fed asynchronous generator (DFAG) wind power park module (WPPM) model used is from [DIg11a], the full converter interface unit (FC) WPPM is a modified version of [DIg11b].

The reactive current gain of the MV wind turbines in the test system is set to 0.2. Normally higher values (often 2) are used, but discussions with DSOs showed that a value of 0.2 can be used in the test system. This is done to reflect the fact that the test system has almost no wind turbines connected at the substation. In reality, only substation connected wind turbines are allowed to feed in additional reactive power during a fault. HV wind turbines are set at the standard value of 2.

C.2.1 Type 3: Doubly fed asynchronous generator (DFAG)

Control parameters for chapter 5

Table C.1: DFAG wind turbine parameters.

Parameter	HV			MV		
	OLD	EEG	SDL	NEW	LVRT	NEW
K_p [p.u.]	4	4	4	4	4	4
T_p [s]	0.1	0.1	0.1	0.1	0.1	0.1
K_q [p.u.]	4	4	4	4	4	4
T_q [s]	0.1	0.1	0.1	0.1	0.1	0.1
X_m [p.u.]	3.5	3.5	3.5	3.5	3.5	3.5
ΔU [p.u.]	0.11	0.11	0.11	0.11	0.11	0.11
$K_{\Delta U}$ [-]	0	2	2	2	0	0.2
i_{\max} [p.u.]	1.31	1.31	1.31	1.31	1.31	1.31
i_{EEG} [0/1]	1	0	1	1	1	1
T_{u_delay} [s]	0.01	0.01	0.01	0.01	0.01	0.01
T_{back_delay} [s]	0	0.5	0	0	0	0
K_{ramp} [p.u./s]	0.01	0.2	99999	99999	0.2	99999
i_{d_max} [p.u.]	1.1	1.1	1.1	1.1	1.1	1.1
i_{q_max} [p.u.]	1	1	1	1	1	1

C.2.2 Type 4: Full converter interface units (FC)

Table C.2: Fault ride-through control mode flags and parameters

Flag or parameter	Description	Unit
Steady state control		
k_p	active power control gain	[p.u.]
T_p	active power control time constant	[s]
k_q	reactive power control gain	[p.u.]
T_q	reactive power control time constant	[s]
Fault period		
$\Delta V_{\text{FRT_DB_FAULT}}$	voltage deadband for fault detection (hysteresis low)	[p.u.]
$\Delta V_{\text{FRT_DB_CLEAR}}$	voltage deadband for fault clearance (hysteresis high)	[p.u.]
$i_{\text{FRT_CL_DB}}$	0 = TC curve; 1 = SDL curve	[0/1]
$T_{\text{FRT_id_v}}$	voltage dependent active current reduction control time constant	[s]
$T_{\text{FRT_detect}}$	time to detect a fault: voltage support delay	[s]
$k_{\text{FRT_CI}}$	short-circuit current gain	[p.u.]
$i_{\text{FRT_CL_MOD}}$	current injection during fault: 0 = total (TC mode); 1 = additional to pre-fault value (SDL mode)	[0/1]
$i_{\text{FRT_CL_PRIO}}$	current priority given to 0 = id; 1 = iq (TC & SDL mode); other = equal (RACI mode)	[0/1/2]
$i_{\text{FRT_CL_PRIO_MOD}}$	current priority mode: 1 = arithmetic (abs); 2 = geometric (sqrt); other = set other value to zero	[0/1/2]
$i_{\text{FRT_CL_STAB}}$	stability improvement during fault by voltage dependent id reduction: 0 = no; 1 = yes	[0/1]
$i_{\text{FRT_CL_ANG}}$	current angle (a)RACI, best set equal to $\varphi = \angle(Z_G)$	[degree]
Post-fault period		
$i_{\text{FRT_CL_CONT}}$	current injection continuation after fault for $T_{\text{FRT_CL_CONT}}$ seconds: 0 = no; 1 = yes	[0/1]
$T_{\text{FRT_CL_CONT}}$	voltage support continuation period after fault for $i_{\text{FRT_CL_CONT}} = 1$	[s]
$i_{\text{FRT_CL_dAPR}}$	delayed active power recovery after fault for $P_{\text{FRT_dAPR_ramp}}$: 0 = no; 1 = yes	[0/1]
$P_{\text{FRT_dAPR_ramp}}$	active power ramp after fault is cleared	[%/s]
Other		
i_{max}	combined current limit	[p.u.]
$i_{\text{d_max}}$	id current limit	[p.u.]
$i_{\text{q_max}}$	iq current limit	[p.u.]
x_m	magnetising reactance at P_{base}	[p.u.]
X	coupling reactance	[%]
u_{max}	maximum allowed internal voltage	[p.u.]

Control parameters for chapter 4

Table C.3: Control Mode Flag and Parameter Values

Flag or parameter	Unit	BLOCK	TC	SDL	NEW
Steady state control					
K_p	[p.u.]	0.5	0.5	0.5	0.5
T_p	[s]	0.05	0.05	0.05	0.05
K_q	[p.u.]	0.5	0.5	0.5	0.5
T_q	[s]	0.5	0.5	0.5	0.5
Fault period					
$\Delta V_{\text{FRT_DB_FAULT}}$	[p.u.]	0.11	0.11	0.11	0.06
$\Delta V_{\text{FRT_DB_CLEAR}}$	[p.u.]	0.09	0.09	0.09	0.04
$i_{\text{FRT_CL_DB}}$	[0/1]	0	0	1	1
$T_{\text{FRT_id_v}}$	[s]	0.005	0.005	0.005	0.005
$T_{\text{FRT_detect}}$	[s]	0.01	0.01	0.01	0.01
$k_{\text{FRT_CI}}$	[p.u.]	0	0, 2, 6	0, 2, 6	0, 2, 6
$i_{\text{FRT_CL_MOD}}$	[0/1]	0	1	1	1
$i_{\text{FRT_CL_PRIO}}$	[0/1/2]	1	1	1	1
$i_{\text{FRT_CL_PRIO_MOD}}$	[0/1/2]	3	1	1	1
$i_{\text{FRT_CL_STAB}}$	[0/1]	0	0	0	1
$i_{\text{FRT_CL_ANG}}$	[degree]	90	90	90	90
Post-fault period					
$i_{\text{FRT_CL_CONT}}$	[0/1]	1	1	0	1
$T_{\text{FRT_CL_CONT}}$	[s]	0.01	0.5	n/a	0.5
$i_{\text{FRT_CL_dAPR}}$	[0/1]	1	1	0	1
$P_{\text{FRT_dAPR_ramp}}$	[%/s]	200	200	200	200
Other					
i_{max}	[p.u.]	1.2	1.2	1.2	1.2
i_{i_max}	[p.u.]	1.15	1.15	1.15	1.15
i_{q_max}	[p.u.]	1.15	1.15	1.15	1.15
x_m	[p.u.]	0	0	0	0
X	[%]	10	10	10	10
u_{max}	[p.u.]	1.1	1.1	1.1	1.1

Note: bold numbers differ between performance classes.

C.3 Photovoltaic power park modules

Control parameters for chapter 5

Table C.5: MV PV system parameters.

Parameter	MV			
	PF100	LVRT	aRCI	NEW
T_{f_ac} [s]	0.002	0.002	0.002	0.002
$T_{q_f_ac1}$ [s]	0.001	0.001	0.001	0.001
i_{base} [A]	0.0507	0.0507	0.0507	0.0507
i_{FRT_APR} [0/1]	0	1	1	1
i_{FRT_Mode} [0/1/2/3]	0	1	2	2
$T_{q_f_ac}$ [s]	0.001	0.001	0.001	0.001
K_{dc} [-]	-12976	-12976	-12976	-12976
K_{q_ac} [-]	-0.226755	-0.226755	-0.226755	-0.226755
T_{q_ac} [s]	0.002205	0.002205	0.002205	0.002205
K_{ac} [-]	-0.5	-0.5	-0.5	-0.5
T_{ac} [s]	0.001	0.001	0.001	0.001
T_{f_dc} [s]	0	0	0	0
T_{dc} [s]	300	300	300	300
T_{L_g} [s]	0.0011	0.0011	0.0011	0.0011
T_{L_d} [s]	0.02323	0.02323	0.02323	0.02323
G [-]	1	1	1	1
i_{Q_Mode} [0/1/2]	0	0	0	0
deadband [p.u.]	0.2	0.1	0.1	0.1
I_{max} [p.u.]	1.1	1.1	1.1	1.1
K_{i_d} [p.u.]	0	0	0.2	0.2
K_{arci} [p.u.]	0	0	0.2	0.2
angle [deg]	90	90	90	90
T_{drop} [s]	60	60	60	60
T_{relay} [s]	0.1	0.1	0.1	0.1
K [p.u.]	1	1	1	1
T [s]	0.01301236	0.01301236	0.01301236	0.01301236
T_{sr} [s]	0	0	0	0
K_1 [p.u.]	1	1	1	1
T_1 [s]	0.01301236	0.01301236	0.01301236	0.01301236
V_b [kV]	0.4718	0.4718	0.4718	0.4718
i_{q_min} [-]	-0.02218	-0.02218	-0.02218	-0.02218
i_{min} [-]	0	0	0	0
Min_{iq} [A]	-0.0507	-0.0507	-0.0507	-0.0507
i_{q_max} [-]	0.02218	0.02218	0.02218	0.02218
i_{max} [-]	0.0507	0.0507	0.0507	0.0507
Max_{iq} [A]	0.0507	0.0507	0.0507	0.0507

Table C.6: LV PV system parameters.

Parameter	LV		
	PF100	PFPOW	NEW
T_{f_ac} [s]	0.002	0.002	0.002
$T_{q_f_ac1}$ [s]	0.001	0.001	0.001
i_{base} [A]	0.0507	0.0507	0.0507
i_{FRT_APR} [0/1]	0	0	see table C.7
i_{FRT_Mode} [0/1/2/3]	0	0	see table C.7
$T_{q_f_ac}$ [s]	0.001	0.001	0.001
K_{dc} [-]	-12976	-12976	-12976
K_{q_ac} [-]	-0.226755	-0.226755	-0.226755
T_{q_ac} [s]	0.002205	0.002205	0.002205
K_{ac} [-]	-0.5	-0.5	-0.5
T_{ac} [s]	0.001	0.001	0.001
T_{f_dc} [s]	0	0	0
T_{dc} [s]	300	300	300
T_{I_g} [s]	0.0011	0.0011	0.0011
T_{I_d} [s]	0.02323	0.02323	0.02323
G [-]	1	1	1
i_{Q_Mode} [0/1/2]	0	0	0
deadband [p.u.]	0.2	0.2	see table C.7
I_{max} [p.u.]	1.1	1.1	1.1
K_{i_d} [p.u.]	0	0	see table C.7
K_{arci} [p.u.]	0	0	see table C.7
angle [deg]	90	90	see table C.7
T_{drop} [s]	60	60	60
T_{relay} [s]	0.1	0.1	0.1
K [p.u.]	1	1	1
T [s]	0.01301236	0.01301236	0.01301236
T_{sr} [s]	0	0	0
K_1 [p.u.]	1	1	1
T_1 [s]	0.01301236	0.01301236	0.01301236
V_b [kV]	0.4718	0.4718	0.4718
i_{q_min} [-]	-0.02218	-0.02218	-0.02218
i_{min} [-]	0	0	0
Min_{iq} [A]	-0.0507	-0.0507	-0.0507
i_{q_max} [-]	0.02218	0.02218	0.02218
i_{max} [-]	0.0507	0.0507	0.0507
Max_{iq} [A]	0.0507	0.0507	0.0507

Table C.7: LV PV_NEW system parameters.

Parameter	LV_NEW			
	nLVRT	BM	aRCI	aRACI
$i_{\text{FRT_APR}}$ [0/1]	0	1	1	1
$i_{\text{FRT_Mode}}$ [0/1/2/3]	0	1	2	3
deadband [p.u.]	0.2	0.1	0.1	0.1
K_{i_d} [p.u.]	0	6	6	6
K_{arci} [p.u.]	0	6	6	6
angle [deg]	90	90	90	acc. PCC impedance

C.4 Combined heat and power plants

Synchronous combined heat and power (CHP) generating facilities are modelled by use of a 6th order synchronous generator model [IEE03a,DIg15] and standard IEEE governors and excitors [IEE06]. The model parameters are provided in this appendix. Values are taken as much as possible manufacturers data sheets. The data for the high voltage connected CHP is taken from [Erl13]. For any missing data, standard DIgSILENT PowerFactory© v15.1 (DGF) values are used.

Control parameters for chapter 5

Table C.8: CHP parameters [Erl13], [Bos14].

Parameter	LV SGCHP	MV SGCHP	HV SGCHP
Generator rating [kW]	10	400	20 000
Power factor [-]	0.8	0.8	0.8
Rotor type [-]	salient	salient	salient
Nominal voltage [kV]	0.4	20	20
Inertia time constant (rated to S_{gen}) [H]	0.31	0.29	3.8
X_d [p.u.]	3.257	3.071	4
X_q [p.u.]	1.661	1.566	2.4
X_d' [p.u.]	0.198	0.227	0.2
X_d'' [p.u.]	0.119	0.159	0.17
X_q'' [p.u.]	0.143	0.211	0.17
T_d' [s]	0.1	0.1	0.18
T_d'' [s]	0.01	0.01	0.018
T_q'' [s]	0.01	0.01	0.001275
X_2 [p.u.]	0.079	0.13	0.2
R_2 [p.u.]	0.1	0.057	0
Stator leakage reactance [p.u.]	0.059	0.079	0.15
Stator resistance [p.u.]	0.0254	0.0143	0.003

Table C.9: Standard AVR parameters (EXAC1A) [DIg13].

T_r [s]	0.025
T_b [s]	1
T_c [s]	2
K_a [p.u.]	400
T_a [s]	0.02
T_e [s]	0.5
K_f [p.u.]	0.01
T_f [s]	1
K_c [p.u.]	0.65
K_d [p.u.]	0.2
E_1 [p.u.]	3.9
S_{e_1} [p.u.]	0.1
E_2 [p.u.]	5.2
S_{e_2} [p.u.]	0.5
K_e [p.u.]	1
V_{r_min} [p.u.]	-10
V_{r_max} [p.u.]	10

Table C.10: Non-standard AVR parameters (EXAC1A) [Bos14].

Parameter	LV SGCHP	MV SGCHP
K_e [p.u.]	1	1
E_2 [p.u.]	6.02	6.26
S_{e_1} [p.u.]	0.32	0.76
E_2 [p.u.]	5.13	5.71
S_{e_2} [p.u.]	0.14	0.39
T_a [s]	0.015	0.022
V_{r_min} [p.u.]	0	0
V_{r_max} [p.u.]	8.6	10

Appendix D

Load modelling

D.1 Exponential load model

$$P_{\text{exp}} = P_0 \cdot \left[a_P \left(\frac{V}{V_0} \right)^{e_{aP}} \right] \quad (\text{D.1})$$

$$Q_{\text{exp}} = Q_0 \cdot \left[a_Q \left(\frac{V}{V_0} \right)^{e_{aQ}} \right] \quad (\text{D.2})$$

Table D.1: Exponential load parameters for constant impedance load.

Parameter		Value
coefficient for voltage dependence of P	a_P	1.0
exponent for voltage dependence of P	e_{aP}	2.0
coefficient for voltage dependence of Q	a_Q	1.0
exponent for voltage dependence of Q	e_{aQ}	2.0

D.2 Detailed induction motor load model

$$\tau_m = \begin{cases} \tau_{m,1} & \text{if } s \leq s_{\tau_{m,\min}} \\ \tau_{m,2} & \text{if } s > s_{\tau_{m,\min}} \end{cases} \quad (\text{D.3})$$

$$\tau_{m,1} = \tau_{m,\min} + (\tau_{m,s=0} - \tau_{m,\min}) \left(\frac{|n_R/n_s| - (1 - s_{\tau_{m,\min}})}{s_{\tau_{m,\min}}} \right)^{e_{\tau_{m,1}}} \quad (\text{D.4})$$

$$\tau_{m,2} = \tau_{m,\min} + (\tau_{m,s=1} - \tau_{m,\min}) \left(1 - \frac{|n_R/n_s|}{1 - s_{\tau_{m,\min}}} \right)^{e_{\tau_{m,2}}} \quad (\text{D.5})$$

with

n_s	synchronous speed	[r/min]
n_R	rotor speed	[r/min]
s	slip speed of the rotor on n_s base	[p.u.]
τ_m	mechanical torque	[p.u.]
$\tau_{m,1}$	torque of 1 st polynomial torque function	[p.u.]
$\tau_{m,2}$	torque of 2 nd polynomial torque function	[p.u.]

Table D.2: Single cage induction motor parameters

Parameter	Symbol	Value	Unit
acceleration time constant on P base	T_{aP}	0.4649	s
stator resistance	r_S	0.031	p.u.
stator reactance	x_S	0.12	p.u.
magnetising reactance	x_m	3.2	p.u.
rotor resistance	r_R	0.036	p.u.
rotor reactance	x_R	0.32	p.u.

Table D.3: Motor-driven machine parameters

Parameter	Symbol	Value	Unit
torque at synchronous speed	$\tau_{m,s=0}$	0.8837	p.u.
torque at standstill	$\tau_{m,s=1}$	0.0465	p.u.
minimum torque	$\tau_{m,\min}$	0.0233	p.u.
slip at minimum torque	$s_{\tau_{m,\min}}$	0.8652	p.u.
exp. of 1 st polynomial torque function	$e_{\tau_{m,1}}$	1.8085	-
exp. of 2 nd polynomial torque function	$e_{\tau_{m,2}}$	1.5779	-

Appendix E

Active Distribution Systems for chapter 5

E.1 Statistical Analysis of German Grid Data

Real German installed DG data are used to determine the amount of DG that is to be installed in the 2012 version of the network [Deu13]. For the 2022 case, a future outlook of the *Bundesnetzagentur* is used [Ger12b]. Data is obtained geographically on German postal code 3 (PLZ-3) resolution.¹ The whole of Germany is made up of 581 PLZ-3s. A PLZ-3 may still be divided further in different ‘region types’, as defined by [Fed11]. The differentiation is made on population density, among other factors. Three region types are distinguished:

Region type 1 Urban

Region type 2 Suburban

Region type 3 Rural

Only region types 2 and 3 are investigated in further detail because distributed generation (DG) penetration levels are highest in the regions.

The goal of the statistical analysis is to find representative values for both the number and size of DG installations connected at the different voltage levels in the network. This information is obtained in two steps. First, the typical installation size per technology and per voltage level is found. Additionally, the typical penetration per technology and per voltage level is determined for the different region types. Combining load data provided by a German DSO with the penetration data yields the number of installations to be used within the different networks per technology and voltage level.

¹German postal codes have 5 digits, the first three digits indicate ever smaller geographic regions.

E.1.1 Typical DG Installation Size

Even though DG installation capacity can be virtually any size, a typical size per technology and per voltage level will greatly reduce the number of variables and simplify the networks to be analysed. When the scale of the simulation network is increased to see how the German network would behave, the installation size should be fitting.

In the database DG units are listed specifying their technology, size, location and connected voltage level. Off-shore wind turbines are not taken into account. One difficulty in analysing the data are multiple units that form one installation, but that have each unit as a separate entry in the database. Without precautions this leads to a very large number of 2 MW installations in the higher voltage levels. To alleviate this problem, installations within a PLZ-3 that are found in the same street in a town are grouped, as are installations with the same connection code and the same installation date. By grouping the installations in this way, bigger installations become visible. Even with this precaution, some of the 2 MW units are falsely counted by themselves.

A second clear problem with the data is a number of small installations that are connected to higher voltage levels. Since installations of only a few kW are never installed on high voltage levels in reality, it must be concluded that this is corrupted data. Entries in the database are at some point entered manually, which makes the possibility of a writing or reading error very real.

In determining the typical size of a certain technology for a voltage level, the median of that technology at that voltage level is used. With half of the installations of smaller size and the other half of larger size, this value gives a representative feel for the 'typical' size of an installation. This does not mean that the typical value occurs (frequently) in reality. Figure E.1a shows the cumulative installed percentage of PV system units for the different voltage levels. The 'typical' installation size is found at the cross-point of the cumulative installed DG units curve and the horizontal line at 50 percent cumulative installed DG units (the median).

In case data on higher voltage levels includes corrupted data as described above, this corrupted data is ignored and the median is taken from the trusted data, see Fig. E.1b showing the cumulative installed percentage of PV systems at a different scale. The data suggests that almost twenty percent of HV connected PV systems is smaller than approximately 3 000 kW in size. This is not realistic due to the way installations are registered in the database, and these systems are subsequently omitted from the determination of the 'typical' size. Thus, instead of the 50 percent line, now the median of the remaining data is used. In this case, the median then lies at almost 60 percent. The 'typical' size is now determined at the cross-point of the cumulative installed DG units curve and the adjusted median. The results of the analysis can be found in [van14]. The obtained typical DG installation sizes per technology and voltage level are given in table E.1.

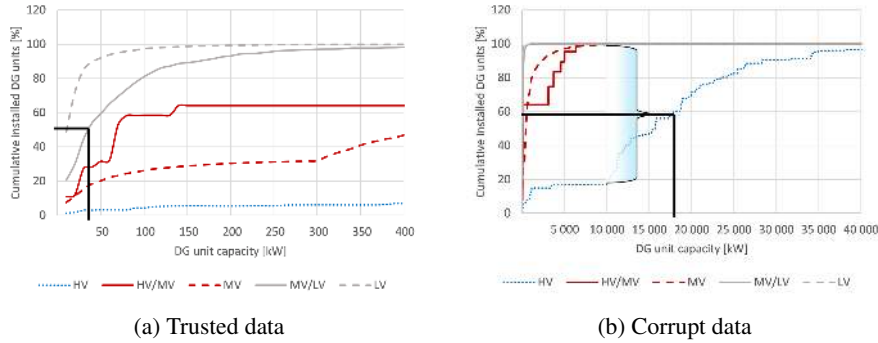


Figure E.1: Determination of typical DG installation size.

Table E.1: Typical DG installation size per voltage level [kW] [Deu13]. MV wind turbine values are changed to represent total park size [Del14].

DG unit size [kW]	eHV	eHV/HV	HV	HV/MV	MV	MV/LV	LV
PV	n.a.	n.a.	34 140	3 690	430	40	10
Wind	4 000	3 000	3 600	[2 000] 10 000	[1 500] 5 000	200	30
CHP	>100 000	n.a.	20 000	5 500	400	230	10

E.1.2 Typical DG penetration

With the typical DG installation size known, the penetration is still required to find the number of typical installations to be installed in the networks. For the statistical analysis, the DG penetration is defined as follows:

(E.1)

Where i = area (PLZ-3, subdivided to region type if applicable).

The penetration for a particular area is thus 100 percent when the installed DG capacity equals the (yearly) peak load in that area. The penetration is calculated for HV, MV and LV levels, where lower voltage levels are included in higher voltage levels, i.e. the MV DG capacity and load include the LV DG capacity and load, and the HV DG capacity and load include the MV DG capacity and load. See Fig. A.4b in section A.6 for a graphical representation.

DG installations per PLZ-3 are provided in [Deu13], but it lacks information on region types. An approximation is made on the basis of area [Fed11], assuming that a larger area will have more DG capacity installed. The capacity for a region type within a PLZ-3 is thus obtained:

$$DGcapacity_i = DGcapacity_{PLZ-3} \cdot \frac{Area_i}{Area_{PLZ-3}} \quad (E.2)$$

There is no data available for the peak load per PLZ-3, even when ignoring region types. However, the DSO that provides the distribution network topology also provides its supply area peak loads per voltage level. This is used as a base for all areas with the population as scaling factor, thereby reflecting the fact that more people use more power:

$$Peakload_i = Peakload_{DSO} \cdot \frac{Population_i}{Population_{DSO}} \quad (E.3)$$

It is clear that this approach does not consider industrial loads that might be spread in a different fashion, but it is the best way available to scale the loads. An overview of the installed loads in the supply area of the DSO is given in table E.2.

Table E.2: Load data DSO supply area [Del13].

HV yearly peak load [MW]	2 960
MV yearly peak load [MW]	2 026
LV yearly peak load [MW]	1 242
Inhabitants [#]	2 225 000

Using equations (E.1) through (E.3), a penetration level is obtained for all areas per voltage level and technology. The same median method as described in section E.1.1 is used. The obtained penetration levels are rounded to the nearest five.

The DG database provides the installed capacity of DG installations. However, starting from 01-01-2012, PV installations ≤ 30 kW are only allowed to generate up to 70 percent of their rated power, unless the owner allows remote control of the installation to the DSO [CE13, BDKP13]. Since this requirement has a large negative economic effect, only 30 percent of these installations are operated with the 70 percent limit [CE13, BDKP13]. Still, this means that 9 percent of the total installed capacity of ≤ 30 kW PV installations installed after 01-01-2012 is not taken into account for the penetration calculations.

While 2012 data is available in the DG database, future installed DG capacity is estimated. Figure E.2 shows an estimate of the development of installed DG in Germany in the next ten years, based on [Deu13] and [Ger12b]. Multiple future scenarios are sketched in the NEP, accounting for different development paths. This thesis uses the 2022 B scenario, which assumes more renewable capacity than the German government now requires for its energy- and climate goals. Additionally, more gas fired power plants are present in this scenario, to increase the flexibility of the power system. This scenario is chosen by the FNN expert network as the future scenario in the study.

The obtained penetration levels are provided in table E.3. The sum of PV, wind and CHP penetration is not always equal to the penetration for all technologies since hydro- and geothermal power are included in the ‘all DG’ category. Rounding may also lead to a small discrepancy between the sum of the three considered technologies and ‘all DG’. Note that especially in rural regions, penetration levels already frequently exceed 100 percent. Expected penetration levels for 2022 indicate that reverse power flows will become common. The complete set of results including region type 1 and Germany as a whole can be found in [van14].

The number of installations obtained by combining typical installation size and typical penetration is rounded to the nearest integer. Whether a DG unit is installed at the sub-

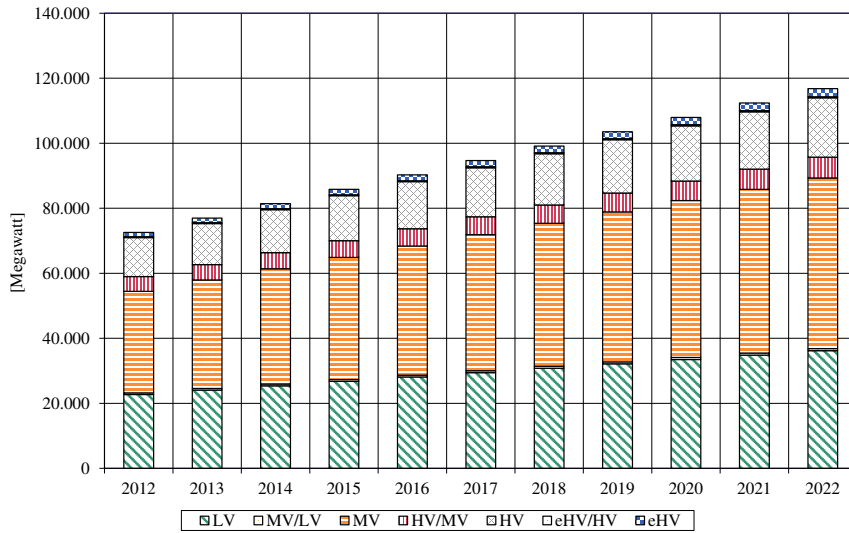


Figure E.2: Cumulative installed DG capacity per voltage level [Deu13], [Ger12b].

Table E.3: Typical DG penetration levels, rounded to nearest 5 percent. ‘All DG’ values include additional additional DG types (hydro, geothermal) and may therefore be larger than the sum of PV, Wind and CHP.

	Region type 2 suburban			Region type 3 rural		
	HV	MV	LV	HV	MV	LV
All DG 2012 [%]	90	105	65	165	205	110
All DG 2022 [%]	145	170	110	265	335	175
PV 2012 [%]	40	55	60	70	95	100
PV 2022 [%]	60	90	100	115	160	165
Wind 2012 [%]	35	30	0	60	50	0
Wind 2022 [%]	50	40	0	95	75	0
CHP 2012 [%]	10	15	5	25	25	5
CHP 2022 [%]	20	25	5	40	45	10

station or within the network is determined by the current ratio of installed capacity at the two locations. Since DG units connected to a substation are assumed substantially larger than those within the network and the loads within the provided LV and MV networks are relatively low, this method leads to a 'loss' of capacity as the capacity that is appointed to the substation level is not enough to justify the connection of a single DG unit. To account for this loss, capacity that is lost at the substation is attributed to the network, which due to the smaller DG installation size may result in additional units. Further rounding errors can not be avoided. Larger discrepancies between the the 'all DG' penetration and summation of the three technologies may occur due to inclusion of hydro- and geothermal power in the 'All DG' category.

E.2 DG legacy performance analysis

Even though each technology type has a single rated installation size per voltage level, there are differences between the (control) capabilities of the installations. Grid codes are a continuous work in progress and thus have been changed in the past more than once. New codes sometimes meant that DG installations had to comply with new requirements, LVRT capability being one example. A historical overview of the grid codes applying to the German grid is presented in appendix [E.2.1](#). Appendix [E.2.2](#) gives an overview per network type and voltage level of the existing (2012) installation capabilities.

E.2.1 Evolution of German grid connection requirements

	1991	1992	1993	1994	1995	1996
eHV						
HV						
MV						
LV	VDEW NS-RL 1991 • no LV/RT • no HV/RT					

Table E.4: APPENDIX: GERMAN GRID CODE DEVELOPMENT part I

	1997	1998	1999	2000	2001	2002
eHV						
HV						
MV		BDEW MS-RL 01-12-1998 • no LV/RT • no HV/RT				
LV					VDEW NS-RL 01-05-2001 • Pre-fault: p/c-1 • no LV/RT • no HV/RT	

Table E.5: APPENDIX: GERMAN GRID CODE DEVELOPMENT part II

	2003	2004	2005	2006	2007	2008
eHV						
HV	<p>VDN TransmissionCode</p> <p>01-02-2004</p> <ul style="list-style-type: none"> • Pre-fault: pf 0.95 by TSO (0.975 ind / 0.9 cap or 0.95 ind / 0.925 cap) • LVRT (no specs) – aRCI – P recovery unspecified • no HVRT 	<p>EEG / HES-RL</p> <p>01-02-2005</p> <ul style="list-style-type: none"> • Pre-fault: pf 0.95 by TSO (0.975 ind / 0.9 cap or 0.95 ind / 0.925 cap) • LVRT – aRCI – P recovery (if near fault with low I¹ contribution) min 20 % of P_{nom} per s, not allowed to draw Q from network • no HVRT 			<p>VDN TransmissionCode</p> <p>01-02-2008</p> <ul style="list-style-type: none"> • Pre-fault: pf by TSO (no specs) • LVRT – aRCI – P recovery 20 % of P_{nom} per s, if STI min 10% of P_{nom} per s, if disconnected max 10% per min • no HVRT 	
MV						<p>BDEW MS-RL</p> <p>01-01-2009</p> <ul style="list-style-type: none"> • Pre-fault: pf 0.95 ind/cap • LVRT (no specs) – aRCI (2010) – Q not allowed >pre-fault, P recovery unspecified • no HVRT
LV			<p>VDE 0126-11 / VDN update</p> <p>01-09-2005</p> <ul style="list-style-type: none"> • Pre-fault: pf ~1 • noLVRT • no HVRT 	<p>VDE 0126-11 update</p> <p>01-02-2006</p> <ul style="list-style-type: none"> • Pre-fault: pf ~1 • noLVRT • no HVRT 		

Table E.6: APPENDIX: GERMAN GRID CODE DEVELOPMENT part III

		2010	2011	2012	2013
eHV	<p>SDLWindV</p> <p>23-07-2009</p> <ul style="list-style-type: none"> • Pre-fault: pf according to TSO • LVVRT • aRCl – P recovery 20 % of P_{nom} per s, if STI min 10 % of P_{nom} per s, if disconnected max 10 % of P_{nom} per min • no HVVRT 				
HV				<p>VDE-AR-N 4120 (concept)</p> <p>01-11-2012 DRAFT</p> <ul style="list-style-type: none"> • Pre-fault: pf range given by TSO • LVVRT – aRCl – P recovery (type II gen): 85 % of pre-fault P within 0.5 - 10 s (by TSO), default 5 s – 4 consecutive faults without thermal overloading • no HVVRT 	
MV	<p>BDEW MS-RL A1</p> <p>01-01-2010</p> <ul style="list-style-type: none"> • Pre-fault: pf 0.95 ind/cap (PV/FC 07-2010) • LVVRT (limited support: PV/FC 07-2010; SG 01-2011) – aRCl (PV/FC 2011) – Q not allowed > pre-fault, P recovery unspecified • no HVVRT 	<p>BDEW MS-RL A2</p> <p>01-01-2010</p> <ul style="list-style-type: none"> • Pre-fault: pf 0.95 ind/cap (PV/FC/Wind 04-2011) • LVVRT – aRCl (PV/FC/Wind 04-2011, Combustion 2013) – Q not allowed > pre-fault, P recovery unspecified • no HVVRT 	<p>BDEW MS-RL A3</p> <p>01-04-2011</p> <ul style="list-style-type: none"> • Pre-fault: pf 0.95 ind/cap (Combustion 2010) • LVVRT – aRCl (Combustion 2013) – Q not allowed > pre-fault, P recovery unspecified • no HVVRT 	<p>BDEW MS-RL A4</p> <p>01-01-2013</p> <ul style="list-style-type: none"> • Pre-fault: pf 0.95 ind/cap (PV/FC 04-2011, Combustion 2010) • LVVRT – aRCl (PV/FC 04-2011) – Q not allowed > pre-fault, P recovery unspecified • no HVVRT 	
LV			<p>VDE 0126-II A1</p> <p>01-05-2011 DRAFT</p> <ul style="list-style-type: none"> • Pre-fault: pf ~1 • no LVVRT • no HVVRT <p>VDE-AR-N 4105</p> <p>01-08-2011 (VDN update 2005 allowed until 2012 (PV) / 07-2012 (other))</p> <ul style="list-style-type: none"> • Pre-fault: pf(P) • no LVVRT • no HVVRT 	<p>CLC 50438</p> <p>01-08-2012 DRAFT</p> <ul style="list-style-type: none"> • <16 A per phase • no LVVRT • no HVVRT <p>CLC 50549-I</p> <p>15-12-2012 DRAFT</p> <ul style="list-style-type: none"> • >16 A per phase • LVVRT – no $i_{d, k}$ specs during fault – 90 % of pre-fault P within 5 s • HVVRT 	

Table E.7: APPENDIX: GERMAN GRID CODE DEVELOPMENT part IV (2009-2013)

E.2.2 Pre-2012 Installation Capabilities

Overviews of the pre-2012 DG installation dates are provided in this appendix. Additionally, the DG types used in this study are linked to installation dates.

High voltage connected DG

Table E.8: HV old installation capabilities.

	PV [MW]	Wind [MW]	CHP [MW] ¹
<01-01-2005	1 [0%]	4 809 [48%]	8 410 [94%]
01-02-2005 - 22-07-2009 (LVRT, aRCI)	53 [3%]	3 322 [33%]	119 [1%]
23-07-2009 - 31-12-2012 (LVRT, aRCI)	1 623 [97%]	1 803 [18%]	451 [5%]
<01-01-2013	1 677 [100%]	9 934 [100%]	39 217 [100%]

¹ Including large CHP that does not count as DG.

Table E.9: HV DG types in test system.

	PV	Wind	CHP
<31-01-2005		OLD	PF100
01-02-2005 - 22-07-2009 (LVRT, aRCI)		EEG	
23-07-2009 - 31-12-2012 (LVRT, aRCI)		SDL	

Medium voltage connected DG

Table E.10: MV old PV and wind capabilities.

	PV [MW]	Wind [MW]
<01-01-2009 (pf=1)	1 012 [11%]	7 421 [25%] ¹
01-01-2009 - 01-04-2011 (LVRT)	2 953 [31%]	10 287 [65%] ¹
01-04-2011 - 31-12-2012 (aRCI)	5 590 [58%]	2 034 [10%]
<01-01-2013	9 556 [100%]	19 747 [100%]

¹ Approx. 7 400 MW (50% of Wind <01-01-2009) has been retrofitted with LVRT [EDB113].

Table E.11: MV old CHP capabilities.

	CHP [MW] ¹
<01-01-2009 (pf=1)	5 813 [73%]
01-01-2009 - 31-12-2010 (pf=0.95)	1 034 [13%]
01-01-2011 - 31-12-2012 (LVRT)	1 095 [14%]
<01-01-2013	7 942 [100%]

¹ Including large CHP that does not count as DG.

Table E.12: MV DG types in test system.

	PV	Wind	CHP
<01-01-2009	PF100		PF100
01-01-2009 - 01-04-2011 (LVRT)	LVRT	LVRT	PF095
01-04-2011 - 31-12-2012 (aRCI)	aRCI		LVRT

Low voltage connected DG

Table E.13: LV old PV and CHP capabilities

	PV [MW]	CHP [MW]
<01-01-2012	17 632 [84%]	1 407 [96%]
01-01-2012 - 31-12-2012	3 376 [16%]	66 [4%]
<01-01-2013	21 008 [100%]	1 473 [100%]

Table E.14: LV DG types in test system.

	PV	CHP
<01-01-2012	PF100	PF100
01-01-2012 - 31-12-2012 (LVRT)	PFPOW	

E.3 Distribution Network expansions

This appendix provides the network planning criteria, and actual expansions that were performed on the networks.

E.3.1 Network Planning Criteria

The inclusion of DG might create a situation where network condition boundaries are crossed, especially in the 2022 networks. The *Deutsche Energie-Agentur* (German Energy Agency) has set up standardised network expansion guidelines in a study investigating the amount of required distribution grid expansion up to 2030 [Ger12a].

High-Voltage Planning Criteria

In the HV network, (n-1)-reliable operation is required during peak load and reverse power flow. Principally, both in the normal case as in the (n-1)-case, the maximum thermal equipment loading is 100 percent (see table E.15). The voltage in the HV network is allowed to deviate ± 6 kV (approximately 5 percent) from the rated voltage. This limit is imposed to allow the HV/MV transformer to regulate the voltage at the MV side such that the voltage at the end-user is acceptable.

To save the effort of investigating each (n-1)-case, as a rule of thumb transformers and lines in the complete network are not allowed to be loaded beyond 60 percent in both normal and reverse power flow.

	Normal power flow [%]	Reverse power flow [%]
eHV/HV transformer	max 100 (60)	max 100 (60)
HV lines	max 100 (60)	max 100 (60)

Table E.15: HV equipment loading, n-1 planning criteria for outage [Ger12a]. In parentheses (n-0)-values.

Medium-Voltage Planning Criteria

There are three criteria to assess whether a MV network requires expansion: thermal loading of equipment, voltage in the network and voltage quality at the customer.

During normal operation, there is a (n-1)-reliable supply requirement for customers in the MV level. To maintain sufficient reserve capacity for the (n-1)-case, the maximum allowed loading at peak load for the HV/MV-transformers, MV cables and MV lines is 60 percent. Currently there is no (n-1)-secure connection criterium for reverse power flow. Following from this lack of (n-1)-criterium, the maximum loading for the HV/MV-transformers, MV cables and MV lines during reverse power flow is 100 percent. Table E.16 summarises the allowable equipment loading in the MV network.

The second parameter determining if the network needs to be expanded is the voltage change due to the introduction of DG in the network. According to [BDE08], the voltage deviation during normal operation caused by the inclusion of all DG in the network is not allowed to change the voltage by more than 2 percent at any node in the network compared

	Normal power flow [%]	Reverse power flow [%]
HV/MV transformer	max 60	max 100
MV cables	max 60	max 100

Table E.16: MV equipment loading, n-1 planning criteria for short-term overloading [Ger12a].

to the network without any DG. If the 2 percent limit is exceeded at any node, the network needs to be expanded or DG has to be taken off-line.

Finally, the voltage quality at the end-user may also require an expansion of the network if it is not sufficient. According to the latest version of [Ver00], the maximum allowable static deviation for the voltage at the customer is ± 10 percent of the rated voltage. This 10 percent is divided over the MV, MV/LV and LV levels as follows:

- ± 4 percent for the MV level;
- ± 2 percent for the MV/LV level;
- ± 4 percent for the LV level.

Low-Voltage Planning Criteria

As for the MV network, the three criteria that are used to assess the need for network expansion in the LV network are thermal loading of equipment, voltage in the network and voltage quality at the customer.

Opposed to the MV-level, there is no (n-1)-secure requirement for customer supply in the LV-level during normal operation. Therefore in all cases the maximum allowable loading for the MV/LV-transformers, LV cables and LV lines is 100 percent, as can be seen in table E.17.

	Normal power flow [%]	Reverse power flow [%]
MV/LV transformer	max 100	max 100
LV cables	max 100	max 100

Table E.17: LV equipment loading, no n-1 planning criteria. [Ger12a]

Similar to what [BDE08] states for the MV network, [For11] states that the voltage deviation during normal operation caused by the inclusion of all DG in the network is not allowed to change the voltage by more than 3 percent at any node in the network compared to the network without any DG. If the 3 percent limit is exceeded at any node, the network needs to be expanded or DG has to be taken off-line.

As stated above in E.3.1, the static voltage at the end-user is not allowed to deviate from the rated voltage more than ± 2 percent for the MV/LV-level and ± 4 percent for the LV-level.

Network Expansion Requirements

To check if any of the three conditions are violated, load flows are executed for different OS. These OS represent the most extreme cases for each condition. In case any of the conditions is violated, the network is expanded accordingly until all conditions are met. To check if the networks provided by the DSO are properly dimensioned for their installed loads, an extra operational scenarios is run before the others. The OS used for the analysis are provided in table E.18.

	Load ₁	Generation ₁	Load ₂	Generation ₂
Load capability	High	No		
Thermal loading	Low	High		
2-3 % V-rule	High	No	Vs High	High
	Low	No	Vs Low	High
10 % V-rule	High	Low		
	Low	High		

Table E.18: Operational scenarios used to evaluate expansion criteria

In table E.18, ‘high load’ means peak load and ‘high generation’ means rated DG power. ‘Low load’ means half of the peak load and ‘low generation’ means half of the DG rated power multiplied by its coincidence factor (see table 5.7 in section 5.3.1).

E.3.2 Actual expansions

Standard expansion variants are provided in [Ger12a] for different violations of voltage quality and equipment ratings. These standard expansion variants were used to expand the complete networks so all voltage and equipment loading requirements are met.

Low Voltage Expansions

Only the suburban PV network is expanded on the LV level. The expansion is required due to violation of the 3 percent rule at the deepest point within the network.

In 2012, two switches are closed and one line is added to the network. The newly added line is of the same line type as the rest of the network, with a length of approximately 2/3 of the length from the substation to the end of the affected feeder.

In 2022, a third switch is closed. Two more parallel lines are added, making for a total of three added parallel lines to the network.

Medium Voltage Expansions

Both suburban networks are expanded with a parallel HV/MV transformer. This is necessary to reduce the thermal loading of the transformer in normal power flow. Multiple parallel lines are added to the rural network in 2012 so that the 2 percent rule is not violated:

- 3 parallel lines between busbar 01 and 10 (between main substation and substation A)
- parallel line between busbar 01 and 19
- parallel line between busbar 01 and 08
- parallel line between busbar 01 and 28

All added lines are again of the same type as the lines in the original network.

For 2022, an extra transformer is added to the rural network. The thermal loading limit for the original transformer is exceeded in RPF. One more parallel line is added between busbars 01 and 41 to remain compliant with the 2 percent rule.

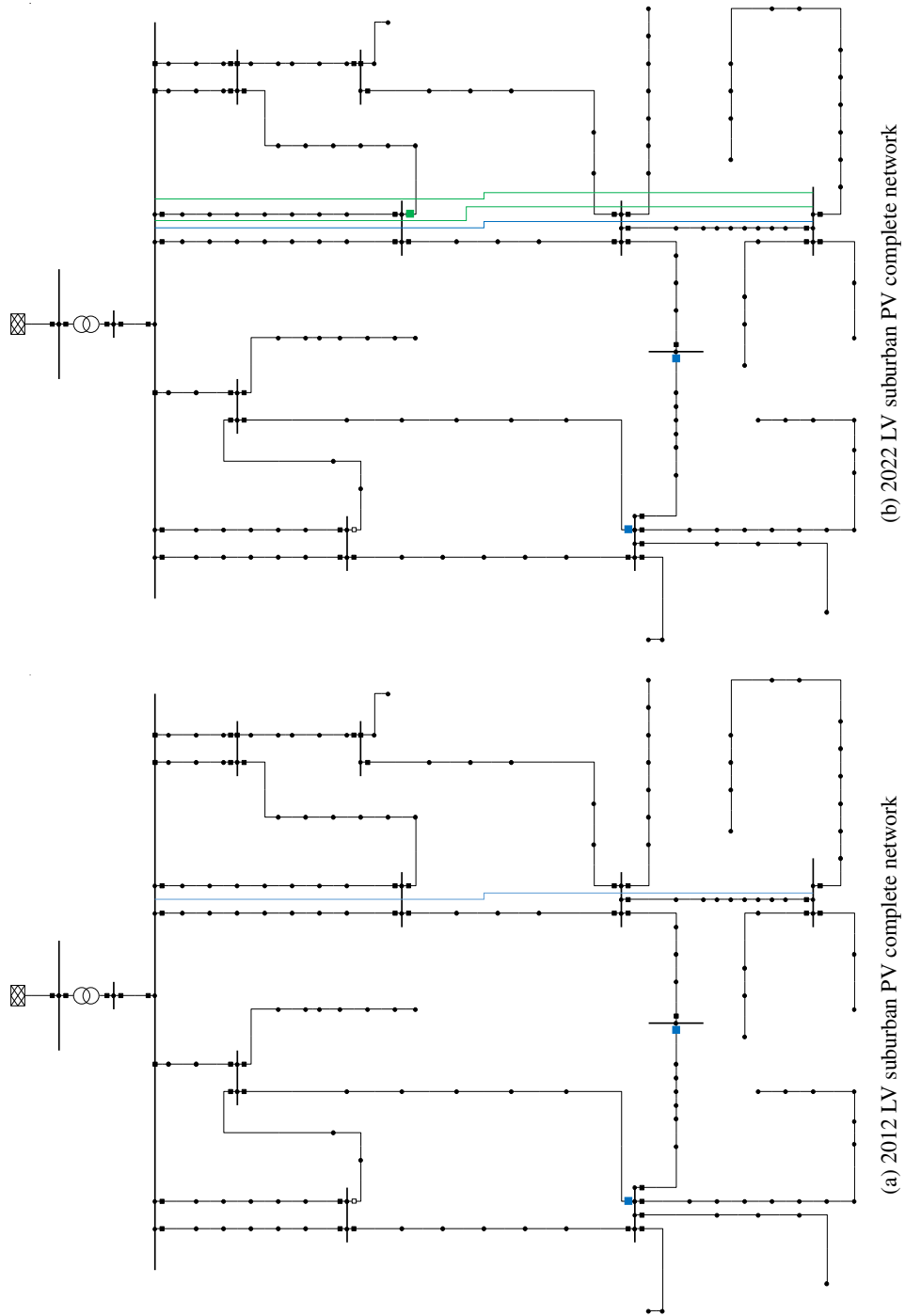


Figure E.3: LV complete network expansions.

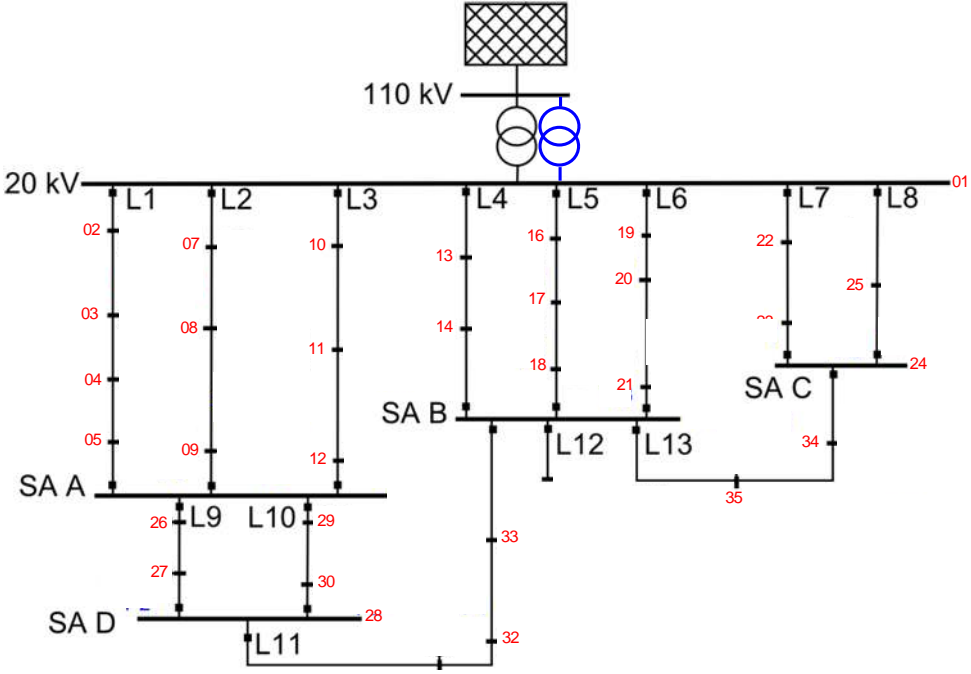
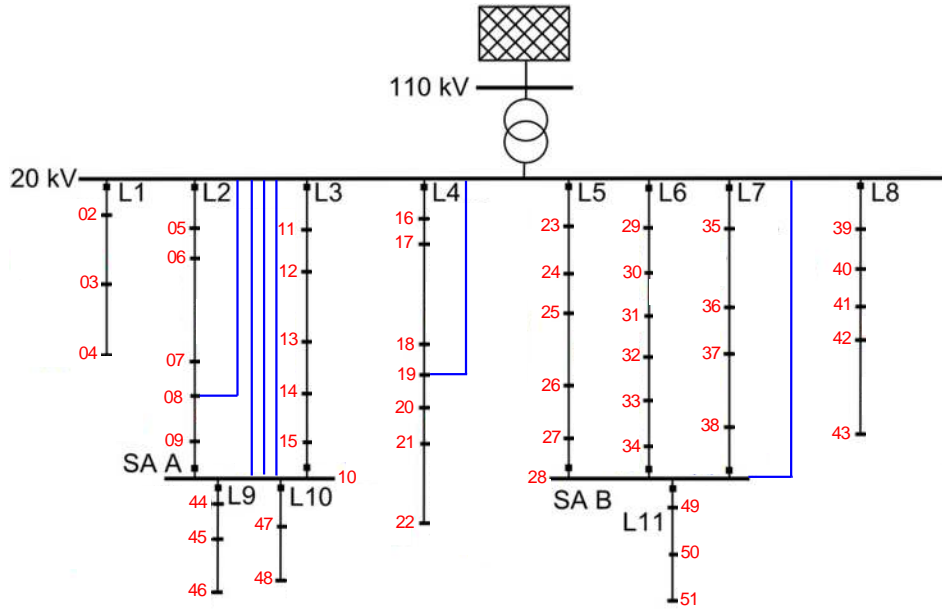
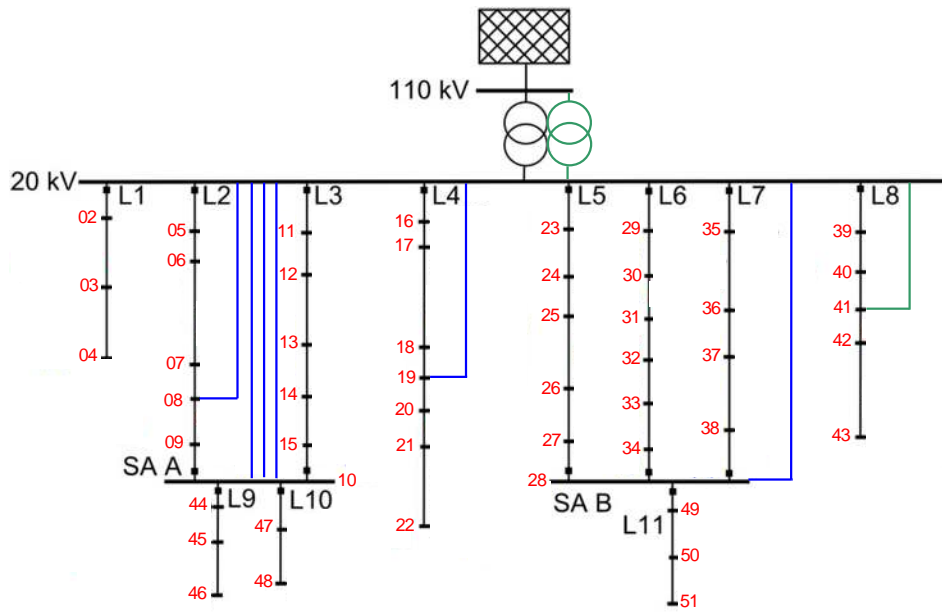


Figure E.4: MV suburban complete network expansions.



(a) 2012 rural MV complete network



(b) 2022 rural MV complete network

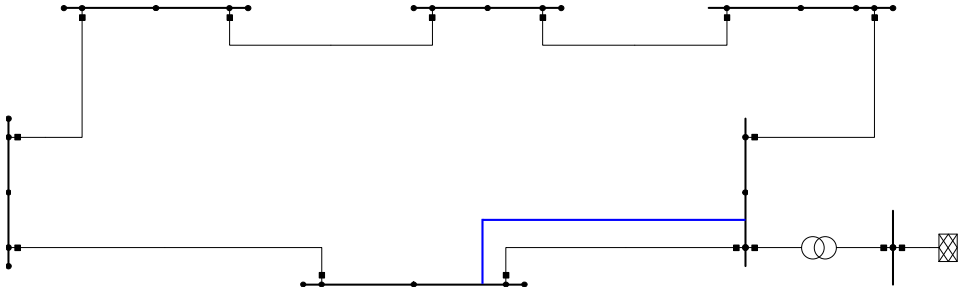
Figure E.5: MV rural complete network expansions.

High Voltage Expansions

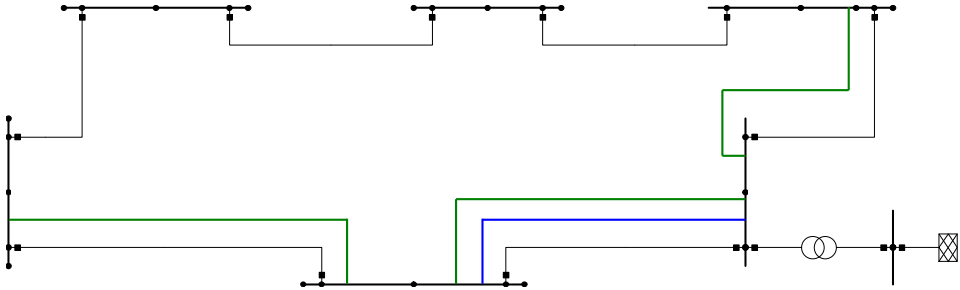
All HV networks are extended with a parallel line between terminals 05 and 06 as the thermal loading of this line is exceeded in the original network. As before, the line type of the added parallel line equals that of the original network.

For 2022, the rural network is further expanded with three additional parallel lines, again to reduce the thermal loading of the lines:

- parallel line between 01 and 06;
- parallel line between 04 and 05;
- parallel line between 05 and 06.



(a) 2012 complete HV networks



(b) 2022 rural HV complete network

Figure E.6: HV complete network expansions.

E.4 Equivalent Models

Due to different characteristics of region types, the topology of the typical distribution systems supplied by the German DSO are very different for the suburban and rural case. Additionally, installed loads differ between the types. The installed loads in the supplied typical networks are combined with the penetration to determine the number of DG installations in each network.

E.4.1 Low Voltage Distribution

The low voltage distribution network operates at 0.4 kV. Based on the statistical analysis presented in section E.1.1, the installation sizes are the smallest at this voltage level. Residential and commercial customers are connected to the LV distribution network in the suburban and rural areas respectively. All of the DG that is installed in the LV network is installed in the feeders. There are no installations connected to the substations, since the total load in the networks is too small to warrant the typically larger substation-connected installations.

All of the LV networks use the same transformers to connect to their respective MV networks. Table E.19 shows the basic data of the MV-LV transformers.

Rated capacity [MVA]	Short-circuit voltage [%]	Losses [kW]
0.4	4	3.85

Table E.19: MV-LV transformer specifications.

—*Suburban German Network*— The peak load within the LV suburban typical network is 153 kW. Two variations are investigated: one with very high penetration of only PV systems in the LV network, the other with a low penetration of only directly coupled SG functioning as CHP plants in the LV network.

Suburban PV Network The LV suburban network has a PV penetration of 60 percent in 2012 and 100 percent in 2022. Tables E.20a and E.20b show the amounts of PV installations connected in the current and future suburban PV networks. More details on the installation capabilities are given in appendix E.2.2.

	Installations [#]	Capacity [kW]		Installations [#]	Capacity [kW]
PV	9	90	PV	15	150

(a) 2012 (b) 2022

Table E.20: DG capacity in suburban LV PV 2012 and 2022 networks.

The single line diagrams for the 2012 and 2022 suburban LV PV networks are given in figure E.7.

The parameters for the obtained equivalent impedances are given in table E.21.

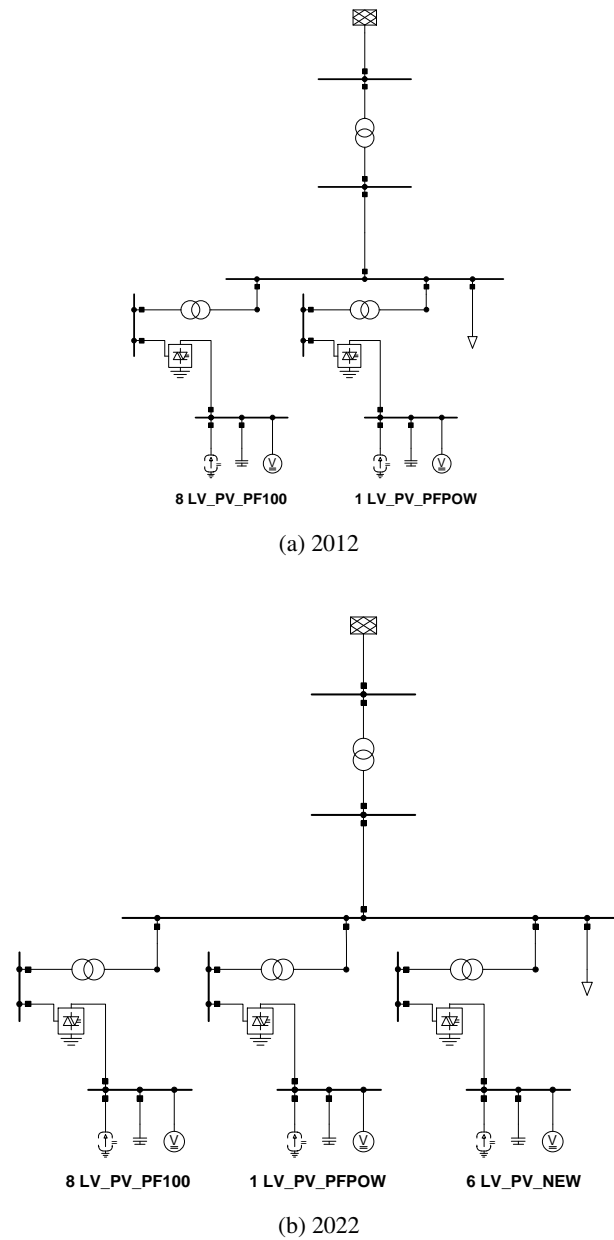


Figure E.7: Single line diagrams aggregated suburban LV PV 2012 and 2022 networks.

R [Ω]	X [Ω]	Z [Ω]	R/X [-]	R [Ω]	X [Ω]	Z [Ω]	R/X [-]
0.0137	0.0008	0.0137	17.1	0.0083	0.0013	0.0084	6.4

(a) 2012 (b) 2022

Table E.21: Equivalent impedances aggregated suburban LV PV 2012 and 2022 networks.

Suburban CHP Network The LV suburban network has a CHP penetration of 5 percent in 2012 and 2022.

As the penetration does not increase, no additional SGCHPs will be installed in 2022. There is thus only one version of the LV suburban CHP network. Installed capacity is given in table E.22. More details on the installation capabilities are given in appendix E.2.2.

	Installations [#]	Capacity [kW]
CHP	1	10

Table E.22: DG capacity in suburban LV CHP 2012/2022 network.

The single line diagram for the 2012/2022 suburban LV CHP network is given in E.8.

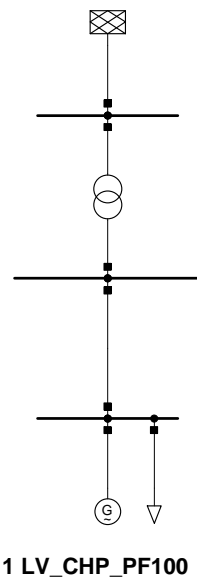


Figure E.8: Single line diagram aggregated suburban LV CHP 2012/2022 network.

The parameters for the obtained equivalent impedance are given in table E.23.

—*Rural German Network*— The peak load in the typical LV rural network is 59 kW. PV penetration in rural regions is currently already 100 percent, leading

R [Ω]	X [Ω]	Z [Ω]	R/X [-]
0.0039	0.0016	0.0042	2.4

Table E.23: Equivalent impedance aggregated suburban LV CHP 2012/2022 network.

to six PV installations in the 2012 network. The 2022 rural LV network is the only LV network with more than one technology type. In 2022 the CHP penetration has increased to 10 percent, warranting one CHP installation. An overview of the LV rural DG installations is given in table E.24. More details on the installation capabilities are given in appendix E.2.2.

Installations			Capacity		
	Installations	Capacity		Installations	Capacity
	[#]	[kW]		[#]	[kW]
PV	6	60		PV	10
				CHP	1
					100
					10

(a) 2012

(b) 2022

Table E.24: DG capacity in rural LV 2012 and 2022 networks.

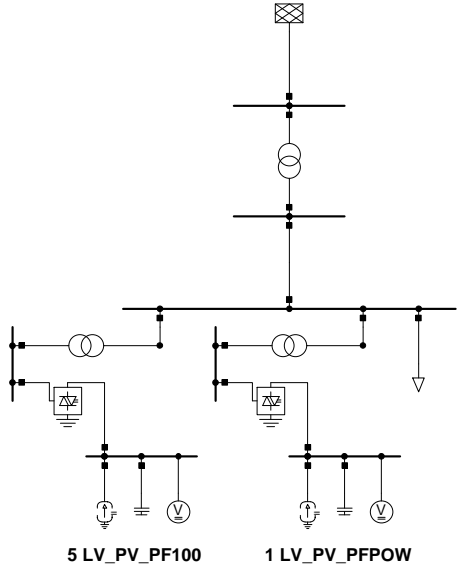
The single line diagrams for the 2012 and 2022 rural LV networks are given in E.9. The parameters for the obtained equivalent impedances are given in table E.25.

R [Ω]	X [Ω]	Z [Ω]	R/X [-]	R [Ω]	X [Ω]	Z [Ω]	R/X [-]
0.0165	0.0064	0.0177	2.6	0.0131	0.0014	0.0131	9.4

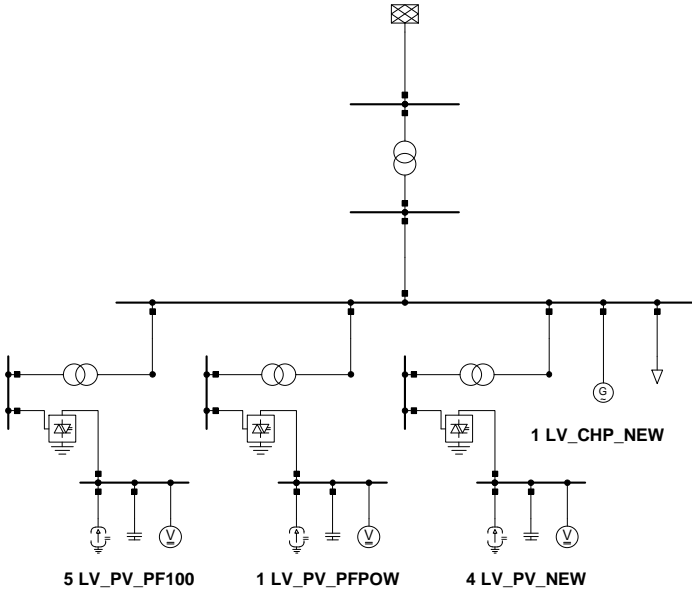
(a) 2012

(b) 2022

Table E.25: Equivalent impedances aggregated rural LV 2012 and 2022 networks.



(a) 2012



(b) 2022

Figure E.9: Single line diagrams aggregated rural LV 2012 and 2022 networks.

E.4.2 Medium Voltage Distribution

The MV distribution networks operate at 20kV and are connected at all of the six busbars of the HV system (see section E.4.3). At this voltage level, industrial and commercial loads are connected within the network.

The original LV loads present in the representative MV networks provided by the DSO are replaced by the aggregated LV networks. The installed LV loads are changed as little as possible by scaling the number of aggregated LV networks connected at each node. Since the LV aggregated networks include generation, the amount of LV-connected DG is also obtained. The amount of MV-connected DG is then determined by the difference between the typical MV penetration and the penetration due to LV-connected DG.

—*Suburban German Network*— The peak load in the MV suburban network is approximately 16.8 MW. Penetration in 2012 is 55, 30 and 15 percent for PV, wind and CHP respectively. In 2022, these penetrations have increased to 90, 40 and 25 percent respectively. Replacing the LV loads connected in the original representative MV suburban network are 84 aggregated LV suburban networks.

Both versions of the suburban network share the same HV-MV transformer. Basic data are given in table E.26. In the simulations, the transformers are set to have continuous automatic tap-changers, making sure the steady-state voltages in the LV networks are optimal.

Rated capacity [MVA]	Impedance [%]	Losses [kW]
31.5	12.3	146.7

Table E.26: HV-MV suburban transformer specifications.

Even though penetration levels for both suburban network types are identical, actual installed penetration of PV installations in the CHP network is much lower. Since the CHP network has no LV-connected PV installations, the amount of MV-connected PV installations would have to be many times larger than it would realistically be. Because the more recently installed MV-connected PV installations already ride through faults, including too many of them in the network would yield unrealistic network response. To make sure behaviour of the CHP network is still realistic, the same number of MV-connected PV installations is used as is found for the PV network.

Suburban PV Network The number of MV-connected DG installations in the suburban PV network is presented in table E.27. More details on the installation capabilities are given in appendix E.2.2.

The single line diagrams for the 2012 and 2022 suburban MV PV networks are given in E.10.

The parameters for the obtained equivalent impedances are given in table E.28.

Suburban CHP Network The number of MV-connected DG installations in the suburban PV network is found presented in table E.29. Note that the number of PV installations is set to equal those in the suburban PV network. The typical PV penetration is thus not adhered to. More details on the installation capabilities are given in appendix E.2.2.

	Installations [#]	Capacity [kW]		Installations [#]	Capacity [kW]
PV	4	1 720		PV	2 150
Wind	1	5 000		Wind	5 000
CHP	6	2 400		CHP	4 000

(a) 2012 (b) 2022

Table E.27: DG capacity in suburban MV PV 2012 and 2022 networks.

R [Ω]	X [Ω]	Z [Ω]	R/X [-]	B [μ S]
0.070	0.070	0.099	1	3 362

(a) 2012

R [Ω]	X [Ω]	Z [Ω]	R/X [-]	B [μ S]
0.025	0.025	0.054	1	3 362

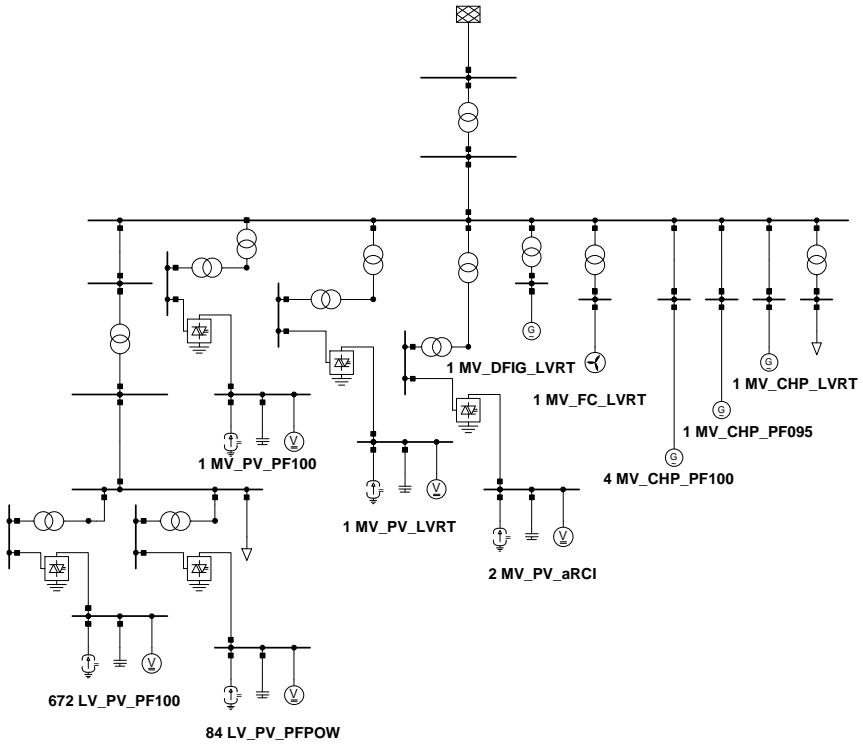
(b) 2022

Table E.28: Equivalent impedances aggregated suburban MV PV 2012 and 2022 networks.

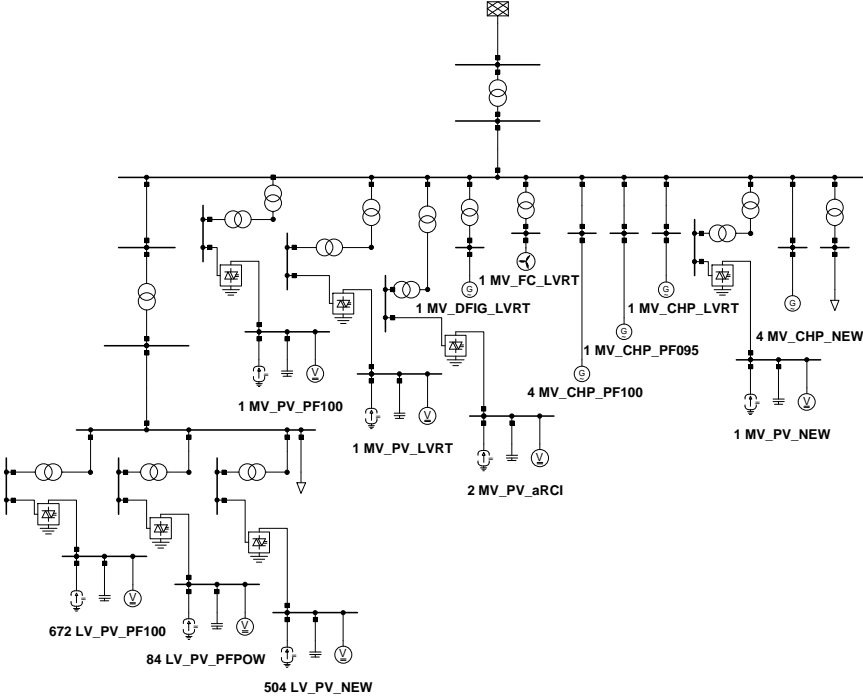
	Installations [#]	Capacity [kW]		Installations [#]	Capacity [kW]
PV*	4	1 720		PV*	2 150
Wind	1	5 000		Wind	5 000
CHP	5	2 000		CHP	3 600

(a) 2012 (b) 2022

Table E.29: DG capacity in suburban MV CHP 2012 and 2022 networks. *Number of MV PV systems equal to suburban PV, not according to penetration.



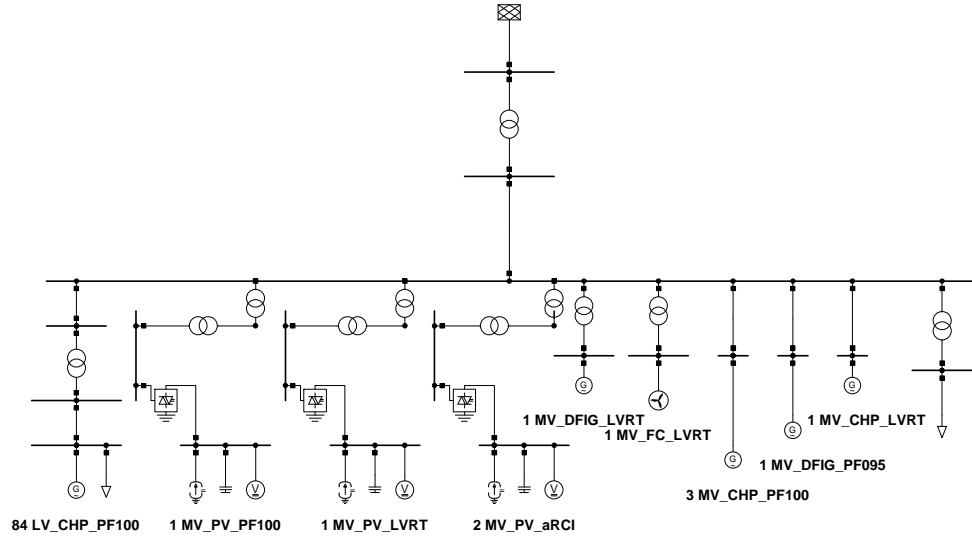
(a) 2012



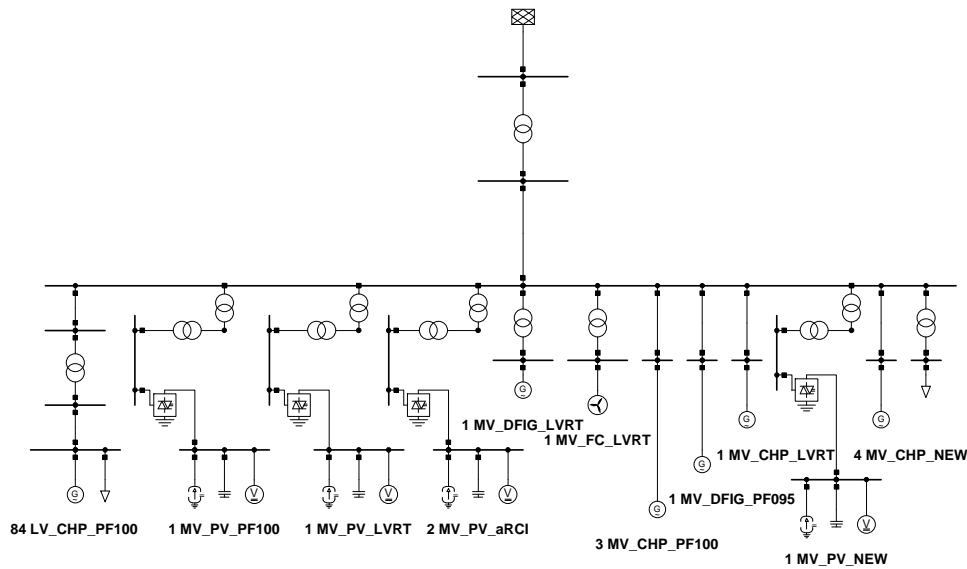
(b) 2022

Figure E.10: Single line diagrams aggregated suburban MV PV 2012 and 2022 networks.

The single line diagrams for the 2012 and 2022 suburban MV CHP networks are given in Fig. E.11.



(a) 2012



(b) 2022

Figure E.11: Single line diagrams aggregated suburban MV CHP 2012 and 2022 networks.

The parameters for the obtained equivalent impedances are given in table E.30.

R [Ω]	X [Ω]	Z [Ω]	R/X [-]	B [μ S]
0.055	0.055	0.077	1	2 589

(a) 2012

R [Ω]	X [Ω]	Z [Ω]	R/X [-]	B [μ S]
0.055	0.055	0.077	1	2 589

(b) 2022

Table E.30: Equivalent impedances aggregated suburban MV CHP 2012 and 2022 networks.

—*Rural German Network*— The peak load in the rural network is approximately 12.6 MW. Like the peak load, the capacity of the rural HV-MV transformer is smaller than that of the suburban networks. Basic data for the transformer are shown in table E.31. In the simulations, the transformers are set to have continuous automatic tap-changers, making sure the steady-state voltages in the LV networks are optimal.

Due to the small size of the LV rural networks, 171 LV networks are connected to each MV rural network.

In 2012, penetration of PV, wind and CHP are 95, 50 and 25 percent respectively. By 2022, penetration has increased to 165, 75 and 45 percent respectively. The resulting amount of DG installations can be found in table E.32. More details on the installation capabilities are given in appendix E.2.2.

Rated capacity [MVA]	Short-circuit voltage [%]	Losses [kW]
25	13.4	124.5

Table E.31: HV-MV rural transformer specifications.

	Installations [#]	Capacity [kW]		Installations [#]	Capacity [kW]
PV	4	1 720	PV	8	3 440
Wind	1	5 000	Wind	2	10 000
CHP	7	2 800	CHP	12	4 800

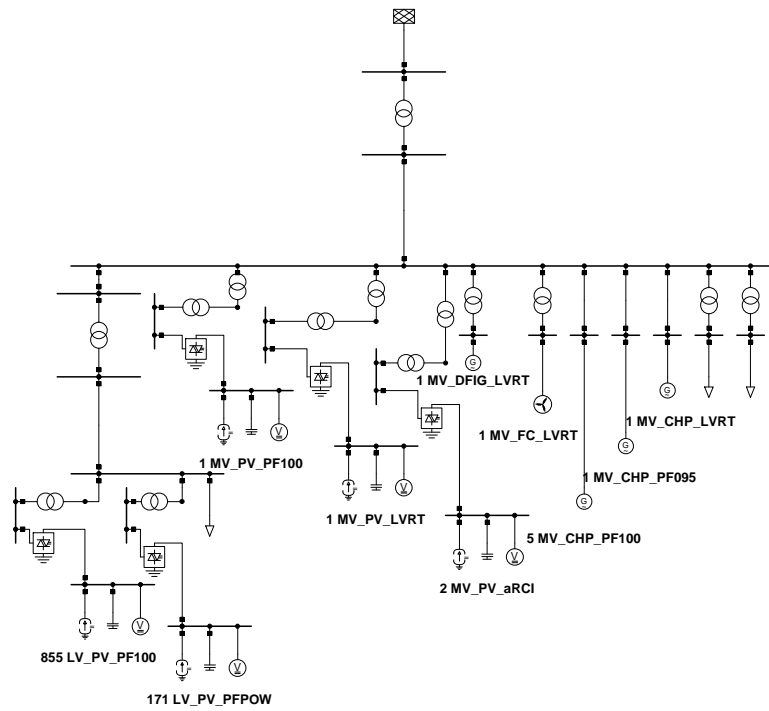
(a) 2012

(b) 2022

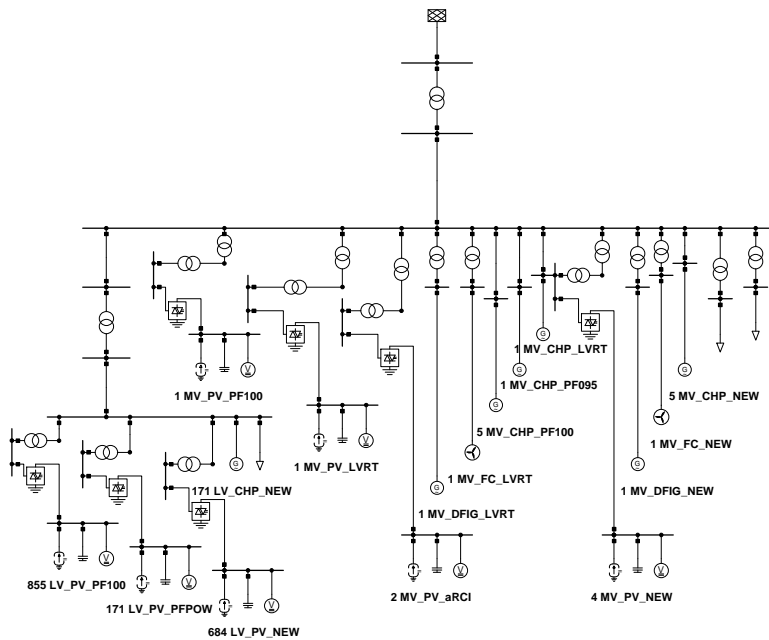
Table E.32: DG capacity in rural MV 2012 and 2022 networks.

The single line diagrams for the 2012 and 2022 rural MV PV networks are given in E.12.

The parameters for the obtained equivalent impedances are given in table E.33.



(a) 2012



(b) 2022

Figure E.12: Single line diagrams aggregated rural MV PV 2012 and 2022 networks.

R [Ω]	X [Ω]	Z [Ω]	R/X [-]	B [μ S]
0.100	0.100	0.141	1	22 386

(a) 2012

R [Ω]	X [Ω]	Z [Ω]	R/X [-]	B [μ S]
0.133	0.133	0.189	1	22 200

(b) 2022

Table E.33: Equivalent impedances aggregated rural MV 2012 and 2022 networks.

E.4.3 Sub-transmission System: Ring Network

The sub-transmission system used is a 6-bus, 110 kV ring network developed at the TU Delft [BvR⁺11a].

In contrast to the distribution networks, the dominant DG technology in the sub-transmission systems is wind power. No PV installations are connected, and only in the rural network one CHP installation is present. This means that the two suburban networks share the same HV network, as they have the same wind turbine penetration in their MV network. It should also be noted that in the rural network there is a substation connected wind turbine with a lower rated capacity than all other HV connected turbines.

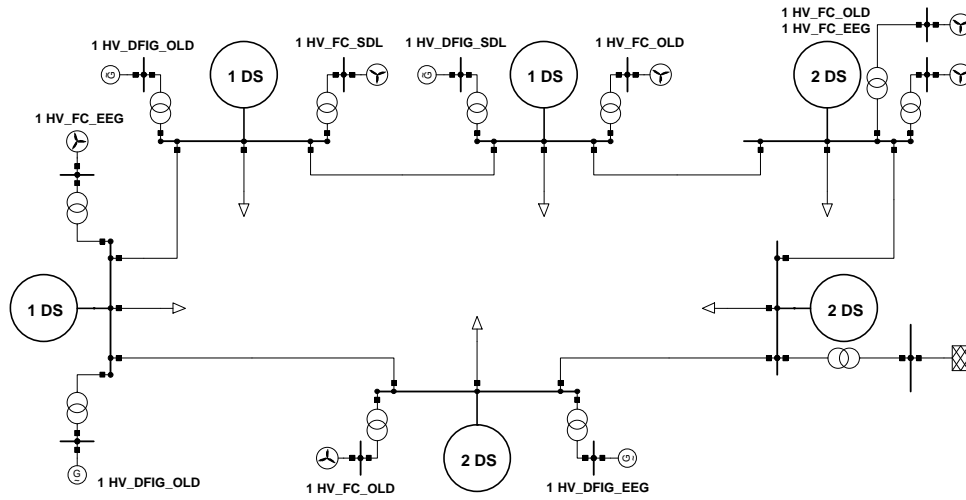
—*Suburban German Network*— The suburban HV sub-transmission networks are connected with a single transformer to the eHV system. Basic transformer data is provided in table E.34. The transformers are set to have continuous automatic tap-changers, making sure the steady-state voltages in the distribution systems are optimal.

Rated capacity [MVA]	Short-circuit voltage [%]	Losses [kW]
250	12	0

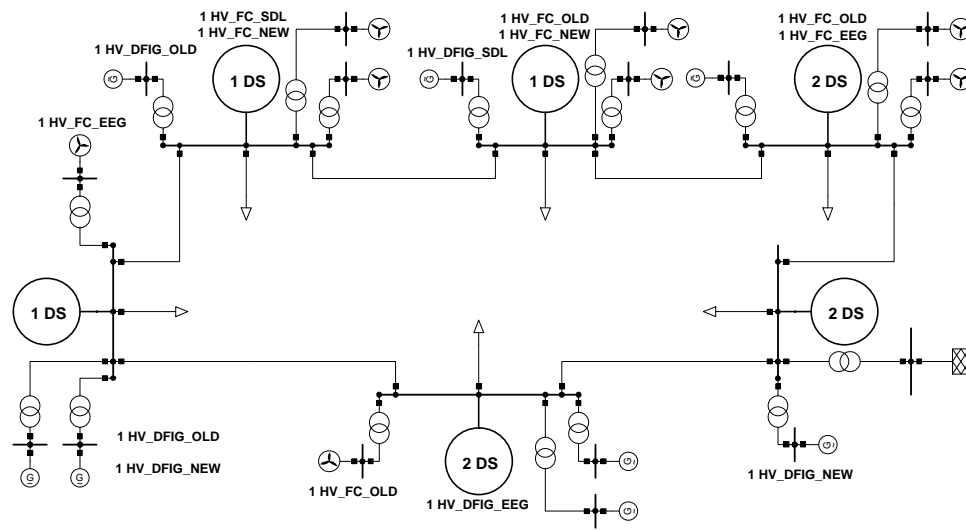
Table E.34: eHV-HV Sub transformer specifications.

Resulting from the DSO supply area HV/MV load ratio and the ‘filling’ of the eHV/HV transformer capacity with load, 9 suburban distribution networks are connected to the ring. At buses 01, 02 and 03, one DS is connected, while two are connected at each of the buses 04, 05 and 06. Figure E.13a shows the single line diagram of the HV suburban network for 2012 and 2022.

Table E.35 provides the number of wind turbines installed in the 2012 and 2022 sub-transmission networks. More details on the installation capabilities are given in appendix E.2.2.



(a) 2012



(b) 2022

Figure E.13: Single line diagrams suburban HV 2012 and 2022 networks.

	Installations [#]	Capacity [kW]		Installations [#]	Capacity [kW]
Wind	10	36 000	Wind	16	57 600

(a) 2012

(b) 2022

Table E.35: DG capacity in suburban HV 2012 and 2022 networks.

—**Rural German Network**— The rural HV sub-transmission network only differs slightly from the suburban HV network. To handle the larger power are connected with a single transformer to the eHV system. Basic transformer data is provided in table E.36. The transformers are set to have continuous automatic tap-changers, making sure the steady-state voltages in the distribution systems are optimal. Figure E.14 shows the 2012 and 2022 rural networks.

Rated capacity [MVA]	Short-circuit voltage [%]	Losses [kW]
300	12	0

Table E.36: eHV-HV Rur transformer specifications.

Resulting from the DSO supply area HV/MV load ratio and the ‘filling’ of the eHV/HV transformer capacity with load, 16 suburban distribution networks are connected to the ring. At buses 01 and 02, two DS are connected, while three are connected at each of the buses 03, 04, 05 and 06.

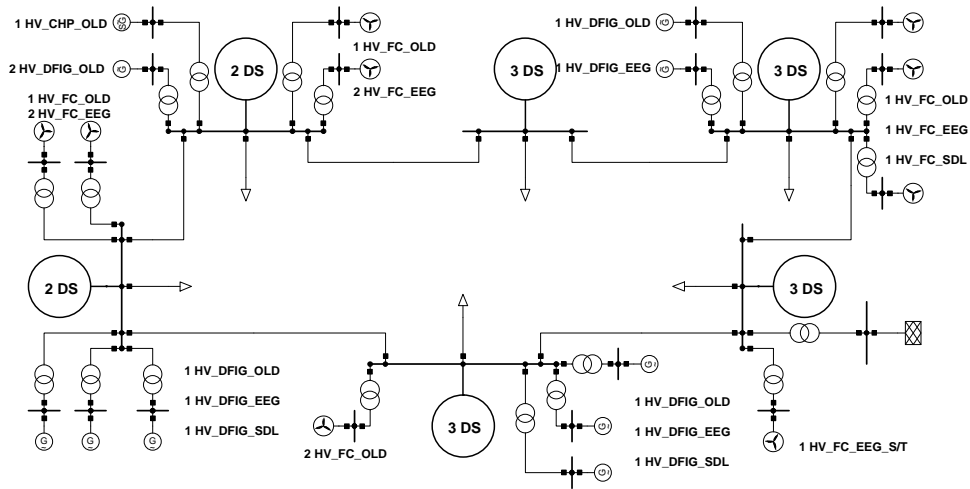
Table E.37a provides the number of wind turbines installed in the 2012 sub-transmission network, while table E.37b gives the number of connected DG installations for 2022. Note that the rural HV network includes one wind turbine at its substation. This is the only substation connected DG installation in the test system. More details on the installation capabilities are given in appendix E.2.2.

	Installations [#]	Capacity [kW]		Installations [#]	Capacity [kW]
Wind	21*	75 000	Wind	36*	129 000
CHP	1	20 000	CHP	1	20 000

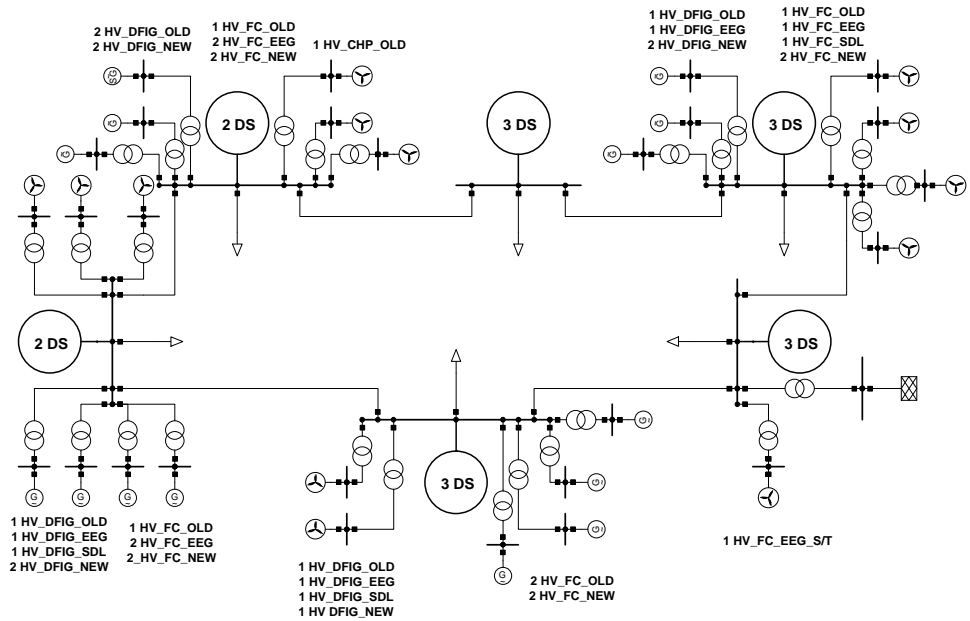
(a) 2012

(b) 2022

Table E.37: DG capacity in rural HV 2012 and 2022 networks. *Includes 1.3 MW turbine connected at the substation.



(a) 2012



(b) 2022

Figure E.14: Single line diagrams rural HV 2012 and 2022 networks.

E.5 Network Data

In this appendix the general parameters for the networks at each voltage level are provided.

E.5.1 Low Voltage Network Data

Equivalent impedance	R [Ω]	X [Ω]	R/X [-]
Suburban PV	0.0137	0.0008	17.1
Suburban CHP	0.0039	0.0016	2.4
Rural	0.0165	0.0064	2.6

Table E.38: Equivalent impedances 2012 aggregated LV networks.

Equivalent impedance	R [Ω]	X [Ω]	R/X [-]
Suburban PV	0.0083	0.0013	6.4
Suburban CHP	0.0039	0.0016	2.4
Rural	0.0131	0.0014	9.4

Table E.39: Equivalent impedances 2022 aggregated LV networks.

Type	R [Ω /km]	X [Ω /km]	R/X [-]	B [μ S/km]
NAYY 4x150SE 0.6/1 kV	0.2067	0.08042478	2.57	260.7522

Table E.40: Complete LV network cable type (2012 and 2022).

E.5.2 Medium Voltage Network Data

Equivalent impedance	R [Ω]	X [Ω]	R/X [-]	B [μ S]
Suburban PV	0.07	0.07	1	3 362
Suburban CHP	0.055	0.055	1	2 589
Rural	0.1	0.1	1	22 386

Table E.41: Equivalent impedances 2012 aggregated MV networks.

Equivalent impedance	R [Ω]	X [Ω]	R/X [-]	B [μ S]
Suburban PV	0.025	0.025	1	3 362
Suburban CHP	0.055	0.055	1	2 589
Rural	0.133	0.133	1	22 200

Table E.42: Equivalent impedances 2022 aggregated MV networks.

Type	R [Ω /km]	X [Ω /km]	R/X [-]	B [μ S/km]
NA2XS2Y 1x150RM 12/20kV ir	0.206	0.1954071	1.05	79.79646

Table E.43: Complete MV network cable type (2012 and 2022).

E.5.3 High Voltage Network Data

Line	R [Ω]	X [Ω]	R/X [-]
eHV-XX_HV-01-02_LINE	0.4090	1.7255	0.237
eHV-XX_HV-02-03_LINE	0.4090	1.7255	0.237
eHV-XX_HV-03-04_LINE	0.6135	2.5882	0.237
eHV-XX_HV-04-05_LINE	0.4090	1.7255	0.237
eHV-XX_HV-05-06_LINE	0.2045	0.8627	0.237
eHV-XX_HV-06-01_LINE	0.4090	1.7255	0.237

Table E.44: Line parameters HV suburban network (2012 and 2022).

Line	R [Ω]	X [Ω]	R/X [-]
eHV-XX_HV-01-02_LINE	0.4090	1.7255	0.237
eHV-XX_HV-02-03_LINE	0.4090	1.7255	0.237
eHV-XX_HV-03-04_LINE	0.6135	2.5882	0.237
eHV-XX_HV-04-05_LINE	0.4090	1.7255	0.237
eHV-XX_HV-05-06_LINE	0.2045	0.8627	0.237
eHV-XX_HV-06-01_LINE	0.4090	1.7255	0.237

Table E.45: Line parameters 2012 HV rural network.

Line	R [Ω]	X [Ω]	R/X [-]
eHV-XX_HV-01-02_LINE	0.4090	1.7255	0.237
eHV-XX_HV-02-03_LINE	0.4090	1.7255	0.237
eHV-XX_HV-03-04_LINE	0.6135	2.5882	0.237
eHV-XX_HV-04-05_LINE	0.2045	0.8627	0.237
eHV-XX_HV-05-06_LINE	0.1363	0.5752	0.237
eHV-XX_HV-06-01_LINE	0.2045	0.8627	0.237

Table E.46: Line parameters 2022 HV rural network.

Load	Active power [MW]	Reactive power [Mvar]	Type [-]
eHV-XX_HV-01_STATLD	8.15	0	Mixed
eHV-XX_HV-02_STATLD	8.15	0	Mixed
eHV-XX_HV-03_STATLD	8.15	0	Mixed
eHV-XX_HV-04_STATLD	16.31	0	Mixed
eHV-XX_HV-05_STATLD	16.31	0	Mixed
eHV-XX_HV-06_STATLD	16.31	0	Mixed

Table E.47: Load ratings suburban HV network.

Load	Active power [MW]	Reactive power [Mvar]	Type [-]
eHV-XX_HV-01_STATLD	11.60	0	Mixed
eHV-XX_HV-02_STATLD	11.60	0	Mixed
eHV-XX_HV-03_STATLD	17.40	0	Mixed
eHV-XX_HV-04_STATLD	17.40	0	Mixed
eHV-XX_HV-05_STATLD	17.40	0	Mixed
eHV-XX_HV-06_STATLD	17.40	0	Mixed

Table E.48: Load ratings rural HV network.

Appendix F

Additional results

F.1 Additional simulation results for chapter 4

F.1.1 Impact with state-of-the-art requirements and $k_{RCI} = 6$ p.u.

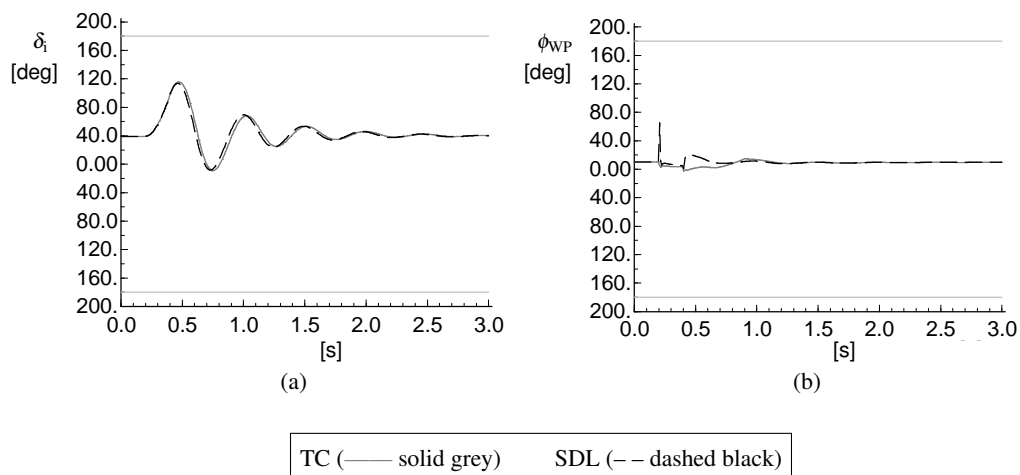


Figure F.1: Impact of fault control mode (TC vs. SDL) with reactive current gain $k_{RCI} = 6$ p.u. during reverse power flow situations on the transient stability of the transmission connected synchronous generator and the excursion of the voltage angle at the WPPM PCC.

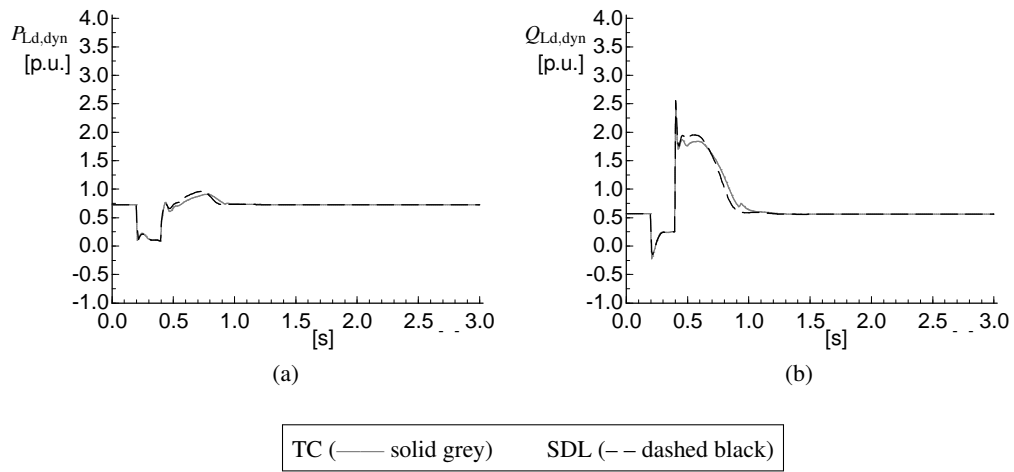


Figure F.2: Impact of fault control mode (TC vs. SDL) with reactive current gain $k_{RCI} = 6$ p.u. during reverse power flow situations on the response of sub-transmission connected induction motor load.

F.1.2 Impedance angle adjusted control mode

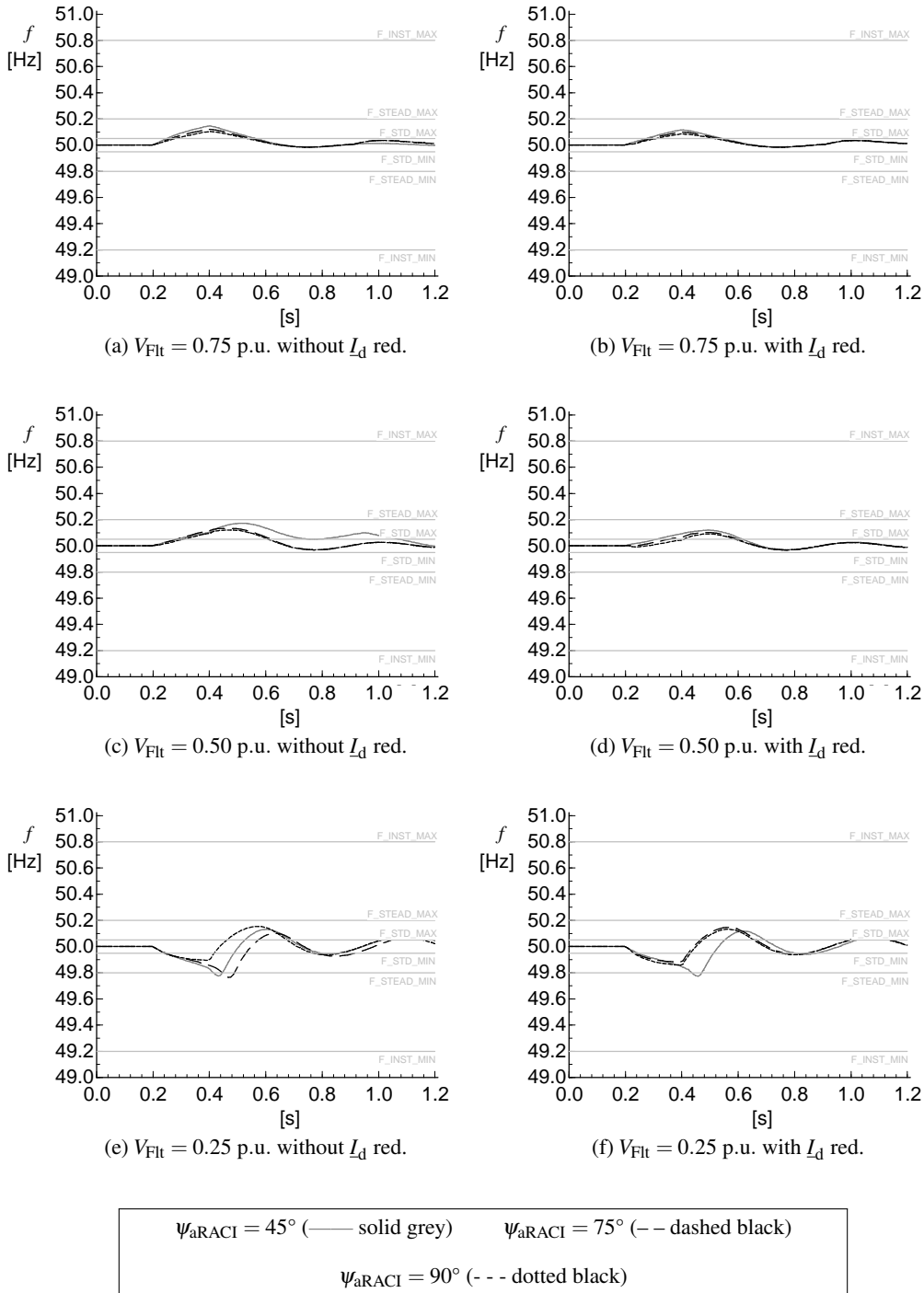


Figure F.3: Impact of additional reactive/active current injection angle ($\psi_{aRACI} = 45^\circ$ vs. 75° vs. 90°) for $k_{RCI} = 2$ p.u. on system frequency f during reverse power flow situations for distribution connected WPPM (DS_RPF_Zdyn). Shallow (top row), medium (middle row) and deep (bottom row) voltage dip. Without (left column) and with (right column) voltage dependent direct-axis current L_d reduction. Taps were in both cases adapted to keep WPPM terminal voltage at 1 p.u. and the pre-fault operating point of the WPPM was in both cases set to $\cos(\varphi) = 1$.

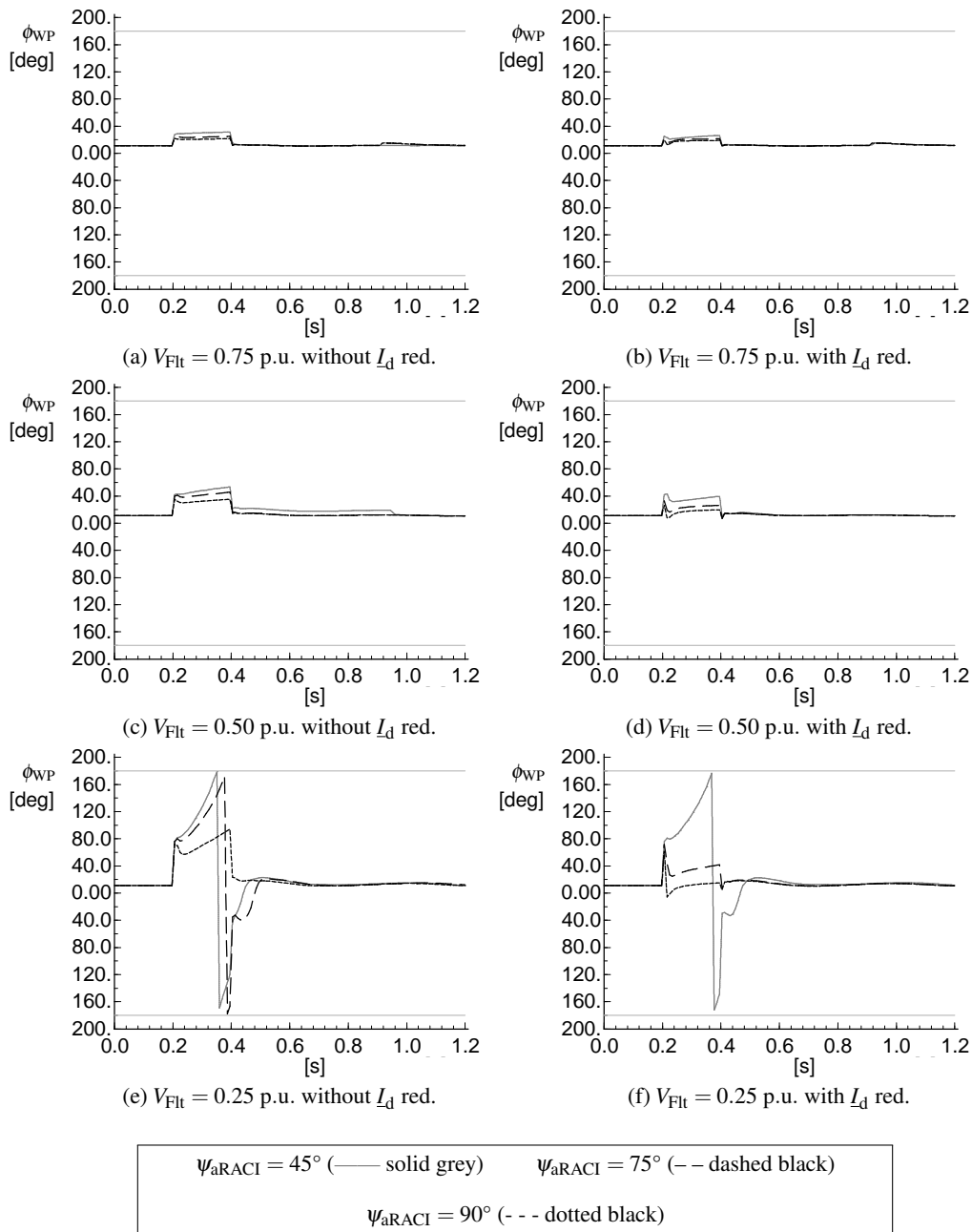


Figure F.4: Impact of additional reactive/active current injection angle ($\psi_{\text{aRACI}} = 45^\circ$ vs. 75° vs. 90°) for $k_{\text{RCI}} = 2$ p.u. on WPPM PCC voltage angle ϕ_{WP} during reverse power flow situations for distribution connected WPPM (DS_RPF_Zdyn). Shallow (top row), medium (middle row) and deep (bottom row) voltage dip. Without (left column) and with (right column) voltage dependent direct-axis current L_d reduction. Taps were in both cases adapted to keep WPPM terminal voltage at 1 p.u. and the pre-fault operating point of the WPPM was in both cases set to $\cos(\varphi) = 1$.

F.2 Operational scenarios for chapter 5

This appendix gives an overview of generation and load in the different operational scenarios. Additionally, power flows between the different voltage levels are provided. Power flow data represents the total power flow within the three instances of that network type measured at the LV side of the transformers. Total power flows in the test system are listed in the last column. Positive numbers represent power export to the next higher voltage level, negative numbers mean power is imported from the next higher voltage level. The share of generation by DG is based on the total generation in the system.

F.2.1 Generation and Load

	Gen _{total} [MW]	Load [MW]	Gen _{DG} [MW]	Share of Gen _{DG} [%]
OS1	6 034	6 021	919	15
OS2	6 068	6 030	1 490	25
OS3	3 249	3 222	1 834	56

Table F.1: Active power generation and load in 2012 operational scenarios.

	Gen _{total} [MW]	Load [MW]	Gen _{DG} [MW]	Share of Gen _{DG} [%]
OS1	6 077	6 041	1 480	24
OS2	6 157	6 123	2 388	39
OS3	3 649	3 605	2 973	81

Table F.2: Active power generation and load in 2022 operational scenarios.

F.2.2 Power Flows

2012 Power Flows

	Suburban PV P [MW]	Suburban CHP P [MW]	Rural P [MW]	Total system P [MW]
HV/eHV	-386.7	-465.2	-365.9	-1 217.8
MV/HV	-236.8	-315.0	-211.8	-763.6
LV/MV	-223.8	-296.8	-285.5	-806.1

Table F.3: Active power flows in 2012, OS 1.

	Suburban PV Q [Mvar]	Suburban CHP Q [Mvar]	Rural Q [Mvar]	Total system Q [Mvar]
HV/eHV	-4.5	-20.2	314.3	289.6
MV/HV	-67.4	-78.9	265.8	119.5
LV/MV	-95.5	-96.9	-155.3	-347.7

Table F.4: Reactive power flows in 2012, OS 1.

	Suburban PV P [MW]	Suburban CHP P [MW]	Rural P [MW]	Total system P [MW]
HV/eHV	-249.9	-323.2	-74.4	-647.5
MV/HV	-148.8	-222.0	-47.3	-418.1
LV/MV	-224.0	-287.5	-285.0	-796.5

Table F.5: Active power flows in 2012, OS 2.

	Suburban PV Q [Mvar]	Suburban CHP Q [Mvar]	Rural Q [Mvar]	Total system Q [Mvar]
HV/eHV	-16.2	-30.1	288.5	242.2
MV/HV	-71.8	-83.1	257.8	102.9
LV/MV	-95.7	-97.1	-155.9	-348.7

Table F.6: Reactive power flows in 2012, OS 2.

	Suburban PV P [MW]	Suburban CHP P [MW]	Rural P [MW]	Total system P [MW]
HV/eHV	120.1	-33.1	592.5	679.5
MV/HV	133.2	-20.1	481.7	594.8
LV/MV	-9.5	-154.1	149.6	-14.0

Table F.7: Active power flows in 2012, OS 3.

	Suburban PV Q [Mvar]	Suburban CHP Q [Mvar]	Rural Q [Mvar]	Total system Q [Mvar]
HV/eHV	20.4	21.3	304.9	346.6
MV/HV	-36.4	-37.0	310.2	236.8
LV/MV	-64.1	-55.5	-105.7	-225.3

Table F.8: Reactive power flows in 2012, OS 3.

2022 Power Flows

	Suburban PV P [MW]	Suburban CHP P [MW]	Rural P [MW]	Total system P [MW]
HV/eHV	-281.2	-412.8	34.3	-659.7
MV/HV	-160.6	-291.9	115.0	-337.5
LV/MV	-171.1	-296.9	-138.4	-606.4

Table F.9: Active power flows in 2022, OS 1.

	Suburban PV Q [Mvar]	Suburban CHP Q [Mvar]	Rural Q [Mvar]	Total system Q [Mvar]
HV/eHV	-2.1	-20.7	345.6	322.8
MV/HV	-66.1	-79.0	255.6	110.5
LV/MV	-98.8	-97.0	-160.5	-356.3

Table F.10: Reactive power flows in 2022, OS 1.

	Suburban PV P [MW]	Suburban CHP P [MW]	Rural P [MW]	Total system P [MW]
HV/eHV	-97.1	-223.1	563.7	243.5
MV/HV	-54.4	-180.3	445.7	211.0
LV/MV	-171.2	-287.5	-121.7	-580.4

Table F.11: Active power flows in 2022, OS 2.

	Suburban PV Q [Mvar]	Suburban CHP Q [Mvar]	Rural Q [Mvar]	Total system Q [Mvar]
HV/eHV	-30.8	-46.2	214.0	137.0
MV/HV	-79.7	-92.3	178.1	6.1
LV/MV	-98.9	-97.2	-171.4	-367.5

Table F.12: Reactive power flows in 2022, OS 2.

	Suburban PV P [MW]	Suburban CHP P [MW]	Rural P [MW]	Total system P [MW]
HV/eHV	335.3	75.9	1 388	1 799.2
MV/HV	290.9	30.7	1 135.5	1 457.1
LV/MV	98.5	-152.7	444.5	390.3

Table F.13: Active power flows in 2022, OS 3.

	Suburban PV Q [Mvar]	Suburban CHP Q [Mvar]	Rural Q [Mvar]	Total system Q [Mvar]
HV/eHV	-34.0	0.6	92.9	59.5
MV/HV	-75.3	-48.8	136.0	11.9
LV/MV	-93.8	-55.5	-188.7	-338.0

Table F.14: Reactive power flows in 2022, OS 3.

References

- [A. 09] A. Eberle GmbH & Co. KG, “REG-D™ Relay for Voltage Control & Transformer Monitoring: Operating Manual,” A. Eberle GmbH & Co. KG, Tech. Rep., 22.02.2009. [Online]. Available: <http://www.a-eberle.de/fr/download-center/finish/24-bediensanleitungen/94-ba-reg-d-gb-pdf.html>
- [AAS01] T. Ackermann, G. Andersson, and L. Söder, “Distributed generation: a definition,” *Electric Power Systems Research*, vol. 57, no. 3, pp. 195–204, 2001.
- [AE03] A. Azmy and E. Erlich, “Dynamic Simulation of Fuel Cells and Micro-turbines Integrated with a Multi-Machine Network,” in *2003 IEEE Bologna PowerTech*, 2003, pp. 550–555.
- [AE04] A. Azmy and I. Erlich, “Identification of Dynamic Equivalents for Distribution Power Networks using Recurrent ANNs,” in *2004 IEEE PES Power Systems Conference & Exposition*, 2004.
- [AE05] ———, “Impact of distributed generation on the stability of electrical power systems,” in *2005 IEEE PES General Meeting*, 2005, pp. 1337–1344.
- [Ant08] Anton Ishchenko, “Dynamics and Stability of Distribution Networks with Dispersed Generation,” Ph.D. dissertation, Technische Universiteit Eindhoven, Eindhoven, 2008.
- [AW15] S. Altschäffl and R. Witzmann, “A modelling approach for dynamic short-circuit analysis of the German power system considering all voltage levels,” in *International ETG Congress 2015*, 2015.
- [BAL09] M. Braun, G. Arnold, and H. Laukamp, “Plugging into the Zeitgeist,” *IEEE Power and Energy Magazine*, vol. 7, no. 3, pp. 63–76, 2009.
- [BBZ⁺11] J. C. Boemer, K. Burges, P. Zolotarev, J. Lehner, P. Wajant, M. Fürst, R. Brohm, and T. Kumm, “Overview of German Grid Issues and Retrofit of German Photovoltaic Power Plants for the Prevention of Frequency Stability Problems in Abnormal System Conditions of the ENTSO-E Region Continental Europe,” in *1st International Workshop on Integration of Solar Power into Power Systems*, October 2011. [Online]. Available: http://www.ecofys.com/files/files/ecofys_2011_paper_on_frequency_stability_challenge.pdf

- [BDE08] “Technical Guideline Generating Plants Connected to the Medium-Voltage Network. Guideline for generating plants’ connection to and parallel operation with the medium-voltage network,” BDEW Bundesverband der Energie- und Wasserwirtschaft e. V., 2008.
- [BDKP13] K. Burges, M. Doering, R. Kuwahata, and G. Papaefthymiou, “Examining the Development of Non-Controllable Photovoltaic and Decentralized Generation Capacity in the Context of Balancing the German Power System,” in *3rd International Workshop on Integration of Solar Power into Power Systems*, 2013.
- [BEW06] U. Bachmann, I. Erlich, and W. Winter, “Advanced Grid Requirements for the Integration of Wind Turbines into the German Transmission System,” in *2006 IEEE PES General Meeting*, 2006.
- [BGK09] J. C. Boemer, M. Gibescu, and W. L. Kling, “Dynamic Models for Transient Stability Analysis of Transmission and Distribution Systems with Distributed Generation: an overview,” in *IEEE PowerTech*, 2009.
- [Bos14] Bosch KWK System GmbH, “Datenblätter zu Generatoren, Erregersystemen, Spannungsreglern, Motoren und Kupplungen: Interne Kommunikation im Rahmen des Projekts “Weiterentwicklung des Verhaltens von Erzeugungsanlagen am Niederspannungsnetz im Fehlerfall - Systemsicherheitsaspekte” durchgeführt an der TU Delft und beauftragt vom Forum Netztechnik/Netzbetrieb im VDE e.V. (internal project communication),” Bosch KWK System GmbH, Tech. Rep., 2014.
- [BRG⁺15] J. C. Boemer, B. G. Rawn, M. Gibescu, M. A. van der Meijden, and W. L. Kling, “Response of Wind Power Park Modules in Distribution Systems to Transmission Network Faults during Reverse Power Flows,” *IET Renewable Power Generation*, vol. 9, no. 8, pp. 1033–1042, November 2015.
- [Brü14] R. Bründlinger, “Grid Codes in Europe for Low and Medium Voltage,” in *6th International Conference on Integration of Renewable and Distributed Energy Resources*, 2014.
- [BvR⁺11a] J. C. Boemer, A. van der Meer, B. G. Rawn, R. L. Hendriks, A. R. Ciupuliga, M. Gibescu, W. L. Kling, and J. A. Ferreira, “Fault Ride-through Requirements for Onshore Wind Power Plants in Europe: the Needs of the Power System,” in *2011 IEEE PES General Meeting*, 2011.
- [BvR⁺11b] J. C. Boemer, A. van der Meer, B. G. Rawn, R. L. Hendriks, M. Gibescu, M. A. van der Meijden, W. L. Kling, and J. A. Ferreira, “Network Fault Response of Wind Power Plants in Distribution Systems during Reverse Power Flows,” in *10th International Workshop on Large-Scale Integration of Wind Power into Power Systems as well as on Transmission Networks for Offshore Wind Power Farms*, October 2011.
- [CBW⁺14] Chandra Mouli, Gautham Ram, P. Bauer, T. Wijekoon, E.-M. Bärthlein, and A. Panosyan, “Design of a Power Electronic Assisted OLTC for Grid Voltage Regulation: unpublished,” *IEEE Transactions on Power Delivery*, 2014.

- [CE13] Consentec GmbH and Ecofys Germany GmbH, “Untersuchungen zur Notwendigkeit einer weitergehenden Systemsteuerung zur Einhaltung der Systembilanz: (Analysis of an advanced system controls for system balancing),” Federal Ministry for Economic Affairs and Energy, Tech. Rep., 31.08.2013. [Online]. Available: <http://www.ecofys.com/de/veroeffentlichung/beitrag-dezentraler-erzeugungsanlagen-zur-versorgungssicherheit/>
- [Ce14] C. A. Cañizares and et al., “Trends in Microgrid Control,” *IEEE Transactions on Smart Grid*, vol. 5, no. 4, pp. 1905–1919, 2014.
- [CEN15a] *Requirements for the micro-generating plants to be connected in parallel with public low-voltage distribution networks*, CENELEC Standard BS EN 50 438:2013, 30.06.2015. [Online]. Available: <http://shop.bsigroup.com/ProductDetail/?pid=000000000030325583>
- [CEN15b] *Requirements for the connection of a generating plant to a distribution system - Part 1: Connection to a LV distribution system and above 16A*, CENELEC Technical Specification CLC/TS 50 549-1:2015, Rev. Standard, January 2015.
- [CEN15c] *Requirements for the connection of a generating plant to a distribution system - Part 2: Connection to a MV distribution system*, CENELEC Technical Specification CLC/TS 50 549-2:2015, Rev. Standard, January 2015.
- [CIG07] CIGRÉ Working Group C4.601, *Modeling and dynamic behavior of wind generation as it relates to power system control and dynamic performance*. Paris (21 rue d’Artois and 75008): CIGRÉ, August 2007.
- [CIG11] CIGRÉ Working Group C6.11, *Development and Operation of Active Distribution Networks: Technical Brochure 457*. Paris: CIGRÉ, April 2011.
- [CIG13] CIGRÉ Joint Working Group C1 / C2 / C 6.18, *Coping with Limits for Very High Penetrations of Renewable Energy*. CIGRÉ, February 2013.
- [CIG14] CIGRÉ Task Force C6.04.02, *Benchmark Systems for Network Integration of Renewable and Distributed Energy Resources: Technical Brochure*. Paris (21 rue d’Artois and 75008): CIGRÉ, 2014, vol. 575.
- [CMKK11] E. Coster, J. Myrzik, B. Kruimer, and W. L. Kling, “Integration Issues of Distributed Generation in Distribution Grids,” *Proceedings of the IEEE*, vol. 99, no. 1, pp. 28–39, 2011.
- [Com14] *Reference technical rules for the connection of active and passive users to the LV electrical Utilities*, Comitato Elettrotecnico Italiano Std. CEI 0-21, Rev. 2014-09, September 2014. [Online]. Available: <http://www.ceiweb.it/doc/norme/13455.pdf>
- [Cos10] E. J. Coster, “Distribution grid operation including distributed generation: Impact on grid protection and the consequences of fault ride-through behavior,” Ph.D. dissertation, Technische Universiteit Eindhoven, Eindhoven, 2010.
- [CPU] CPUC. Interconnection (Rule 21). [Online]. Available: <http://www.cpsc.ca.gov/PUC/energy/rule21.htm>

- [CT07] L. Cipcigan and P. Taylor, "Investigation of the reverse power flow requirements of high penetrations of small-scale embedded generation," *IET Renewable Power Generation*, vol. 1, no. 3, p. 160, 2007.
- [CTN⁺14] T. Chinuki, H. Taniguchi, T. Nakajima, Y. Ota, and H. Suzuki, "System Reduction of Power System with Penetration of Photovoltaic Generations," *Electrical Engineering in Japan*, vol. 188, no. 4, pp. 31–43, 2014.
- [DBA11] V. Diedrichs, A. Beekmann, and S. Adloff, "Loss of (Angle) Stability of Wind Power Plants. The Underestimated Phenomenon in Case of Very Low Short Circuit Ratio," in *10th International Workshop on Large-Scale Integration of Wind Power into Power Systems as well as on Transmission Networks for Offshore Wind Power Farms*, October 2011. [Online]. Available: http://www.fh-oow.de/fbi/we/ee/Common/fue/Netzdynamik/Paper_WIW11-024.pdf
- [DBB⁺12] V. Diedrichs, A. Beekmann, K. Busker, S. Nikolai, and S. Adloff, "Control of wind power plants utilizing voltage source converter in high impedance grids," in *2012 IEEE PES General Meeting*, 2012, pp. 1–9.
- [Del13] Delft University of Technology, "Annual peak load per voltage level and population in service area: E-Mail message," December 2013.
- [Del14] —, "Weiterentwicklung des Verhaltens von Erzeugungsanlagen am Niederspannungsnetz im Fehlerfall: Systemsicherheitsaspekte," Forum network technology / network operation (FNN) in the VDE e.V., Berlin, Tech. Rep., August 2014.
- [Deu09] Deutscher Bundestag, "Gesetz über die friedliche Verwendung der Kernenergie und den Schutz gegen ihre Gefahren (Atomgesetz)," *Bundesgesetzblatt*, vol. I, p. 556, 2009.
- [Deu13] Deutsche Gesellschaft für Sonnenenergie (DGS) e.V. (2013) EnergyMap.info: Konsolidierte und plausibilisierte Datenbank der Stammdaten von EEG-Anlagen in Deutschland (Consolidated and plausibilised database of the EEG power plant registry in Germany). [Online]. Available: <http://energymap.info/>
- [DIg08] DIgSILENT GmbH, "General Load Model: Manual," DIgSILENT GmbH, Gomaringen, Tech. Rep., 30-10-2008.
- [DIg11a] —, "DFIG Template: Manual," DIgSILENT GmbH, Gomaringen, Tech. Rep., 02.05.2011.
- [DIg11b] —, "Fully Rated WTG Template: Manual," DIgSILENT GmbH, Gomaringen, Tech. Rep., 02.05.2011.
- [DIg12a] —, "Induction Machine: Manual," DIgSILENT GmbH, Gomaringen, Tech. Rep., 2012.
- [DIg12b] —, "Motor Driven Machine: Manual," DIgSILENT GmbH, Gomaringen, Tech. Rep., 2012.
- [DIg13] —, *PowerFactory 15.1 Manual*. Gomaringen: DIgSILENT GmbH, 2013.

- [DIg15] —, “Synchronous Machine: Technical Reference Documentation,” DIGSILENT GmbH, Gomaringen, Tech. Rep., 2015.
- [Eco08] Ecofys, “Verbesserte Netzintegration von Windenergieanlagen im EEG 2009: (Legal Measures for Improved Grid Integration of Wind Turbines in the Revised Renewable Energy Sources Act 2009),” German Federal Ministry for the Environment, Nature Conservation and Nuclear Safety, Berlin and Germany, Tech. Rep., 30.06.2008.
- [Eco10] —, “Facilitation of Renewables. Work Package 3 Final Report,” in *All Island TSO Facilitation of Renewables Studies*, EirGrid plc and SONI, Ed. EirGrid, 2010.
- [Eco11] —, “Impact of Large-scale Distributed Generation on Network Stability During Over-Frequency Events and Development of Technical Mitigation Measures: Executive Summary,” Forum network technology / network operation (FNN) in the VDE e.V. and EnBW Transportnetze AG and German Solar Industry Association (BSW-Solar), Berlin, Tech. Rep., September 2011. [Online]. Available: http://www.ecofys.com/files/files/ecofys_ifk_2011_50_2_hz_summary.pdf
- [EDBI13] Ecofys Germany GmbH, Deutsche Windguard GmbH, Becker Büttner Held, and Institut für Feuerungs- und Kraftwerkstechnik der Universität Stuttgart, “Entwicklung einer Nachrüstungsstrategie für Erzeugungsanlagen am Mittel- und Niederspannungsnetz zum Erhalt der Systemsicherheit bei Über- und Unterfrequenz: Studie im Auftrag des Bundesministeriums für Wirtschaft und Technologie,” Bundesministerium für Wirtschaft und Technologie (BMWi), Tech. Rep., 06.12.2013. [Online]. Available: <http://www.ecofys.com/de/news/systemsicherheit-notwendige-nachrustung-von-dezentralen-erzeugungsanlagen/>
- [EDML00] F. Edwards, G. Dudgeon, J. McDonald, and W. Leithead, “Dynamics of distribution networks with distributed generation,” in *2000 IEEE Power Engineering Society Summer Meeting*, 2000, pp. 1032–1037 vol. 2.
- [EE10] ENTSO-E, “European Wind Integration Study (EWIS). EWIS Final Report,” European Network of Transmission System Operators for Electricity (ENTSO-E), Brussels, Tech. Rep., 31 March 2010, 31 March. [Online]. Available: http://www.wind-integration.eu/downloads/library/EWIS_Final_Report.pdf
- [EE13a] —. (22.03.2013) Dispersed Generation Impact on CE Region Security: Dynamic Study: Final Report. Brussels. [Online]. Available: https://www.entsoe.eu/fileadmin/user_upload/_library/publications/entsoe/RG_SOC_CE/130322_DISPERSED_GENERATION_final_report.pdf
- [EE13b] —. (28.06.2013) Network Code on Load-Frequency Control and Reserves. Brussels. [Online]. Available: <https://www.entsoe.eu/major-projects/network-code-development/load-frequency-control-reserves/>
- [EE13c] —. (8 March 2013) ENTSO-E Network Code for Requirements for Grid Connection applicable to all Generators. Brussels. [Online].

- Available: <https://www.entsoe.eu/major-projects/network-code-development/requirements-for-generators/Pages/default.aspx>
- [EE13d] EWEA and EPIA. (January 2013) ENTSO-E Network Code for Requirements for Grid Connection applicable to all Generators: EWEA and EPIA main concerns and proposals for solutions. Brussels.
- [EE14] ENTSO-E, “Dispersed Generation Impact on CE Region Security: Dynamic Study: 2014 Report Update,” European Network of Transmission System Operators for Electricity (ENTSO-E), Brussels, Tech. Rep., December 12, 2014.
- [Eir10] EirGrid plc and SONI, Ed., *All Island TSO Facilitation of Renewables Studies*. EirGrid, 2010.
- [Eir13] EirGrid plc, “EirGrid Grid Code: This version comes into effect 07/10/2013,” EirGrid plc, Tech. Rep., 2013.
- [Ell09] A. Ellis, “Memorandum on dynamic performance of WTG models in PSSE and PSLF,” Western Electricity Coordinating Council, Tech. Rep., 22 September 2009.
- [Ene13] Enercon GmbH, “Model Documentation: ENERCON Wind Energy Converter Model ExF3v2 for DIgSILENT PowerFactory,” Enercon GmbH, Aurich and Germany, Tech. Rep., 15/03/2013.
- [ENT12a] ENTSO-E Drafting Team on RfG, “Meeting with DSO Technical Expert Group on 22 November 2012,” Brussels, 18.12.2012.
- [ENT12b] ENTSO-E User Group, “Meeting on “Network Code for Requirements for Grid Connection applicable to all Generators” (NC RfG) on 22 November 2012,” Brussels, 17.12.2012.
- [E.O01] E.ON Netz GmbH, “Ergänzende Netzanschlussregeln für Windenergieanlagen: Zusätzliche technische und organisatorische Regeln für den Netzanschluss von Windenergieanlagen innerhalb der E.ON Netz GmbH: Additional grid connection requirements for wind power plants: Additional technical and organisational rules for the grid connection of wind power plants to the E.ON Netz GmbH,” E.ON Netz GmbH, Bayreuth, Tech. Rep., 2001.
- [E.O03] —, “Netzanschlussregeln Hoch- und Höchstspannungsnetz: Grid connection requirements high- and extra-high voltage networks,” E.ON Netz GmbH, Bayreuth, Tech. Rep., August 2003.
- [EPR13] EPRI, “Protecting the Modern Distribution Grid: EPRI Survey on Distribution Protection with Emphasis on Distributed Generation Integration Practices: 3002001277,” Electric Power Research Institute (EPRI), Tech. Rep., December 2013. [Online]. Available: <http://www.epri.com/abstracts/Pages/ProductAbstract.aspx?ProductId=000000003002001277>
- [EPR14] —, “Common Functions for Smart Inverters,” Electric Power Research Institute (EPRI), Tech. Rep. 3002002233, February 2014. [Online]. Available: <http://www.epri.com/abstracts/Pages/ProductAbstract.aspx?ProductId=00000000001026809>

- [EPR15a] —, “Are Current Unintentional Islanding Prevention Practices Sufficient for Future Needs? Technical Brief (members only): #3002003291,” Electric Power Research Institute (EPRI), Tech. Rep., March 2015. [Online]. Available: <http://www.epri.com/abstracts/Pages/ProductAbstract.aspx?ProductId=00000003002003291>
- [EPR15b] —, “Recommended Settings for Voltage and Frequency Ride-Through of Distributed Energy Resources: Minimum and Advanced Requirements and Settings for the Performance of Distributed Energy Resources During and After System Disturbances to Support Bulk Power System Reliability and Their Respective Technical Implications on Industry Stakeholders: 3002006203,” Electric Power Research Institute (EPRI), Palo Alto, CA, Tech. Rep., May 2015. [Online]. Available: <http://www.epri.com/abstracts/Pages/ProductAbstract.aspx?ProductId=00000003002006203>
- [Erl13] I. Erlich, “Vergleich der Reaktion von direkt netzgekoppelten Synchrongeneratoren und umrichterbasierten Erzeugungseinheiten auf netzseitige Kurzschlüsse,” *TÜV NORD-Forum: Geprüfte Netzkonformität von BHKWs*. 25 September 2013, Düsseldorf, 2013.
- [ESBR08] M. El-Shimy, M. Badr, and O. Rassem, “Impact of large scale wind power on power system stability,” in *2008 12th International Middle-East Power System Conference MEPCON 2008*, 2008, pp. 630–636. [Online]. Available: <http://ieeexplore.ieee.org/ielx5/4545824/4562294/04562365.pdf?tp=&arnumber=4562365&isnumber=4562294>
- [ESE⁺09] I. Erlich, F. Shewarega, S. Engelhardt, J. Kretschmann, J. Fortmann, and F. Koch, “Effect of wind turbine output current during faults on grid voltage and the transient stability of wind parks,” in *2009 IEEE PES General Meeting*, 2009, pp. 1–8. [Online]. Available: [10.1109/PES.2009.5275626](https://doi.org/10.1109/PES.2009.5275626)
- [ESPM05] C. Eping, J. Stenzel, M. Pöller, and H. Müller, “Impact of Large Scale Wind Power on Power System Stability,” in *Proceedings. 5. International workshop on large-scale integration of wind power and transmission networks for offshore wind farms*, T. Ackermann and J. Matevosyan, Eds. Royal Institute of Technology, Stockholm, 2005, 2005.
- [Ess12] P. Esslinger, “Studie Q(U),” Technische Universität München, München, Tech. Rep., 31.08.2012. [Online]. Available: <http://www.hsa.ei.tum.de/fileadmin/tueihsa/www/Forschung/StudieQU-Schlussbericht.pdf>
- [Eur04] Eurelectric Thermal Working Group, “Ancillary Services: Unbundling Electricity Products - an Emerging Market,” EURELECTRIC, Brussels, Tech. Rep. Ref: 2003-150-0007, February 2004.
- [Eur08] *Voltage characteristics of electricity supplied by public distribution systems*, European Committee for Electrotechnical Standardization EN EN 50 160:2008-04, Rev. 2007, April 2008.
- [Eur09a] “Directive 2009/28/EC of the European Parliament and of the Council of 23 April 2009 on the promotion of the use of energy from renewable sources and

- amending and subsequently repealing Directives 2001/77/EC and 2003/30/EC: Directive 2009/28/EC,” Directive 2009/28/EC, European Parliament and European Council, 2009. [Online]. Available: <http://eur-lex.europa.eu/LexUriServ/LexUriServ.do?uri=OJ:L:2009:140:0016:0062:EN:PDF>
- [Eur09b] “Directive 2009/29/EC of the European Parliament and of the Council of 23 April 2009 amending Directive 2003/87/EC so as to improve and extend the greenhouse gas emission allowance trading scheme of the Community: Directive 2009/29/EC,” Directive 2009/29/EC, European Parliament and European Council, 2009. [Online]. Available: <http://eur-lex.europa.eu/LexUriServ/LexUriServ.do?uri=CELEX:32009L0029:EN:NOT>
- [Eur09c] “Directive 2009/72/EC of the European Parliament and of the Council of 13 July 2009 concerning common rules for the internal market in electricity and repealing Directive 2003/54/EC: Directive 2009/72/EC,” Directive 2009/72/EC, European Parliament and European Council, 2009. [Online]. Available: <http://eur-lex.europa.eu/LexUriServ/LexUriServ.do?uri=CELEX:32009L0072:en:NOT>
- [EW10] I. Erlich and M. Wilch, “Primary frequency control by wind turbines,” in *2010 IEEE PES General Meeting*, 2010, pp. 1–8. [Online]. Available: <http://ieeexplore.ieee.org/ielx5/5577387/5588047/05589911.pdf?tp=&arnumber=5589911&isnumber=5588047>
- [Fec10] C. A. Fechner, *Die 4. Revolution: Energy autonomy; freie Energie für Alle!* Immendingen: FechnerMedia, 2010.
- [Fed11] Federal Statistical Office (Destatis), “Regional statistics: Towns and villages,” Federal Statistical Office (Destatis), Tech. Rep., 31.03.2011. [Online]. Available: <https://www.destatis.de/DE/ZahlenFakten/LaenderRegionen/Regionales/Gemeindeverzeichnis/Gemeindeverzeichnis.html>
- [FEK⁺08] C. Feltes, S. Engelhardt, J. Kretschmann, J. Fortmann, F. Koch, and I. Erlich, “High voltage ride-through of DFIG-based wind turbines,” in *2008 IEEE PES General Meeting*, 2008.
- [FEK⁺09] —, “Comparison of the grid support capability of DFIG-based wind farms and conventional power plants with synchronous generators,” in *2009 IEEE PES General Meeting*, 2009, pp. 1–7. [Online]. Available: <10.1109/PES.2009.5275441>
- [FGW14] FGW, “Technical Guidelines for Power Generating Units: Part 4 -Demands on Modelling and Validating Simulation Models of the Electrical Characteristics of Power Generating Units and Systems,” FGW e.V. Fördergesellschaft Windenergie und andere Erneuerbare Energien, Kiel, Tech. Rep., 07.04.2014.
- [FLB07] X. Feng, Z. Lubosny, and J. W. Bialek, “Identification based Dynamic Equivalent,” in *2007 IEEE Lausanne Power Tech*, 2007, pp. 267–272.
- [For10] *VDE-AR-N 100 (VDE-AR-N 4000) Erarbeitung von VDE-Anwendungsregeln im FNN*, Forum network technology / network operation (FNN) in the VDE

- e.V. Anwendungsregel VDE-AR-N 100:2010-01, 2010. [Online]. Available: <http://www.vde.com/de/fnn/dokumente/seiten/vde-ar-n100.aspx>
- [For11] *Generators in the low voltage distribution network. Application guide for generating plants' connection to and parallel operation with the low-voltage network*, Forum network technology / network operation (FNN) in the VDE e.V. VDE Application Guide VDE-AR-N 4105, 01.08.2011.
- [For12] Forum Netztechnik / Netzbetrieb (FNN) im VDE e.V., "VDEIFNN-Roadmap identifiziert weiteren Entwicklungsbedarf zum Umbau der Netze: Pressemitteilung," Berlin, 07.12.2012.
- [For13] J. Fortmann, "Modeling of Wind Turbines with a Doubly Fed Generator System," Ph.D. dissertation, Universität Duisburg-Essen, Duisburg, 30.08.2013.
- [For15a] *Technische Bedingungen für den Anschluss und Betrieb von Kundenanlagen an das Hochspannungsnetz (TAB Hochspannung)*, Forum Netztechnik / Netzbetrieb (FNN) im VDE e.V. VDE-Anwendungsregel VDE-AR-N 4120, Januar 2015. [Online]. Available: <http://www.vde.com/de/fnn/arbeitsgebiete/seiten/n4120.aspx>
- [For15b] *Technical requirements for the connection and operation of customer installations to the high voltage network (TAB high voltage)*, Forum Netztechnik / Netzbetrieb (FNN) im VDE e.V. VDE-Application-Guide VDE-AR-N 4120, January 2015. [Online]. Available: <http://www.vde.com/de/fnn/arbeitsgebiete/seiten/n4120.aspx>
- [Fra13] Fraunhofer ISE, "Levelized Cost of Electricity- Renewable Energy Technologies," Fraunhofer Institute for Solar Energy Systems ISE, Freiburg and Germany, Tech. Rep., November 2013.
- [Fra15] Frankfurt School of Finance & Management gGmbH, "Global Trends in Renewable Energy Investment 2015," Frankfurt School of Finance & Management gGmbH, Frankfurt am Main, Tech. Rep., 2015.
- [Gal13] E. Galinas, "Sensitivity Analysis for Expansion of Transmission Systems with High Amounts of Renewables," Ph.D. dissertation, Delft University of Technology, Delft, 15 March 2013.
- [Geo09] K. Georg, "Empfehlung zur Richtlinie zum Anschluss von Erzeugungsanlagen an das Niederspannungsnetz," Fachgebiet Elektrische Energieversorgungsnetze. Technische Universität München, München, Tech. Rep., 15/05/2009. [Online]. Available: http://www.hsa.ei.tum.de/Publikationen/2009/2009_Empfehlung_Richtlinie_Niederspannung.pdf
- [Ger01] German Electricity Association (VDEW), *Generating Plants Connected to the Low-Voltage Network. Guideline for generating plants' connection to and parallel operation with the low-voltage network*, 4th ed. Frankfurt am Main: VDEW Energieverlag GmbH, 2001.

- [Ger09] German Government, “Verordnung zu Systemdienstleistungen durch Windenergieanlagen (Systemdienstleistungsverordnung – SDLWindV) (Ordinance for Ancillary Services of Wind Power Plants (Ancillary Services Ordinance - SDLWindV),” *Federal Law Gazette*, vol. I, no. 39, pp. 1734–1746, 2009.
- [Ger12a] German Energy Agency, “dena Distribution Grid Study: German electricity distribution grids in need of significant expansion by 2030,” German Energy Agency, Berlin, Tech. Rep., December 2012. [Online]. Available: <http://www.dena.de/en/projects/energy-systems/dena-distribution-grid-study.html>
- [Ger12b] German TSOs, “Netzentwicklungsplan Strom 2012 (Network Development Plan Electricity 2012): 2. überarbeiteter Entwurf der Übertragungsnetzbetreiber (2nd revised draft of the transmission system operators),” German TSOs, Berlin-Dortmund-Bayreuth-Stuttgart, Germany, Tech. Rep., 15/08/2012. [Online]. Available: <http://www.netzentwicklungsplan.de>
- [GILM03] F. M. Gatta, F. Iliecto, S. Lauria, and P. Masato, “Modelling and computer simulation of dispersed generation in distribution networks. measures to prevent disconnection during system disturbances,” in *2003 IEEE Bologna PowerTech*, 2003, pp. 659–668.
- [GPP08] D. N. Gaonkar, G. N. Pillai, and R. N. Patel, “Dynamic performance of micro-turbine generation system connected to a grid,” *ELECTRIC POWER COMPONENTS AND SYSTEMS*, vol. 36, no. 10, pp. 1031–1047, 2008.
- [GTB⁺14] Ö. Göksu, R. Teodorescu, C. L. Bak, F. Iov, and P. C. Kjaer, “Instability of Wind Turbine Converters During Current Injection to Low Voltage Grid Faults and PLL Frequency Based Stability Solution,” *IEEE Transactions on Power Systems*, vol. 29, no. 4, pp. 1683–1691, 2014.
- [Gut02] R. Guttromson, “Modeling distributed energy resource dynamics on the transmission system,” *Power Systems, IEEE Transactions on*, vol. 17, no. 4, pp. 1148–1153, 2002.
- [HALJS05] F. M. Hughes, O. Anaya-Lara, N. Jenkins, and G. Strbac, “Control of DFIG-based wind generation for power network support,” *Power Systems, IEEE Transactions on*, vol. 20, no. 4, pp. 1958–1966, 2005.
- [HSU15] HSU HH, “Wirksame Verfahren zur Inselnetzerkennung in 0,4-kV-Netzen: (Effective methods for islanding detection in 0.4 kV networks): Draft,” Helmut Schmidt University, Hamburg, Tech. Rep., 8 October 2015.
- [IEC15] *Wind turbines - Part 27-1: Electrical simulation models – Wind turbines*, IEC Standard IEC 61 400-27-1, Rev. Ed. 1.0, 13.02.2015.
- [IEE] IEEE Standards Coordinating Committee 21. IEEE 1547 Standard for Interconnecting Distributed Resources With Electric Power Systems: Workshop Meeting Minutes, December 3 - 4, 2013, New Brunswick, NJ. [Online]. Available: http://grouper.ieee.org/groups/scc21/1547_series/docs/minutes/1547-Workshop-20131204-Minutes.pdf

- [IEE03a] *IEEE Guide for Synchronous Generator Modeling Practices and Applications in Power System Stability Analyses*, IEEE Standard IEEE Std. 1110-2002, 11 November 2003.
- [IEE03b] *Standard for Interconnecting Distributed Resources with Electric Power Systems*, IEEE Std. IEEE Std. 1547-2003, 28 July 2003.
- [IEE04] IEEE/CIGRÉ Joint Task Force on Stability Terms and Definitions, “Definition and Classification of Power System Stability,” *IEEE Transactions on Power Systems*, vol. 19, no. 3, pp. 1387–1401, 2004.
- [IEE06] *IEEE Recommended Practice for Excitation System Models for Power System Stability Studies*, IEEE Standard IEEE Std 421.5-2005, 1 May 2006.
- [IEE13] IEEE Standards Coordinating Committee 21. (19.03.2013) IEEE SA - P1547.8 - Recommended Practice for Establishing Methods and Procedures that Provide Supplemental Support for Implementation Strategies for Expanded Use of IEEE Standard 1547. [Online]. Available: <http://standards.ieee.org/develop/project/1547.8.html>
- [IEE14a] *Standard for Interconnecting Distributed Resources with Electric Power Systems*, IEEE Standard. Amendment 1 IEEE Std. 1547a-2014, Rev. 1, 21 May 2014. [Online]. Available: <http://standards.ieee.org/findstds/standard/1547a-2014.html>
- [IEE14b] IEEE PES PSDPC. (2014) Homepage of the Power System Stability Controls Subcommittee: Task Force on Contribution to Bulk System Control and Stability by Distributed Energy Resources connected at Distribution Networks. [Online]. Available: http://ewh.ieee.org/soc/pes/psdpc/index_PSSC.htm
- [IEE16] *Draft Standard for Interconnection and Interoperability of Distributed Energy Resources with Associated Electric Power Systems*, IEEE Draft 3 IEEE P1547/D3, Rev. 3, January 2016. [Online]. Available: http://grouper.ieee.org/groups/scc21/1547_revision/1547revision_index.html
- [IMK07] A. Ishchenko, J. Myrzik, and W. L. Kling, “Dynamic equivalencing of distribution networks with dispersed generation using Hankel norm approximation,” *IET Generation, Transmission & Distribution*, vol. 1, no. 5, p. 818, 2007.
- [IVG12] IVGTF Task Force 1-3, “2012 Special Assessment: Interconnection Requirements for Variable Generation,” NERC, Atlanta, GA, Tech. Rep., September 2012. [Online]. Available: http://www.nerc.com/files/2012_IVGTF_Task_1-3.pdf
- [JEA13] JEAC, *Grid-interconnection Code: JEAC 9701-2012*, ser. JESC E0019 (2012). Japan Electric Association, 31-3-2013.
- [JT05] A. Johnson and N. Tleis, “The development of grid code requirements for new and renewable forms of generation in Great Britain,” *Wind Engineering*, vol. 29, no. 3, 2005.

- [Kli09] J. Klimstra, "Fault ride-through capability of engine-driven power plants," in *2009 POWER-GEN Europe*, 2009.
- [Kob12] H. Kobayashi, "Fault Ride Through Requirements and Measures of Distributed PV Systems in Japan," in *2012 IEEE PES General Meeting*, 2012.
- [Kun94] P. Kundur, *Power system stability and control*. New York: McGraw-Hill, Inc., 1994.
- [KW08] G. Kerber and R. Witzmann, "Statistische Analyse von NS-Verteilungsnetzen und Modellierung von Referenznetzen: (Statistical Distribution Grid Analysis and Reference Network Generation)," *Ew*, vol. 107, no. 6, pp. 22–26, 2008.
- [LKP05] V. Levi, M. Kay, and I. Povey, "Reverse Power Flow Capability of Tap-Changers," in *18th International Conference on Electricity Distribution*, 2005, pp. 1–5. [Online]. Available: <http://ieeexplore.ieee.org/stamp/stamp.jsp?arnumber=05427965>
- [LMO05] G. Lalor, A. Mullane, and M. O'Malley, "Frequency control and wind turbine technologies," *Power Systems, IEEE Transactions on*, vol. 20, no. 4, pp. 1905–1913, 2005.
- [LSS⁺15] J. Langstädtler, B. Schowe-Von der Brelie, M. Schellschmidt, S. Schrobsdorff, J. Scheffer, and C. Kahlen, "Relevance of High-Voltage-Ride-Through Capability and Testing," in *23rd International Conference on Electricity Distribution*, 2015.
- [MBE⁺06] E. Muljadi, C. P. Butterfield, A. Ellis, J. Mechenbier, J. Hochheimer, R. Young, N. Miller, R. Delmerico, R. Zavadil, and J. C. Smith, "Equivalent the collector system of a large wind power plant," in *2006 IEEE Power Engineering Society General Meeting*, 2006, p. 9 pp.
- [MBPE07] E. Muljadi, C. P. Butterfield, B. Parsons, and A. Ellis, "Effect of Variable Speed Wind Turbine Generator on Stability of a Weak Grid: Invited Paper," *IEEE Transactions on Energy Conversion*, vol. 22, no. 1, pp. 29–36, 2007.
- [MF10] L. Meegahapola and D. Flynn, "Impact on transient and frequency stability for a power system at very high wind penetration," in *2010 IEEE PES General Meeting*, 2010, pp. 1–8. [Online]. Available: <http://ieeexplore.ieee.org/ielx5/5577387/5588047/05589908.pdf?tp=&arnumber=5589908&isnumber=5588047>
- [MHKF06] J. Morren, S. d. Haan, W. L. Kling, and J. Ferreira, "Wind turbines emulating inertia and supporting primary frequency control," *Power Systems, IEEE Transactions on*, vol. 21, no. 1, pp. 433–434, 2006.
- [MM13a] S. Mat Zali and J. V. Milanovic, "Generic Model of Active Distribution Network for Large Power System Stability Studies," *IEEE Transactions on Power Systems*, 2013.

- [MM13b] J. V. Milanovic and S. Mat Zali, "Validation of Equivalent Dynamic Model of Active Distribution Network Cell," *IEEE Transactions on Power Systems*, vol. 28, no. 3, pp. 2101–2110, 2013.
- [MNP08] E. Muljadi, T. B. Nguyen, and M. A. Pai, "Impact of Wind Power Plants on Voltage and Transient Stability of Power Systems," in *IEEE Energy 2030*. IEEE, 2008, pp. 1–7.
- [Mol12] D. Molina, "Progress report on the development and validation of DIgSILENT PowerFactory model of the 39-Bus benchmark system for stability controls: Addressed to IEEE Task Force on Benchmark Systems for Stability Controls: Working Paper," Georgia Institute of Technology, Tech. Rep., 25-09-2012. [Online]. Available: <http://www.sel.eesc.usp.br/ieee/IEEE39/main.htm>
- [Mor06] J. Morren, "Grid support by power electronic converters of Distributed Generation units," Ph.D. dissertation, Delft University of Technology, Delft, 2006.
- [MPR⁺11] A. Marinopoulos, F. Papandrea, M. Reza, S. Norrga, F. Spertino, and R. Napoli, "Grid integration aspects of large solar PV installations: LVRT capability and reactive power/voltage support requirements," in *2011 IEEE Trondheim PowerTech*, 2011, pp. 1–8. [Online]. Available: <http://ieeexplore.ieee.org/stamp/stamp.jsp?arnumber=6019324>
- [Muh06] Muhamad Reza, "Stability analysis of transmission systems with high penetration of distributed generation," Ph.D. dissertation, Delft University of Technology, Delft, 2006.
- [MWA01] N. Miller, R. Walling, and A. Achilles, "Impact of distributed resources on system dynamic performance," in *2001 IEEE/PES Transmission and Distribution Conference and Exposition*, Oct. 2001, pp. 951–952 vol.2.
- [MY03] N. Miller and Z. Ye, "Report on Distributed Generation Penetration Study," National Renewable Energy Laboratory, Golden, Colorado and USA, Tech. Rep., August 2003. [Online]. Available: <http://www.nrel.gov/docs/fy03osti/34715.pdf>
- [Nat09] National Grid, "How the National Grid System Operates," National Grid, Tech. Rep., 2009. [Online]. Available: http://www.nationalgridus.com/niagamohawk/non_html/ee_conference/systemoper.pdf
- [Nav05] I. R. Navarro, "Dynamic Power System Load Estimation of Parameters from Operational Data," Ph.D. dissertation, Lund University, 16/3/2005.
- [NE12] T. Neumann and E. Erlich, "Modelling and Control of Photovoltaic Inverter Systems with Respect to German Grid Code Requirements," in *2012 IEEE PES General Meeting*, 2012.
- [NER09] NERC, "A Technical Reference Paper Fault-Induced Delayed Voltage Recovery: White Paper," North American Electric Reliability Corporation, Princeton, NJ, Tech. Rep., June 10, 2009. [Online]. Available: http://www.nerc.com/docs/pc/tis/fidvr_tech_ref%20v1-2_pc_approved.pdf

- [NER12] —, “Emerging Issue #RAS–8: Assessment of Fault-Induced Delayed Voltage Recovery (FIDVR) Simulations,” North American Electric Reliability Corporation, Tech. Rep., 15-6-2012. [Online]. Available: http://www.nerc.com/docs/pc/ras/2012_Issue_8_FIDVR.pdf
- [NER15] —, “Fault-Induced Delayed Voltage Recovery (FIDVR) & Dynamic Load Modeling: U.S. DOE-NERC Workshop, September 30, 2015 - October 1, 2015, Alexandria, WA,” North American Electric Reliability Corporation, Tech. Rep., October 2015. [Online]. Available: <http://www.nerc.com/comm/PC/System%20Analysis%20and%20Modeling%20Subcommittee%20SAMS%20201/2015%20FIDVR%20Workshop%20Takeaways.pdf>
- [NP14] S. I. Nanou and S. A. Papathanassiou, “Modeling of a PV system with grid code compatibility,” *Electric Power Systems Research*, vol. 116, pp. 301–310, 2014.
- [NWDE15] T. Neumann, T. Wijnhoven, G. Deconinck, and I. Erlich, “Enhanced Dynamic Voltage Control of Type 4 Wind Turbines During Unbalanced Grid Faults,” *IEEE Transactions on Energy Conversion*, pp. 1–10, 2015.
- [NWJ03] Nicholas W. Miller, William W. Price, and Juan J. Sanchez-Gasca, “Dynamic Modeling of GE 1.5 and 3.6 Wind Turbine-Generators,” GE Power Systems Energy Consulting, Tech. Rep., 27 October 2003, 27 October.
- [Pal14] S. Palm, “Grundlagen der Detektierbarkeit und Detektionsverfahren von Inselnetzen,” 8. *FNN/ETG-Tutorial Schutz- und Leittechnik. Düsseldorf, Deutschland, 05.-06.02.2014*, 2014.
- [PHS05] S. Papathanassiou, N. Hatziargyriou, and K. Strunz, “A benchmark low voltage microgrid network,” *CIGRÉ Symposium on Power Systems with Dispersed Generation, Athens, Greece, April 2005*, 2005.
- [PKD⁺13] G. Papaefthymiou, R. Kuwahata, M. Doering, K. Burges, and J. C. Boemer, “Assessment of the Frequency Settings from Distributed Generation in Germany for the Prevention of Frequency Stability Problems in Abnormal System Conditions,” in *12th International Workshop on Large-Scale Integration of Wind Power into Power Systems as well as on Transmission Networks for Offshore Wind Power Farms*, 2013.
- [Pöl03] M. Pöller, “Doubly-fed induction machine models for stability assessment of wind farms,” in *2003 IEEE Bologna PowerTech*, 2003, p. 6.
- [QH08] W. Qiao and R. G. Harley, “Effect of Grid-Connected DFIG Wind Turbines on Power System Transient Stability,” in *2008 IEEE PES General Meeting*, 2008, pp. 4084–4090. [Online]. Available: <http://ieeexplore.ieee.org/ielx5/4584435/4595968/04596912.pdf?tp=&arnumber=4596912&isnumber=4595968>
- [RERV⁺02] S. M. Rovnyak, D. Ernst, D. Ruiz-Vega, M. Pavella, P. Hirsch, and D. Sobajic, “Discussion of ‘A unified approach to transient stability contingency filtering, ranking, and assessment’ [and closure],” *IEEE Transactions on Power Systems*, vol. 17, no. 2, pp. 527–529, 2002.

- [REvD12] S. d. Rijcke, H. Ergun, D. van Hertem, and J. Driesen, "Grid Impact of Voltage Control and Reactive Power Support by Wind Turbines Equipped With Direct-Drive Synchronous Machines," *IEEE Transactions on Sustainable Energy*, vol. 3, no. 4, pp. 890–898, 2012.
- [RKTb94] S. Rovnyak, S. Kretsinger, J. Thorp, and D. Brown, "Decision trees for real-time transient stability prediction," *IEEE Transactions on Power Systems*, vol. 9, no. 3, pp. 1417–1426, 1994.
- [RL07] F. O. Resende and J. A. P. Lopes, "Development of Dynamic Equivalents for MicroGrids using System Identification Theory," in *2007 IEEE Lausanne Power Tech*, 2007, pp. 1033–1038.
- [RMM13] F. O. Resende, J. Matevosyan, and J. V. Milanovic, "Application of dynamic equivalence techniques to derive aggregated models of active distribution network cells and microgrids," in *2013 IEEE Grenoble PowerTech*, 2013, pp. 1–6.
- [RWE14] RWE Germany AG, "Anschlusspraxis von Erzeugungsanlagen hinsichtlich einer dynamischen Netzstützung (connection practice for generating plants regarding dynamic network support): Interner Bericht der RWE Deutschland AG (internal report of RWE Germany AG)," RWE Germany AG, Essen, Tech. Rep., March 2014.
- [SAB⁺12] P. Sørensen, B. Andresen, J. Bech, J. Fortmann, and P. Pourbeik, "Progress in IEC 61400-27," in *11th International Workshop on Large-Scale Integration of Wind Power into Power Systems as well as on Transmission Networks for Offshore Wind Power Farms*, 2012.
- [SBv⁺14] K. Skaloumpakas, J. C. Boemer, E. van Ruitenbeek, M. Gibescu, and M. van der Meijden, "Response of Low Voltage Networks with High Penetration of Photovoltaic Systems to Transmission Network Faults," in *3rd Renewable Power Generation Conference (RPG 2014)*, 2014, p. 8.27.
- [SED⁺12] A. Samadi, R. Eriksson, Della Jose, F. Mahmood, M. Ghandhari, and L. Söder, "Comparison of a Three-Phase Single-Stage PV System in PSCAD and PowerFactory," in *2nd International Workshop on Integration of Solar Power into Power Systems*, November 2012.
- [SER09] F. Shewarega, I. Erlich, and J. L. Rueda, "Impact of large offshore wind farms on power system transient stability," in *2009 IEEE/PES Power Systems Conference and Exposition PSCE '09*, 2009, pp. 1–8.
- [SHPK03] J. G. Slootweg, S. W. H. d. Haan, H. Polinder, and W. L. Kling, "General model for representing variable speed wind turbines in power system dynamics simulations," *IEEE Transactions on Power Systems*, vol. 18, no. 1, pp. 144–151, 2003.
- [SK02a] J. G. Slootweg and W. L. Kling, "Modelling and analysing impacts of wind power on transient stability of power systems," *Wind Engineering*, vol. 26, no. 1, pp. 3–20, 2002.

- [SK02b] J. Slootweg and W. Kling, "Impacts of distributed generation on power system transient stability," in *2002 IEEE Power Engineering Society Summer Meeting*, 2002, pp. 862–867.
- [SK03] J. G. Slootweg and W. L. Kling, "The impact of large scale wind power generation on power system oscillations," *Electric Power Systems Research*, vol. 67, no. 1, pp. 9–20, 2003.
- [Ska14] K. Skaloumpakas, "Response of Low Voltage Networks with High Photovoltaic Systems Penetration to Transmission Network Faults," M.Sc. thesis, Delft University of Technology, Delft, 29/01/2014.
- [SKL12] B. Schowe-Von Der Brelie, F. Kalverkamp, and J. Langstädtler, "Dynamic system performance of renewable power generation units - useful and doubtful grid code requirements," in *CIGRE Workshop*, 2012, p. 209. [Online]. Available: <http://ieeexplore.ieee.org/ielx5/6296793/6302339/06302437.pdf?tp=&arnumber=6302437&isnumber=6302339>
- [SKMC14] S. Soni, G. G. Karady, M. Morjaria, and V. Chadliev, "Comparison of full and reduced scale solar PV plant models in multi-machine power systems," in *2014 IEEE/PES Transmission & Distribution Conference & Exposition (T&D)*, 2014, pp. 1–5.
- [SKN⁺10] S. Sugita, Y. Kataoka, S. Naoi, Y. Noro, and R. Ichikawa, "Study of modeling method of distributed generators considering partial dropout for trunk transmission system," in *2010 International Power Electronics Conference-ECCE Asia*, 2010, pp. 975–980.
- [SSS13] F. Sulla, J. Svensson, and O. Samuelsson, "Wind Turbines Voltage Support in Weak Grids," in *2013 IEEE PES General Meeting*, 2013.
- [Str11] E. Strickland, "24 hours at Fukushima," *IEEE Spectrum*, vol. 48, no. 11, pp. 35–42, 2011.
- [TGTB13] A. Tuohy, A. Gaikwad, J. Taylor, and D. Brooks, "The Impact of Low Voltage Disconnection of Distributed PV on Bulk Electricity System Reliability," in *3rd International Workshop on Integration of Solar Power into Power Systems*, 2013.
- [Tho00] M. Thomson, "Automatic voltage control relays and embedded generation: Part 1," *Power Engineering Journal*, vol. 14, no. 2, pp. 71–76, 2000.
- [TQLA⁺06] T. Tran-Quoc, L. Le Thanh, C. Andrieu, N. Hadjsaid, C. Kieny, J. C. Sabonnadiere, K. Le, O. Devaux, and O. Chilard, "Stability Analysis for the Distribution Networks with Distributed Generation," in *2005/2006 IEEE PES Transmission and Distribution Conference and Exhibition*, 2006, pp. 289–294.
- [U.S05] "Interconnection for Wind Energy: Order No. 661-A," Order No. 661-A, U.S.A. Federal Energy Regulatory Commission, 12 December 2005.

- [van14] E. van Ruitenbeek, "Impact of Large Amounts of Photovoltaic Installations in Low-Voltage Networks on Power System Stability During Transmission System Faults," M.Sc. thesis, Delft University of Technology, Delft, 17.06.2014.
- [vBR⁺14] E. van Ruitenbeek, J. C. Boemer, J. L. Rueda, M. Gibescu, and M. A. van der Meijden, "A Proposal for New Requirements for the Fault Behaviour of Distributed Generation Connected to Low Voltage Networks," in *4th International Workshop on Integration of Solar Power into Power Systems*, 2014.
- [VDN04] VDN, "EEG-Erzeugungsanlagen am Hoch- und Höchstspannungsnetz. Leitfaden für Anschluss und Parallelbetrieb von Erzeugungsanlagen auf Basis erneuerbarer Energien an das Hoch- und Höchstspannungsnetz in Ergänzung zu den NetzCodes (Renewable Energy Generating Plants connected to the High- and Extra-High Voltage Networks. Guideline for renewable energy generating plant's connection to and parallel operation with the high- and extra-high voltage networks in addition to the grid codes)," German Association of Network Operators, since beginning of 2008 part of BDEW, Tech. Rep., August 2004. [Online]. Available: http://www.vde.com/de/fnn/dokumente/documents/rl_eeg_hh_vdn2004-08.pdf
- [Ver98] Vereinigung Deutscher Elektrizitätswerke - VDEW - e. V., "Generating Plants Connected to the Medium-Voltage Network. Guideline for generating plants' connection to and parallel operation with the medium-voltage network," Frankfurt am Main, 1998.
- [Ver00] *Merkmale der Spannung in öffentlichen Elektrizitätsversorgungsnetzen*, Verband der Elektrotechnik, Elektronik Informationstechnik e.V. DIN EN DIN EN 50 160:2000-03, 17.03.2000.
- [Ver03] Verband der Netzbetreiber - VDN - e.V. beim VDEW, "TransmissionCode 2003. Netz- und Systemregeln der Deutschen Übertragungsnetzbetreiber (Network and System Rules of the German Transmission System Operators)," Verband der Netzbetreiber - VDN - e.V. beim VDEW, Tech. Rep., August 2003.
- [Ver07] "TransmissionCode 2007. Network and System Rules of the German Transmission System Operators," Verband der Netzbetreiber - VDN - e.V. beim VDEW (German Association of Network Operators, since beginning of 2008 part of BDEW), August 2007. [Online]. Available: <http://www.vde.com/de/fnn/dokumente/documents/transmissioncode2007.pdf>
- [WEC10] WECC Modeling and Validation Work Group, "WECC Wind Power Plant Dynamic Modeling Guide," Western Electricity Coordinating Council, Tech. Rep., November 2010.
- [WEC11] —, "WECC Guide for Representation of Photovoltaic Systems In Large-Scale Load Flow Simulations," Western Electricity Coordinating Council, Tech. Rep., January 2011.
- [WEC12] WECC Renewable Energy Modeling Task Force, "Generic Solar Photovoltaic System Dynamic Simulation Model Specification," Western Electricity Coordinating Council, Tech. Rep., September 2012.

- [WEC14] —, “WECC Solar Power Plant Dynamic Modeling Guidelines,” Western Electricity Coordinating Council, Tech. Rep., April 2014. [Online]. Available: <https://www.wecc.biz/Reliability/WECC%20Solar%20Plant%20Dynamic%20Modeling%20Guidelines.pdf>
- [Wei13a] B. Weise, “Beeinflussung der Netzstabilität durch die Wirkstromreduktion im LVRT-Modus von Stromrichter-Erzeugungseinheiten und den Gradienten der Wirkleistungssteigerung nach Fehlerklärung: Impact of Active Current Reduction in LVRT Mode of Generating Units connected via Converters and of Active Power Ramping Speed after Fault Clearance on Network Stability,” in *Internationaler ETG-Kongress*, 2013.
- [Wei13b] —, “Optimal K-Factor and Active Current Reduction during Fault-Ride-Through of Converter-Connected Generating Units for Power System Stability,” in *12th International Workshop on Large-Scale Integration of Wind Power into Power Systems as well as on Transmission Networks for Offshore Wind Power Farms*, 2013.
- [Wei14] —, “Angle Instability of Generating Units with Fully Rated Converters in Cases of Low Voltages,” in *Chinese Wind & Solar Grid Integration Conference*, 2014.
- [Wei15] —, “Impact of K-factor and active current reduction during fault-ride-through of generating units connected via voltage-sourced converters on power system stability,” *IET RENEWABLE POWER GENERATION*, vol. 9, no. 1, pp. 25–36, 2015.
- [YC13] K. Yamashita and A. Cerretti, “Modelling and dynamic performance of inverter based generation in power system transmission and distribution studies: Proposal for the creation of a new joint working group: JWG* CC2013/2.C4/C6.35,” CIGRÉ Study Committee C4 and CIRED, Tech. Rep., 28 October 2013.
- [YDG⁺11] A. Yazdani, A. R. Di Fazio, H. Ghoddami, M. Russo, M. Kazerani, J. Jatskevich, K. Strunz, S. Leva, and J. A. Martinez, “Modeling Guidelines and a Benchmark for Power System Simulation Studies of Three-Phase Single-Stage Photovoltaic Systems,” *IEEE Transactions on Power Delivery*, vol. 26, no. 2, pp. 1247–1264, 2011.
- [Zho13] Z. J. Zhou, “Co-ordination of Converter Controls and an Analysis of Converter Operating Limits in VSC-HVdc Grids,” Ph.D. dissertation, The University of Manitoba, Winnipeg and Manitoba and Canada, 21-8-2013.

List of Publications

Journal papers

- [BRG⁺15] J. C. Boemer, B. G. Rawn, M. Gibescu, M. A. van der Meijden, and W. L. Kling, "Response of Wind Power Park Modules in Distribution Systems to Transmission Network Faults during Reverse Power Flows," *IET Renewable Power Generation*, vol. 9, no. 8, pp. 1033-1042, 2015.

Conference papers

- [BGK09] J. C. Boemer, M. Gibescu, and W. L. Kling, "Dynamic Models for Transient Stability Analysis of Transmission and Distribution Systems with Distributed Generation: an overview," in *IEEE PowerTech*, 2009.
- [BvR⁺11a] J. C. Boemer, A. van der Meer, B. G. Rawn, R. L. Hendriks, A. R. Ciupuliga, M. Gibescu, W. L. Kling, and J. A. Ferreira, "Fault Ride-through Requirements for Onshore Wind Power Plants in Europe: the Needs of the Power System," in *2011 IEEE PES General Meeting*, 2011.
- [BvR⁺11b] J. C. Boemer, A. van der Meer, B. G. Rawn, R. L. Hendriks, M. Gibescu, M. A. van der Meijden, W. L. Kling, and J. A. Ferreira, "Network Fault Response of Wind Power Plants in Distribution Systems during Reverse Power Flows," in *10th International Workshop on Large-Scale Integration of Wind Power into Power Systems as well as on Transmission Networks for Offshore Wind Power Farms*, October 2011.
- [vBR⁺14] J. C. Boemer, K. Skaloumpakas, M. Gibescu, M. A. van der Meijden, and W.L. Kling, "Response of Low Voltage Networks with High Penetration of Photovoltaic Systems to Transmission Network Faults," in *3rd International Workshop on Integration of Solar Power into Power Systems*, 2013.
- [SBv⁺14] K. Skaloumpakas, J. C. Boemer, E. van Ruitenbeek, M. Gibescu, and M. van der Meijden, "Response of Low Voltage Networks with High Penetration of Photovoltaic Systems to Transmission Network Faults," in *3rd Renewable Power Generation Conference (RPG 2014)*, 2014, p. 8.27.

- [vBR⁺14] E. van Ruitenbeek, J. C. Boemer, J. L. Rueda, M. Gibescu, and M. A. van der Meijden, "A Proposal for New Requirements for the Fault Behaviour of Distributed Generation Connected to Low Voltage Networks," in *4th International Workshop on Integration of Solar Power into Power Systems*, 2014.

M.Sc. theses and project reports

- [Ska14] K. Skaloumpakas, "Response of Low Voltage Networks with High Photovoltaic Systems Penetration to Transmission Network Faults," M.Sc. thesis, Delft University of Technology, Delft, 29/01/2014.
- [van14] E. van Ruitenbeek, "Impact of Large Amounts of Photovoltaic Installations in Low-Voltage Networks on Power System Stability During Transmission System Faults," M.Sc. thesis, Delft University of Technology, Delft, 17.06.2014.
- [Del14] Delft University of Technology, "Weiterentwicklung des Verhaltens von Erzeugungsanlagen am Niederspannungsnetz im Fehlerfall: Systemsicherheitsaspekte," Forum network technology / network operation (FNN) in the VDE e.V., Berlin, Tech. Rep., August 2014.

Acknowledgements

This dissertation has been a life-changing journey for me and my family throughout the past seven years. I started my research part-time while working for Ecofys just around the same time that my wife-to-be traded her life in Seattle, WA for our joint life in Berlin, Germany. In the fourth year of this dissertation, our daughter Elle Aradena was born and only a few months later we moved to Delft in the Netherlands where I dedicated myself fully to this research. After another international move to the United States, and coming aboard the U.S.-based Electric Power Research Institute (EPRI), it took me almost another two years to complete the thesis. Throughout this long journey I have met exceptional people whose company, thoughtfulness, and encouragements I will deeply appreciate for a life time and whom I would like to thank in the following remarks.

Prof.ir. W.L. Kling (Wil), who accepted my research exposé and wholeheartedly supported me during this dissertation in his lifetime, passed away unexpectedly on Saturday, March 14th, 2015. He died from natural causes, in Hangzhou, China during a business trip shortly before returning home to the Netherlands. Wil will be remembered for his outstanding contributions that combined academic knowledge with practical insights. He was a true mentor and friend to me and will continue to inspire me with his tremendous work ethic, personal integrity, and good humour. Without his passionate and caring attitude, this dissertation would not have been possible. Special thanks and thoughts go to his wife Mirjam for hosting me many times at their home in Helmond and a wonderful visit to 's-Hertogenbosch that opened my eyes for the beauty of the Netherlands.

Prof.ir. M.A.M.M. van der Meijden (Mart) was a wonderful promotor. His broad yet deep professional knowledge and experience across distribution and transmission systems planning and operations provided essential guidance for this thesis. Dr. M. Gibescu (Madeleine), my co-promotor from the very first day, continuously challenged my explanations and conclusions and did a tremendous job in scrutinizing this thesis. Dr. B. Rawn (Barry) has been a loyal scientific sparring partner over the years whose passion and wit delight me truly. I also want to thank Prof.dr.eng. J.A. Ferreira and Dr.eng. P. Bauer for contributing to this thesis in various roles, the secretaries Sharmila, Ellen, and Laura for their patience and flexible support, and all the other researchers in the Department of Electrical Sustainable Energy with whom I interacted on a regular basis.

I owe many thanks to my Master Students Ir. Evangelos (Vagelis) Galinas, Ir. Konstantinos (Kostis) Skaloumpakas and Ir. Emmanuel van Ruitenbeek whose absolute dedication to their work and patience with my never-ending demands contributed significantly to this thesis. A special thanks goes to Emmanuel who worked so thoroughly and independently on the research project for the Forum network technology / network operation in the VDE (FNN) that I was able to advance in other parts of my research at the same time.

I am grateful to Ing. W. Bartels of Westnetz GmbH, Dr. W. Winter of TenneT TSO GmbH, Prof. Dr.-Ing. habil. Z.A. Styczynski of University of Magdeburg, Dr.-Ing. T. Kumm of EWE Netz GmbH, and Dipl.-Ing. H. Kerber as well as Dipl.-Ing. J. Suckow of the FNN for advocating my research as a valuable scientific contribution to the ongoing revision of the *VDE Application Guide for generating plants' connection to and parallel operation with the low-voltage network (VDE-AR-N 4105)*. The numerous technical discussions with those utilities and vendors that were represented in the responsible FNN expert group on distributed generation were crucial for the development of a solid understanding of distribution system-related concerns and DG technology-specific modelling assumptions. The scientific collaboration with Dipl.-Ing. S. Altschäffl of Technische Universität München, Dipl.-Ing. S. Laudahn of Technische Universität Braunschweig, and Dipl.-Ing. M. Dietmannsberger of Helmut Schmidt-Universität Hamburg helped me link my research to adjacent fields of study. I further express my appreciation to Ecofys Germany GmbH and my former colleagues Dr.-Ing. K. Burges, Dr.-Ing. C. Nabe, C. Petersdorff, and K. van der Leun for supporting my part-time research with their resources and understanding.

The numerous discussions with colleagues inside and outside the Intelligent Electrical Power Grids group have been very illuminating. My office mate Arjen van der Meer was always eager to help in deepening my understanding of fundamental power system theory. Dr.ing. Edward Coster of Stedin B.V. reminded me of the practical value of my research.

My neighbours Carole and Lissa were meticulous proof readers of my manuscript. Arjen, Emmanuel, and Mart helped with the edits to the Dutch thesis summary. My wife Becky created the cover illustration literally overnight. I would also like to mention my appreciation for the unexpected encouragement from The Pike Market PenMaker in the final weeks of my work, whose gifted hand-made pen and enthusiasm for bringing renewable energy to the United States reminded me of the value of my work.

I am deeply thankful to my parents who nurtured me with a unique combination of scientific curiosity (through my mother Brigitte) and social responsibility (through my father Norbert). I wish to thank my sister Eva for competing with me to see who would finish our dissertations first (which I lost big-time) and my sister Ronja, who reminded me of the importance of my non-academic life. I also thank my dear friends who encouraged me throughout the years of my research in various ways, in particular Dr. Martin Mienkina who tirelessly challenged me in our regular conversations to carefully decide on the very next step to take.

Finally, I wish to thank my dearest ones, my wise and beautiful wife Becky for her love and everlasting support during this challenging chapter of our marriage, and our daughter Elle for her (un)conscious reminders of the most important things in life. Without Becky, I would not have been able to complete this dissertation.

Thank you to you all.

Jens C. Boemer,
Bainbridge Island, WA, June 2016.

Curriculum Vitae

Jens C. Boemer was born on May 8, 1980 in Dortmund, Germany. He studied Electrical Engineering at Technical University of Dortmund, Germany (1999–2005) including a six-month research stay at University of Chile, Santiago, Chile (2004). He received his Dipl.-Ing. in Electrical Engineering with a thesis on *‘Provision of Ancillary Services by Distributed Generation’* in 2005 at a time when the German *‘Energiewende’* was still in its infancy.

After an abridged *‘Postgraduate Programme in International Affairs’* run by the distinguished Robert Bosch Foundation and German National Academic Foundation in co-operation with the German Federal Foreign Office (2005–2006), he consulted the German Government, network operators, non-government organizations and project developers as an expert for grid integration of renewable and distributed generation. He started his career working as an independent consultant (2006–2007) and later worked as a Senior Consultant in the Power Systems and Markets Group at Ecofys, Berlin, Germany (2007–2012). His industry contributions during that period include technical support in the drafting of the *‘Ancillary Services Ordinance for Wind Power Plants (SDLWindV)’*, the development of an operational strategy for the Irish transmission system operator EirGrid/SONI with regard to very high instantaneous shares of wind power in the *‘All Island Facilitation of Renewables Studies’*, and a study on the so-called *‘50.2 Hz-Problem’* that guided the German Government to pass legislation for a massive retrofitting programme of photovoltaic systems.

During a sabbatical term (2013–2014), he conducted research with the Intelligent Electrical Power Grids group of the Electrical Sustainable Energy department at the Delft University of Technology, The Netherlands on the *‘Network Fault Response of Transmission Systems with Very High Penetration of Distributed Generation’*. In this period, he also consulted the Forum network technology / network operation in the VDE (FNN) on revisions to the German *‘Application Guide VDE-AR-N 4105’* by leading a research study on future voltage ride-through requirements for distributed generation in low voltage networks.

In November 2014 he joined the Grid Operations and Planning, Modeling and Simulation group in the Power Delivery and Utilization sector at the Electric Power Research Institute (EPRI) in Palo Alto, CA, as a remote employee based in the Greater Seattle Area, WA. In his current position as a Senior Technical Leader he leads research on the grid integration of renewable and distributed energy resources with a focus on power system stability issues. He contributes to the timely revision of *‘IEEE Standard 1547’*, particularly on the frequency and voltage ride-through clauses and was the lead author of an EPRI white paper that provides recommendations for *‘Minimum and Advanced Requirements and Settings for the Performance of Distributed Energy Resources During and After System Disturbances to Support Bulk Power System Reliability and Their Respective Technical Implications on Industry Stakeholders’*. He is member of IEEE, CIGRÉ, and VDE.

